TESIS DE LA UNIVERSIDAD DE ZARAGOZA

2022 61

Sonia García Embid

Encapsulation of biologically active agents in emulsions stabilized by natural polymers

Director/es
Martínez De La Fuente, Jesús
De Matteis, Laura

ISSN 2254-7606

Prensas de la Universidad
Universidad Zaragoza

ISSN 2254-7606

Universidad Zaragoza
1542

Tesis Doctoral

ENCAPSULATION OF BIOLOGICALLY ACTIVE AGENTS IN EMULSIONS STABILIZED BY NATURAL POLYMERS

Autor

Sonia García Embid

Director/es

Martínez De La Fuente, Jesús
De Matteis, Laura

UNIVERSIDAD DE ZARAGOZA
Escuela de Doctorado

Programa de Doctorado en Bioquímica y Biología Molecular

2022

Encapsulation of biologically active agents in emulsions stabilized by natural polymers

Memoria presentada para optar al grado de Doctor por la Universidad de Zaragoza

Sonia García Embid

Directores:

Jesús Martínez de la Fuente
Laura de Matteis

INMA
INSTITUTO DE NANOCIENCIA Y MATERIALES DE ARAGÓN

Programa de doctorado en Bioquímica y Biología Molecular

Zaragoza, 2020

Prof. Jesús Martínez de la Fuente y Dra. Laura de Matteis,

INFORMAN:

Que Sonia García Embid, graduada en Biotecnología y con título de Máster en Materiales Nanoestructurados para Aplicaciones Nanotecnológicas, ha realizado en el grupo de Biofuncionalización de Nanopartículas y Superficies de la Universidad de Zaragoza bajo su dirección el trabajo descrito en la presente memoria, que lleva por título “Encapsulation of biologically active agents in emulsions stabilized by natural polymers”, y que presenta para optar al grado de Doctor.

Zaragoza, 2021

Prof. Jesús Martínez de la Fuente

Dra. Laura de Matteis

Table of contents

Chapter 3. Encapsulation of disulfiram for its repurposing as an anticancer and antimicrobial agent

Chapter 4. Encapsulation of cloroperoxidase and magnetic nanoparticles for their use as catalytic microsupports

Chapter 5: Encapsulation of holmium vanadate nanoparticles for their use as contrast agents

Abstract

The use of nanocarriers for the encapsulation of different molecules has been explored over the recent years for multiple applications. They have been used for the vehiculization of hydrophobic molecules in aqueous media (or hydrophilic ones in oily media), protection of sensitive molecules or immobilization of different molecules in supports.

Among the different nanocarriers that have been developed, polymeric nanocapsules have attracted the interest of many researchers thanks to their great advantages. In this thesis, polysaccharide coated nanoemulsions have been developed as potential nanocarriers for the encapsulation of different molecules. Thanks to their versatility, these nanocarriers allow the encapsulation of hydrophobic in the oily core, while hydrophilic ones can be entrapped in the polymer coating. Besides, the components of the nanocapsules can be modified upon the needs of the final application.

All the developed nanocapsules were coated with the adequate polymer depending on the final application and the characteristics that needed to be achieved. Both chitosan, alginate and xanthan were used successfully.

The developed nanocapsules have proven to be very effective for the encapsulation of antibiotics such as bedaquiline and daptomycin used the treatment of *Mycobacterium tuberculosis* and Methicillin-resistant *Staphylococcus aureus* (MRSA) infections, respectively. An exploratory research has been also carried out

to encapsulate the drug disulfiram for its repurposing for the treatment of pancreatic cancer and MRSA infections. The developed nanocapsules have shown great capability as immobilizing agents of the enzyme chloroperoxidase and the encapsulation of magnetic nanoparticles (NP). They have also been able to encapsulate holmium vanadate NP for their use as contrast agents.

Physicochemical characterization as well as efficacy test for the different purposes were performed in all the cases. For all the tested applications, the developed nanocapsules showed great versatility for their use as nanocarriers of many different drugs, enzymes and nanoparticles as well as being able to modify the surface with different polymers to meet the application requirements.

Resumen

El uso de nanotransportadores para la encapsulación de diferentes moléculas ha sido explorado a lo largo de los últimos años para múltiples aplicaciones. Ha sido utilizado por ejemplo para la vehiculización de moléculas hidrofóbicas en medios acuosos (y de hidrofílicas en medios oléicos), la protección de moléculas sensibles o la inmovilización de diferentes moléculas en soportes.

Entre los diferentes tipos de nanotransportadores que han sido desarrollados, las nanocápsulas poliméricas han atraído la atención de multitud de investigadores debido a sus grandes ventajas. En esta tesis, nanoemulsiones recubiertas de polisacáridos han sido desarrolladas para su utilización como nanotransportadores de diferentes moléculas. Gracias a su versatilidad, estas nanocápsulas permiten la encapsulación de moléculas hidrofóbicas en el interior aceitoso, mientras que las moléculas hidrofílicas pueden ser atrapadas en la recubierta polimérica. Además, los componentes de las nanocápsulas pueden ser modificados a demanda de la aplicación final.

Las nanocápsulas desarrolladas han demostrado ser muy efectivas para la encapsulación de antibióticos como bedaquilina y daptomicina para su uso en el tratamiento de infecciones causadas por *Mycobacterium tuberculosis* y *Staphylococcus aureus* resistente a la meticilina (SARM), respectivamente. Han sido utilizadas también en un estudio exploratorio para la encapsulación del fármaco disulfiram y su utilización alternativa en el tratamiento del cáncer de páncreas e

infecciones causadas por SARM. También han mostrado gran capacidad como soportes para la inmovilización de la enzima cloroperoxidasa así como la encapsulación de partículas magnéticas. Por último, también han sido desarrolladas nanocápsulas para la encapsulación de nanopartículas de vanadato de holmio para su utilización como agentes de contraste.

Todas las nanocápsulas desarrolladas han sido recubiertas con el polímero adecuado teniendo en cuenta la aplicación final y las necesidades que se debían cubrir. Tanto el quitosano como el alginato y el xantano han sido utilizados para este propósito de manera satisfactoria. Se han realizado las caracterizaciones fisicoquímicas así como las pruebas de eficacia necesarias para cada aplicación. En todos los casos, estas nanocápsulas han demostrado tener un gran versatilidad como agentes nanotransportadores de diferentes fármacos, enzimas y nanopartículas así como ser capaces de modificar su superficie con diferentes polímeros para conseguir los requerimientos de la aplicación final.

Chapter 1

Introduction

1. Nanotechnology

1.1. Definition

Nanoscience breakthroughs in almost every field of science and represents millions of dollars of investment each year. Nanoscience and nanotechnology represent an expanding research area, which involves structures, devices, and systems with novel properties and functions, but what are they exactly? The prefix ‘nano’ is referred to a Greek prefix meaning ‘dwarf’ or something very small and depicts one thousand millionth of a meter (10^{-9} m). However, we should distinguish between nanoscience and nanotechnology first. Nanoscience is the study of structures and molecules on the scales of nanometers ranging between 1 and 100 nm, and the technology that utilizes it in practical applications is called nanotechnology. Despite being official definition stablished by the US National Nanotechnology Initiative (NNI)[1], experts have cautioned against an overly rigid definition, expanding the range to the submicrometric scale[2]. This is of great important in the pharmaceutical industry, in which the desired property of the “nanomaterial” (improved bioavailability, lower dose, reduce in the side effects…) may be achieved in a size range greater than 100 nm and not strictly in the 1 to 100 nm. Regulation in the

European Commission does not differ, and also considers nanotechnology as the design, characterization, production and application of structures, devices and systems by controlling shape and size at the nanoscale (having one or more dimensions of the order of 100 nm or less.[3] From the practical point of view, in the field of nanomedicine and pharmaceutical industry the term nanoscale and nanomaterial is used more vaguely and usually materials up to 500 nm are referred to as nanomaterials and in this thesis the term will be used like this for ease in the terminology as many materials are in the submicrometric range.

1.2. Discovery and origin

The American physicist and Nobel Prize Richard Feynman is considered the father of nanotechnology. In 1959, during the annual meeting of the American Physical Society he presented the now worldwide known lecture ‘There’s Plenty of Room at the Bottom’ in which he made the hypothesis of writing the entire 24 volumes of the Encyclopedia Britannica on the head of a pin.[4] He described a vision of using machines to construct smaller machines down to the molecular level and this novel idea demonstrated new ways of thinking that has been proven Feynman’s hypotheses correct.[5]

15 years after Feynman’s lecture, in 1974, the Japanese researcher Norio Taniguchi, was the first to use ‘‘nanotechnology’’ to describe semiconductor processes that occurred on the order of a nanometer. He described nanotechnology as the processing, separation, consolidation and deformation of materials by one atom or one molecule.[5]

After these discoveries, the golden era of nanotechnology began in the 1980s. Firstly, Binnig and Rohrer invented the first scanning tunneling microscope in 1981, providing visualization of individual atoms and bonds, and allowing the first manipulation of individual atoms in 1989.[6] 4 years later, in 1985, Kroto, Smalley and Curl discovered fullerenes.[7] Later on, Eric Drexler published the book ‘‘Engines of Creation: The Coming Era of Nanotechnology’’ in which he proposed the idea of a nanoscale assembler with the ability of building a copy of itself and of other items of arbitrary complexity. In 1991, the Japanese scientist Iijima developed carbon nanotubes.[8]

Despite the fact that nanoparticles (NP) and nanotechnology was given a name after Feynman’s lecture, nanoparticles and structures have been used by humans from a long time ago. For example, the Lycurgus cup is the oldest famous example of dichroic glass, which describes two different types of glass which changes color in certain lighting conditions. The cup, which was created in the IV century in the Roman Empire, has two different colors depending if the light reaches in the cup in direct form (green) or through the glass (red-purple) (The British Museum). In 1990, Barber *et al.* analyzed the cup using transmission electron microscopy (TEM) to explain the phenomenon of dichroism (Barber_1990).[9] They discovered that the dichroism is due to the presence nanoparticles with 50–100 nm in diameter. Using X-ray analysis, the research concluded that nanoparticles were composed of a silver-gold (Ag-Au) alloy, with a ratio of Ag:Au of about 7:3, containing in addition about 10% copper (Cu) dispersed in a glass matrix. The Au nanoparticles produce a red color as result of light absorption (~520 nm). The red-purple color is due to the

absorption by the bigger particles while the green color is attributed to the light scattering by colloidal dispersions of the Ag nanoparticles with a size greater than 40 nm. This effect is not exclusive to the cup and a similar effect is seen in late medieval church windows, shining a luminous red and yellow colors due to the fusion of Au and Ag nanoparticles into the glass.

After Feynman had discovered this new field of research, many scientists got new interest developing two approaches describing the different possibilities for the synthesis of nanostructures. These manufacturing approaches fall under two categories: top-down and bottom-up, which differ in degrees of quality, speed and cost.

The top-down approach consists on breaking down a bulk material into smaller particles. Some of these techniques are ball milling or lithography.[10] On the other side, the bottom-up approach consists on building-up nanostructures by assembly of atoms or molecules to obtain the final material.[10] Current research tries to improve bottom-up methodologies and it is desired that all nanomaterials in the future are synthesized by bottom-up approaches, although we are still far from this specially in the industry.[10]

1.3. Advantages and new characteristics of nanomaterials

Now we know the definition and origin or nanomaterials, but, why are they so important? Once the size of the system decreases, several phenomena become pronounced, such as statistical mechanical effects, as well as quantum mechanical effects. One of these effects is known as the "quantum size effect", in which the electronic properties of solids are altered with great reductions in particle size. These

quantum effects become significant when the nanometer size range is reached, usually at distances of 100 nanometers or less; this parameter is called the quantum realm. Additionally, depending on the type of nanoparticles, other mechanical, electric or optical properties change in comparison with macroscopic systems. For example, the increase in surface area to volume ratio altering mechanical, thermal and catalytic properties of materials. This is of great importance in the interaction with biomaterials, which usually range in the same scale. Nanoparticles can also reach to inaccessible sites, including i.e. tumor cells or inflamed tissue. Besides, some properties can completely change and some nanomaterials can become transparent, combustible, soluble or reactive at the nanoscale.[11]

1.4. Applications

Nanoparticles, due to their unique properties, have attracted researchers from many different fields. Among the nanotechnology consumer products, health fitness products are the largest category, followed by electronics and computers.[12] Nanotechnology is considered as the next revolution in many industries such as food processing or packaging, energy harvesting or even medicine.[13] Nanoparticles can be classified into inorganic or organic, and their applications will depend on that thanks to the different properties they have

Inorganic nanoparticles are composed of metal and semi-metal materials and have gained a lot of interest in the past years. Their main advantages are the scalable synthesis, simple modification of the surfaces, high stability and controlled drug release. Besides, depending of the material of the inorganic nanoparticle, they can combine other properties to the carrier.

The unique properties of semiconductor and metal nanoparticles have make them especially interesting in electronic applications. They are currently investigated, for example, for the development of new transistors used in for the amplification or switch of electronic signals. They also have great potential to be used in the storage of information in hard disks or energy in cells and batteries. Other applications in the electronics field are high voltage insulators, nanorobotics or nanowires.[14]

Related with this field, nanoparticles are also being used in energy harvesting. It is widely known that fossil fuels are limited so research is concentrated in the development of new strategies to generate renewable energies from easily available resources with cheap costs. Due to their large surface area, optical properties and catalytic nature, nanoparticles have been proposed as the best candidates. They have been used in water splitting, solar cells and piezoelectric generators, among others.[12]

Nanoparticles have also been extensively used in environmental applications. They have been applied in water and waste water treatment, remediation, removal of pollutants or sensing. For example, nanoadsorbents, nanocatalysts or nanomembranes have been used for the removal of pollutants from wastewater to reduce the cost of potable water production. They have been also used for the removal of contaminants from groundwater, soils or sediments, both in situ or ex situ.[15] They have also been applied for the development of sensors, for example for the detection heavy metals such as lead, cadmium or mercury but also contaminant in the food industry[16] or extracellular vesicles in liquid biopsies[17].

In the food industry, nanoparticles have been used in both food processing and food packaging. In food processing, several authors have used nanotechnology to improve texture, taste and appearance of food. For example, nanoencapsulation has been used to improve flavor release or to improve stability of instable molecules with biological activity. It has been also used to protect bioactive molecules from degradation by the acidic conditions of the stomach or increase the shelf-life of manufactured foods. In food packaging, nanoparticles have been used as antimicrobial agents to inhibit or retard microbial growth or even as detectors of food contaminants.[18]

Nanoparticles have been also applied in biomedical applications. They have been applied for the treatment of numerous illnesses such as cancer, infections or Alzheimer's disease. For example, Artiga and coworkers[19] used gold nanoparticles for the treatment of cancer. Thanks to the photothermal properties, gold nanoparticles are able to produce heat after irradiation with an adequate laser, killing surrounding cells. Iron oxide nanoparticles have also been used for this purpose, but in this case heat is produced upon application of a magnetic alternate field.[20] However, one of the most promising application of nanoparticles in the biomedical field is their use as nanocarriers, which is the main topic of this thesis. Their use is so important in this topic, that even the newly developed Covid-19 vaccines produced by Pfizer-BioNTech or Moderna encapsulate their mRNA construct into lipid nanoparticles. This allows easy internalization of the mRNA into cells, as well as protects them from early degradation.[21]

2. Nanocarriers

Nanocarriers are nanomaterials used to transport another substance. They have been used for the encapsulation of both small molecules (drugs, vitamins…) and macro size ones such as proteins or other nanoparticles. The term nanocarriers comprises different types of organic nanoparticles such as nanospheres, nanocapsules, nanoemulsion, and nano-sized vesicular carriers but also inorganic nanoparticles such as gold or iron oxide NP (Figure 1).

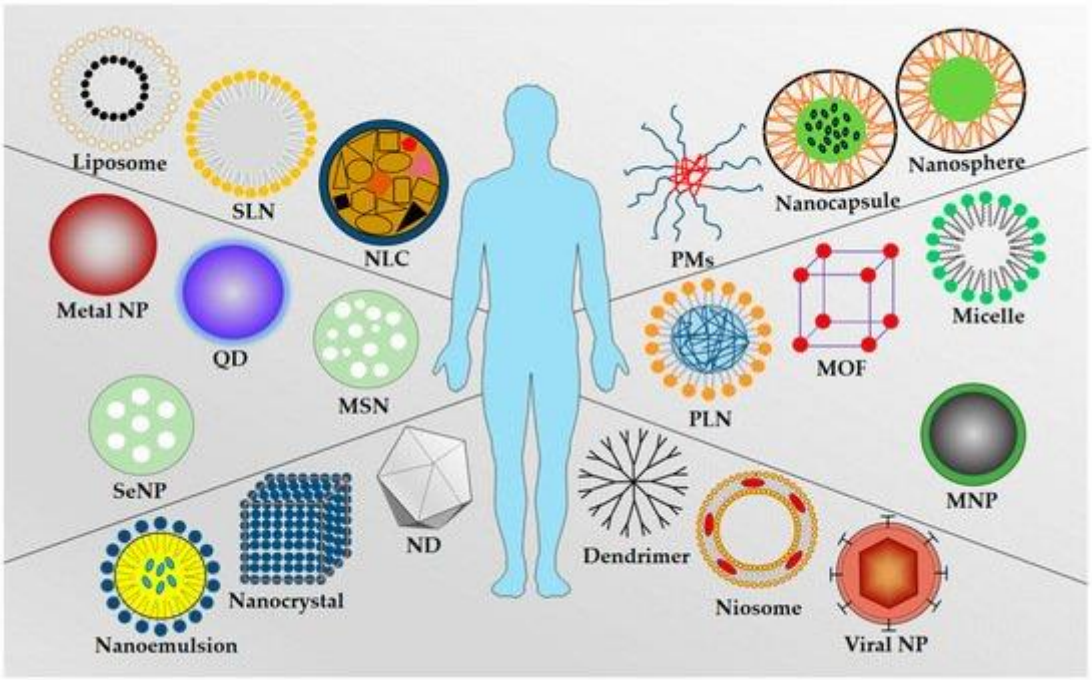

Figure 1. Schematic representation of the commonly used nanocarrier types: Liposome, solid lipid nanoparticle (SLN), nanostructured lipid carrier (NLC), polymeric micelles (PMs), nanocapsule, nanosphere, metal nanoparticle, quantum dot (QD), mesoporous silica nanoparticle (MSN), polymer–lipid hybrid nanoparticle (PLN), metal–organic framework (MOF), micelle, selenium nanoparticle (SeNP), magnetic nanoparticle (MNP), nanoemulsion, nanocrystal, nanodiamond (ND), dendrimer, niosome, and viral nanoparticle. Adapted from Wei et al.[22]

Although there are also inorganic nanocarriers, due to their more extensive use and the main topic of this thesis, we will be focusing here in the organic ones.

Among the organic nanocarriers, liposomes are the most commonly used ones. They are composed of lipid bilayers made of phospholipid having enclosed aqueous compartment. They can be used for the delivery of smaller molecular weight therapeutics, imaging agents, peptides, proteins and nucleic acid.[23,24]

Similar to liposomes, solid lipid nanoparticles (SLN) present great advantages such as economical large-scale production, long-term stability, and controlled drug release. However, they have low drug loading capacity in comparison with other vehicles. Nanostructured lipid carriers (NLC) are second generation SLN with high drug loading and composed of a mixture of lipids that favors the encapsulation of different drugs.[23,25]

Micelles are another type of lipid nanostructures that are formed by amphiphilic surfactants that spontaneously aggregate in water into vesicles. The hydrophobic core facilitates encapsulation of low-water soluble drugs but there are not commonly used due to poor chemical versatility and structural instability.[23,26]

Polymeric micelles consist of a hydrophilic external shell and a hydrophobic internal core. The major improvement in comparison with regular micelles is their chemical versatility that improves both drug loading and target specificity. Thanks to the polymeric external shell, the surface can be modified to provide steric stability as well as the possibility to have target delivery.[23,27]

Polymer-based nanocarriers are organic polymer compound assemblies that form nanospheres or nanocapsules. While nanospheres are solid particles, nanocapsules are hollow spheres with a space in the center. They can be formed by both natural or synthetic polymers and their main advantage is the extend circulation time and controlled drug release.

Similar to polymer-based nanocarriers, dendrimers are branched polymers with a symmetric spherical shaped that are chemically produced. Drugs are either entrapped in the core or covalently attached to the surface. Their advantages are their high stability, water solubility, low immunogenicity or antigenicity but the multistep synthesis highly increases the productions costs, which limits their use.[28]

Niosomes are similar to liposomes but with higher stability. They are formed by nonionic surfactants as they were developed to overcome the low stability of liposomes due to phospholipid oxidation. Their main advantages, besides increased stability is the lower manufacturing costs. However, their main disadvantage is the low encapsulation ability.[23]

Nanocrystals are pure solid nanoparticles with a crystal structure. They have increased surface area to volume ratio, continuous dissolution rates, enhanced stability and high drug-loading.

Bionanoparticles are widely used in lab scale, but have low scalability to the industry due to high cost and manufacturing time. This kind of nanocarriers include viral nanoparticles or protein based nanocarriers.

Exosomes are naturally produced nanoparticles secreted by all types of cells that can be found in several body fluids. They van store water soluble drugs in their hydrophilic core and possess natural targeting capacity, which is one of their main advantages. Besides, they are highly stable, low immunogenic, and are able to pass through various biological barriers. However, due to their complex structure and difficult identification more research is needed in order to develop commercial nanocarriers.[23]

The last type of organic nanocarriers are nanoemulsions, that are the main topic of this thesis and will be discussed in the next section.

3. Nanoemulsions

An emulsion consists of two immiscible liquids (usually oil and water), being one of them dispersed as small spherical particles in the other. A nanoemulsion can be considered to be a conventional emulsion in which the dispersed particles are very small particles.[29] They can be also referred to as miniemulsions, ultrafine emulsions, unstable microemulsion o submicrometer emulsions,[30] but they should not be confused with microemulsion[29,31]. The major reason for the confusion created between micro and nanoemulsions comes from the prefix used for their names. Although it would be expected that nanoemulsions (nano means 10^{-9}) would be much smaller than microemulsions (micro states for 10^{-6}), the reality is that the opposite usually happens. [32]

The term microemulsion was first used in 1961[33] while the first article using the term nanoemulsion was published in 1996[34]. Thus, the term ‘‘microemulsion’’ was well-established among researchers before the term ‘‘nanoemulsion’’ was introduced and

the use of both terms became widespread before they were clearly distinguished form each other.[31] The fundamental method for their distinction nowadays is their thermodynamical stability. Microemulsion are thermodynamically stable and they are spontaneously formed. They also have a smaller diameter and are therefore translucent. Besides, they are stable while their range of conditions (temperature, pH…) does not change. Nanoemulsions, on the other hand, are thermodynamically unstable as kinetically stable.[31] This kinetically stability means that they can have long-term stability in the right conditions. They have a bigger diameter than microemulsions and the solution is turbid. They usually need and input of energy and will break down over time if they are not stabilized in further steps (this will be discussed in Section 3.3). The main advantage of nanoemulsions over microemulsions, and the main reason why they were chosen in this thesis, is that nanoemulsions can be synthesized with lower amounts of surfactants. Also, nanoemulsion can made from a wider range of surface active agents.[31]

Nanoemulsions are great nanocarriers as they offer the possibility to encapsulate lipophilic or hydrophilic active agents depending on their composition. There are 3 types of nanoemulsions: oil-in-water (O/W) in which the oil is dispersed in water; water-in-oil (W/O) in which water is dispersed in oil and bi-continuous nanoemulsions, which include two types: oil in water in oil (O/W/O) in which O/W act as a dispersed phase and oil act as a dispersion medium and water in oil in water (W/O/W) where W/O oil act as a dispersed phase while water act as a dispersion medium. Usually, O/W are the most commonly used for the drug delivery of lipophilic drugs as they can be dispersed in the aqueous media of the body.

3.1. Components

The basic components required for fabrication of nanoemulsions are oil, stabilizers, co-solvent and water.

The selection of the oil used for the preparation of the emulsion is a critical parameter and should be selected based on polarity, water-solubility, interfacial tension, viscosity or density, among other physicochemical characteristics. The choice of oil will greatly influence the formation stability and properties of the emulsion as well as will limit the type of homogenization method that can be used for the nanoemulsion synthesis. For example, increase in density of the oil will increase creaming rate, destabilizing the emulsion and decreasing shelf-life.[35] Some of the oils usually used can be triacylglycerols, diacylgycerols or monoacylglycerols, fatty acids, essential oils, waxes, oil-soluble vitamins, amongst others.[29,35]

Besides the use of water, the aqueous phase may also contain other polar components such as co-solvents, carbohydrates, minerals or proteins. These components will determine some of the chemical characteristics of the phase impacting also formation and stability of the nanoemulsion.[35]

The use of stabilizers is necessary to stabilize the nanoemulsion and help increase long-term stability. If only the oil and the aqueous phases are mixed, the system will break down due to several mechanisms: Ostwald ripening, coalescence, flocculation… so the use of stabilizers is essential. The selection of the appropriate one will reduce interfacial tension and improve nanoemulsion stability. The emulsifier is the surface-active molecule able to absorb to the oil droplet surface protecting them from aggregation.[36,37] It will also impact in the synthesis method used as it

facilitates droplet disruption, so the synthesis method selected will also depend on the surfactant used.

Different molecules can be used as stabilizers, mainly small molecule surfactants, phospholipids, proteins and polysaccharides. Surfactants are usually the most effective ones, and can be used for almost all synthesis methods. On the other hand, proteins and polysaccharides, although not as suitable for the formation of small emulsions, are natural products, biodegradable and are catching more attention.

Surfactants can be classified into three groups: ionic, zwitterionic and non-ionic.Ionic surfactants can be positively charged such as quaternary ammonium alkyl salts or hexadecyltrimethylammonium bromide; or negatively charged for example sodium lauryl sulfate. Although they can be used mostly in all preparation methods, their utilization may be limited in products where high-surfactant levels are required because they tend to cause irritation.[38]

Zwitterionic surfactants can have a net neutral, positive or negative charge depending on the pH thank to having at least two ionizable groups on the same molecules. The most common zwitterionic surfactants are phospholipids and are usually used in combination with cosurfactants, as they are not good stabilized by themselves.[39,40]

Non-ionic surfactants are the most widely used as they have low toxicity and can easily form nanoemulsion using all synthesis methods. They include sugar ester surfactants, polyoxyethylene ether surfactants and ethoxylated sorbitan esters. Non-ionic surfactants are stabilized by dipole and hydrogen bonding interaction and produce more stable nanoemulsions than ionic ones, as these last ones are affected by salt concentration and pH.[41]

Combinations of emulsifiers is usually preferred to the use of a single one, as stability and formation of the emulsions is improved. This fact is more important in the case of low-energy methods (See next section), in which the presence of a co-surfactant (or sometimes a co-solvent) is required.[42]

Cosurfactants are surface active amphiphilic molecules that cannot stabilize an emulsion by themselves due to small size and polar head groups, but help stabilizers. They can be short and medium chain alcohols than fluidize the interface, optimize the disperse-to-continuous phase viscosity ratio, reduce the electrical repulsion between the ionic surfactants acting as spacers and induce appropriate interfacial curvature.[42]

In some cases, texture modifiers and weighting agents are also needed to improve stability. Texture modifiers thickens or gels the aqueous phase while weighting agents are added to the oily phase to match its density to the aqueous one. (McClements_2005).[43,44]

3.2. Synthesis methods

With all the components already mentioned, several synthesis methods can be used for the synthesis of nanoemulsions. These are generally classified as high-energy and low-energy approaches depending on the input energy needed.[29,35,45]

Nowadays, high-energy methods are the most common approach for the synthesis in nanoemulsion in the industry. They are easy to prepare, scalable and several starting materials can be used.[46,47] On the other hand, low-energy approaches rely on the spontaneous formation of the emulsion when the solution or the environmental conditions of the oil-water-emulsifier are altered. [29,45,48,49]

Table 1. Summary of nanoemulsion synthesis methods

		Mechanism of formation/force
High-energy methods	High-pressure valve homogenizer	Piston pump
	Microfluidizer	Impact between two streams
	Ultrasonic homogenizer	Ultrasonic waves
Low-energy methods	Spontaneous emulsification	Spontaneous formation by mixing two phases with a partially miscible component
	Phase-inversion temperature (PIT)	Change in the optimum curvature of surfactant due to change in temperature
	Phase-inversion composition (PIC)	Change in the optimum curvature of surfactant due to change in formulation
	Emulsion-inversion point (EIP)	Catastrophic-phase inversion by increase (or decrease) in volume fraction of the dispersed phase

3.2.1. High-energy approaches

In high energy approaches, mechanical devices generate extremely intense disruptive forces than produce tiny droplets to form nanoemulsions.[29] High energy is needed because disruptive forces created by this mechanical device have to exceed restoring forces holding the spherical droplet's shape. The smaller the emulsion droplet, the more difficult to break them. Therefore, the homogenizer design,

operating conditions, sample composition, environmental conditions and physicochemical properties of the phases are crucial parameters for droplet size. [35] High energy approaches are highly versatile, as they can be used for a lot of different oil and emulsifier combinations. There are several devices developed for the synthesis of nanoemulsions using high-energy methods: high-pressure valve homogenizers, microfluidizers and ultrasonic homogenizer.

3.2.1.1. High pressure valve homogenizer

High pressure valve homogenizers are the most common high pressure devices.[50] This type of devices has a piston pump that forces a previously mixed coarse emulsion through a valve with a specific gap. The coarse emulsion is produced with a high shear mixer and its essential for the correct operation of the homogenizer. Droplets are disrupted due to the laminar and turbulent flow at the valve, breaking larger droplets into smaller ones. Droplets with less than 100 nm in radius are difficult to produce, and special conditions are needed: high emulsifier amounts, appropriate viscosity ratios and low interfacial tensions. Besides, it is usually required to operate at high pressures and complete multiple passes.[35,51] A schematic representation is shown in Scheme 1.

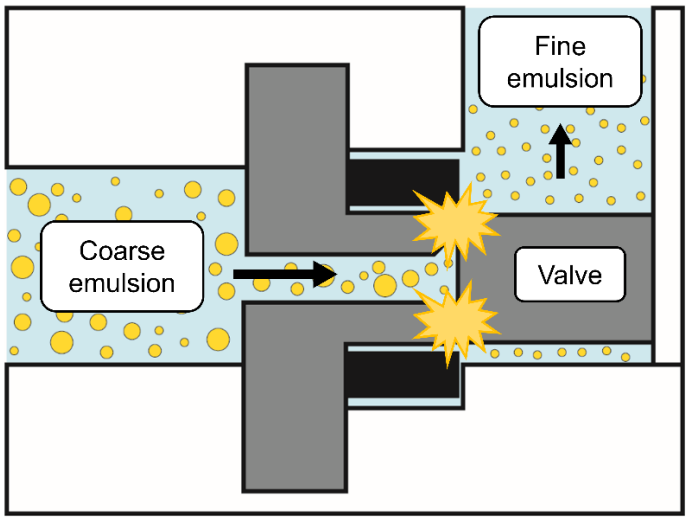

Scheme 1. High-pressure valve homogenizer

3.2.1.2. Microfluidizers

As high pressure valve homogenizer, microfluidizers work at high pressures, forcing a coarse emulsion to be separated into two different streams. These streams are passed through two channels and then redirected at each other to interact in a mixing chamber. The impact in a 180º angle creates disruptive forces due to high turbulence and shear, creating smaller droplets. As in high pressure valve homogenizers, usually several cycles are needed to achieve the desirable droplet size.[35,50,51] A schematic representation is shown in Scheme 2.

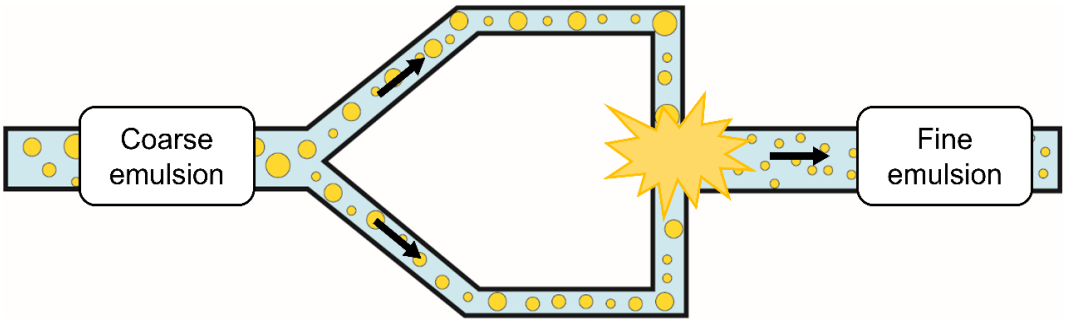

Scheme 2. Microfluidizer

3.2.1.3. Ultrasonic homogenizer

Ultrasonic homogenizers use high intensity ultrasonic waves creating disruptive forces that break up both aqueous and oil phases into small droplets. This sonicator tip is placed between the two phases, crating the disruptive forces. The greater the intensity of the ultrasonic wave or the residence time, the lower the droplet size obtained. This method has the advantage of being cheaper, but it is not suitable for all applications, as the high sonication intensities used can lead to destruction of some of the components of the emulsion: protein denaturalization or polysaccharide depolymerization among others.[35,50,51] A schematic representation is shown in Scheme 3.

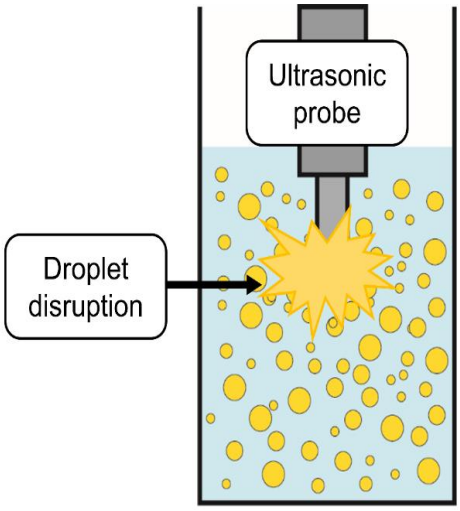

Scheme 3. Ultrasonic homogenizer

The main advantage of these methods is their reproducibility and easiness to develop in the industry. However, one of the main drawbacks is their cost, as they need expensive equipment and require a lot of energy input. Besides, due to the operational process, such as high pressure and forces, they may not be suitable for certain molecules that are sensitive to the operational conditions.[35,44,52]

3.2.2. Low-energy approaches

Synthesis of nanoemulsions using low energy approaches relies on the spontaneous formation by alteration of composition or environment of the oil-water-emulsifier mixtures.[29,35,45,48,51] They have the advantage of being more cost effective and produce smaller droplets than high-energy approaches. However, their main disadvantage is that there is a high limitation in the types of oils and emulsifiers that can be used.[35,51]

3.2.2.1. Spontaneous emulsification

In spontaneous emulsification, emulsion is formed spontaneously by mixing of two liquids.[45] This method can be carried out by different mechanism: 1. Change in the composition of the phases; 2. Change in the environmental conditions; 3. Change in the mixing conditions. The organic phase can be added to the aqueous phase[48,53] or water can be added to the organic one[54]. A schematic representation is shown in Scheme 4.

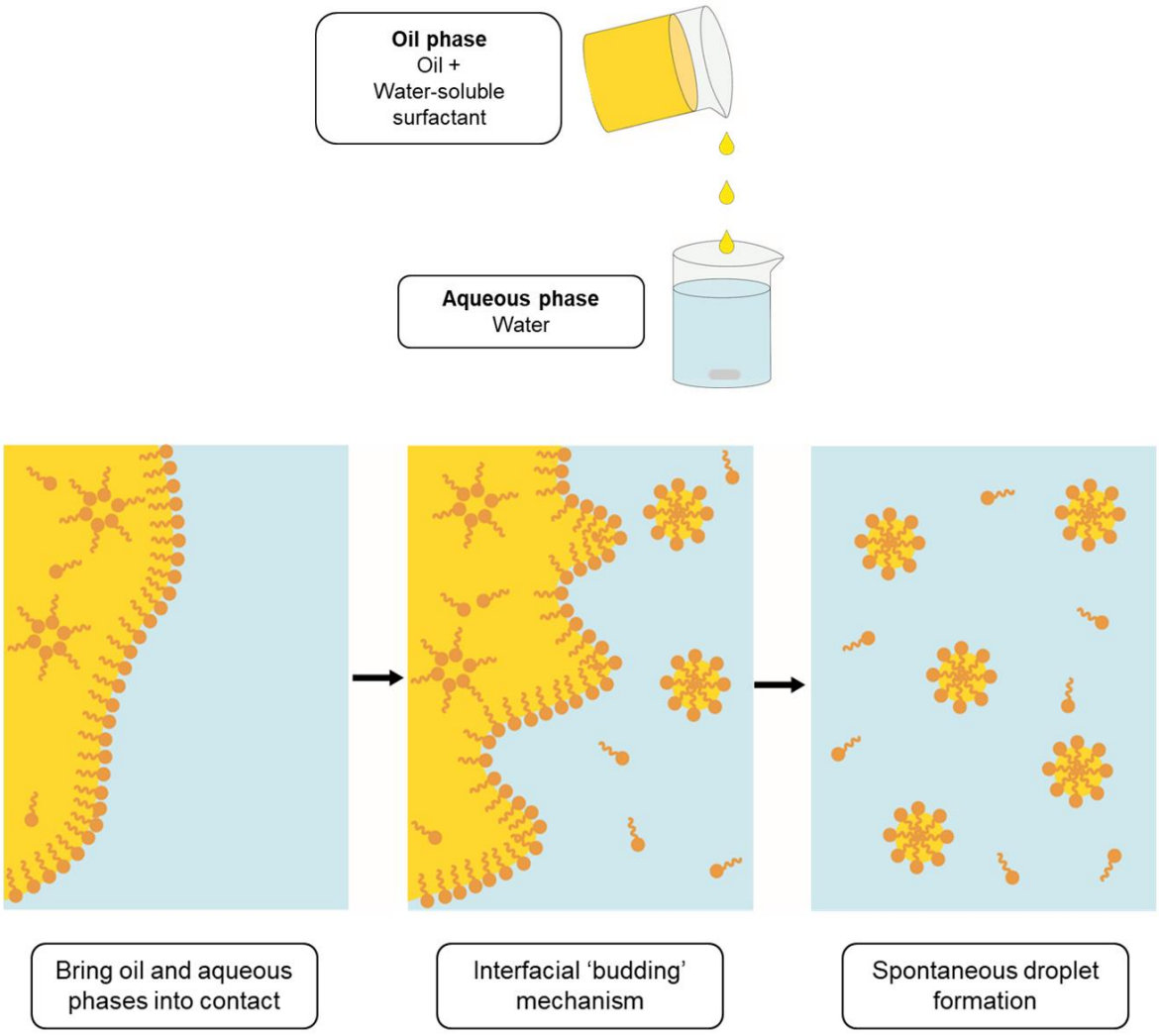

Scheme 4. Spontaneous emulsification

When two phases are put in contact, each of them has some components that are immiscible with the other one (i.e. oil and water) and others that are partially miscible (i.e. surfactant). After contact of both phases, some of the partially miscible component will move from one phase to the other, increasing oil-water interfacial area and turbulence, causing spontaneous formation of the emulsion droplets. The size of this droplets will vary depending on the composition of the phases and the mixing conditions (temperature, stirring…).[35]

In surfactant-free systems, Ouzo or Pastis effect produces self-emulsification. Ouzo is an alcoholic beverage that, when mixed with water, becomes cloudy instantaneously. Ouzo is composed of water, ethanol and trans-anethol (an ethanol soluble, water insoluble molecule). Upon addition of water into the beverage, some alcohol molecules move from the organic to the aqueous phase, causing the formation of small oil droplet of trans-anethol due to loss of solubility.[55] This method has been applied for the formation of surfactant free nanoemulsion in literature.[56]

There is not full understanding on how the dynamics and the mechanisms of spontaneous emulsification works.[57] However, it is known that the addition of a surfactant allows the obtaining of smaller nanoemulsion droplets in comparison with surfactant-free systems. This method has been widely used in pharmaceutical applications, but has some limitations in the food industry for example, due to a limited availability of food-grade surfactants.[58]

Several mechanisms can be developed in spontaneous emulsification, so there is not consensus in the final classification. For example, Solans *et al.*[59] *c*onsider that phase inversion does not occur in spontaneous emulsification, while Anton *et al.*[45] do.

3.2.2.2. Phase-inversion

There are three approaches: phase-inversion temperature (PIT), phase-inversion composition (PIC) and emulsion-inversion point (EIP). In all of them, phase transitions usually involve inversion of the surfactant film curvature from positive to negative: meaning that O/W are transformed into W/O and vice versa. However, it has also been reported that transitions from structures with zero average curvature are especially important. A schematic representation of PIT and PIC is shown in Scheme 5 and of EIP in Scheme 6.

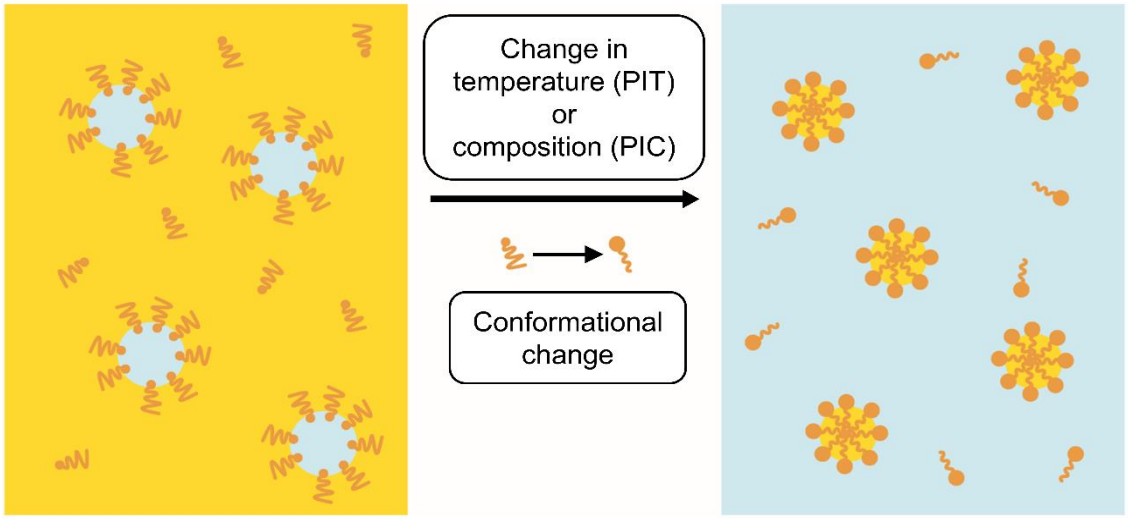

Scheme 5. Phase-inversion Temperature (PIT) and Phase-inversion Composition (PIC)

In PIT, phase inversion occurs due to changes in the optimum curvature or solubility of non-ionic surfactants with a change in temperature.[53] In PIC, the optimum curvature of the surfactant is modified by a change in the formulation of the system instead of temperature, for example, by addition of salts or a change in pH.[53]

Generally speaking, PIC method is preferred in industry as it is easier to add one component to the emulsion than to produce a sudden change in temperature.

Besides, it is preferred when working with certain molecules with temperature stability problems such as proteins.[56]

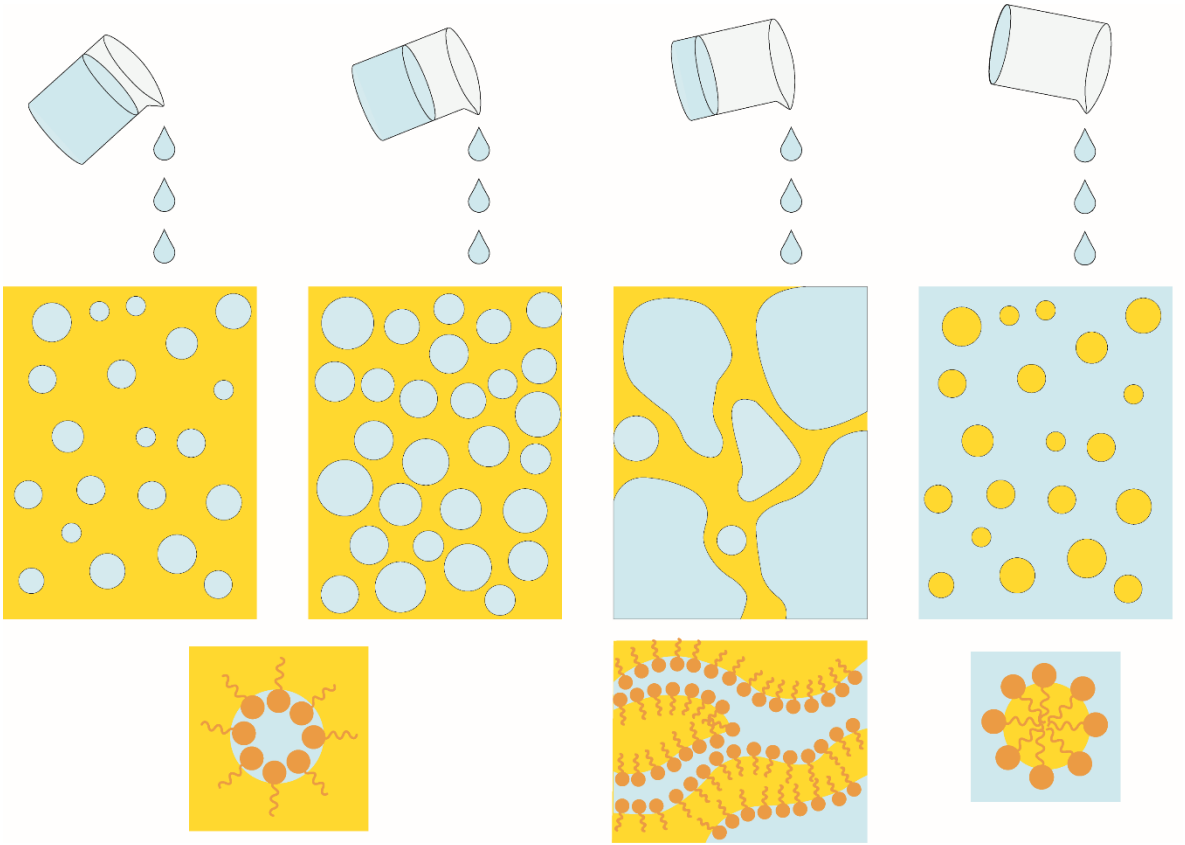

Scheme 6. Emulsion-inversion point (EIP)

In both PIC and PIT methods, the phase inversion occurs through change in the properties of the surfactant. The EIP method takes place when there is a catastrophic-phase inversion by changing of the oil-to-water phases. This occurs when the volume fraction of the dispersed phase in increased (or decreased) above (or below) a critical level. This method is not as versatile, as only small molecule surfactants that are able to stabilize both O/W and W/O emulsions can be used.[35]

3.3. Stability of nanoemulsions

Due to the fact that nanoemulsions are not thermodynamically stable, but kinetically stable, several mechanisms can lead to breakdown over time. Some of these are: gravitational separation, droplet aggregation, Ostwald ripening and chemical degradation.[60]

Gravitational separation can take form of creaming or sedimentation, depending on the densities of the phases of the nanoemulsion. Droplets usually have different density to the surrounding liquid so gravitational forces act upon them. Creaming occurs when the dispersed phase has lower density than the continuous one, leading to the upward movement of the droplets. In sedimentation, droplets move downwards, as they have higher density. This is one of the most common forms of instability in nanoemulsions with diameters higher than 70 nm, as in smaller diameter nanoemulsions, Brownian motion dominates particle movement rather than gravitational forces. Gravitation separation can be prevented by increase of the shell layer thickness (layer surrounding the emulsion). The shell layer can reduce the density contrast between the particles and the surrounding fluid if it has a higher density than the oil or the dispersion phase. The thickness of this layer can be increased by absorption of addition material to the droplet surface after synthesis.[35]

There are two types of droplet aggregation: flocculation and coalescence. Due to the continuous movement of emulsion droplets, there are continuous collision between neighbors. Depending on the attractive and repulsive forces between them, droplets may tend to stay aggregated or move apart again. Flocculation is the process in which two or more droplets aggregate but retaining their individual integrity. In coalescence, droplets merge to form one single larger particle. Droplet aggregation

can be reduced by increasing the repulsive forces between droplets, i.e. increasing electrical charge or reducing collision frequency by increase in the viscosity of the dispersion phase.[60]

Ostwald ripening is a process in which oil molecules diffuse from small to larger droplets through the dispersion liquid, increasing nanoemulsion mean size diameter over time. This effect is explained by the fact that an oil contained in a spherical droplet is more soluble in water as the size of the droplet decreases. This means that there is a higher concentration of oil in water around small droplets than around bigger ones. This creates a concentration gradient than makes oil molecules to move from the smaller particles to the bigger ones. This problem is more noticeable in emulsions prepared with oils with higher water solubility such as short triglyceride, flavor oils and essential oils.[46] Ostwald ripening can be retarded by the addition of a ripening inhibitor. These substances are non-polar molecules that are insoluble in water but soluble in the oil phase, generating entropy of mixing that counterbalances Ostwald ripening.[35,60]

The last factor affecting nanoemulsions stability is chemical stability. This effect is usually more noticeable in nanoemulsions as the size decreases. More lipid phase will be exposed to the aqueous phase with a decrease in diameter, as the oil-water surface area increases. As chemical degradation usually occurs at the interface, the smaller the particles, the greater the reaction rate. Besides, smaller particles, which are usually transparent, are more exposed to degradation by UV or visible light than bigger opaque emulsions. Protection of the emulsion surface can reduce chemical degradation of the oils.[35]

3.4. Finishing techniques

Several finishing techniques can help overcome these problems. Finishing techniques are a variety of methods that are carried out after nanoemulsion synthesis to change droplet characteristics and improve stability. Some of them include: emulsifier or oil exchange, droplet crystallization, solvent evaporation/displacement or coating.

Solvent evaporation or displacement are finishing methods to reduce nanoemulsion droplets size. In both methods, the nanoemulsion are formed by oil-solvent. In the solvent displacement method, the aqueous phase is initially saturated with a partially miscible solvent. After addition of more water, the solvent in the oil droplets moves to the aqueous phase, shrinking the emulsion droplets. In the solvent evaporation method, the organic solvent is removed from the emulsion droplets by evaporation, causing shrinking of the droplets and therefore a reduction in size. The overall reduction of the droplets diameter will depend on the solvent characteristics, amount of solvent and original size.

The oil composition of a nanoemulsion can be changed by lipid phase exchange. When two emulsions with different oil compositions are mixed together, it is possible that oil exchange is produced between them due to ripening effects until a steady-state is reached. This allows the introduction of different lipophilic components into emulsions after their synthesis.[35]

The oil emulsion droplets can be changed from liquid to solid state to achieve novel functional properties.[61] For this method, the selection of oil and synthesis temperature is the most important factor. Emulsion synthesis is performed above the melting temperature of the oil and cooled in a controlled rate to crystalize it.

The last finishing techniques modify emulsion interface to stabilize the droplets or alter the nature for different applications. This is especially interesting when the emulsifier used is highly suitable for the synthesis process, but is not able to stabilize the emulsion for the final application. Several methods can be used for this purpose. Emulsifier can be changed by interfacial displacement, in which a new surfactant competes at the oil-water interface with the existing one.[60] Depending on the emulsifier used during the synthesis process, it is possible to crosslink them. This is usually carried out when the emulsifiers are proteins or polysaccharides.[62] Lastly, the interface can be modified by addition of a molecule to the droplet surface. In this case, a molecule able to absorb to the droplet surface is added to the solution. This can be used to create multilayers and change functional properties of the emulsion.[58,63]

Regarding this last approach, it is one of the most promising, as it allows the modification of the surface to achieve the characteristics desirable for the final applications. Several molecules have been used for this purpose: polysaccharide, proteins or other surfactants[64,65] and also several techniques.

One strategy is the layer-by-layer method (LbL). In this technique, the previously synthesized nanoemulsion is prepared using an ionic emulsifier that rapidly adsorbs to the surface of the oil droplet. Then, an oppositely charged biopolymer is added. This polymer is adsorbed to the droplet creating an emulsifier-biopolymer interfacial layer. This process can be repeated several times creating multilayered nanoemulsions that have proved to be more stable to environmental stresses than conventional emulsion in some circumstances.[58]

Another method for the deposition of polymers to coat nanoemulsion surfaces is by coacervation. In this method, the polymer is added to the nanoemulsion and polymer solvation is decreased. This can be done by increase or decrease in temperature, addition of electrolytes o dehydration agents. The decrease in solvation causes polymer precipitation forming a film around the emulsion. This can be then stabilized by crosslinking the polymer, either using a cross-linking agent (ionic or covalent), or modifying pH and/or temperature.[66]

A third approach is the deposition of the polymer triggered by solvent evaporation. In this case, the emulsion is formed and the polymer is added later to the solution. Once the solvent is evaporated, the polymer is coating the nanoemulsion.[67]

All these methods have been used for the coating of nanoemulsions using different kind of synthetic polymers such as poly(methyl methacrylate) (PMMA), poly(methacrylate) (PMA) or natural polymers such as polysaccharides.

4. Polysaccharides as emulsion stabilizers

Polysaccharides are high molecular weights derivatives of monosaccharide with repeating units. Polysaccharides have been widely used for the stabilization of nanoemulsions working as thickening or gelling agents. More recently, they have been used as a coating to modify the oil-water surface.[35,58,68,69] Among the different polysaccharides available, in this thesis only chitosan, alginate and xanthan gum are going to be used, as they present good characteristics for each of the objectives.

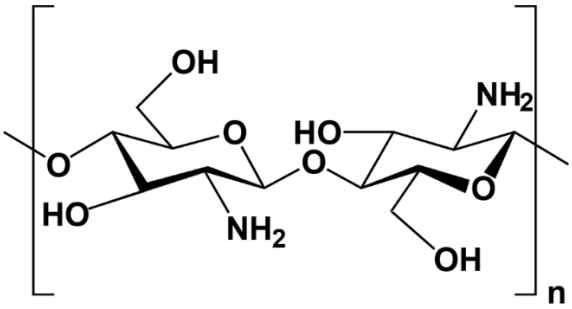

Scheme 7. Structure of chitosan

Chitosan is one of the most abundant polymers in nature. It is obtained by deacetilation of chitin, present in the exoskeleton of crustaceans and cell walls of fungi. It is a linear polysaccharide composed of randomly distributed β-(1→4)-linked D-glucosamine (deacetylated unit) and N-acetyl-D-glucosamine (acetylated unit), which makes it one of the richest biopolymer in amino groups (Scheme 7). To be considered chitosan, the deacetylation degree needs to be between 60 and 100%. Chitosan has a positive charge at physiological pH, as the pK_a value of its amino groups is 6.5. The presence of amino groups confers it mucoadhesive properties and easy functionalization with molecules such as antibiodies, saccharides or polyethylene glycol.[70,71] Besides, it is biocompatible and its degradation products are not toxic.[72] Chitosan films and coatings have a homogeneous matrix, stable structure and good water barrier.[73] Its positive charge is also expected to interact with cell membranes and bacterial membranes, that are mainly negatively charged due to the presence of phospholipids.[74,75]

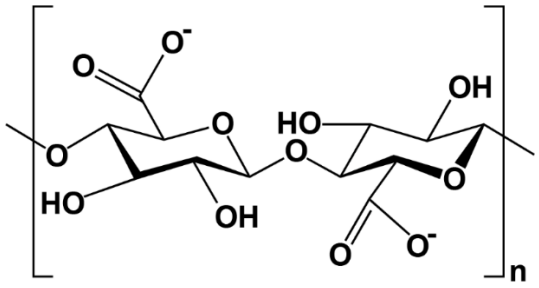

Scheme 8. Structure of alginic acid

Sodium alginate is one of the salts of alginic acid. Alginic acid is a polysaccharide present in the cell walls of brown algae. It is a linear copolymer with homopolymeric blocks of (1→4)-linked β-D-mannuronate (M) and α-L-guluronate (G) residues, respectively, covalently linked together in different sequences or blocks (Scheme 8). The presence of these carboxyl groups confers alginic acid a negative charge which enables an easy interaction with biomolecules of interests as well as with other positively charged polymers, such as the already mentioned chitosan. Sodium alginate is biocompatible, nonimmunogenic, has low toxicity and low cost.[76]

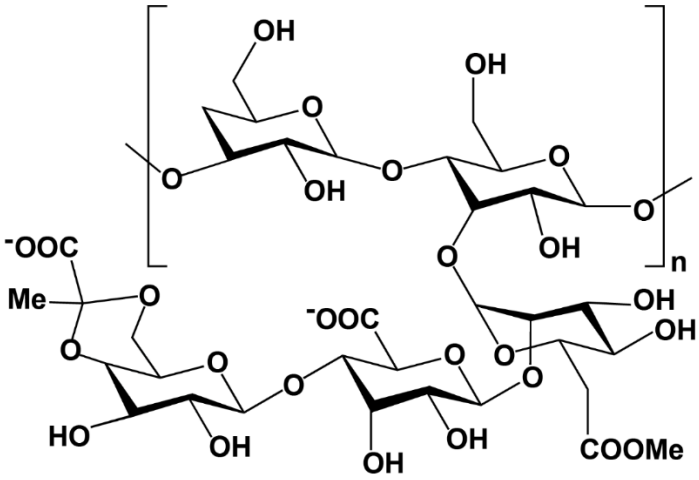

Scheme 9. Structure of xanthan gum

Xanthan gum is polysaccharide that consists on a β1-4-D-glucose backbone. Alternate glucose units have a sugar side chain made of two mannose residues separated by a glucuronic acid (Scheme 9). The internal mannose can be acetylated and the external one may carry a pyruvate residue. It is produced from simple sugars using fermentation process in bacteria such as *Xantomonas campestris.* As alginic acid, it has a negative change and it is nontoxic. In fact, it is widely used in the food industry as a texture modifier and thickener.[77]

Polysaccharide offer great advantages for the coating of both nanoemulsions or other types of nanoparticles. They are biocompatible, soluble and can be easily modified which can increase their applicability in nanomedicine. Besides, they have good biocompatibility and biodegradability. It has been demonstrated that polysaccharide coated nanocapsules have higher circulation life time in blood stream.[78]

However, one of the main drawbacks of polysaccharides is their high variability due to their natural origin. This can be overcome by chemical modification or futher characterization to completely understand the properties of this polymers. Despite dis variability, the high versatility of this polymers makes the one of the most common biomaterials for the preparation of nanoparticles for drug delivery. Further research need to be conducted in order to understand the mechanism of interaction with cells or how they affect drug absorption and metabolism.[79]

The use of different polysaccharides in nanoemulsion stabilization offers the possibility of modify nanocapsule surface properties. For example, chitosan is

expected to interact more efficiently with cell membranes due to its positive surface while alginate may stabilize the emulsion more efficiently in the presence of negative ions in the media. Xanthan has proven to be the most effective and most used one in the stabilization of emulsions, so it may be more suitable for the stabilization of nanoemulsion with stability issues. Having different options as surface modifiers will allow the possibility to adequate it to the final application of the system or to improve its stability.

5. Objectives

The general objective of this thesis is the synthesis of nanocapsules to be used as encapsulating agents. Based on a nanoemulsion core synthesized by spontaneous emulsification, different types of polysaccharides will be used for the stabilization and modification of the surface properties. Depending on the final application, some modifications will be done to the polymer after nanocapsule synthesis.

These developed nanocapsules will be used for the encapsulation of both small molecules, proteins and nanoparticles. These molecules will be encapsulated either in the nanocapsule core, entrapped in the polymer coating or covalently linked to it depending on the nature of the nature of the agent to be encapsulated to study the versatility of these systems.

The developed nanocapsules will be applied to solve different industrial or biomedical problems, to prove the versatility of the developed nanocapsule, that can be tailored depending on the final application.

Finally, the nanoemulsion core will be modified in an attempt to reduce the use of synthetic surfactants.

The objectives of the different chapters are:

- **In Chapter 2** nanocapsules will be developed for the treatment of infectious diseases: Multidrug-resistant *Mycobacterium tuberculosis* (MDR-TB) and Meticillin-resistant *Staphylococcus aureus* (MRSA). The main objective will be the encapsulation of two different antibiotics for the treatment of MDR-TB and MRSA: bedaquiline and daptomycin, respectively in chitosan-coated nanocapsules. The different hydrophobicity of this two small molecules will give the opportunity to evaluate the versatility of the nanocarrier in encapsulating molecules with different hydrophilicity. Antibacterial activity will be also studied both *in vitro* and *in vivo*, as well as biodistribution in a murine model to evaluate the efficacy of the developed system.
- **In Chapter 3** nanocapsules will be sued to encapsulate and repurpose disulfiram. In this case, the nanoemulsion will be coated using both chitosan and xanthan, in order to evaluate how charge and structure of the polymer affects the final application. The developed nanocapsules will be applied for the treatment of MRSA and pancreatic cancer, as disulfiram probed to be effective for the treatment of both illnesses. This will allow the evaluation and comparison of the effectiveness of the same type of nanocapsules against two different targets.
- **In Chapter 4** nanocapsules will be used for the encapsulation of bigger molecules such as the protein Cloroperoxidase (CPO) and magnetic

nanoparticles (MNPs). This will allow to probe that nanocapsules are really versatile and not only capable of encapsulating small molecules. These capsules will be applied in the industrial catalysis of a model reaction to evaluate its suitability as enzyme immobilizers.

- **In Chapter 5** nanocapsules will be used for the encapsulation of bigger hydrophobic nanoparticles made of holmium vanadate for their use as contrast agents. The suitability of the developed nanocapsules will be evaluated for the encapsulation of bigger nanoparticles and their use as contrast agents for cancer detection. Biodistribution of these nanocapsules as well as toxicity and relaxibity will be evaluated.
- **Chapter 6** will explore the future perspectives of these nanocapsules. In all of the previous chapters only the nature of the encapsulated agent or the nanocapsule surface will be modified. In this case, the nanoemulsion composition will be modified to explore the use of different oils and surfactants to evaluate stability of the empty system for their application in future works. Synthesis optimization as well stability and toxicity of these nanocapsules will be tested and compared with the ones formed by synthetic surfactants.

6. References

(1) Council, N. S. and T. *Natl. Nanotechnol. Initiat. Overv. Strateg. Plan* **2011**, 89–187.

(2) Bawa, R. *Curr. Drug Deliv.* **2012**, *8* (3), 227–234.

(3) Commission, E. **2006**, No. March.

(4) Feynman, R. P. *Engineering and Science*. 1960, pp 22–36.

(5) Hulla, J. E.; Sahu, S. C.; Hayes, A. W. *Hum. Exp. Toxicol.* **2015**, *34* (12), 1318–1321.

(6) Binnig, G.; Rohrer, H. *IBM J. Res. Dev.* **1986**, *30* (4), 355–369.

(7) Kroto, H. W.; Heath, J. R.; O'Brien, S. C.; Curl, R. F.; Smalley, R. E. *Nature* **1985**, *318* (6042), 162–163.

(8) Iijima, M.; Shinozaki, M.; Hatakeyama, T.; Takahashi, M.; Hatakeyama, H. *Carbohydr. Polym.* **2007**, *68* (4), 701–707.

(9) Barber, D. J.; Freestione, I. C. *Archaeometry* **1990**, *32* (1), 33–45.

(10) Arora, A. *Adv. Eng. Mater.* **2004**, *6* (4), 244–247.

(11) Lubick, N. *Environ. Sci. Technol.* **2008**, *42* (11), 3910.

(12) Khan, I.; Saeed, K.; Khan, I. *Arab. J. Chem.* **2019**, *12* (7), 908–931.

(13) Laghari, M.; Darwis, Y.; Memon, A. H.; Khan, A. A.; Abdulbaqi, I. M. T.; Assi, R. A. *Trop. J. Pharm. Res.* **2016**, *15* (1), 201–211.

(14) Payal; Pandey, P. *Recent Pat. Nanotechnol.* **2021**, *15*.

(15) Pathakoti, K.; Manubolu, M.; Hwang, H. M. *Nanotechnology applications for environmental industry*; Elsevier Inc., 2018.

(16) Li, Y.; Wang, Z.; Sun, L.; Liu, L.; Xu, C.; Kuang, H. *TrAC - Trends Anal. Chem.* **2019**, *113*, 74–83.

(17) Martín-Gracia, B.; Martín-Barreiro, A.; Cuestas-Ayllón, C.; Grazú, V.; Line, A.; Llorente, A.; De La Fuente, J. M.; Moros, M. *J. Mater. Chem. B* **2020**, *8* (31), 6710–6738.

(18) Singh, T.; Shukla, S.; Kumar, P.; Wahla, V.; Bajpai, V. K. *Front. Microbiol.* **2017**, *8* (AUG), 1–7.

(19) Alfranca, G.; Artiga, Á.; Stepien, G.; Moros, M.; Mitchell, S. G.; de la Fuente, J. M. *Nanomedicine (Lond.)* **2016**, *11* (22), 2903–2916.

(20) Beola, L.; Asín, L.; Roma-Rodrigues, C.; Fernandez-Afonso, Y.; Fratila, R. M.; Serantes, D.; Ruta, S.; Chantrell, R. W.; Fernandes, A. R.; Baptista, P. V.; de la Fuente, J. M.; Grazu, V.; Gutierrez, L. *ACS Appl. Mater. Interfaces*

2020, *12* (39), 43474–43487.

(21) Pilkington, E. H.; Suys, E. J. A.; Trevaskis, N. L.; Wheatley, A. K.; Zukancic, D.; Algarni, A.; Al-Wassiti, H.; Davis, T. P.; Pouton, C. W.; Kent, S. J.; Truong, N. P. *Acta Biomater.* **2021**, *131*, 16–40.

(22) Wei, Q. Y.; Xu, Y. M.; Lau, A. T. Y. *Cancers (Basel).* **2020**, *12* (10), 1–37.

(23) Patel, S.; Bhirde, A. A.; Rusling, J. F.; Chen, X.; Gutkind, S. J.; Patel, V. *Pharmaceutics* **2011**, *3* (1), 34–52.

(24) Drulis-Kawa, Z.; Dorotkiewicz-Jach, A. *Int. J. Pharm.* **2010**, *387* (1–2), 187–198.

(25) Cacciatore, I.; Ciulla, M.; Fornasari, E.; Marinelli, L.; Di Stefano, A. *Expert Opin. Drug Deliv.* **2016**, *13* (8), 1121–1131.

(26) Huo, Q.; Zhu, J.; Niu, Y.; Shi, H.; Gong, Y.; Li, Y.; Song, H.; Liu, Y. *Int. J. Nanomedicine* **2017**, *12*, 8631–8647.

(27) Bonferoni, M. C.; Sandri, G.; Dellera, E.; Rossi, S.; Ferrari, F.; Mori, M.; Caramella, C. *Eur. J. Pharm. Biopharm.* **2014**, *87* (1), 101–106.

(28) Kolhe, P.; Misra, E.; Kannan, R. M.; Kannan, S.; Lieh-lai, M. **2003**, *259*, 143–160.

(29) Tadros, T.; Izquierdo, P.; Esquena, J.; Solans, C. *Adv. Colloid Interface Sci.* **2004**, *108–109*, 303–318.

(30) Wahid, H.; Ahmad, S.; Nor, M. A. M.; Rashid, M. A. *Fundamentals and applications of controlled release drug delivery*; 2017; Vol. 51.

(31) McClements, D. J. *Soft Matter* **2012**, *8* (6), 1719–1729.

(32) Laxton, A. W.; Stone, S.; Lozano, A. M. *Stereotact. Funct. Neurosurg.* **2014**, *92* (5), 269–281.

(33) Schulman, J. H.; Montagne, J. B. *Ann. N. Y. Acad. Sci.* **1961**, *92* (2), 366–371.

(34) Calvo, P.; Vila-Jato, J. L.; Alonso, M. J. *J. Pharm. Sci.* **1996**, *85* (5), 530–536.

(35) McClements, D. J.; Rao, J. *Crit. Rev. Food Sci. Nutr.* **2011**, *51* (4), 285–330.

(36) Kralova, I.; Sjöblom, J. *J. Dispers. Sci. Technol.* **2009**, *30* (9), 1363–1383.

(37) McClements, D. J.; Decker, E. A.; Weiss, J. *J. Food Sci.* **2007**, *72* (8), 109–124.

(38) Solè, I.; Maestro, A.; González, C.; Solans, C.; Gutiérrez, J. M. *Langmuir* **2006**, *22* (20), 8326–8332.

(39) Trotta, M.; Cavalli, R.; Ugazio, E.; Gasco, M. R. *Int. J. Pharm.* **1996**, *143* (1), 67–73.

(40) Hoeller, S.; Sperger, A.; Valenta, C. *Int. J. Pharm.* **2009**, *370* (1–2), 181–186.

(41) Kale, S.; Deore, S. *Syst. Rev. Pharm.* **2017**, *8* (1), 39–47.

(42) Joos, A.; Weiss, J.; McClements, D. J. *Food Biophys.* **2015**, *10* (1), 83–93.

(43) Choi, S. J.; McClements, D. J. *Food Sci. Biotechnol.* **2020**, *29* (2), 149–168.

(44) McClements, D. J. *Adv. Colloid Interface Sci.* **2018**, *253*, 1–22.

(45) Anton, N.; Benoit, J. P.; Saulnier, P. *J. Control. Release* **2008**, *128* (3), 185–199.

(46) Leong, T. S. H.; Wooster, T. J.; Kentish, S. E.; Ashokkumar, M. *Ultrason. Sonochem.* **2009**, *16* (6), 721–727.

(47) Gutiérrez, J. M.; González, C.; Maestro, A.; Solè, I.; Pey, C. M.; Nolla, J. *Curr. Opin. Colloid Interface Sci.* **2008**, *13* (4), 245–251.

(48) Bouchemal, K.; Briançon, S.; Perrier, E.; Fessi, H. *Int. J. Pharm.* **2004**, *280*, 241–251.

(49) De Matteis, L.; Alleva, M.; Serrano-Sevilla, I.; García-Embid, S.; Stepien, G.; Moros, M.; De La Fuente, J. M. *Mar. Drugs* **2016**, *14* (10), 175.

(50) Lee, L.; Hancocks, R.; Noble, I.; Norton, I. T. *J. Food Eng.* **2014**, *131*, 33–37.

(51) Jafari, S. M.; Paximada, P.; Mandala, I.; Assadpour, E.; Mehrnia, M. A. *Encapsulation by nanoemulsions*; Elsevier Inc., 2017.

(52) Tan, C.; McClements, D. J. *Foods* **2021**, *10* (4).

(53) Anton, N.; Vandamme, T. F. *Int. J. Pharm.* **2009**, *377* (1–2), 142–147.

(54) Sonneville-Aubrun, O.; Babayan, D.; Bordeaux, D.; Lindner, P.; Rata, G.; Cabane, B. *Phys. Chem. Chem. Phys.* **2009**, *11* (1), 101–110.

(55) Carteau, D.; Bassani, D.; Pianet, I. *Comptes Rendus Chim.* **2008**, *11* (4–5), 493–498.

(56) Solans, C.; Solé, I. *Curr. Opin. Colloid Interface Sci.* **2012**, *17* (5), 246–254.

(57) Solans, C.; Morales, D.; Homs, M. *Curr. Opin. Colloid Interface Sci.* **2016**, *22*, 88–93.

(58) McClements, D. J. *J. Food Sci.* **2010**, *75* (1), 30–42.

(59) Solans, C.; Izquierdo, P.; Nolla, J.; Azemar, N.; Garcia-Celma, M. J. *Curr. Opin. Colloid Interface Sci.* **2005**, *10*, 102–110.

(60) McClements, D. J.; Gumus, C. E. *Adv. Colloid Interface Sci.* **2016**, *234*, 3–26.

(61) Weiss, J.; Decker, E. A.; McClements, D. J.; Kristbergsson, K.; Helgason, T.; Awad, T. *Food Biophys.* **2008**, *3* (2), 146–154.

(62) Littoz, F.; McClements, D. J. *Food Hydrocoll.* **2008**, *22* (7), 1203–1211.

(63) Iwanaga, D.; Gray, D.; Decker, E. A.; Weiss, J.; McClements, D. J. *J. Agric. Food Chem.* **2008**, *56* (6), 2240–2245.

(64) Grigoriev, D. O.; Miller, R. *Curr. Opin. Colloid Interface Sci.* **2009**, *14* (1), 48–59.

(65) Guzey, D.; McClements, D. J. *Adv. Colloid Interface Sci.* **2006**, *128–130* (2006), 227–248.

(66) Mora-huertas, C. E.; Fessi, H.; Elaissari, A. *Int. J. Pharm.* **2010**, *385*, 113–142.

(67) Prego, C.; Fabre, M.; Torres, D.; Alonso, M. J. *Pharm. Res.* **2006**, *23* (3), 549–556.

(68) Xu, X.; Luo, L.; Liu, C.; McClements, D. J. *Food Hydrocoll.* **2017**, *64*, 112–122.

(69) Dickinson, E. *J. Sci. Food Agric.* **2013**, *93* (4), 710–721.

(70) Tavares, I. S.; Caroni, A. L. P. F.; Neto, A. A. D.; Pereira, M. R.; Fonseca, J. L. C. *Colloids Surfaces B Biointerfaces* **2012**, *90* (1), 254–258.

(71) Mazzarino, L.; Coche-Guérente, L.; Labbé, P.; Lemos-Senna, E.; Borsali, R. *J. Biomed. Nanotechnol.* **2014**, *10* (5), 787–794.

(72) Shelma, R.; Sharma, C. P. *Colloids Surfaces B Biointerfaces* **2011**, *84* (2), 561–570.

(73) Chaudhary, S.; Kumar, S.; Kumar, V.; Sharma, R. *Int. J. Biol. Macromol.* **2020**, *152*, 154–170.

(74) Liu, H.; Du, Y.; Wang, X.; Sun, L. *Int. J. Food Microbiol.* **2004**, *95* (2), 147–155.

(75) Krajewska, B.; Wydro, P.; Jańczyk, A. *Biomacromolecules* **2011**, *12* (11), 4144–4152.

(76) Santana, B. P.; Nedel, F.; Piva, E.; De Carvalho, R. V.; Demarco, F. F.; Carreño, N. L. V. *Biomed Res. Int.* **2013**, *2013*.

(77) Baumgartner, S.; Pavli, M.; Kristl, J. *Eur. J. Pharm. Biopharm.* **2008**, *69* (2), 698–707.

(78) Seidi, F.; Jenjob, R.; Phakkeeree, T.; Crespy, D. *J. Control. Release* **2018**, *284* (May), 188–212.

(79) Zhang, X.; Tu, R.; Peng, J.; Hou, C.; Wang, Z. *Chem. Eng. J.* **2021**, *404* (May 2020), 126553.

Chapter 2

Encapsulation of antibiotics for the treatment of resistant pathogens

1. Introduction

The discovery of antibiotics has saved thousands of lives but misuse has also lead to the appearance of multidrug resistant (MDR) pathogens worldwide.[1] Although acquisition of antimicrobial resistance is a natural process that occurs through different mechanisms such as gene transfer and gene mutations due to exposure to the drugs, it is worsen by misuse and inadequate surveillance.[2] It is estimated that around 700.000 people die each year due to the appearance of multidrug resistant pathogens and that this value can increase up to 20 million by 2050, although estimation is this field is difficult.[3] Despite the fact that lots of efforts were made to stop the lack of effective therapies against multidrug resistant bacteria, only 13 new antibacterial agents have been approved by US Food and Drug Administration (FDA) between 1999 and 2011[4] as the actual unfavorable economics of antibiotic development had a chilling effect on industrial discovery programs[5]. Due to the enormous human and economic losses that this increase in the appearance of MDR pathogens is causing, World Health Organization (WHO) endorsed a global action plan to tackle antimicrobial

resistance.[6] Besides, in 2017, World Health Organization released a priority list ranking the 13 bacteria or bacterial families that urgently need new or more effective treatment.[7] These include: *Mycobacterium tuberculosis* (MDR-TB), *carbapenem-resistant Acinetobacter baumannii, Pseudomonas aeruginosa* and *Enterobacteriaceae;* 3rd gen. cephalosporin-resistant *Enterobacteriaceae* and *Neisseria gonorrhoeae*; vancomycin-resistant *Enterococcus faecium* and *Staphylococcus aureus*; c*larithromycin-resistant Helicobacter pylori*; methicillin-resistant *Stapylococcus aureus*; and fluoroquinole-resistant *Salmonella and Campylobacter* species.

Amongst them, *Mycobacterium tuberculosis* (TB) is considered the global priority for five different reasons. Firstly, TB is the number one global infectious disease killer, causing 1.8 million deaths per year, from which 250000 deaths are caused by multidrug-resistant TB (MDR-TB). Secondly, management of MDR-TB is difficult, as it needs complex and prolonged multidrug treatment, and only 52% of patients are successfully treated globally. Besides, in about 50% of MDR-TB patients worldwide, treatment regimens are already compromised by second-line drug resistance and treatment of extensively drug-resistant disease (XDR-TB) is successful in only one in three patients at best. Moreover, patients with M/XDR-TB face agonizing, prolonged suffering and often permanent disability while on treatment, compounded by devastating economic hardship, stigma and discrimination. Lastly, only two new antibiotics have reached the market for the hospital treatment of MDR-TB in the last 70 years due to low investment in scientific research: bedaquiline and delamanid.[7]

From 2014 to 2015, the rate of decline in TB incidence remained at only 1.5% while it was expected to be around 4-5% annual by 2020 according to the

milestone set by WHO in the End TB Strategy.[7] Achievement of this milestone requires the implementation of a mix of biomedical, public health and socioeconomic interventions, as well as major breakthroughs in research and innovation. One of the fundamental strategies proposed by WHO is the development of new tools such as a new vaccine, point-of care tests and new anti-TB agents. As the development of new drugs is expensive and requires long periods of time, more attention is paid to the development of new systems to provide improved efficiency and safety of the existing treatments.[7]

Among of all the above mentioned bacteria, MRSA is another priority since it represents one of the major causes of morbidity and mortality worldwide. MRSA is a frequent cause of hospital-acquired infections, especially in patients with risk factor or underlying conditions with associated long hospital stay and high costs.[7] It is one of the principal resistant pathogens which causes difficult skin infections and hospital acquired infections, especially bloodstream infections and ventilator-associated pneumonia.[8] Although it has been observed a decrease in the incidence of MRSA, a recent study found out that there has not been any improvement in the 30-day mortality rates between 200 and 2015, probably due to a lack of effective treatments.[9] For all these reasons, meticillin-resistant S. aureus (MRSA) was selected as another target for the development of improved therapies.

As the development of new drugs is a long and expensive process, the current research interest lays on the improvement of the efficiency of conventional antibacterial drugs.[10] In this aspect, nanomaterials can play an important role in enhancing the effectiveness of the existent treatment because of several reasons. Due to the small size of these novel drug delivery systems, they are in

the same order of magnitude as cellular organelles, which allows direct interaction of the nanomaterial with cells.[11] Besides, their high surface to volume ratio increases interaction with target cells and the possibility of modifying both structurally and functionally the nanomaterials, allows to control their biodistribution *in vivo*. They also allow drug protection from degradation before reaching the target and they can improve biocompatibility of hydrophobic drugs. Nanovehicles offer selective transport to the site of infection and tunable release, allowing for decreasing frequency of drug administration.[12]

In the case of drug-resistant infections, the development of effective and safe nanotherapy methods has particular interest, as high and frequent doses are usually given. Local higher concentration of the antibiotic at the site of infection can be achieved by functionalizing the nanocarrier with molecules that directs it to the pathogen or infected cells, enabling lower doses in circulation, which would reduce the adverse effects. This increase in the local concentration of the antibiotic will turn into an increase in the therapeutic index which may allow the use of antibiotics that could not be used before due to the high doses needed.[4,13–15]

Amongst the different types of nanocarriers developed in the last decades, in this work we used nanocapsules for the delivery of different antibiotics. As mentioned in Chapter 1 (introduction), nanocapsules are a type of nanovehicle that consist on a polymeric protective shell that surrounds a hydrophobic oily core. In this case, the oily core was synthesized by a spontaneous emulsification process and then coated with polysaccharides to improve the low stability of the emulsion and modify the surface properties.

This type of nanocarrier, thanks to its structure, offers a great versatility in terms of the type of molecules that can be encapsulated. Hydrophobic molecules can be encapsulated into the oily core, while hydrophilic drugs can be entrapped into the polymeric shell. This offers great opportunities for the application of the nanocapsules in the treatment of different diseases.

We selected two different antibiotics of interest and of different nature to be loaded into nanocapsules as treatment for MRSA or MDR-TB: daptomycin and bedaquiline. Daptomycin (DP) is one of the three membrane-active antimicrobial peptides approved by the U.S. Food and Drug Administration (FDA) (Huang_2020). DP is currently used for the management of MRSA infections as it has activity against a broad range of gram-positive bacteria, including pathogens resistant to methicillin, vancomycin, and other currently available agents.[16] It was the first available agent from a new class of antibiotics, the cyclic lipopeptides, and its structure consists of a 13-member aminoacid cyclic lipopeptide with a decanoyl side-chain. This side chain is believed to be inserted into the bacterial cell membrane in a calcium-dependent manner, which causes an efflux of potassium from the bacterial cell. This will turn into cell death as a loss of potassium disrupts macromolecular synthesis in the cell.[17,18]

Due to the hydrophilic nature of daptomycin, the hypothesis is that encapsulation of the drug into the nanocapsules is achieved by insertion of the decanoyl side-chain into the nanoemulsion core, while the rest of the molecule would be protected by the external chitosan coating. Negative charge of daptomycin at pH 7 could favor its interaction with positively charged chitosan coating layer. Encapsulation of daptomycin into this type of nanocapsules is expected to increase the effectiveness of the antibiotic by increasing its local concentration,

and therefore contributing to reduce the required doses. This will greatly reduce the chances of appearance of bacterial resistances and adverse effects, as treatments with high doses of DP result in myopathy.[18]

The second antibiotic that was chosen is bedaquiline (BQ). Bedaquiline is a new drug approved by the FDA in 2012 and the EMA in 2013 for the treatment of MDR-TB.[19] BQ is a diarylquinoline that has been associated with accelerated sputum-culture conversion, which means that sputum from patients treated with bedaquiline is free from the bacteria earlier than for the ones treated with other regimen.[20] Bedaquiline has a unique and specific antimycobacterial activity as it inhibits specifically the proton pump of mycobacterial ATP synthase, which is a critical enzyme in the ATP synthesis of M. tuberculosis. However, there are several concerns about its safety, since it can cause arrhythmias and about 11.4% of patients taking bedaquiline died during clinical trials compared with 2.5% of those taking placebos. For this reason, its use is allowed only in patients who do not have other treatment options.[21]

Encapsulation of bedaquiline into the core of the nanocapsule will be highly favored by the hydrophobic nature of the drug. Besides, the vehiculation of bedaquiline will increase the effectiveness of the antibiotic by increase of the local concentration, and therefore contribute to reduce the required doses. This will mean a reduction of adverse effects and therefore an important improvement of the applicability of the drug to a wider segment of patients.

The results obtained in this chapter are framed within the European project Nanotherapeutics for antibiotic resistant emerging bacterial pathogen (NAREB), whose main objective was the development of different nanoformulations of

antibacterial therapeutics in order to improve the efficacy of treatments for multi-drug resistant (MDR) tuberculosis (TB) and MRSA infections in European MDR patients.

2. Results and discussion

2.1. Synthesis and optimization of bedaquiline-loaded nanocapsules

The method selected for the synthesis of bedaquiline-loaded nanocapsules has been adapted from a previous work regarding the synthesis of empty nanocapsules[22], that are formed by a nanoemulsion core coated by a shell made of the natural polymer chitosan. The structure of the developed system, thanks to its nature is capable of encapsulate both hydrophobic and hydrophilic drugs in the core or the polymer structure, respectively. Thanks to the lipophilicity of the nanocapsule core and due to the hydrophobicity of bedaquiline, it seemed highly suitable for the encapsulation of this drug.

The synthesis method of these nanocapsules is based on a spontaneous nanoemulsification method followed by the coating with the polysaccharide chitosan by ionotropic gelation. Components and quantities ratios involved in the construction of the nanocapsules were maintained the same as for the synthesis of the empty nanocapsules (See Table 1).

Table 1. mg and ratios of the different components of the nanocapsules synthesis

	Tween 20	**Span 85®**	**Oleic acid**	**Chitosan**
mg of molecule	13.6	8.6	40	2.5
mg molecule/ mg total	0.12	0.076	0.35	0.022

An organic phase composed of oleic acid and the lipophilic surfactant Span 85 is added to an aqueous phase that contains the hydrophilic surfactant Tween 20. In the case of bedaquiline encapsulation, different quantities of the drug (2.5, 5, 10 and 25 mg) were mixed with the organic phase, because of its hydrophobic nature. The addition of increasing quantities of bedaquiline into the mixture for nanoemulsion formation, allowed to evaluate its loading capacity, which is the maximum amount of drug that the emulsion can encapsulate.[23] This is an important value to determine since when we reach this capacity, encapsulation efficiency will decrease. As a consequence, drug will be wasted, increasing the cost of the method without any improvement in the yield.

After the dropwise addition of the organic phase into the Tween 20 water solution, the bedaquiline-loaded nanoemulsion is spontaneously formed. The spontaneous emulsification occurs thanks to the rapid diffusion of the organic solvent into the water phase which causes an increase in oil-water interfacial area, interfacial turbulence and spontaneous formation of droplets. An increase in the turbidity of the solution indicates that the emulsion is forming.[24] After 15 minutes of stirring the equilibrium of the system is reached[25] and the chitosan solution is added for the coating and stabilization of the emulsion. As stated in Chapter 1, nanoemulsions are not thermodynamically stable systems and need further modifications to improve long term-stability. This chitosan coating increases the stability of the nanoemulsion towards changes in the environment, improves interaction with cells and allows an easy functionalization of nanocapsule surface.

The solution was stirred for another 15 minutes to obtain a homogeneous distribution of the polymer chains around the nanoemulsion surface and then, the ionotropic gelation was carried out. This time was stabilized in a previous thesis by Dra. Inés Serrano Sevilla and was determined as the optimum time. This process consists on the ionic crosslinking of the positively charged chitosan amine groups with a negative divalent ion, in this case sulfate ion, after addition to a sodium sulfate solution. As demonstrated by several authors in literature, sodium sulfate is able to crosslink chitosan chains and therefore produce chitosan microspheres.[26,27] Besides, it has been demonstrated by the same authors, that chitosan solubility is decreased in the presence of sodium salts, which will therefore contribute to the compactness of the polymer coating. As demonstrated in a previous study from De Matteis *et al (2016)*[22], developed during the PhD project of Dr. Inés Serrano from our research group, coacervation process was of great importance for the formation of the final capsule. When this step was skipped, nanocapsule nuclei were not correctly coated as the polymer was not able to settle around the nanocapsules forming a stable coating. This was demonstrated by the fact that although chitosan has a positive charge, the obtained nanocapsules presented a negative zeta potential. Also the measurement of the amount of amino groups on the surface (only due to the presence of chitosan), further demonstrated the absence of the polymeric coating. Another experiment was also performed using a sonication treatment during the coacervation with sodium sulfate. However, no improvement was observed in comparison with the magnetic stirring so it was discarded as sonication is not easy to perform at large scale in the industry.

After the ionotropic gelation, we washed the developed nanocapsules with water by applying two ultracentrifugation steps. Excess reactants and non-encapsulated drug are eliminated from the final suspension of nanocapsules. A schematic representation of the proposed structure for bedaquiline loaded nanocapsules and their main components structure is shown in Scheme 1.

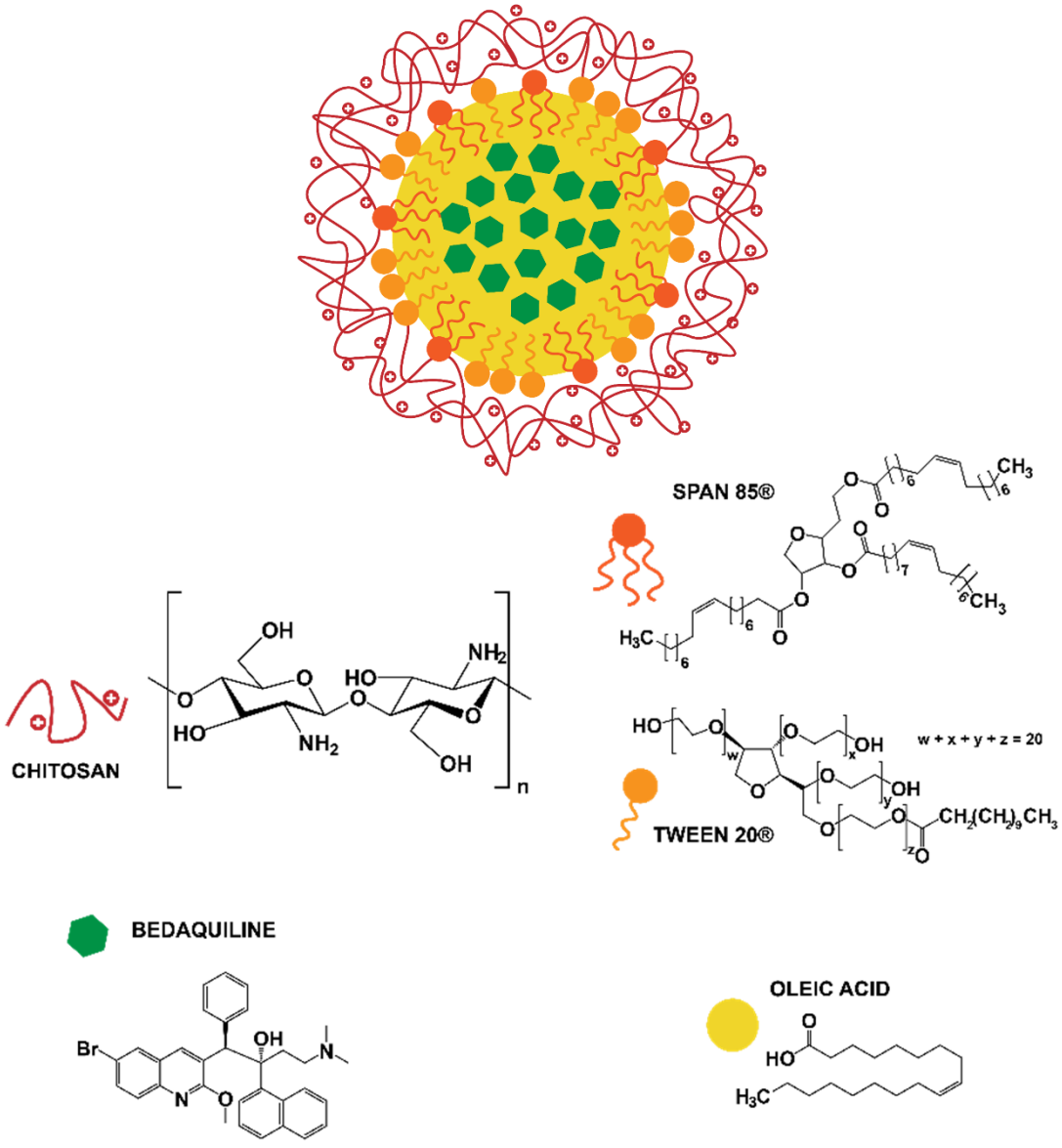

Scheme 1. Proposed structure for bedaquile-loaded nanocapsules and chemical strucure of its components

As this system is new for the development of bedaquiline-loaded nanocapsules, it is important to evaluate how well it works. To evaluate the suitability for the encapsulation of bedaquiline, the encapsulation efficiency and drug loading of bedaquiline into nanocapsules were evaluated. Encapsulation efficiency (EE%) is defined as the amount of drug encapsulated per amount of drug initially added; while the drug loading (DL%) is described as the milligrams of drug encapsulated per mg of nanocapsule obtained. These two parameters are important factors to take into account in the pharmatheutical industry as they are highly related to the economy of the process and the profitability of the developed system. For the determination of these two parameters, it was necessary to quantify the nanocapsule concentration as well as bedaquiline content. Nanocapsule concentration was calculated by freeze-drying of an aliquot of the suspension and subsequent quantification of the dry weight. This allowed the quantification of the total amount of nanomaterial, meaning nanocapsule and antibiotic.

To determine the amount of encapsulated antibiotic, we needed to develop a method for the extraction of the antibiotic, as direct measurement was not possible. Measuring the amount of bedaquiline encapsulated directly without extraction was impossible due to high dispersion of the nanocapsules in UV-vis spectrophotometry as well as measurement of the non-encapsulated bedaquiline in the supernatant of the synthesis. It was necessary to extract the antibiotic from the nanocapsules into a suitable solvent. In a first attempt, freeze dried nanocapsules were mixed with dichloromethane (DCM), which destroyed the nanocapsule structure and dissolved bedaquiline. UV-vis spectrometry was used for the quantification. Bedaquiline has a unique absorbance spectrum with four different peaks (Figure 1A)

A

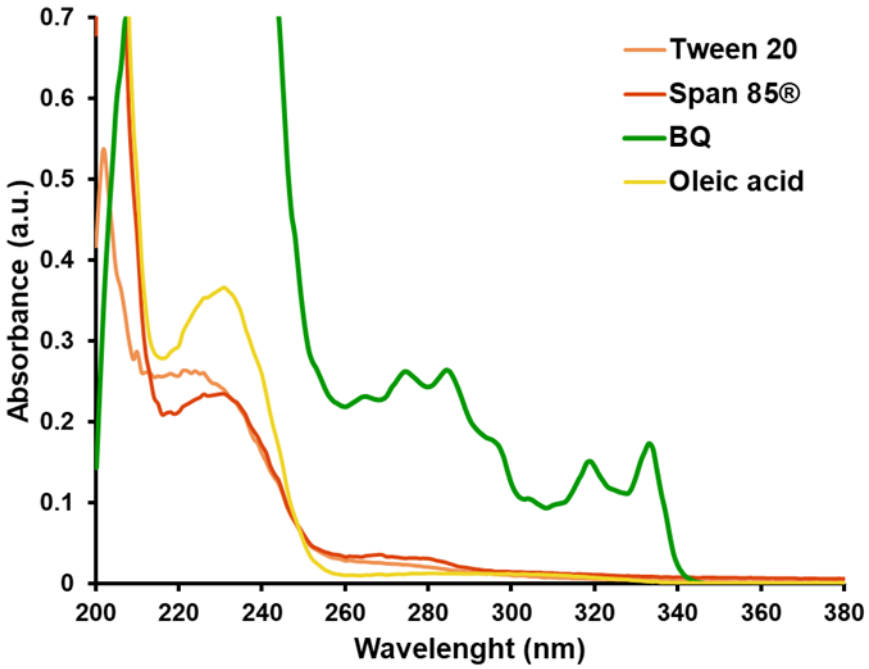

B

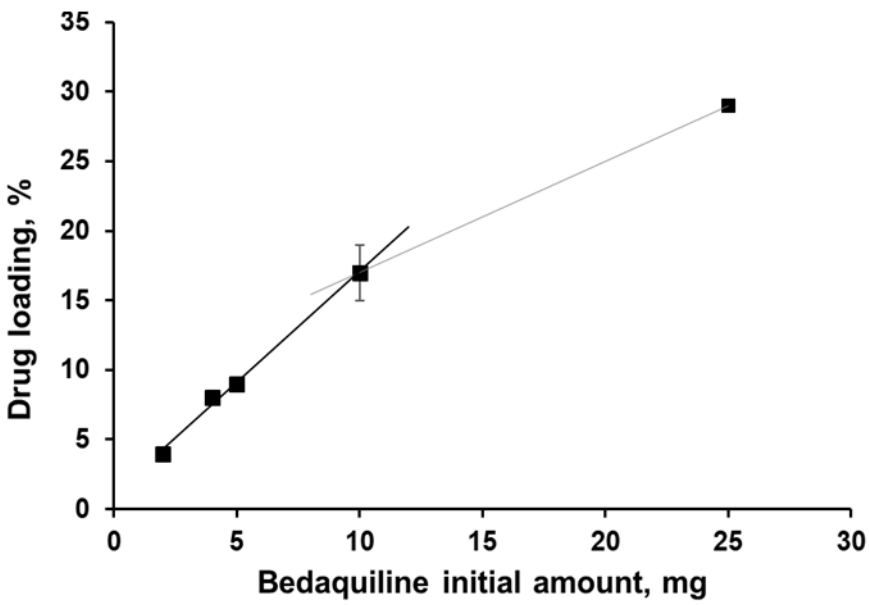

C

Bedaquiline initial amount, mg	Drug loading, %
2	4 ± 0
4	8 ± 0
5	9 ± 0
10	17 ± 2
25	29 ± 3

Figure 1. A) Absorbance spectra of BQ, tween 20, Span 85, Tween 20 and olic acid in methanol. B) Relationship between the bedaquiline initial amount and drug loading into nanocapsules. C)Table showing the DL% for each initial amount of BQ.

The absorption at 333 nm was used as it does not interfere with the absorbance peaks of the rest of the components of the nanocapsules (Tween 20, Span 85, and oleic acid), whose absorbance spectra show peaks at a wavelength below 280 nm, as shown in Figure 1A. To check the suitability of this method, an analysis using HPLC separation was also carried out, achieving the same results

To ease bedaquiline quantification and so nanocapsule characterization, the freeze drying step was eliminated, as it required at least 12 hours before bedaquiline concentration measurement. For this purpose, DCM was substituted by methanol that is miscible with water and can extract bedaquiline directly from the nanocapsule suspension. Nanocapsules were mixed with methanol and sonicated for 30 minutes to get the complete extraction of bedaquiline. First of all, the new method was compared with DCM extraction to confirm that the extraction was achieved. Quantification was performed by UV-vis spectroscopy as for DCM extraction, but with the appropriate calibration curve in methanol. The drug loading achieved is reported for the amount of bedaquiline initially added to the synthesis and it is shown in Figure 1B and C.

As it can be observed in Figure 1B, the increase in DL% is linear for bedaquiline nominal loadings below 10 mg. Above this value, linearity is lost. At 25 mg, a DL% of 28 ± 2 % is obtained. Therefore, we selected this quantity as the optimum one, as we obtained high DL% values without compromising EE%, which reached values of 70 ± 7 %. Upon addition of more bedaquiline, we would not be able to increase much more the DL% as we will reach the maximum loading capacity. This is evidenced by the fact that DL% is not linear with the initial amount of bedaquiline above 10 mg of added antibiotic which would mean that EE% would

decrease and the antibiotic would be wasted. Hereon, we will always refer to BQ-loaded nanocapsules as the ones with 25 mg initially added.

Up to our knowledge, these values are comparable to the ones achieved by other authors in the literature. For example, Soria-Carrera *et al.*[28] developed bedaquiline-loaded polypeptidic micelles coated with alginate reaching EE% values of 58.3 ± 10.0% and DL% of 19.2 ± 3.0%. De Matteis *et al.*[29] developed lipid nanocapsules achieving more than 90% EE, but with a much lower DL of 2.8 ± 0.15%. Poh *et al.*[30] developed D, L-lactide-co-glycolide nanoparticles loaded with Q203, bedaquiline and iron oxide superparamagnetic nanoparticles reaching 57% EE%. Finally, Ritsema *et al.* [31] developed nanoparticles via double emulsion technique loaded with bedaquiline, reaching EE% values between 95 and 99%, depending on the system, but with DL% of 8.6 to 9%. Comparing this results to the ones obtained in this study, EE% is comparable with other studies. However, DL% is higher than other ones found in literature, meaning that these nanocapsules are able to encapsulate bedaquiline with great capacity. This represents a great advantage for the final application, as the higher the DL%, the lower the amount of nanocapsules that have to be administered to the patient. This higher DL% means that the number of nanocapsules that need to be uptaken by cells is less to achieve the same BQ dose, which will translate into lower side effects due to nanocapsules components and better economy of the process.

2.2. Characterization of bedaquiline-loaded nanocapsules

According to the literature, surface charge, together with size, highly influence nanoparticle stability and interaction with biological membranes[32], so the nature of the surface and size of our nanoparticles are always important parameters to take into account. Besides, it allows to study if the capsule is correctly

synthesized, as the surface charge will depend on whether the capsule is coated or not. For this purpose, bedaquiline-loaded nanocapsules were characterized by Photo Correlation Spectroscopy (PCS) to determine hydrodynamic diameter, size distribution and ζ potential.

Nanocapsules are first measured in the storage media (water in this case) to determine size distribution and mean diameter in basal conditions. Results are shown in Figure 2.

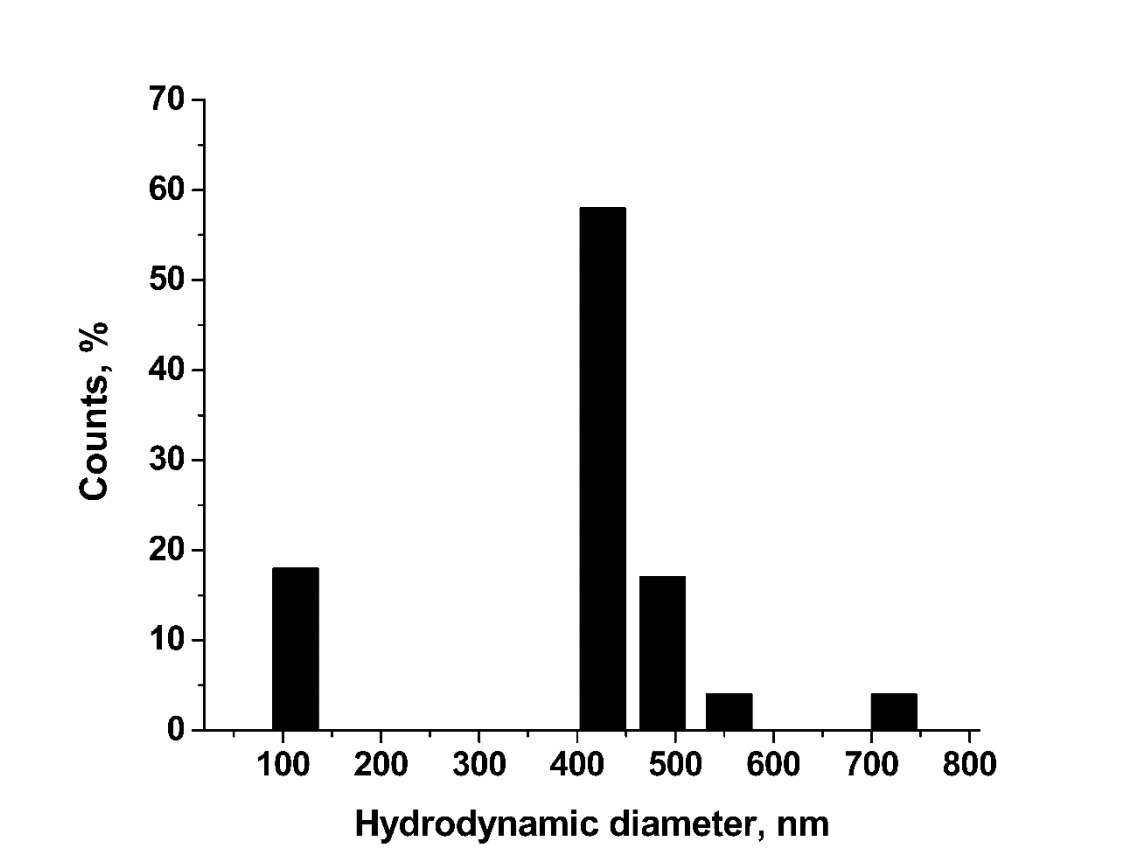

Figure 2. Size distribution measured by Dynamic Light Scattering (DLS) of bedaquiline-loaded nanocapsules in water

From the results reported in Figure 2, nanocapsules present a mean diameter for the DP-loaded nanocapsules of 400 nm in water. However, there are two

populations: A very small population with a mean diameter of 110 nm and a bigger one around 450 nm. As mentioned before, nanoparticle size is an important factor for cell uptake, especially in macrophages. Particle size can greatly affect uptake efficiency by influencing adhesion of the particles and interaction with cells.[33] Besides, larger nanoparticles have the advantage that they might coalesce within the cell membrane, making them easier to be phagocytized in a shorter time.[34] Couvreur *et al.*[35] found out that nanoparticles with size from 100 to 200 nm are usually internalized by receptor-mediate endocytosis, while larger nanoparticles were taken up by phagocytosis which can only be performed by phagocytic cells. Yu *et al.*[36] studied the internalization of PEGylated iron oxide micelles into macrophages *in vitro*. In their study they found that there was a great increase in nanoparticle uptake with diameters higher than 100 nm, being greatly reduced in the 30 and 40 nm nanoparticles of the study. On another study, Li *et al.*[37] studied the internalization of PLA nanoparticles, founding that internalization was higher for mean diameter higher than 200 nm. He *et al.*[38] in a 2010 study, also found out that uptake of polymeric nanoparticles in murine macrophages increased with increased diameter, while the tendency was opposite for non-phagocytic cells. This means that bedaquiline loaded nanoparticles, with a diameter of around 400 nm would be well internalized by macrophages, which in the case of TB infection are the target cells, as they are the infected tissue.

As well as the measurement of the particles characteristics in the storage media, it is important to determine its size in the media of administration, to know if these solutions are suitable for this purpose. Nanocapsules are sensitive to the presence of salts in the medium and they can tend to aggregate in physiological

media. This is because the presence of ions and proteins can produce a crosslinking between the capsules themselves due to their adsorption onto the surface (and even a salting out-like effect). So the presence of high amounts of salt will decrease the solubility of the nanocapsules.

Nanocapsules were put in contact with PBS and NaCl 0.9% solutions as these solutions are usually used for the intravenous administration. This via of administration was selected in the NAREB project, in which this study is framed. For this reason, the nanocapsules developed in this Chapter will be tested in this media. Results of the size distribution of nanocapsules in PBS and NaCl 0.9% in comparison with the distribution in water is shown in Figure 3A and B respectively.

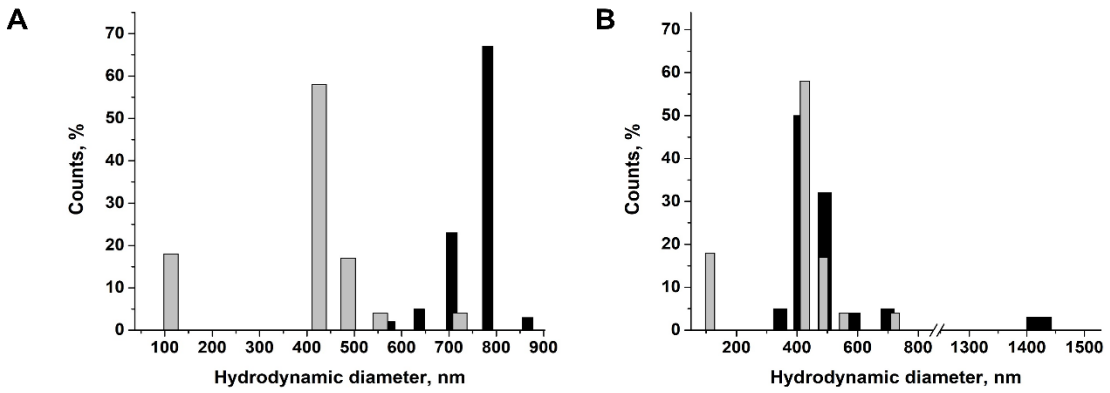

Figure 3. Size distribution measured by Dynamic Light Scattering (DLS) of bedaquiline-loaded nanocapsules in PBS (A) and NaCl 0.9% (B) (black bars) in comparison with water (grey bars)

From the results reported in Figure 3, we obtain a mean diameter for the BQ-loaded nanocapsules of 755 nm in PBS and 500 nm in NaCl 0.9%. Size distribution in PBS (Figure 3A, black bars), in comparison with water (grey bars),

has a bigger size, ranging from 550 nm up to 900 nm. For the NaCl 0.9%, size distribution is similar to the bigger population of the nanoparticles in water although there is also a small population of around 5% of nanocapsules, with a bigger size of around 1400 nm, probably corresponding to aggregates. From these results, it can be concluded that the physiological solution in which the nanocapsules are more stable is NaCl 0.9%, as the size distribution in this medium and in water is similar. Nanoparticles showed an increase in the diameter when they were dissolved in PBS, indicating aggregation of the nanocapsules. This effect can be explained by the presence of phosphate ions negatively charged in PBS at pH 7.4. The divalent negative ion is able to ionically interact with the chitosan positive amino groups in the nanocapsule surface. This leads to aggregation of nanocapsules because of the ionic crosslinking of the amino groups of different nanocapsules through the phosphate bridge.[39] NaCl 0.9% solution, was selected for administration of nanocapsules in the *in vivo* experiments.

In addition to the measurement of the hydrodynamic diameter, we studied the nanoparticle surface charge by measurement of its ζ potential. We obtained a value of potential of +25 mV for the BQ-loaded nanocapsules in KCl solution. This indicates that the particles are correctly coated by chitosan as the presence of positively charged amino groups from chitosan on the nanocapsule surface leads to a positive ζ potential. As explained before, in a previous study with empty nanoparticles it was demonstrated that a positive charge indicates that nanoemulsion is correctly coated in opposition with a negative charge that was observed for the naked emulsion.[22]

ζ potential is also an indicator of the systems stability. It has been reported as general condition, that an absolute value of ζ potential over 25-30 mV is enough for the nanoparticles to be considered as a stable colloidal suspension, as the repulsion between the charges of the nanoparticles is enough to avoid aggregation.[40] For this reason, we can consider our BQ-loaded nanocapsules as a stable colloidal system.

As well as size, charge also affect nanoparticle internalization in macrophages and other type of cells. For example, He *et al.* observed that macrophage uptake increased with surface charge, and for the same absolute value of ζ potential, positively charged nanoparticles showed higher internalization. However, charge was not determining for non-phagocytic cell lines.[38] Yu and coworkers observed similar results, and nanoparticles with higher absolute values of ζ potential presented higher macrophages uptake, although they determined that size was a stronger determinant factor for non-specific uptake by macrophages.[36] This would mean that the positively charged chitosan-coated nanoparticles are a promising system for internalization in macrophages in comparison with other coated nanoparticles.

2.3. Bedaquiline release study

Once colloidal stability was studied, the next step was to determine the stability of the loaded nanocapsules. This means the study of the release of the antibiotic, in this case bedaquiline, in different media of relevance. Studying the release profile of the antibiotic in different media used in the *in vitro* studies is important to correlate results of the antimicrobial activity with material characteristics. Besides, the study of the release profile in the administration media would allow to determine the best media for administration to preserve the properties of the

nanoparticles as best as possible. Also, studying the release profile in the storage media would allow to understand the best conditions for nanocapsules preservation.

The first step was the selection of the release media to study. In literature, most authors evaluate the release profile of the drugs in PBS pH 7.4 to evaluate the release kinetics for the system. For example, Ritsema *et. al.* studied the release profile of bedaquiline loaded mPEG-PLGA, mPEG-PLBMGA and mPEG-PLHMGA nanoparticles in PBS (pH 7.4). In their study, 10% fetal bovine serum (FBS) was added to the water-based release solution to bind the released drug and achieve full dissolution into the release medium, due to poor solubility of bedaquiline in water.[31] This method allowed them to determine that bedaquiline is released *via* diffusion in these conditions. This method is suitable for the determination of release kinetics in laboratory conditions, but it does not provide information of the behavior of the nanoparticles in real condition *in vivo* or *in vitro*. Release profile *in* vivo or *in* vitro will depend on the specific pH, salt concentration or presence of other components of each media, which is not represented in this assay. In the case of our study, we looked for the conditions that can better mimic real assays conditions, that is nanocapsules suspended in the same medium to be studied. Several media were selected as they were considered of importance for the present study: water, PBS, NaCl 0.9%, Middlebrook 7H9 Broth (7H9), Roswell Park Memorial Institute (RPMI) cell culture medium, gastric simulated (GS) medium and intestinal simulated (IS) medium.

Water is the storage media, and so it will be considered as the control. PBS and NaCl 0.9% were selected because of their use in intravenous administration of drugs and therefore they will be tested to be selected as administration media for

the *in vivo* experiments. It is of great importance to be aware of the behavior of the nanocapsules in the medium in which that they will be administered, to avoid a loss in the nanocapsules activity or a change in their properties.

Middlebrook 7H9 broth is the bacterial culture medium used for *Mycobacterium tuberculosis.* The amount of free antibiotic in the bacterial culture media is an important parameter to be related with the antibacterial activity. For example, if the concentration of encapsulated bedaquiline needs to be double than free bedaquiline to inhibit bacterial growth, and release in this media is 50%, this would mean that the activity observed is due to released antibiotic and not due to nanocapsules internalization. However, if the observed activity is the same than for the same concentration of free bedaquiline, and considering that the released bedaquiline is only 50%, it should be an effect in the antibacterial activity coming from the encapsulation. Therefore, the study of the release in this media would indicate if the encapsulated antibiotic or the one prematurely released are responsible for the activity *in vitro.* Regarding RPMI media, *Mycobacterium tuberculosis* is an intracellular parasite of macrophages that are cultivated in this medium. Release studies would allow determining possible relations between *in vitro* experiments and the presence of free bedaquiline.

Although the framework of the NAREB project stated that the nanocapsules were going to be administered intravenously, we decided to test the stability of the cargo in Gastric Simulated (GS) and Intestinal Simulated (IS) in view of a possible oral administration. According to the literature, oral administration has several advantages over IV administration: reduced risks, such as cannular-related infections, lower costs and earlier discharge from hospital.[41] For this reason, we selected gastric and intestinal simulated media[42] to evaluate the stability of the

nanocapsules in the stomach and the intestine and evaluate the suitability for oral administration.

After selection of the media, the release profile method was developed to try to mimic the real conditions as best as possible. Nanoparticles were incubated for 7 days, as efficacy *in vitro* experiments last this amount of time. Check points were established at 1, 2 and 3 days to follow the progress of the experiment. For the same reason, 37 ºC were selected as incubation temperature, as it is both the temperature of *in vitro* and *in vivo* experiments and the human corporal temperature. Nanocapsules were incubated with each release medium and the concentration of bedaquiline was analyzed at each time point. To determine the amount of released bedaquiline, one of the most important steps of the method was the separation of the bedaquiline still encapsulated from the released one.

For this purpose, authors in the literature used different methods. Some authors charge the nanoparticles inside dialysis membranes and at different time points take out samples from the release media.[43] In some other cases, nanocapsules are separated from the release media via ultracentrifugation. These two methods were not suitable for this project. In the dialysis method, bedaquiline crystals may precipitate inside the dialysis bag, which would avoid their measurement in the release media. Usually, this is avoided by addition of a protein that is able to dissolve bedaquiline in the media, but this is not suitable for our project as we wanted to mimic real conditions.[31] In the case of separation by ultracentifugation, in our case it was impossible to reach a complete precipitation of the bedaquiline-loaded nanocapsules making impossible to obtain a correct measure of the released antibiotic.

For this reason, we used a separation method in which the nanocapsules were retained in an appropriate PVDF syringe filter. Released bedaquiline was able to pass through the membrane, while the nanocapsules containing non-released bedaquiline are retained in the membrane. Then, both free bedaquiline and non-released bedaquiline are measured to assure that all bedaquiline is measured. To check that free bedaquiline was not retained in the filter, free bedaquiline at the maximum concentration of the experiment was passed through the filter dissolved in each media. Concentration was checked and it was corroborated that no free bedaquiline was retained by the filter. A scheme of the method is shown in Figure 4.

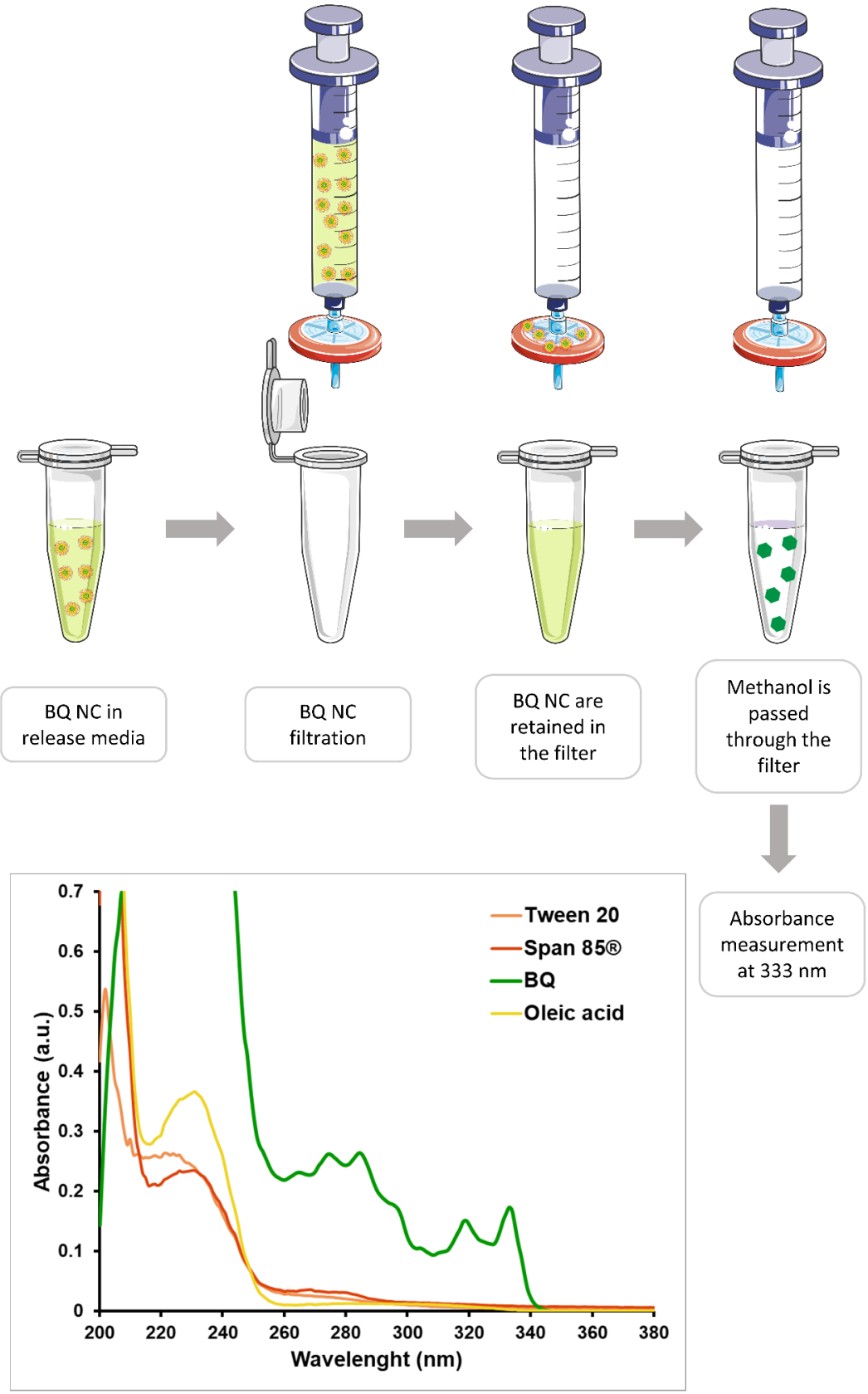

Figure 4.Schematic representation of the method for BQ quantification and absorbance spectra of BQ, Tween 20, Span 85 and oleic acid in methanol

To measure released bedaquiline, the filtrated portion, corresponding to the released bedaquiline, was freeze-dried and resuspended in methanol, in which bedaquiline is highly soluble. To measure non-released bedaquiline inside the capsules, methanol was passed through the filter to break nanocapsules and dissolve and release bedaquiline from the filter membrane. Both solutions were measured by UV and after quantification of bedaquiline using a calibration curve, it was calculated that total amount of bedaquiline was equal to initial one. The % of release was calculated as percent ratio between the amount of released bedaquiline and the amount initially added to the assay.

This method is just an approximation of what really happens in the *in vitro* experiments, as interaction with bacteria and cells will also contribute to nanocapsule stability, however, it is a very useful approach to observe possible burst releases of the drug in different media and allows explanation of some of the antibacterial results. Data from release experiments are represented as release profiles of bedaquiline in Figure 5.

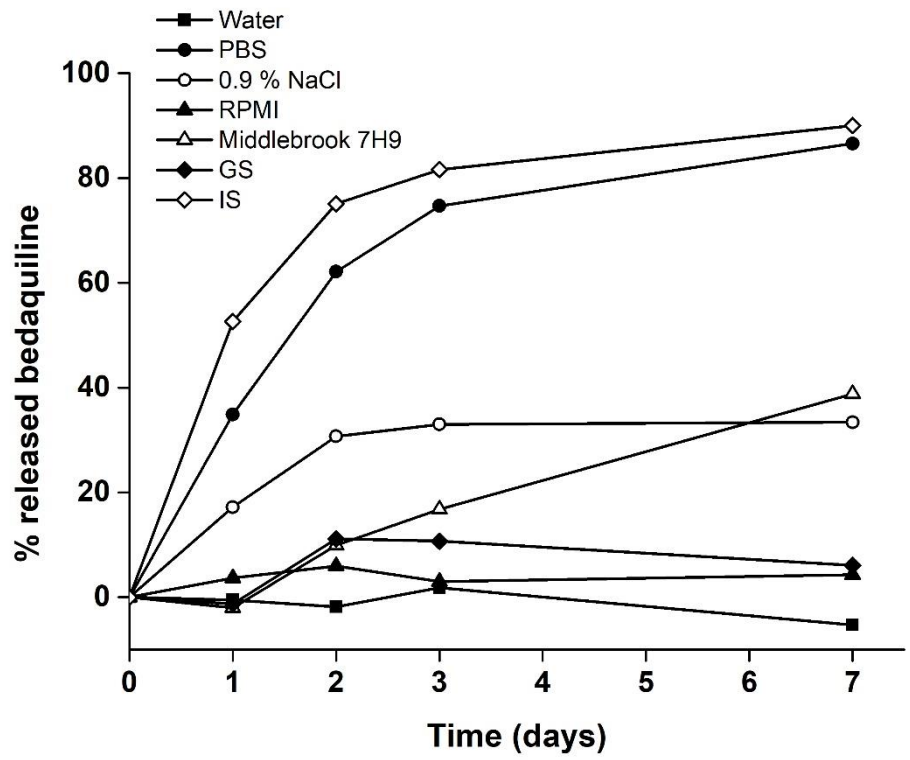

Figure 5. Release profile of bedaquiline-loaded nanocapsules in different media of interest

In the control media (Figure 5, black square), water in our case, it can be observed that bedaquiline maintains its DL% after one week of incubation at 37ºC, indicating that the capsules are stable in this media. This is probably because bedaquiline is a hydrophobic drug and will prevent leakage from the hydrophobic core into water.

Long term stability was also measured in water. Nanocapsules were preserved at 5 ºC for six months and drug loading was measured after that time. DL% was 90% ± 10% of the initial one. This is of great importance for the industry as allows the preservation of the nanocapsules for long periods of time without requiring continuous synthesis of fresh nanocapsules upon demand.

The behavior of nanocapsules in media other than water are represented and discussed in detail in the following figures.

If we observe the release in the two possible in vivo administration media, as stated before, PBS and NaCl 0.9%, we can determine that the stability is highly different (Figure 6).

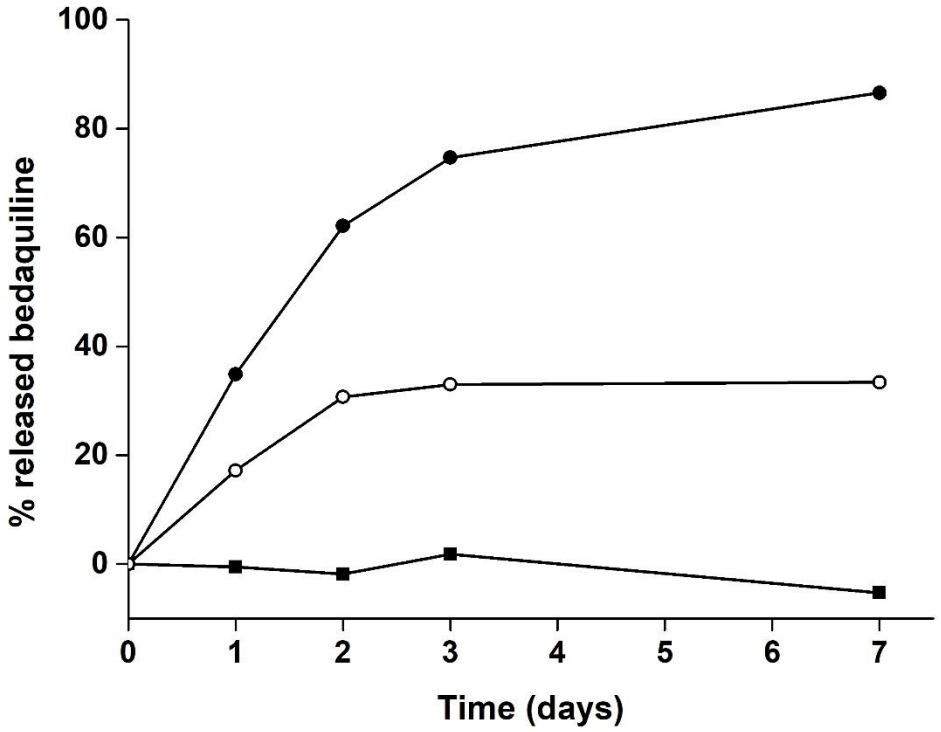

Figure 6. Release profile of bedaquiline-loaded nanocapsules in water (■), NaCl 0.9% (○) and PBS (●)

After 7 days of incubation almost 90% of bedaquiline is released in the PBS solution and only 40% in NaCl 0.9%. This difference is even more noticeable after 1 day of incubation, in which less than 20% antibiotic is released in NaCl 0.9 % while it is more than 50% for PBS. NaCl 0.9% confirmed to be the best

administration option for this particles, since they are not stable enough in PBS. This correlates with the results of stability towards aggregation measured by DLS.

In Figure 7, it can be observed that release in RPMI is less than 10 % even after one week of incubation, being similar than in water.

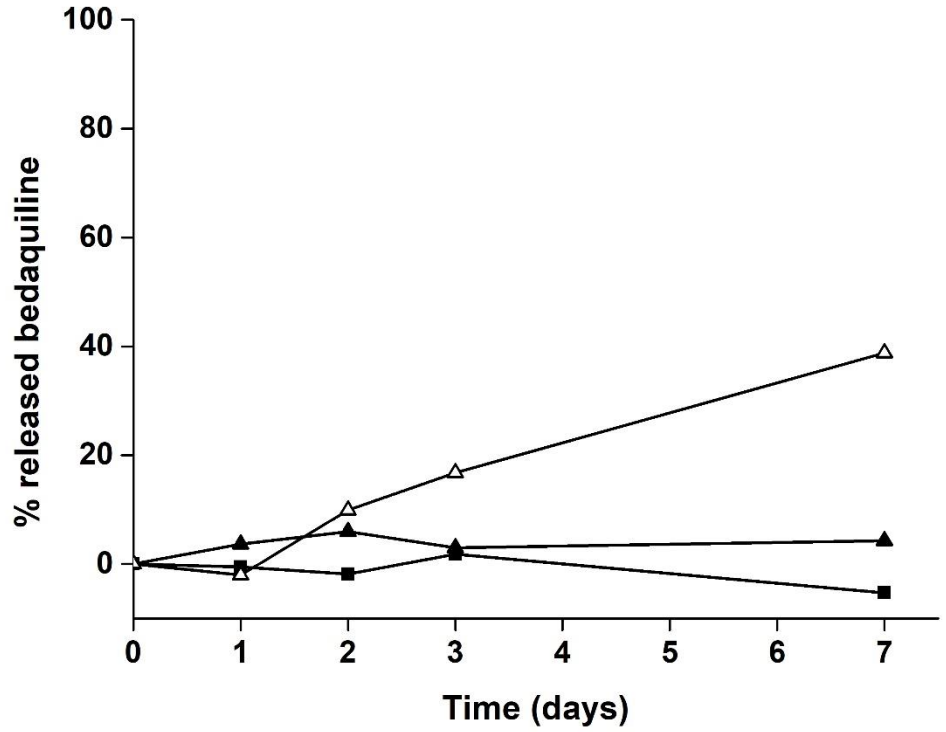

Figure 7 .Release profile of bedaquiline-loaded nanocapsules in water (■), RPMI (▲) and Middlebrook 7H9 (△)

This means that the effects observed in the experiments with macrophages performed in this medium would be due to bedaquiline-loaded nanocapsules and not free bedaquiline, as the release in this media is very low. In the case of the other cell culture medium, Middlebrook 7H9 broth, release is almost 40% after 7 days of incubation. This would mean that the presence of free bedaquiline in the antibacterial activity experiments need to be taken into account, as the amount

of free bedaquiline in the experiment will be almost the same as the encapsulated one.

In the simulated media for the oral delivery (Figure 8), we can observe an important difference in the release profile.

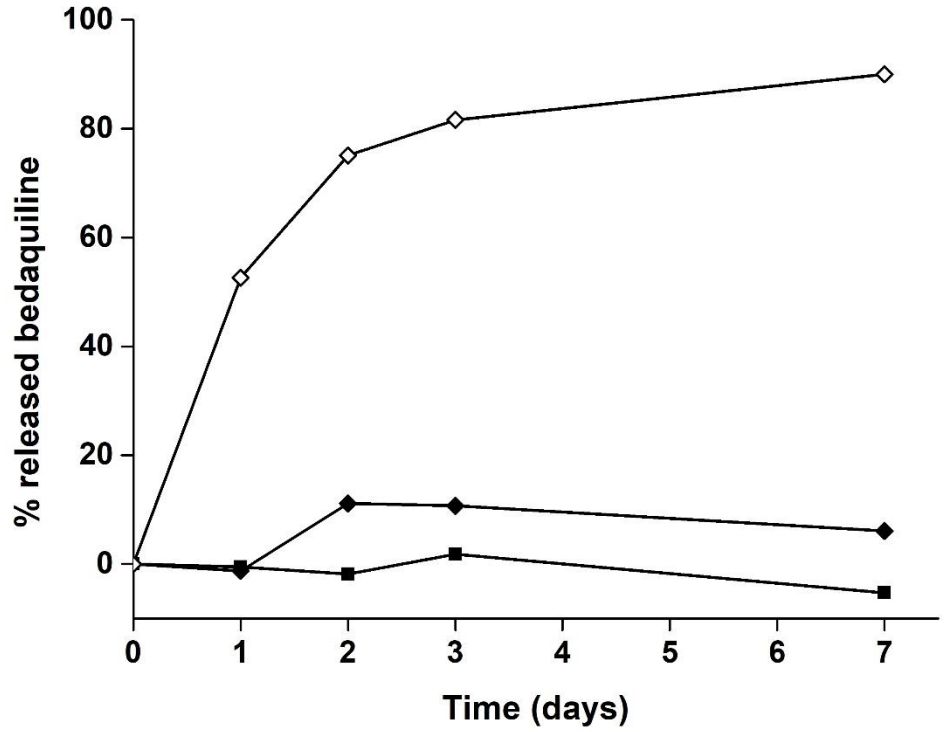

Figure 8. Release profile of bedaquiline-loaded nanocapsules in water (■), GS (◆) and IS (◇)

In the case of GS, bedaquiline release is less than 10% after one week of incubation, while for IS is 90% and even 80% after only 2 days of incubation. This would mean that nanocapsules can be used as oral delivery vehicles of bedaquiline as the drug is protected in the stomach, while release in the intestine would allow absorption and distribution to the body. However, the high release observed in the intestine means that only free bedaquiline is going to be absorbed

and not the whole nanocapsule. This would mean that nanoparticles will not act as a vehicle for target delivery and many of the advantages of encapsulation will be lost (target delivery, reduction of side effects). However, they can act as a vehicle to solubilize it until its absorption in the intestine.

In Figure 9, we can observe that release profile for Intestinal simulated media and PBS is really similar.

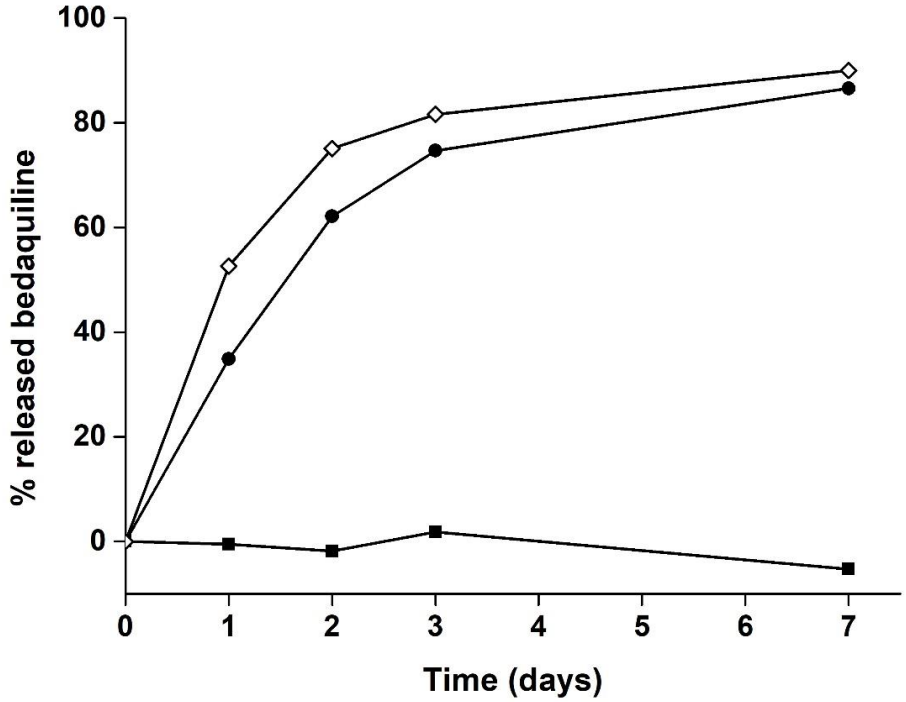

Figure 9. Release profile of bedaquiline-loaded nanocapsules in water (■), PBS (●) and IS (◇)

The fact that both IS and PBS show the highest release of drug and a similar release profile (Figure 9) can be explained by the high concentration of phosphate ions in both media. It has been described in literature that phosphate can disrupt the chitosan coating of the nanocapsules, therefore triggering drug release.[39]

According to this results, intravenous administration of the nanoparticles is recommended to be performed in NaCl 0.9%, in which release is less than 20% after 24 hours, indicating that nanocapsules are stable enough for this route of administration.

2.4. Surface grafting of bedaquiline-loaded nanoparticles

Surface grafting offers the possibility to modify the surface of nanoparticles to change their properties. Different objectives can be accomplished through this strategy. First of all, the specific recognition of the target tissue or cell can be achieved by adding a specific recognizing molecule to the surface. For this purpose, surface can be grafted with antibodies, proteins or specific ligands of the target cells, to improve nanocapsule adhesion to the tissue. and to decrease the nanocarrier dose.[44,45] However, nanoparticle surface can also be grafted for other purposes, such as the avoidance of recognition by serum proteins o cells or to avoid aggregation. This is usually carried out by the attachment of hydrophilic molecules to coat de nanocapsules surface, such as polyethylene glycol (PEG).[46,47]

In this thesis, the surface of the bedaquiline-loaded nanocapsules was modified by grafting the surface with PEG to achieve two different objectives. Firstly, to decrease the aggregation of the nanocapsules in physiological media. Secondly, this was developed as a proof-of-concept for the optimization of the functionalization of nanocapsules which will allow the application of the surface grafting method to other ligands.

The surface grafting was carried out by linking a PEG spacer modified with an amino group to the amino groups of the nanocapsules surface through the

homobifunctional crosslinker, bis(sulfosuccinimidyl)suberate (BS^3). This method has already been applied for the grafting of empty nanocapsules.[22] Here the method has been slightly modified to be adapted to the number of amino groups available. The structure of PEG, BS^3 and a schematic representation of the link to the NC surface is shown in Figure 10.

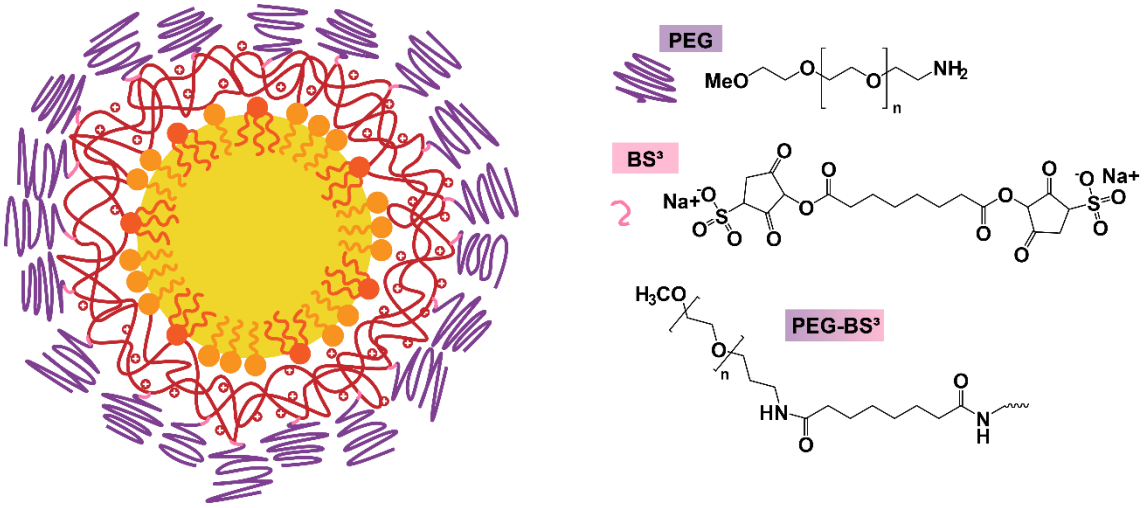

Figure 10. BS^3 and PEG structure and structure of the linking of PEG and BS^3 to the surface of nanocapsules.

PEG was selected to reduce the surface charge of the chitosan, which allows to reduce the interaction with proteins and salts and so confers better stability in several physiological media. Amino groups of the chitosan coating of the nanocapsule, which are positively charged at physiological pH, can interact with negative ions in solution which can lead to the formation of aggregates. PEG grafting is expected to reduce this aggregation as it can reduce the amount of amino groups available by direct linking or masking. Besides, as PEG is a widely known molecule that has shown great biocompatibility and is easy to obtain, it can be used as a coating molecule in a first approach to optimized the grafting protocol.[48]

The amount of BS^3 and PEG added to graft the surface was optimized with respect to the number of available amino groups on the nanocapsule surface. To determine this value, we used a spectrophotometric assay based on the compound Orange II.[22]

This method was optimized for the measurement of available amino groups on empty nanocapsules.[22] It is based on a pH-dependent interaction between positively charged amino groups and $-SO^{3-}$ group of Orange II dye. This spectrophotometric method not expensive and simple to use. Besides, the relationship between amino groups and the reactants is 1:1, allowing a direct and reliable quantification. In this thesis, the method was slightly modified to use syringe filters as support for the separation of nanocapsules from the solution during all the washing steps. Briefly, Orange II method for quantification of available amino groups is based on the reversible electrostatic interactions between the negatively charged sulfonated group in Orange II and the positive charge of protonated amino groups of chitosan in acidic solution. Then, under alkaline conditions (pH 12), the amino groups become neutral so Orange II is released into the solution.

A double measurement is carried out in order to check that our system works properly, and both bonded and unbounded Orange II is measured. First, nanocapsules are mixed with Orange II solution at pH 3 for the binding of the molecule to the amino groups in chitosan. Then, unbounded Orange II (excess of reagent) is recovered after the filtration of the capsules and its concentration determined by spectrophotometry. Later, bonded dye was detached from the capsules surface using an alkaline solution (pH 12), as in this conditions Orange II is not able to bind to the amino groups and it is released. The pH of this

detached Orange II solution was then changed to a pH 3 for the measurement. Finally, bounded and detached Orange II quantities are summed up to check that all the initial amount of Orange II is measured. This double measurement allows us to check that all the dye is recovered, and that our set up is suitable for the system.

To correlate the absorbance of the solution with the amount of Orange II and therefore of amino groups, a calibration curve is performed at pH 3. With this calibration curve and measuring the absorbance of the Orange II solutions from the nanocapsules, we determined that the available amino groups in the non-grafted nanocapsules are 400 nmol/mg. Taking in mind this value, 100 nmol BS^3/mg were added for the grafting. With this value, only 25% of the amino groups in nanocapsules will be linked to a PEG molecule. It was considered that this was enough to reduce the number of amino groups available in the nanocapsules surface to avoid aggregation of the nanocapsules, but not too high to produce crosslinking between the nanocapsules. However, we observed that upon the addition of this amount of crosslinker, nanoparticles aggregated macroscopically during the grafting. It is possible that the amount of linker was still too high, linking too many amino groups, reducing charge which would be insufficient to guarantee a good stability of the nanocapsules. Besides, high amount of BS^3, as it is the previous step before PEG addition, may crosslink to many amino groups of different capsules between them, leading also to aggregation. Therefore, the amount of BS^3 was reduced to 50 nmol/mg and no macroscopic aggregation was observed in this case, so this amount was used for the rest of the experiments.

2.5. PEG-grafted bedaquiline-loaded nanocapsules characterization

As in the case of non-grafted nanocapsules, size and ζ potential of the grafted nanocapsules was studied by Dynamic Light Scattering (DLS) in order to compare them with the non-grafted ones.

The hydrodynamic diameter and size distribution of the PEG-grafted capsules optimized before was studied using Dynamic Light Scattering in water to compare the size distribution of the non-grafted nanocapsules with the PEG-grafted ones (Figure 11).

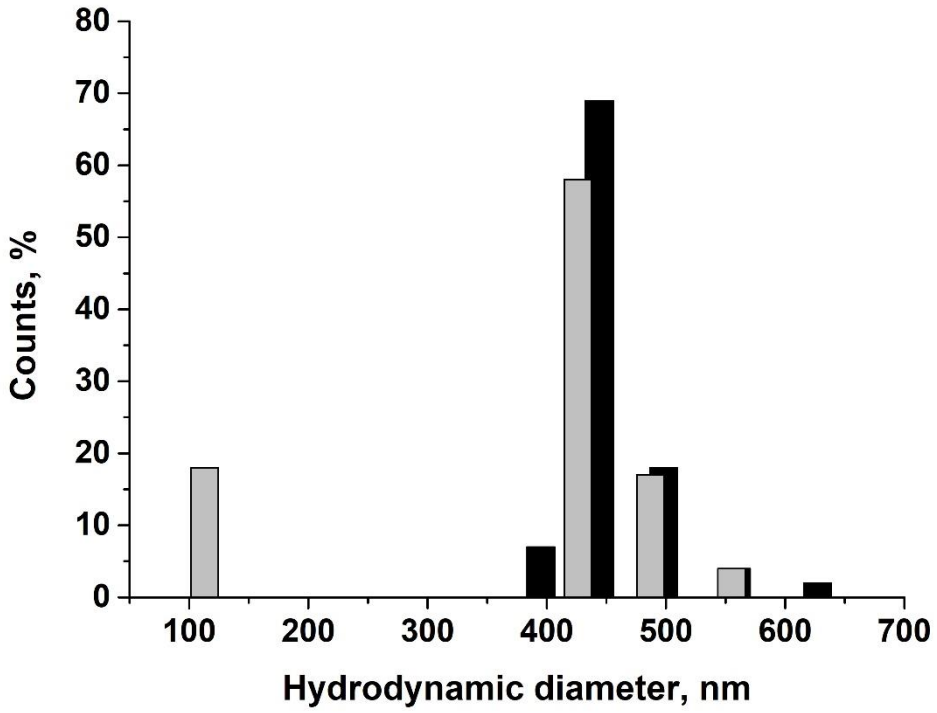

Figure 11. Size distribution of non-functionalized (grey) and PEG-grafted (black) bedaquiline-loaded nanocapsules in water

The mean diameter can be calculated from the size distribution observed in Figure 11 and is 460 nm for the grafted nanocapsules while for the non-grafted

is 400 nm (Figure 2A). This increase in the mean diameter is in agreement with the extra coating in the nanocapsule surface due to PEG presence, which is an indication that the capsules have been grafted. This increase in size should not affect the cellular uptake of the nanocapsules by macrophages, as explained before, it was observed that macrophage uptake could be increased when nanoparticle size increases.[37,38,49]

To confirm the grafting of the surface, we measured the ζ potential of the nanocapsules. Due to the positive charge of the amino groups of the chitosan coating the nanocapsules, a positive ζ potential of the non-grafted nanocapsules was expected (the value was +25 mV: SEE Section 2.2). However, it is expected that the positive ζ Potential should be lower in the grafted nanocapsules, as some of the amino groups are now establishing bonds with PEG and thus, they do not contribute to the positive surface. Besides, PEG around the surface may change the interaction with the ions of the solution, therefore changing the ζ potential of the nanocapsule. After measuring the ζ potential, it was obtained a value of -10 mV for the PEG-grafted nanocapsules, while the non-grafted nanocapsules provided a value +25 mV. These results confirmed that the surface was modified.

To further study the surface grafting and the nature of the coating of both non-grafted and grafted nanocapsules, the available amino groups of the grafted and the non-grafted nanocapsule were compared using the spectrophotometric assay based on Orange II. Amino groups on grafted and non-grafted nanocapsules were analyzed using the same method. It was determined that the free amino groups of the PEG grafted nanocapsules was 280 nmol/mg, while for the non-grafted ones the value was 400 nmol/mg. This experiment confirmed that the surface of the nanocapsules has been modified with PEG.

It should be pointed out that results from Orange II interaction only represented the amount of amino groups available for the interaction with dye molecule. It is supposed that the decrease of the number of amino groups would be due to bond formation with PEG molecules. However, also the structure and arrangement of the PEG around the surface may interfere with this estimation, generating even a higher decrease than expected.

As in the case of non-grafted nanocapsules, PBS and NaCl 0.9% solutions were used to study the aggregation of the capsules in the administration media and to compare if the aggregation is reduced. Results are shown in Figure 12.

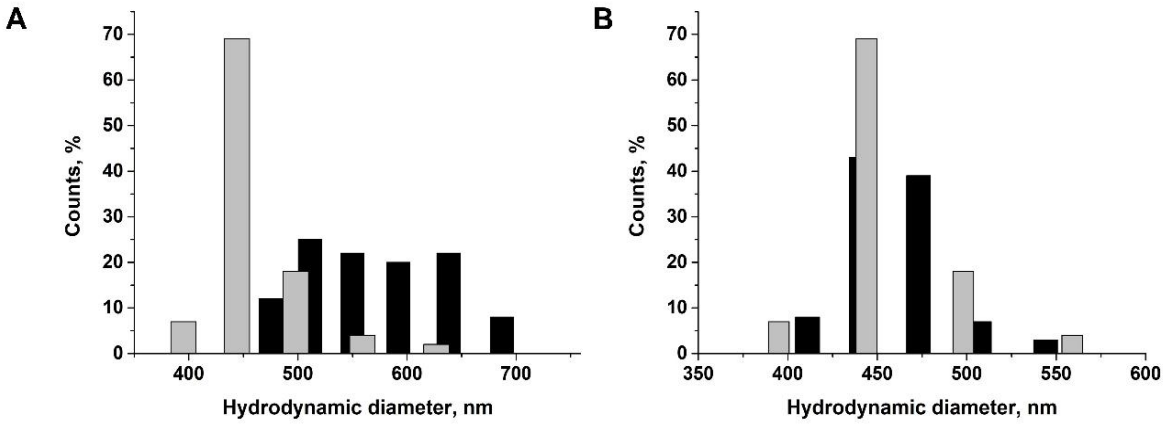

Figure 12. Size distribution of PEG-grafted nanocapsules in water (grey) and (A) NaCl 0.9% (black) and (B) PBS (black)

As one of the objectives of PEG grafting was to avoid aggregation of the nanocapsules in physiological media such as PBS and NaCl 0.9%, it was important to measure the size distribution and hydrodynamic diameter of the PEG-grafted nanocapsules in these media.

The results presented in Figure 3 for the non-grafted nanocapsules and Figure 12 for the grafted ones, show that the aggregation tendency in this media

changes depending on the grafting. In the case of NaCl 0.9% no effect was observed (Figure 12A). The mean diameter of the capsules changes from 460 nm to 570 nm, which is similar to the effect observed in the non-grafted ones, which varies from 400 nm to 500 nm (Figure 12A). In the case of PBS, no aggregation is observed after grafting, as the mean diameter of the nanocapsules is 465 nm, compared with the measurement in water was 460 nm. The size distribution is similar too, indicating that we obtained a protective effect from phosphate salts by grafting PEG molecules onto the surface of the nanocapsules (Figure 11B).

It can be deduced from these results that the aggregation observed in PBS is due to crosslinking between nanoparticles induced by the presence of phosphate salts. This effect is prevented by the surface modification with PEG, which will prevent the amine groups of the capsule surface to interact with the negatively charged phosphate ions. On the other hand, the effect on the increase of the nanocapsule diameter observed in the presence of NaCl 1% should be caused by other mechanisms, such as salting out-like effect, in which the PEG-grafting does not improve the stability. The salting-out effect is based on the removal of the water barrier between nanoparticles with an increase in salt concentration due to the attraction of water molecules to the salt ions. This would lead to an increase in the interaction of the nanocapsules with each other, and the precipitation and apparent increase in size.[50] Therefore, PEG-grafting would not be able to lower this effect and avoid aggregation, as interaction between PEG molecules on the nanoparticle surface is still possible.

2.6. Release profile of PEG-grafted bedaquiline-loaded nanocapsules

Release profile of PEG-grafted bedaquiline-loaded nanocapsules was studied in the same conditions and following the same method than for the non-grafted ones. This allowed to determine how grafting of the surface affects the release profile of bedaquiline in comparison with non-grafted ones. Figure 12 shows the release profiles of the PEG-grafted nanoparticles in the different media studied.

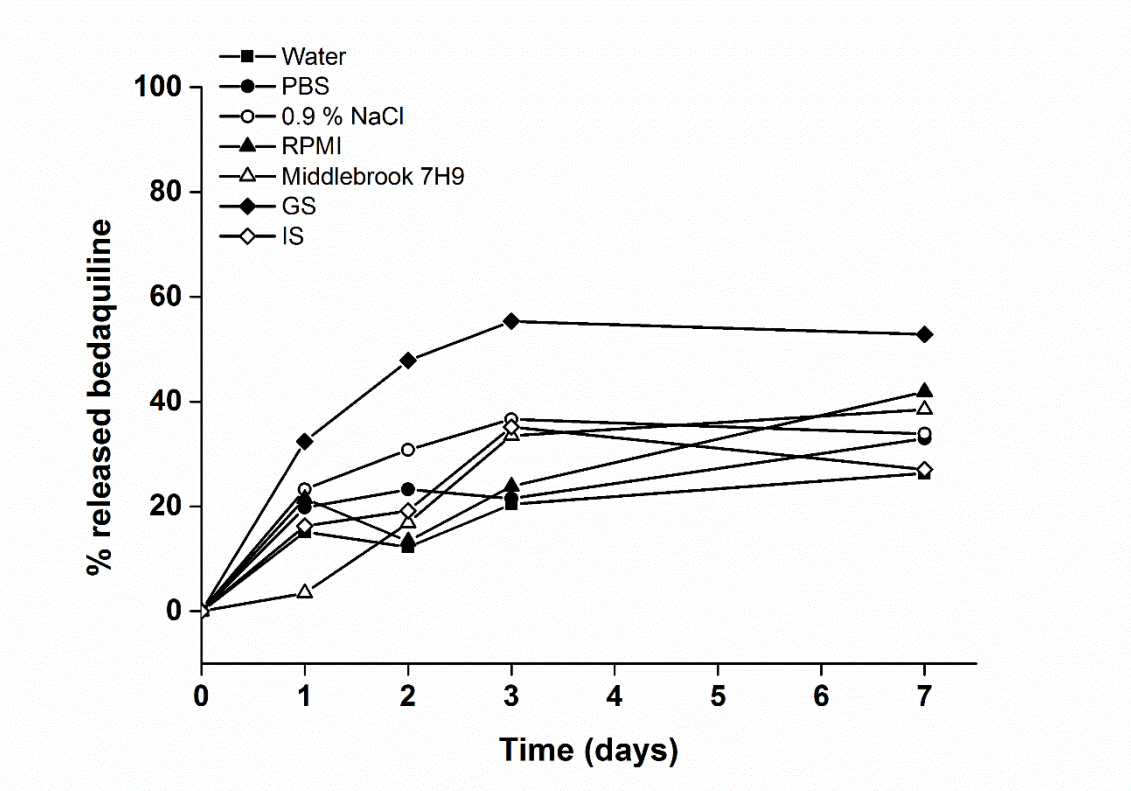

Figure 13. Release profile of PEG-grafted bedaquiline-loaded nanocapsules in different media of interest

In Figure 13, we can observe that in the case of PEG-grafted nanocapsules, bedaquiline release shows a similar profile in all the media. Final % released bedaquiline varies between 20 and 60%, in comparison with non-grafted nanocapsules, in which release varied from 0 to almost 100%. Graphs comparing

non-grafted and PEG-grafted nanocapsules have been plotted for each media individually in order to compare the behavior of each type of nanocapsules in the different media,

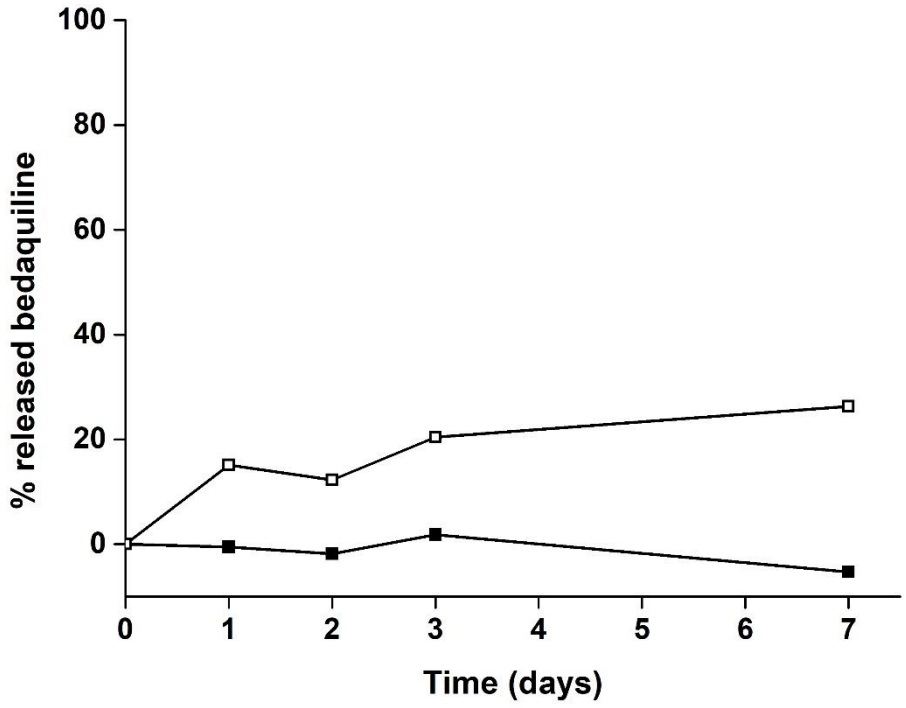

Figure 14. Release profile of non-grafted (■) and PEG-grafted (□) bedaquiline-loaded nanocapsules in water

As observed in Figure 14, non-grafted nanocapsules prove to be more stable than the PEG-modified ones in terms of drug load in water. This can be explained by the fact that the use of borate buffer during the grafting process can weaken the chitosan structure surrounding the nanocapsule core, and therefore promoting diffusion of bedaquiline into the media. Borate is a negatively charged ion that can interact with the positively charged amino groups in chitosan structure. These amino groups would stop interacting with the sulfate for the nanocapsule structure that crosslinks and reinforces the polymer coating,

weaking the its structure. This would make bedaquiline release easier in the PEG-grafted nanocapsules.

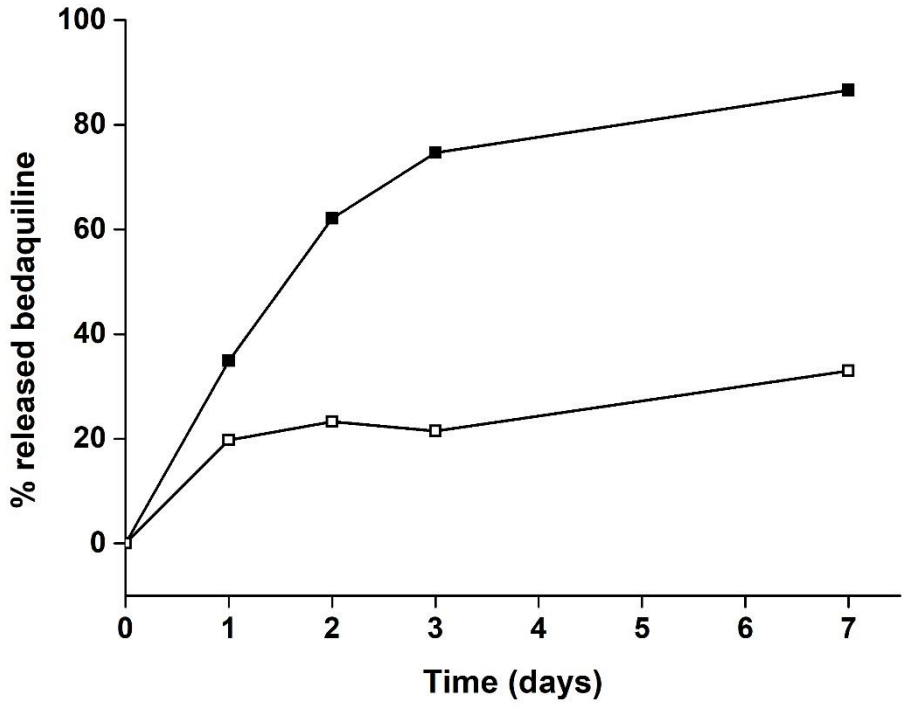

Figure 15. Release profile of non-grafted (■) and PEG-grafted (□) bedaquiline-loaded nanocapsules in PBS

In Figure 15, release profile in PBS shows great differences between grafted and non-grafted nanocapsules. PEG-grafted nanocapsules show 50% less release in comparison with the non-grafted ones. This correlates with the stability in terms of aggregation, as grafted nanocapsules show higher stability too. It can be said that PEG-grafting improves the stability of the nanosystems in the presence of phosphate salts.

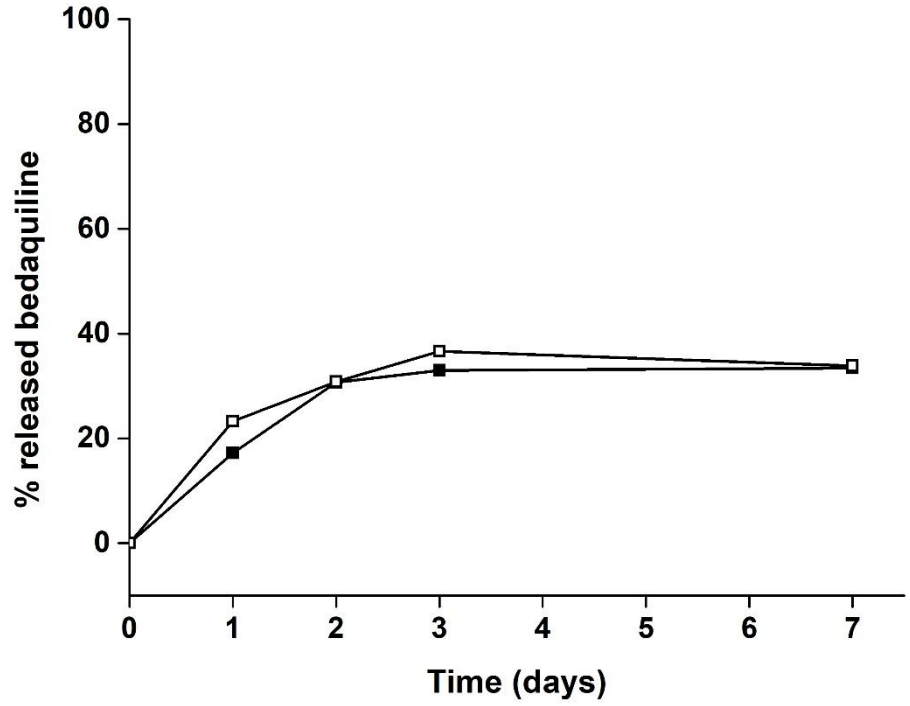

Figure 16. Release profile of non-grafted (■) and PEG-grafted (□) bedaquiline-loaded nanocapsules in NaCl 0.9%

As observed in Figure 16, the release in NaCl 0.9% shows almost the same profile for non-grafted and PEG-grafted nanocapsules. As in the case of stability toward aggregation, PEG-grafting does not show any improvement in stability in the presence of NaCl. This would mean that PEG does not interact with NaCl nor modifies the mechanism of action of the salt in bedaquiline release.

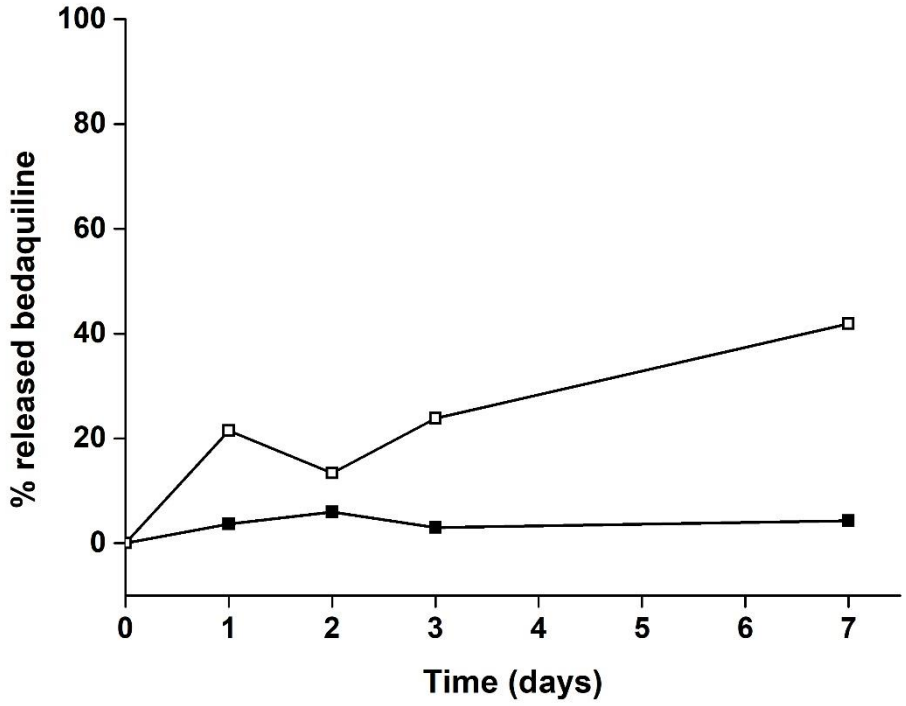

Figure 17. Release profile of non-grafted (■) and PEG-grafted (□) bedaquiline-loaded nanocapsules in RPMI

Comparison of Figure 17 (RPMI) with 13 (water) shows that the tendency in PEG-grafted versus non-grafted is different. In both cases, non-grafted nanocapsules show almost none release while this value is increased up to 40% after 7 days for the PEG-grafted ones. As explained for the case of water, grafting in the presence of borate ions may destabilize the chitosan coating, favoring bedaquiline release.

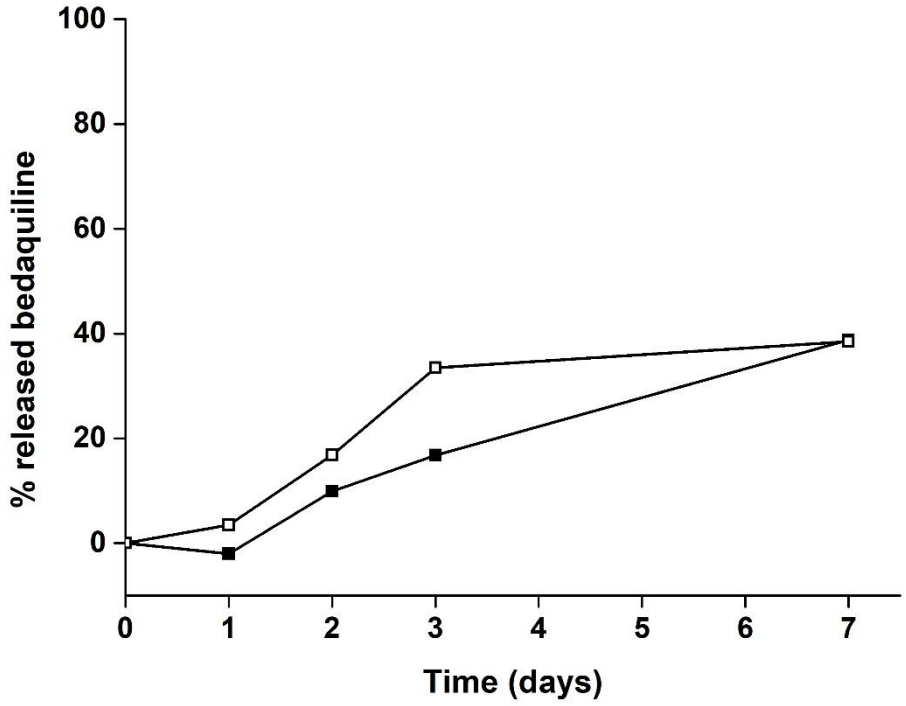

Figure 18. Release profile of non-grafted (■) and PEG-grafted (□) bedaquiline-loaded nanocapsules in Middlebrook 7H9

Figure 18 shows the release profile of nanocapsules in the bacterial culture media Middlebrook 7H9. In this case, although release slope is slightly different (steeper in the case of PEG-grafted), the final result is similar for both cases at 7 days. However, the tendency is different, as it seems that non-grafted nanocapsules have a lineal tendency while PEG-grafted ones seem to have a plateau. As stated before, release in Middlebrook 7H9 medium is very important as it could be correlated to the antibacterial activity. If the MIC observed for the encapsulated bedaquiline correlated with the amount of BQ released, this would mean that the antibacterial activity is likely to be due to the breakup of the capsules.

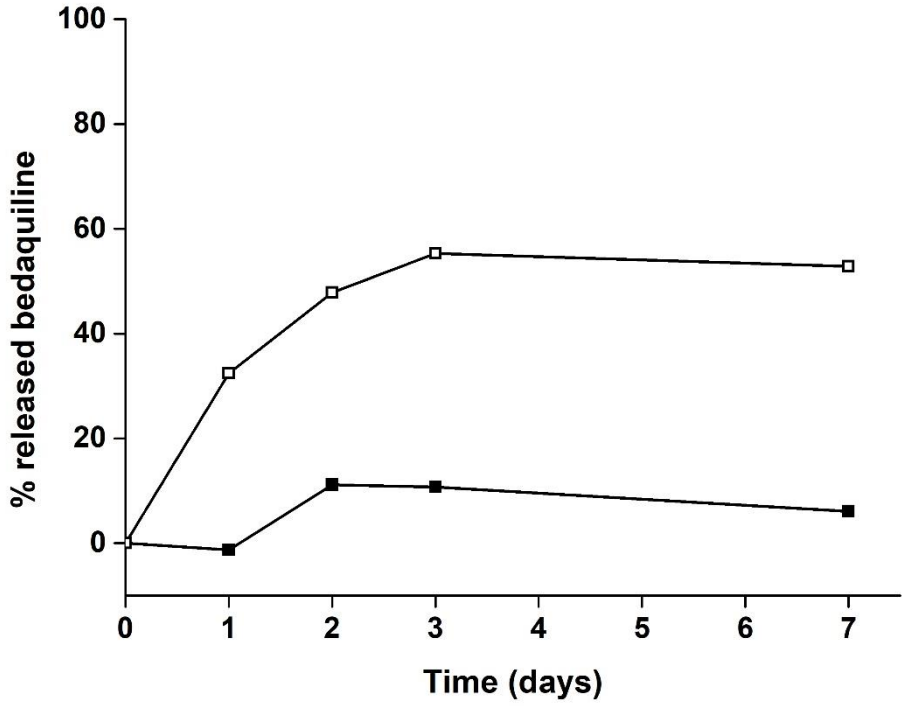

Figure 19. Release profile of non-grafted (■) and PEG-grafted (□) bedaquiline-loaded nanocapsules in gastric simulated medium

In Figure 19 can be observed that there is a huge difference in the behavior of non-grafted and PEG-grafted nanocapsules in gastric simulated medium. After 7 days of incubation, bedaquiline release increases from almost 10% for the non-grafted nanocapsules to more than 50% in PEG-grafted ones. This means that PEG-grafted nanocapsules are more sensitive to lower pH in gastric simulated media. It is known that pH affects PEG conformation[51] which can lead to destabilization of the nanocapsule surface by opening of the polymer structure and subsequent release of bedaquiline.

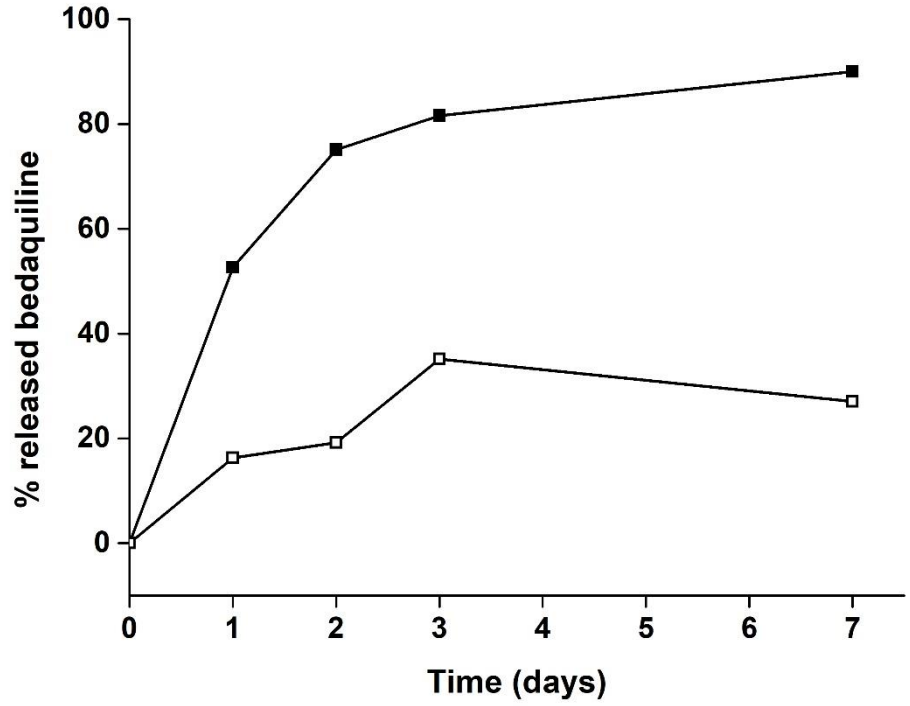

Figure 20. Release profile of non-grafted (■) and PEG-grafted (□) bedaquiline-loaded nanocapsules in intestinal simulated medium

Similar tendencies can be again observed in phosphate based media. As in PBS (Figure 20), PEG- grafted nanocapsules show 50% less released bedaquiline in comparison with the non-grafted ones. This can be explained by an improvement on the stability of nanocapsules in the presence of phosphate ions due to the modification of the surface by PEG chains.

We can conclude that PEG-grafting highly improves stability in the presence of phosphate ions, both in terms of tendency toward aggregation and bedaquiline release. Grafted nanocapsules would be more suitable for the application in this medium.

For the rest of the media, no improvement or even worsening is observed. Higher release percentages are obtained for water, GS and RPMI, which would mean that unless necessary for other purposes, non-grafted nanocapsules have the best characteristic for this application.

2.7. Antimicrobial activity of bedaquiline-loaded nanoparticles against *Mycobacterium tuberculosis*

Once nanoparticles have been characterized *in vitro,* antimicrobial activity was tested.

In vitro antimicrobial activity of the nanocarriers against *M. tuberculosis* H37Rv was tested by Dr. Ainhoa Lucía as part of the NAREB project. The strain H37Rv does not belong to a MDR *M.* tuberculosis strain, but it was used as a first approximation to study antimicrobial effect of the nanocapsules against TB cultures.

In this study, both non-grafted and PEG-grafted nanocapsules were tested to evaluate the antimicrobial activity of both developed nanovehicles and to determine if grafting affects the activity. Grafting can affect stability of the nanocapsules, release of the cargo and internalization into bacterial, which can affect the overall activity.

The antimicrobial activity was determined using the established REMA assay[52], in which a range of concentrations of bedaquiline-loaded nanocapsules was tested against *M. tuberculosis* to determine the Minimum Inhibitory Concentration (MIC) after 7 days of incubation. MIC was compared to that of free bedaquiline to evaluate if bedaquiline efficacy is improved after encapsulation or if its activity drastically decreases. Besides, it is important to test empty carriers MIC to ensure

that within the range of concentrations used in the assay, the antibacterial effect was only due to the antimicrobial drug and not to the nanocarrier itself.

After 7 days of incubation, the MIC value obtained for free BQ was 0.03 µg/mL. However, this value was 0.03-0.06 µg/mL for the non-grafted BQ-loaded nanocapsules and 0.06-0.13 µg/mL for the PEG-grafted ones. This variability is due to different values obtained in different assays. This means that the efficacy of BQ is decreased in encapsulated BQ as more BQ is needed to kill bacteria. Besides, this is more pronounced after PEG-grafting. If this result is compared with BQ release of both types of nanocapsules in Middlebrook 7H9, release is about 40% after 7 days of incubation. If MIC would be due only to released BQ, MIC for non-grafted nanocapsules would be 0.06-0.13 mg/mL, as only 40% of the total added encapsulated BQ would be free in the media. This means that the different MIC values do not depend only in free released BQ in the medium, but also internalization and bacterial interaction with nanocapsules may play a role.

It can be concluded that bedaquiline was at least partially active against M. tuberculosis after encapsulation in any of the carriers, as the lower activity may be due to loss of activity of BQ. Although efficacy is not improved, if biodistribution and cell targeting is upgraded, side effects can be decreased and nanocapsules would improve the overall treatment with BQ.

2.8. Fluorescent bedaquiline-loaded nanoparticles surface grafting

Besides *in vitro* studies, the project in which these nanocapsules were going to be applied included the study of the efficacy and biodistribution of the nanocapsules *in vivo.* The developed nanocapsules needed three different

features. Firstly, bedaquiline had to be internalized into the core, to study its efficacy. Secondly, the nanocapsules needed to be fluorescent to be able to follow their fate and study their biodistribution *in vitro*. Lastly, nanocapsules needed to be functionalized with a ligand to increase internalization in TB-infected macrophages.

For this purpose, the first step was the selection of the fluorescent probe. For *in vivo* studies, it is important that the excitation and emission wavelengths of the fluorophore of choice are within the biological window. This biological window comprises the region from 650 nm to 950 nm, in which tissues present lower autofluorescence values and minimum absorption, in order to clearly visualized the fluorophore for *in vivo* studies.[53] Besides, as the fluorophore will be coencapsulated into the nanocapsules core with bedaquiline, the molecule of choice had to be hydrophobic. The fluorophore that was chosen was DiD oil (DiIC18(5) oil (1,1'-Dioctadecyl-3,3,3',3'-Tetramethylindodicarbocyanine Perchlorate)) a hydrophobic molecule whose excitation and emission wavelengths maximums are 644 and 665 nm, respectively.

Thanks to the hydrophobicity of the fluorophore, it was expected that encapsulation into the core of the nanocapsules was successful. The nanocapsules synthesis was carried out in the same way than for the non-fluorescent nanocapsules, but in this case, also 100 or 200 µg of the DiD oil molecule were added to the organic phase before its addition to the aqueous phase. These quantities of DiD oil were used to evaluate which amount worked better. It was expected that, as the amount of DiD is low compared to the amount of bedaquiline, it will not compete with BQ encapsulation, and there was no decrease in DL% or EE% of the antibiotic.

All the excess reactants were washed as in the previous nanocapsules, so the non-encapsulated fluorophore was eliminated.

We carried out a fluorescent excitation and emission spectra of both the free DiD and the fluorescent nanocapsules to confirm that the synthesized nanocapsules were fluorescent in the region of interest. This let us confirm the presence of the fluorophore encapsulated into the nanocapsules and that the emission and excitation wavelength were in the region of interest (the first biological window) for the *in vivo* biodistribution experiments. 100 µg of fluorophore added to the reaction was selected as the optimum initial amount. Results for 200 µg showed that fluorescence did not increase in comparison with 100 µg and excess fluorophore appeared in the supernatant, so this quantity was discarded to avoid waste of fluorophore. Emission spectra of the nanocapsules loaded with 100 µg at a excitation wavelength of 344 nm is shown in Figure 21.

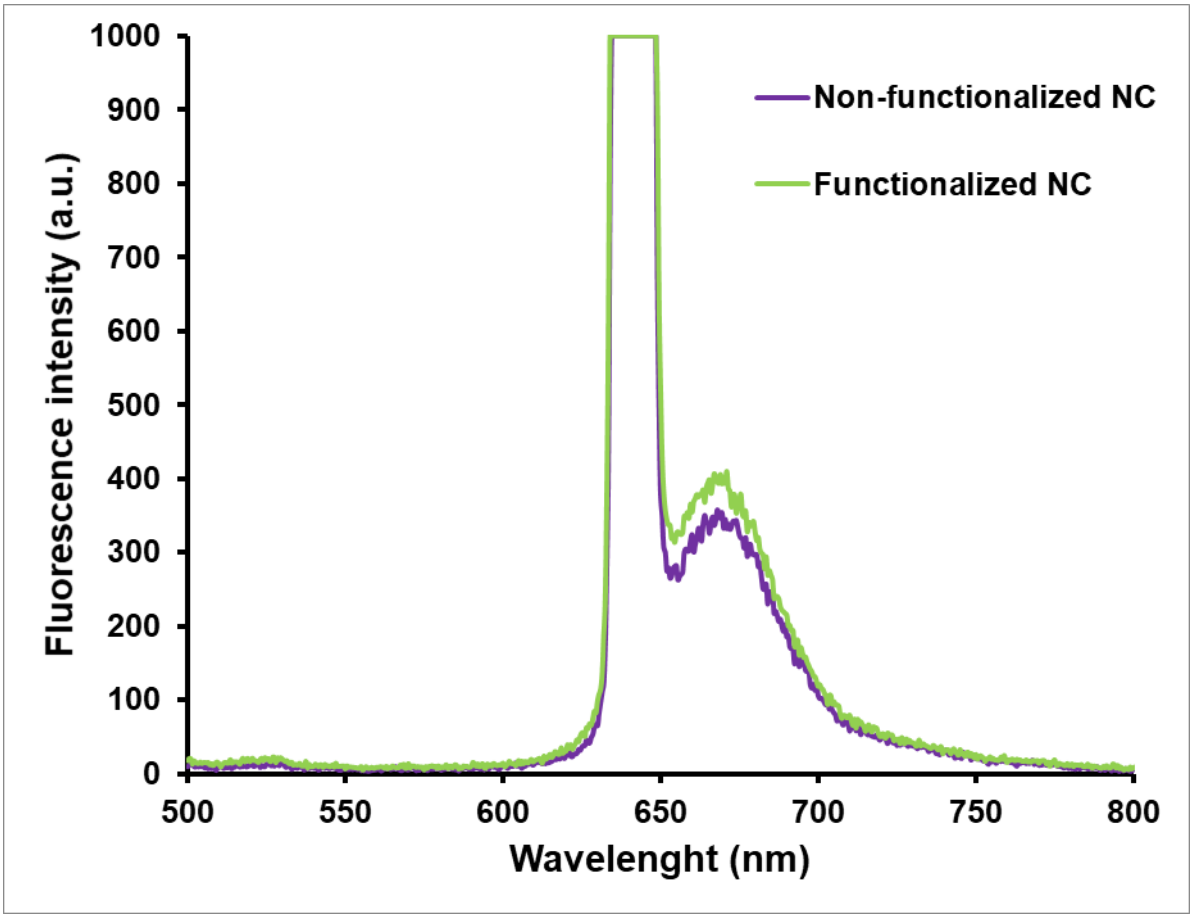

Figure 21. Emission spectra of encapsulated DID oil in bedaquiline loaded nanocapsules at an excitation wavelength of 644 nm before (purple) and after functionalization (green)

After this confirmation, the second step consisted in the grafting of the nanocapsules surface with a targeting ligand, to increase internalization in TB-infected macrophages. The molecule that we selected for this purpose was a trimannose ligand, which is able to interact with the mannose receptors in macrophages surface and therefore enhance internalization in these cells.[54] To check that the protocol was suitable for these nanocapsules, fluorescence of both washing steps of the functionalization and of the final nanocapsules obtained was measured. It was observed that nanocapsules lost their fluorescence due to release of the fluorophore (that appeared in the supernatant of the washing steps), so the protocol had to be optimized. For this purpose, the first approach

was to avoid the blocking step with TRIS, as it was the only step that could be avoided.

The rest of the protocol was maintained the same and again the fluorescence was measured in both washing steps and nanocapsules. In this case, no fluorescence of DID oil was detected in the supernatants. Fluorescence of the functionalized nanocapsules was 85% in comparison with the non-functionalized at the same concentration (Figure 21). This can be explained by an increase in nanocapsule mass or a slight loss of fluorophore during the process.

After the nanocapsules functionalization was complete, we measured also the amount of bedaquiline in order to confirm that we did not lose the drug loading fluorescence of the nanocapsules after functionalization. The extraction method of bedaquiline was performed in the same way that for the non-fluorescent, non-functionalized nanocapsules. Measurement of the absorbance at 333 nm confirmed that the drug loading for the developed nanocapsules decreased from 30% to 27%, which could be related to a slight loss of antibiotic during the functionalization or an increase in the nanocapsule overall mass due to the addition of ligands to the surface.

This DL% and fluorescent values were enough to continue with the next characterization steps to check stability of nanocapsules and use them the *in vivo* experiments.

As well as for the non-fluorescent bedaquiline-loaded nanocapsules, fluorescent bedaquiline-loaded nanocapsules were characterized by Photo Correlation Spectroscopy (PCS) to determine hydrodynamic diameter, size distribution and ζ potential. As explained before, surface charge and size are important parameters

influencing nanoparticle stability and interaction with biological membranes and it allows us to determine if the capsule is correctly synthesized and coated.[32] It is of special importance to study these characteristics in both functionalized and non-functionalized nanocapsules to evaluate how functionalization may affect particle size. Results for both nanocapsules are shown in Figure 7.

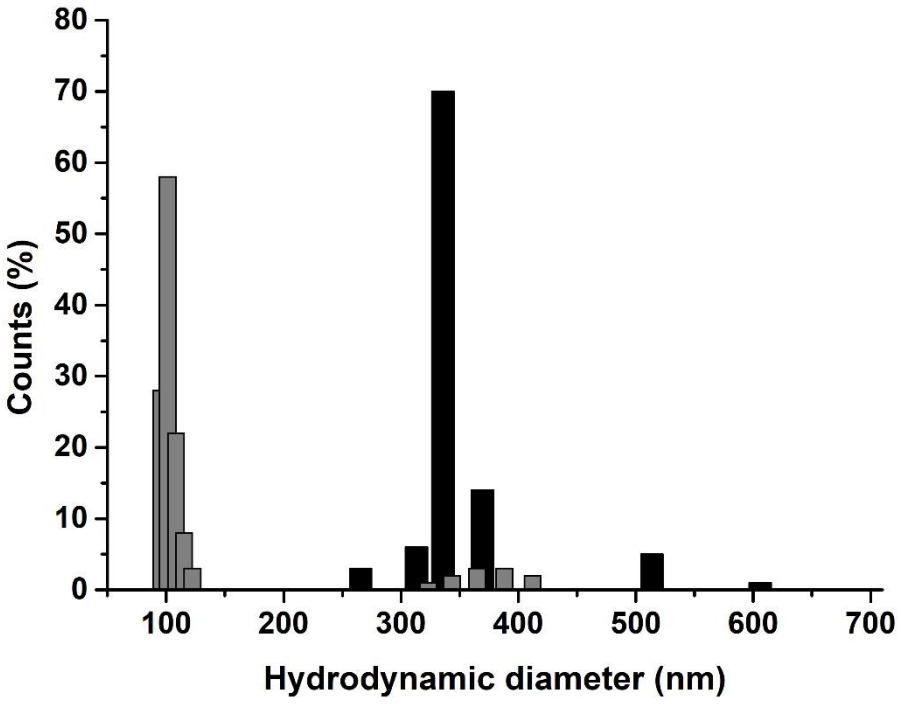

Figure 22. Size distribution of non-functionalized (grey) and trimannose-functionalized fluorescent bedaquiline (black) loaded nanocapsules

As it can be calculated from the size distribution in Figure 22, the mean diameter for the non-functionalized fluorescent nanocapsules is 130 nm which is similar to the small population observed in non-fluorescent nanocapsules. The one for the trimannose-functionalized ones is 430 nm (Figure 22). This increase in the mean diameter is probably due to an aggregation effect of the nanocapsules in water, as we observed that the functionalized sample is not as stable as the non-

functionalized. In fact, it was observed during manipulation of samples that functionalized nanocapsules were not stable in contact with plastic surfaces and stuck to the surface. This effect was also observed in the samples blocked with TRIS, so it is not due to the skipping of that step.

To confirm the grafting of the surface, we measured the ζ potential of the nanocapsules, as variations between the grafted and non-grafted nanocapsules might be an indicator that the grafting was successful. ζ potential for the non-functionalized nanocapsules was +28 mV, while it was of +31 mV for the trimannose-functionalized nanocapsules. As in the case of PEG-grafted nanocapsules, the number of free amino groups decrease after functionalization. However, in this case, ζ potential does not change from positive to negative as observed in PEG grafted ones, probably due to the contribution of the trimannoside. However, these results do not confirm the modification of the surface as we do not observe a change in the ζ potential, so further test needed to be done, to study the nanocapsule surface.

As in the case of PEG-grafted nanocapsules, a free amino group measurement by the Orange II assay was performed. After the analysis with the same protocol carried out previously, it was determined that the free amino groups of the non-functionalized nanocapsules was 740 nmol/mg, while for the trimannose functionalized ones the value was 560 nmol/mg. This reduce in the amino free amino group measurement sets the evidence that nanocapsules were functionalized by the trimannoside, so these nanoparticles were suitable for its use in *in vivo* biodistribution assays.

With all the results above mentioned, it can be concluded that nanocapsules were suitable for their application in the *in vivo* experiments. Bedaquiline DL% show similar results than for the non-fluorescent nanocapsules and, as evidenced in the *in vitro* antibacterial activity experiments, BQ concentration is enough to kill bacteria. Regarding fluorescence, it is expected that it is enough to follow the fate of the nanocapsules in the *in vivo* experiments, as fluorescence could not be increased as when 200 µg of fluorophore were added, fluorescence did not increase and excess DID oil was not encapsulated.

As previously stated, trimannose can interact with mannose receptors in macrophages surface and therefore enhance internalization in these cells.[54] It is expected that this will increase internalization in macrophages in comparison with non-grafted nanocapsules.

2.9. Optimization of daptomycin-loaded nanocapsules

The synthesis method used in this work to obtain nanocapsules containing daptomycin is the same one than the one used for the encapsulation of bedaquiline. As explained before, the nanocapsules is based in the synthesis of a nanoemulsion and a subsequent coating with the polysaccharide chitosan.

The antibiotic to be encapsulated can be added in several steps of the synthesis or mixed with different phases: organic or aqueous. In this case, the optimization of the nanocapsule synthesis and antibiotic encapsulation was carried out by adding 25 mg of the antibiotic to the aqueous phase or the organic phase before the start of the synthesis to evaluate which method presents better encapsulation efficiency and drug loading. We would expect that daptomycin encapsulation would work better in the aqueous phase, due to its higher solubility in water.

However, due to the small hydrophobic region in its structure and (see Figure 22), addition to the organic phase was also tested. The amount of antibiotic was selected based on the results obtained in the case of bedaquiline. The synthesis steps were similar for both cases: daptomycin was added to the water or ethanol solution in each case and the emulsion was synthesized as previously described for bedaquiline (See section 2.1).

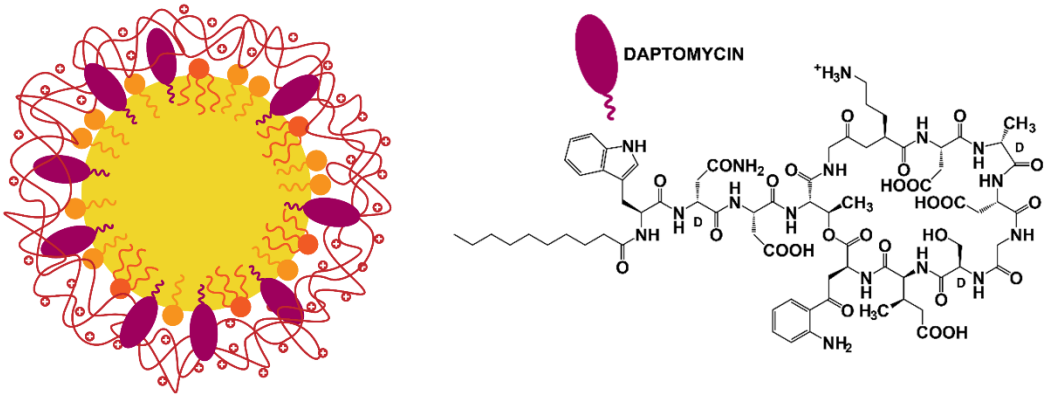

Figure 23. Schematic representation of daptomycin-loaded nanocapsules and the chemical structure of daptomycin

After the synthesis, the first characterization performed was the evaluation of the encapsulation efficiency and drug loading of the nanocapsules. As in the case of bedaquiline, nanocapsule concentration was determined by measurement of the dry weight after freeze-drying. Then, daptomycin concentration was determined by extraction of the antibiotic in methanol, following the same method that for bedaquiline.

Results show that in the case of addition in the aqueous phase, EE% and DL% was 60 and 40%, respectively, while for the organic phase was 14 and 12%, respectively. These high EE% and DL% in the aqueous phase is due to a higher

solubility of the antibiotic in water. During the synthesis, it was observed that daptomycin was not soluble enough in ethanol, as it formed small crystals that probably make difficult the encapsulation of the antibiotic during nanocapsule formation.

Santos Ferreira *et al.*[55] developed poly-epsilon-caprolactone microparticles loaded with daptomycin for the treatment of staphylococcal biofilms. They obtained EE% of 83% with almost 20% DL%. This same authors obtained 95% EE% and 12% DL% for Eudragit RL 100 microparticles[56] and similar results for poly(methyl methacrylate)(PMMA) Eudragit RL 100 (EUD)[57]. The nanocapsules developed in this thesis show higher DL%, although compromising EE% in comparison with other studies. This higher DL% has promising advantages since for the final application lower doses of nanocapsules will be administered to achieve the same concentration of daptomycin.

Hereon, it will always be referred to the daptomycin loaded nanocapsules as the ones synthesized following the method of daptomycin addition to the aqueous phase, as they are the ones that present better results for EE% and DL%. The high values obtained for this parameters are again especially important from the point of view of the economy of the process, to limit the waste of active molecule, and in view of future transfer of this technology to pharmaceutical industry.

2.10. Characterization of daptomycin-loaded nanocapsules

Daptomycin-loaded nanocapsules were characterized by Photo Correlation Spectroscopy (PCS) to determine hydrodynamic diameter, size distribution and ζ potential. As explained before, surface charge and size are important parameters

influencing nanoparticle stability and interaction with biological membranes and it allows us to determine if the capsule is correctly coated.[32]

Water will be the first media of study as daptomycin-loaded nanocapsules are stored as water suspension. Besides, we tested how the presence of salts in the medium affect the nanocapsule stability, as ions can crosslink the nanocapsules due to absorption onto the surface, leading to their aggregation. As in the previous case, nanocapsules were put in contact with PBS and NaCl 0.9% solutions as they are used for the intravenous administration of drugs in clinic and their size distribution was studied by DLS. Results of the size distribution of nanocapsules are shown in Figure 24.

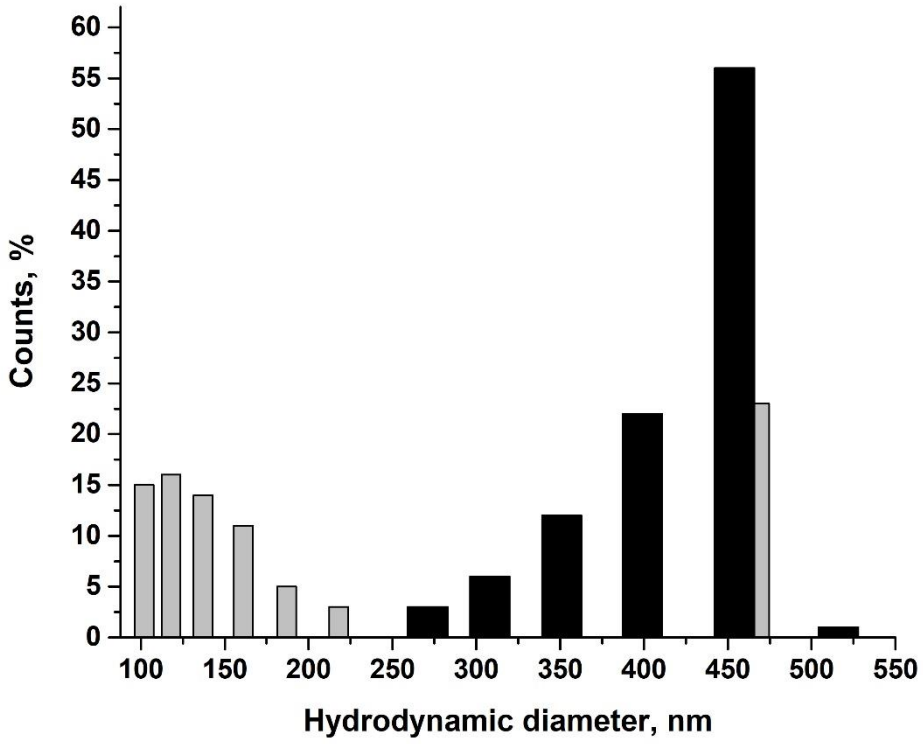

Figure 24. Size distribution measured by Dynamic Light Scattering (DLS) of daptomycin-loaded nanocapsules in water (grey) and NaCl 0.9% (black)

Results observed in Figure 8 show mean diameter for the DP-loaded nanocapsules in water of 280 nm and 420 nm in NaCl 0.9%. However, there is a clear difference in nanocapsule size distribution in this media. In water they present two main populations, one with a mean diameter centered around 140 nm and a bigger one with 460 nm, while in NaCl 0.9% presents a broad size distribution with a bigger mean diameter. Nanocapsules were macroscopically aggregated in PBS so stability in this media was not enough to be able to measure the size distribution by DLS. As in the case of BQ-loaded nanocapsules, it is possible that phosphate ions, with a divalent negative charge, ionically crosslink chitosan chains by its positively charged amino groups, leading to aggregation of the nanocapsules and instability of the whole system.[39]

In view of these results, we selected NaCl 0.9 % as the best physiological solution for the administration of DP-loaded nanocapsules, as nanocapsules are not stable in PBS due to precipitation, although stability is not optimum either in this medium.

We also carried out measurements of surface ζ potential. This will allow to determine if nanocapsules are correctly coated and if the surface ζ potential is enough for the nanocapsules to be considered as a colloidal stable system. Daptomycin-loaded nanocapsules present a ζ potential value of +24 mV, which is an indication of the presence of chitosan on the surface of the capsule. Besides, as explained for BQ-loaded nanocapsules, a value of +24 mV is considered to be enough for the nanoparticles to be considered as a stable colloidal suspension, as the repulsion between the surface charges will be enough to avoid aggregation of the system (Kumer_2017). Another advantage of the positively charged surface at physiological pH is that *Staphylococcus aureus*

has a negatively charged bacterial wall. This means that nanoparticle interaction with cell surface would be improved thanks to the chitosan coated surface of nanocapsules.[58]

2.11. Daptomycin release profile study

Studying the release profile of the antibiotic in different media of relevance is important. It allows to be able to preserve the properties of the nanocapsules for longer periods if the antibiotic is released in one medium less than in other. It can also correlate the antimicrobial activity with the release profile in the media of the *in vitro* assays.

The incubation protocol followed for this medium is similar to the one developed for the bedaquiline loaded nanocapsules. However, some conditions are changed to mimic the antibacterial assay. In this case, as the antimicrobial efficacy assay only last for 24 hours, this was also the incubation time for the release assay, with checkpoints at 30 minutes, 1 and 3 hours.

We selected 6 different media of interest: water, PBS, NaCl 0.9%, Muller Hinton II (MHII) bacterial culture broth, gastric simulated (GS) medium and intestinal simulated (IS) medium. As in the case of the stability in terms of hydrodynamic diameter, water is the storage medium, and will be also considered as the control, while PBS and NaCl 0.9% were selected because of their use in intravenous administration of drugs. Although in this case it was already determined that PBS is not suitable for administration due to lack of stability of nanocapsules, release assay was performed to complete the characterization of nanocapsules.

MHII is the bacterial culture medium in which *Staphylococcus aureus* is cultured and in which the antibacterial activity assays were performed. Understanding the

release during time in this particular medium will allow us to better interpret the results from the antimicrobial activity assays.

Gastric Simulated (GS) and Intestinal Simulated (IS) media were selected to observe the stability of the nanocapsules in view of a possible oral administration.

Measurement of the released antibiotic was performed following a different method compared with BQ-loaded nanocapsules. If we recall from SECTION 2.3, released antibiotic was separated from encapsulated one using a syringe filter. However, after passing daptomycin through both cellulose, PVDF and Nylon filters, more than 50% daptomycin was retained inside. For this reason, a new separation method was developed in which samples were centrifuged at 13000 rpm for 30 minutes to precipitate nanocapsules and separate them from released daptomycin. Released daptomycin was measured in each medium by UV-vis spectroscopy. To check that recovery of released antibiotic was complete, encapsulated bedaquiline remaining inside the nanocapsules was also measured by extraction in methanol. In all of the cases, sum of released and remaining bedaquiline was 100% compared with the initial amount.

The results of release profiles of daptomycin are shown in Figure 25.

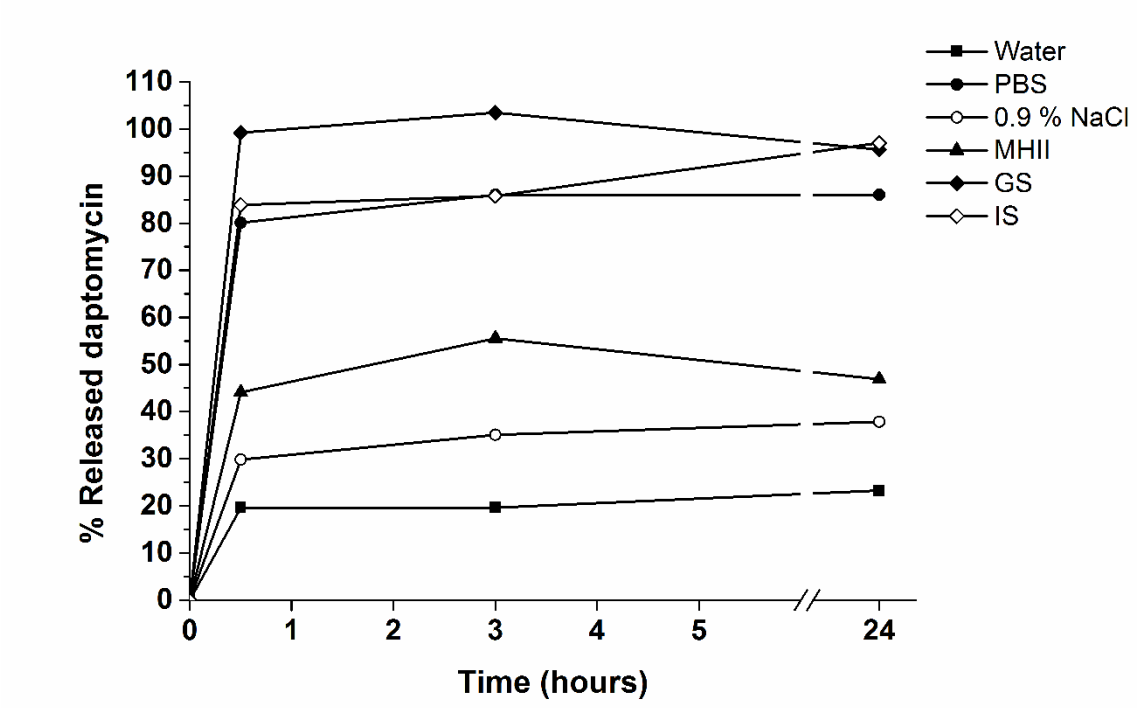

Figure 25. Release profile of daptomycin-loaded nanocapsules in different media of interest

As observed in Figure 25, the daptomycin release profile shows a burst release in the first 30 minutes in all the media studies, but the amount of released drug in very different for each case. In all cases, this release does not increase after 24 hours of incubation. For the storage medium (water), the burst release is the lowest observed, corresponding to 20% of the total daptomycin. This would be considered as the basal state and the rest of the media will be compared with this storage medium. Release is stable after the first 30 minutes, which could mean that after the first burst release, the nanocapsule cargo is stable.

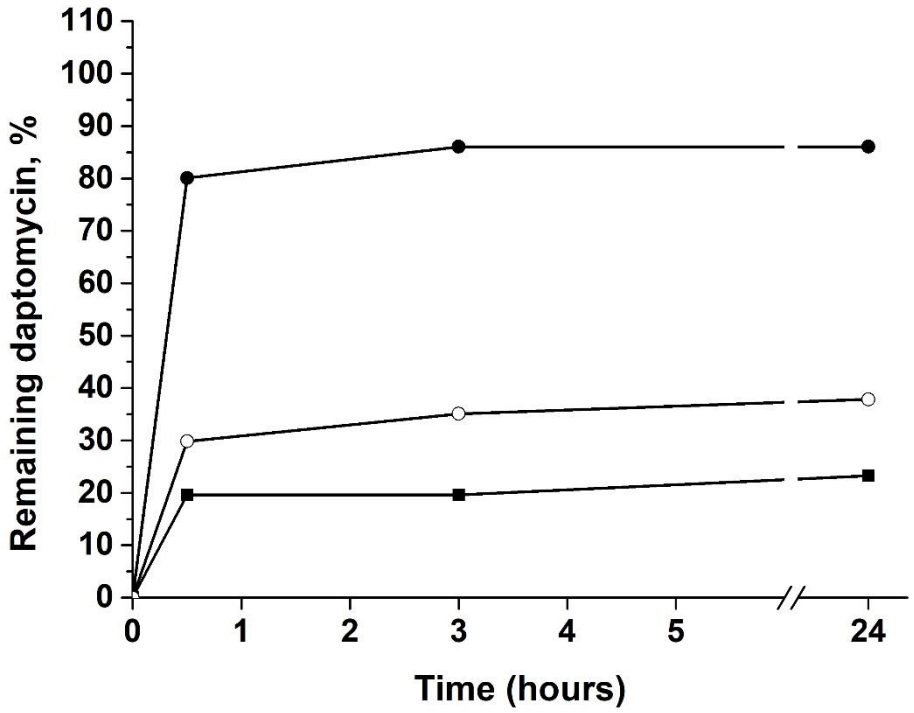

Figure 26. Release profile of daptomicin-loaded nanocapsules in water (■), PBS (●) and NaCl 0.9% (○)

As observed in Figure 26, the amount of daptomycin released in PBS and NaCl 0.9% is very different. In the case of NaCl 0.9%, about 30% release is achieved after 30 minutes, while this value is 80% for PBS. Again, as in the size distribution and as for the case of BQ-loaded nanocapsules, NaCl 0.9% shows better results in terms of stability. This fact agrees with the lower stability towards aggregation observed by DLS, which would mean that daptomycin nanocapsules are not compatible with PBS. For these reasons, NaCl 0.9% will be selected as the administration medium for the rest of the experiments.

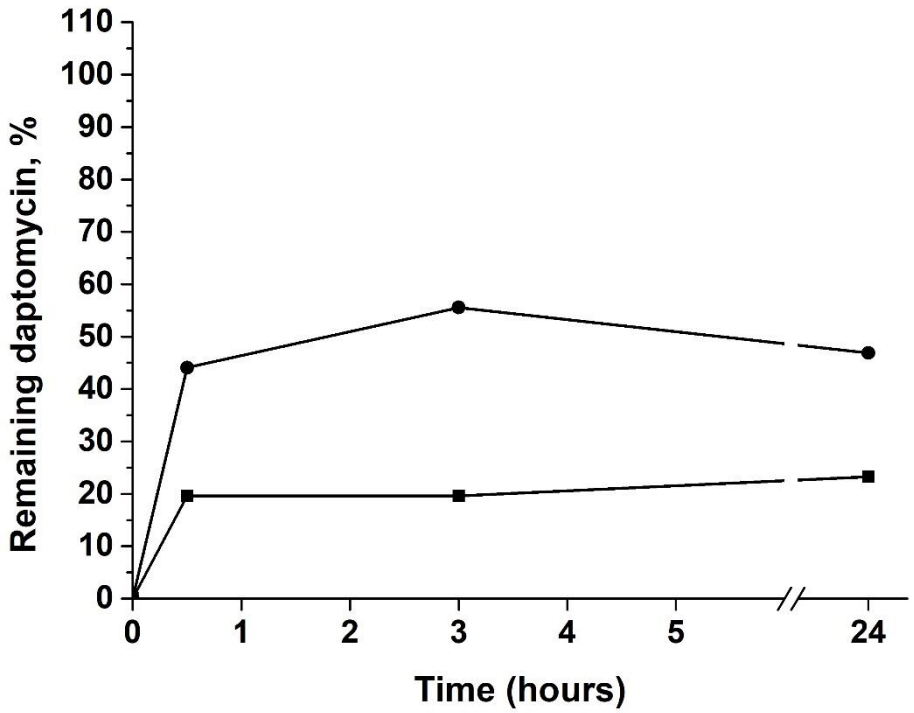

Figure 27. Release profile of daptomycin-loaded nanocapsules in water (■) and MHII (●)

In the case of MHII (Figure 27), burst release is 45% after 24 hours. This value may help us understand the results of the antimicrobial results. MHII is the bacterial culture medium for *Staphylococcus aureus*. As release is almost 50% after only 24 hours, if antimicrobial activity for encapsulated-daptomycin is half in comparison with the same concentration of free daptomycin, only released daptomycin would have antimicrobial activity. This result will allow interpretation of antimicrobial activity assays.

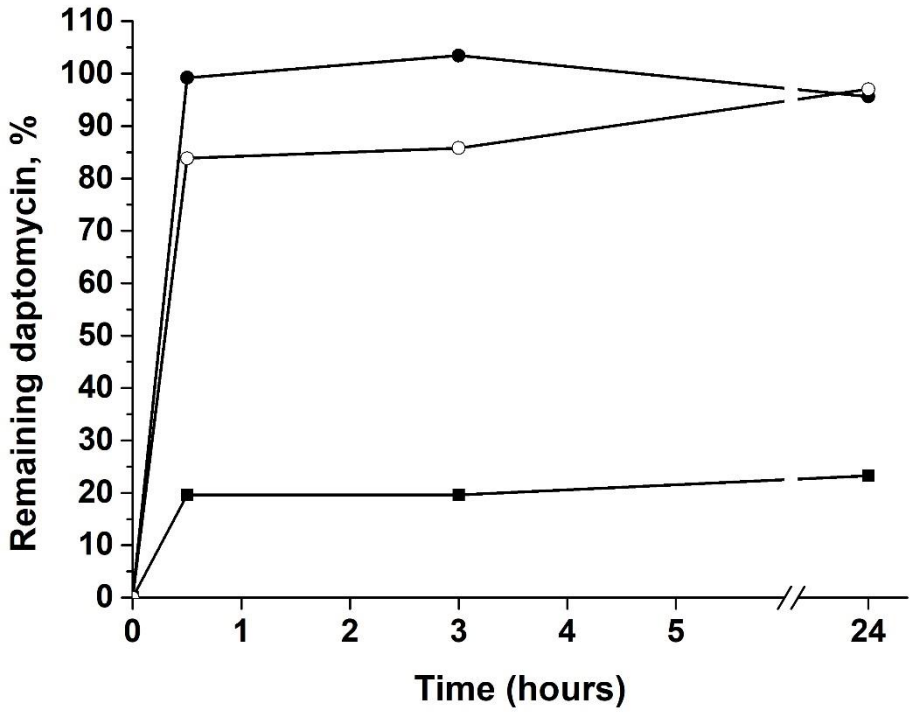

Figure 28. Release profile of daptomycin-loaded nanocapsules in water (■), GS (●) and IS (○)

In Figure 28, it can be observed that our nanocapsules are not good candidates for the oral administration of daptomycin. For both GS and IS media, daptomycin release is more than 80% after 30 min and 90 % after 24 hours. In the case of GS medium, the strong burst release observed may be due to the low pH. This pH changes daptomycin structure which makes it insoluble and can disrupt nanocapsules integrity.[59] This means that this nanocapsules are not suitable for the oral delivery of daptomycin, as cargo is released in the gastric media before absorption in the intestine.

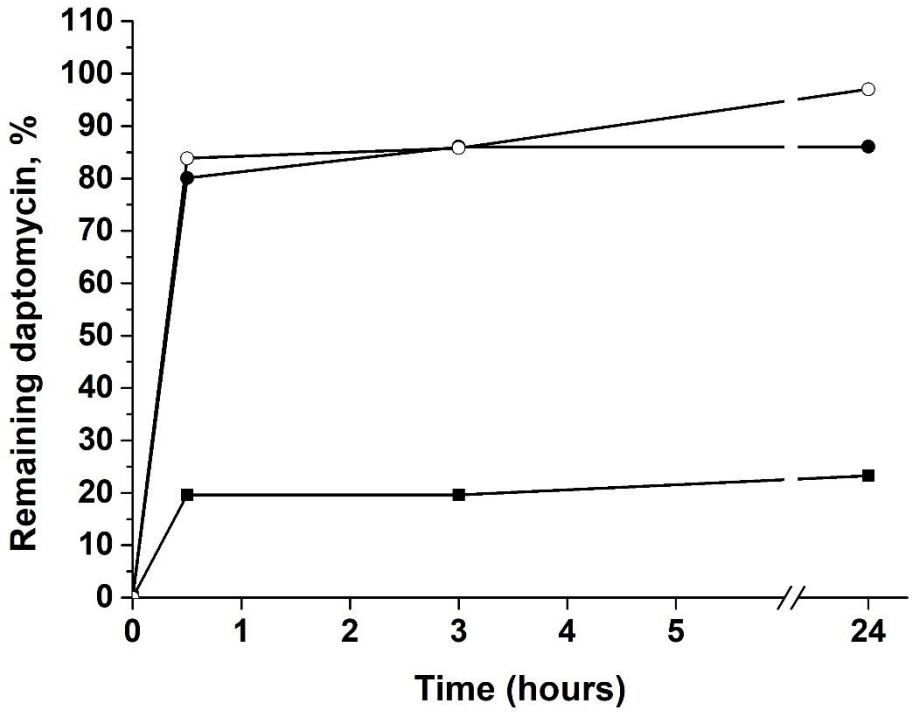

Figure 29. Release profile of daptomycin-loaded nanocapsules in water (■), PBS (●) and IS (○)

As in BQ-loaded nanocapsules, DP-loaded ones are sensitive to the presence of phosphate ions in solution. As observed in the comparison in Figure 29, high values of burst release are observed for the media containing phosphates: PBS and IS. This instability of the drug loading in phosphate media is the same than the one observed for bedaquiline and it seems to depend on the coating of the capsule and not on the encapsulated molecule. The presence of phosphate ions and their interaction with the amino groups in the nanocapsule coating may cause a weakening of the hydrogel coating around the nanoemulsion and therefore lead to loss of antibiotic.

Despite this burst release observed for all the cases, daptomycin drug loading remains the same for the duration of the experiment (24 hours). Although this

burst release is not the ideal behaviour, usually controlled and sustained release is preferred to maintain a stable amount of antiobiotic over time, this study will help understand the antimicrobial effects observed. Also, it allowed the selection of NaCl 0.9% as administration media and discarding of a possible oral delivery due to low stability of the cargo in gastric simulated media. Besides, after the first 30 minutes, no more daptomycin is released, so this first burst release would be a stabilization of the nanocapsule in the media and it is not too high in the media of interest such as MHII or NaCl 0.9 %.

2.12. Antibacterial activity against *Staphylococcus aureus* of daptomycin-loaded nanocapsules

After evaluation of the stability and characteristic of daptomycin-loaded nanocapsules, the next step was to evaluate its antimicrobial activity. The antibacterial activity was studied against two strains of *Staphylococcus aureus*: the strain CECT 794, a meticillin-sensitive pathogen, and the strain CECT 5190, a meticillin-resistant strain. It is important to test the nanocapsules against both types of strains, as the treatment of *Staphylococcus aureus* meticillin-resistant bacteria is very challenging and daptomycin is one of the antibiotics that are being used to fight these infections, as it has proven to be very effective against this strains. However, we should also check its effectiveness against a sensitive strain as a control.

The antibacterial activity was studied in terms of Minimal Inhibitory Concentration (MIC), which is the minimum concentration of the antibiotic that inhibits the growth of the bacteria in a cell culture. This MIC value for encapsulated daptomycin was compared with the activity of the free antibiotic as a control.

Bacteria were cultured following a standard protocol. Different amounts of the antibiotic, either free or encapsulated, were incubated with bacteria for 18 hours and the viability of the culture was tested by adding resazurin to the culture. Resazurin is a blue-colored compound that is reduced to resorufin by living cells, producing a change in color from blue to pink. This change in color allows to determine the presence of viable cells in the cell or bacterial culture in this case. (See Figure 30).

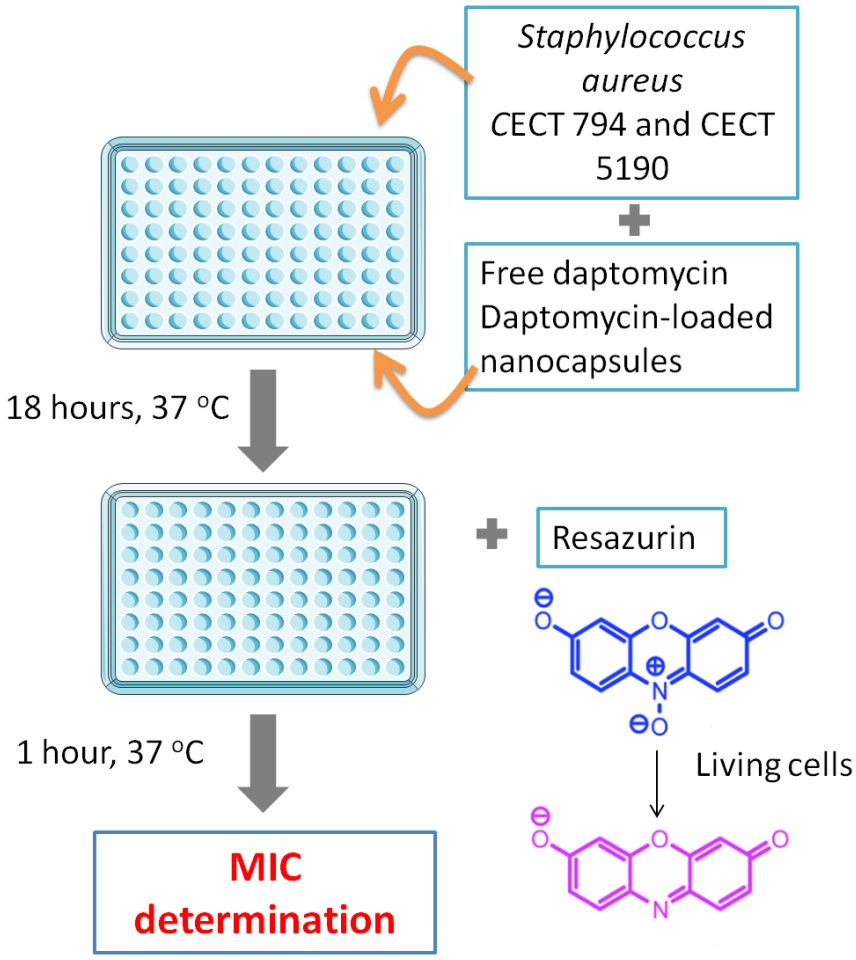

Figure 30. Resazurin assay squeme for the determination of MIC of daptomycin-loaded nanocapsules against MSSA and MRSA

The results obtained showed good antibacterial activity of the nanocapsules as the MIC observed is the same as for the free antibiotic for both strains and has a value of 0.25 mg/mL. If we recall from Figure 27, the amount of antibiotic released

after 24 hours in MHII medium (the medium used in the experiment) was about 50% of the total daptomycin in the experiment. This means that free daptomycin in the nanocapsule well is only 50% of the total antibiotic added and the other half is still encapsulated. As the MIC the same for both free and encapsulated daptomycin, it can be concluded that antimicrobial activity of daptomycin-loaded nanocapsules is not only due to released daptomycin and encapsulated one is playing a role in order to achieve the same activity. Nanocapsules might be internalized or adhere to the cell, producing an increase in the amount of the antibiotic against the bacteria that would lead to the antimicrobial activity observed. This is in agreement with the fact that bacterial cell wall is negatively charged and it would be easy that the positively charged nanoparticles would interact with it, facilitating nanocapsule internalization. However, this hypothesis has not been checked yet. To check it, in the future, fluorescent daptomycin-loaded nanocapsules can be produced to check the fate of nanocapsules and observe internalization.

Although it is unclear how the nanocapsules have the same activity than free daptomycin, it can be hypothesized that nanocapsules are able to deliver daptomycin near the bacterial membrane or even internalize and release the cargo inside the bacteria. The most positive result is that the antibiotic keeps its antibacterial activity after the encapsulation and the process does not affect the antibiotic effectiveness. This nanovehicles were therefore applied to *in vivo* studies to evaluate antimicrobial activity and biodistribution.

3. Conclusions

In this chapter, we presented the optimization of the synthesis of drug-loaded nanocapsules for the treatment of infectious diseases. Two different drugs have been successfully encapsulated into the same type of nanocarrier and the developed nanocapsules have been characterized.

The synthesis process was already optimized for the development of empty nanocapsules in a previous work, but here we tested the suitability for the encapsulation of both hydrophobic and hydrophilic drugs. The tested drugs present good encapsulation efficiencies and drug loadings, regardless of the nature of the antibiotic. It was expected that bedaquiline, due to its hydrophobic nature, showed good compatibility with the hydrophobic core of the nanocapsules, which was demonstrated by the good EE% results. However, we could observe also good EE% and DL% values for the hydrophilic drug daptomycin, which is probably explained by the amphiphilic nature of the molecule. The hydrophobic tail of the antibiotic can be inserted into the surfactant layer, which would explain the good results.

After characterization of the nanoparticle size distribution, we could observe that all the developed nanocapsules presented a mean diameter in the submicrometric range (100-400 nm), which, as already mentioned, is in an appropriate range to promote interaction with living cells. Besides, ζ Potential was in agreement in all of the cases with the polymer coating used, which therefore served as an indicator that the nanocapsules were correctly coated. Besides, mean diameter of bedaquiline-loaded nanocapsules was appropriate for internalization into macrophages, which are the target tissue of this nanoparticles.

For both antibiotic-loaded nanocapsules, administration was chosen to be carried out in a saline solution containing NaCl 0.9%, as we observed that PBS destabilized the capsules leading to aggregation of the samples. This destabilization was in agreement with the data obtained in the release profiles assays of these drugs in the presence of PBS, in which the cargo was not stable either. This led to the conclusion that phosphate ions interact with chitosan amino groups, crosslinking nanocapsules and weakening polymer coating around the nanoemulsion core.

This aggregation in the presence of PBS was partially avoided in bedaquiline-loaded nanocapsules by the grafting of the surface with PEG molecules, which allowed to obtain more stable nanocapsules both in terms of tendency to aggregation and drug release. This protocol also served as an optimization of the grafting process of the nanocapsules surface as a model to be applied for other biomolecules. In our case, we carried out trimannose fuctionalization of the surface of fluorescent bedaquiline-loaded nanocapsules. Trimannose molecule can interact with the receptors of infected macrophages, therefore increasing internalization of the nanocapsules and in the end, increasing effectiveness of the treatment.

In the end, antimicrobial assays of the nanocapsules against *Staphylococcus aureus* or *Mycobacterium tuberculosis*, depending on the antibiotic encapsulated, showed that all of the nanocapsules present antimicrobial activity, which indicated that the cargo is protected in the core, and the encapsulation process does not damage the drug. In both cases, both released antibiotic in the media and encapsulated one played a role in the antimicrobial activity, so internalization or interaction of nanoparticles with bacterial surface need to play a role.

4. Materials and methods

4.1. Materials

Tween® 20 and absolute ethanol were purchased from Panreac. Span® 85 (sorbitane trioleate), oleic acid (90%), chitosan (medium molecular weight) and resazurin were obtained from Sigma-Aldrich. Bedaquiline was adquired from AURUM Pharmatech LLC (Franklin Park, NJ, USA). Daptomycin was purchased from Selleckchem.com. Bis(sulfosuccinimidyl) suberate (BS3) was purchased from Pierce Biotechnology Inc (Rockford, IL, USA) and α-methoxy-ω-amino poly(ethylene glycol) (PEG-MW 5000 Dalton) from IRIS Biotech GmbH (Marktredwitz, Germany). 4-aminobutyl 2-O-(a-D-mannopyranosyl) 2-O-(a-D-mannopyranosyl) a-D-mannopyranoside was obtained from Omicron Biochemicals Inc. The fluorophore DiD oil (DiD' oil; DiIC18(5) oil (1,1'-Dioctadecyl-3,3,3',3'-Tetramethylindodicarbocyanine Perchlorate) was from ThermoFisher.

Phosphate Buffered Saline (PBS) without PBS without Ca^{++}, Mg^{++} or phenol red and RPMI (Roswell Park Memorial Institute) medium were obtained from Lonza. BBL™ Mueller Hinton II (MHII) Broth Cation Adjusted is from BD Diagnostics. Middlebrook 7H9 medium is from Difco and it is supplemented with 10% ADC (0.5% bovine serum albumin, 0.2% dextrose, 0.085% NaCl, 0.0003% beef catalase) also from Difco, and with glycerol (0.5%). BBL™ Mueller Hinton II (MHII) Broth Cation Adjusted is from BD Diagnostics.

Gastric Simulated medium (GS) and Intestinal Simulated medium (IS) were prepared as an enzyme free version of Marques et al (Marques, 2011). GS

contains 34.2 mM NaCl and pH 1.3. Intestinal simulated medium (IS) 2.7 mM KCl, 136.9 mM NaCl, 10.1 mM HNa_2HPO_4, 1.8 mM KH_2PO_4 and pH 7.

Millipore Biomax 300kDa Ultrafiltration Discs were purchased from Merck Millipore.

4.2. Synthesis of bedaquiline-loaded nanocapsules

The general method for the synthesis of bedaquiline-loaded nanocapsules was slightly modified from the already reported protocol for the obtaining of empty nanocapsules (De Matteis *et al.*, 2016). Firstly, different amounts of bedaquiline (2, 3.5, 5, 10 or 25 mg) were mixed with 100 µL absolute EtOH and 40 mg of oleic acid. Then, this solution was incorporated to an organic solution composed of 8.6 mg Span 85 in 4 mL absolute ethanol. This solution was added dropwise to an aqueous phase containing 13.6 mg Tween 20 in 8 mL MilliQ water under magnetic stirring. The solution was left under stirring for 15 minutes for the formation of the nanoemulsion and then we added 2.5 mg of a 5 mg/mL chitosan solution in acetic acid 1% (v/v). After another 15 minutes of stirring, the chitosan-coated nanoemulsion was added to 15 mL of 50 mM Na_2SO_4 under manual stirring. Capsules were separated from Na_2SO_4 through ultracentrifugation (24000 rpm, 30 minutes, 10˚C), washed with 10 mL of milliQ water, centrifuged again and resuspended in water. The concentration of the nanocapsules in water suspension was obtained by measuring the weight of 200 µL of sample after freeze-drying.

4.3. Synthesis of fluorescent bedaquiline-loaded nanocapsules

The method for the synthesis of fluorescent nanocapsules was similar to the previously reported one. In this case, 100 µg of the fluorophore DiD oil was mixed with the organic phase before its addition to the aqueous phase. The rest of the protocol was kept the same.

4.4. Synthesis of daptomycin-loaded nanocapsules

The method for the synthesis for the daptomycin-loaded nanocapsules was similar that for the bedaquiline-loaded ones, but in this case, due to the hydrophilicity of the antibiotic, DP was mixed with the aqueous phase instead than with the organic one. 25µL of daptomycin were mixed with 100 µL absolute ethanol for sterilization and then added to the aqueous phase containing 13.6 mg Tween 20. Then, the organic phase containing 8.6 mg Span 85 and 40 mg oleic acid in 4 mL absolute ethanol was added dropwise to the aqueous phase under magnetic stirring. As for the bedaquiline-loaded nanocapsules, the solution was left under stirring for 15 minutes for the formation of the nanoemulsion and then we added 2.5 mg of a 5 mg/mL chitosan solution in acetic acid 1% (v/v). After another 15 minutes of stirring, the chitosan-coated nanoemulsion was added to 15 mL of 50 mM Na_2SO_4 under manual stirring. Capsules were separated from Na_2SO_4 through ultracentrifugation (24000 rpm, 30 minutes, 10˚C), washed with 10 mL of milliQ water, centrifuged again and resuspended in water. The concentration of the nanocapsules in water suspension was obtained by measuring the weight of 200 µL of sample after freeze-drying. Determination of drug encapsulation efficiency and drug loading

For all the types of nanocapsules, 1.5 mg of particles were mixed with 900 µL methanol and sonicated for 30 minutes, in order to extract the encapsulated drug. The absorbance of the sample was measured at the adequate for each drug using a Varian Cary 50 UV/Vis spectrophotometer. Previously, a calibration curve of the drug in methanol was obtained.

The absorbance at 333 nm was used for bedaquiline and at 369 nm for daptomycin.

Two values are calculated for the evaluation of the efficiency of the process, encapsulation efficiency and drug loading:

- **Encapsulation efficiency:** is the parameter that expresses the total amount of the drug that was successfully encapsulated in comparison to the amount initially added to the synthesis.

- **Drug loading:** this value expresses the amount of drug inside the capsules with respect to the total amount of capsules mass.

4.5. Characterization of the nanocapsules

Dynamic Light Scattering (DLS) analysis has been carried out using a Brookhaven 90Plus DLS instrument. Nanoparticle hydrodynamic diameter and polydispersity index (PDI) has been measured in milliQ water at the concentration of 0.05 mg/mL.

Electrophoretic mobility (Z Potential) of nanoparticles has been determined by measuring the potential of a 0.1 mg/mL nanoparticle suspension in 1 mM KCl with a Plus Particle Size Analyzer (Brookhaven Instruments Corporation).

4.6. Stability of nanocapsules

Nanocapsules hydrodynamic diameter was measured in PBS and NaCl 1% at a concentration of 0.05 mg/mL and compared with the measurement in pure water in order to determine the stability and tendency to aggregate in the presence of salts.

4.7. Surface amino content of bedaquiline-loaded nanocapsules

The amount of amino groups on nanocapsule surface was measured by the Orange II spectrophotometric assay. 0,5 mg of nanocapsules were mixed with 1 mL of 2 mM Orange II sodium salt solution in pH 3 HCl solution and kept for 30 minutes at 40 °C. Capsule suspension was passed through a syringe membrane filter (Millex syringe-driven filter unit, PVDF filter with 0,22 µm pores, purchased from Merck Millipore) to retain nanocapsules in the membrane to separate them from the Orange II solution. After that, a pH 3 HCl solution was passed through the same filter until all the unbound dye was removed from the nanocapsules (verified by UV/Vis spectrophotometric measurement of the filtrated fractions). Then, a pH 12 NaOH solution was passed in order to desorb the bound dye from amino groups in the surface of the capsules. The washing fractions were collected and the pH was adjusted at 3. The final volume was measured and the absorbance of these solutions was measured at 480 nm using a Varian Cary 50 UV/Vis spectrophotometer in order to determine the amount of bound and unbound dye. A calibration curve was done to determine the molar extinction coefficient of the compound at pH 3.

4.8. Grafting of the bedaquiline-loaded nanocapsule surface with PEG5000 or trimannoside

Bedaquiline-loaded nanocapsules were grafted with PEG5000, while the fluorescent ones were functionalized with trimannoside (4-aminobutyl 2-O-(α-d-mannopyranosyl) 2-O-(α-d-mannopyranosyl) α-d-mannopyranoside). In both cases, 20 mg of nanocapsules at a concentration of 2 mg/mL in borate buffer 10 mM pH 8.3 were put in contact with 1 µmol of the linker bis(sulfosuccinimidyl) suberate (BS^3) (50 nmol/mg_{NC}) and they were kept under stirring for 30 minutes. Then, a double amount of the corresponding ligand was added and the mixture was kept under stirring for 2 hours at 37 ˚C. Finally, 20 mL of Tris-HCl buffer 10 mM pH 8.0 was added to quench the linker that eventually didn't reacted with PEG. In the case of fuctionalization with trimannoside, quenching was not carried out to avoid leakage of the fluorophore.

Grafted nanocapsules were filtered in an Amicon Ultrafiltration unit using Millipore Biomax 300 kDa Ultrafiltration Discs to separate them from unreacted PEG or trimannoside. Then, they were washed with milliQ water and concentrated to a final volume of 2 mL.

4.9. Release study of bedaquiline-loaded nanocapsules

Release profile of the bedaquiline-loaded nanocapsules and the PEG-grafted bedaquiline-loaded nanocpaules was studied in water, phosphate buffer solution (PBS), Middlebrooke 7H9, RPMI cell culture medium, GS and IS media. For each media and time point, 50 µL of a 30 mg/mL capsules solution was mixed with 0.95 mL of each studied medium and incubated at 37 °C during 1, 2, 3 and 7 days. At each time point, the solution was passed through a syringe membrane filter (Millex syringe-driven filter unit, PVDF filter with 0.22 µm pores, from Merck

Millipore) to separate the nanocapsules from the medium. Then, 900 µL methanol were passed through the filter to break the capsules and extract the antibiotic. The concentration was measured spectrophotometrically at 333 nm. The amount of released bedaquiline was obtained as the difference between the measured amount and the initial amount of drug. At least three replicas were performed for each point.

4.10. Release study of daptomycin-loaded nanocapsules

Release profile of the daptomycin-loaded nanocapsules was studied in water, phosphate buffer solution (PBS), MHII, gastric simulated medium (GS) and intestinal simulated medium (IS). 50 µL of a 20 mg/mL capsules solution was mixed with 0.95 mL of each medium and incubated at 37 °C during 0.5, 3 and 24 hours. The solution was centrifuged for 30 minutes, at 13000 r.p.m. to separate the nanocapsules from the medium and the supernatants were collected. The amount of daptomycin in the media was measured spectrophotometrically at 365 nm. At least three replicas were performed for each point.

4.11. *In vitro* antimicrobial activity assessment of bedaquiline-loaded nanocapsules

The following experiments were performed by Dr. Ainhoa Lucía Quintanar, as part of the NAREB project.

Mycobacterium tuberculosis (reference strain, H37Rv) cultures were routinely grown at 37 °C in Middlebrook 7H9 medium supplemented with 10% ADC and 0.05% Tween® 80. The Minimum Inhibitory Concentration (MIC) was determined using the Resazurin Microtiter Assay Plate (REMA) (Palomino_2002). Briefly, a range of concentrations of bedaquiline-loaded nanocapsules were added in 96-

well plates to 100 µL of Middlebrook 7H9 medium supplemented with 10% ADC and 0.5% glycerol. As a control, both empty nanoparticles and free bedaquiline were also tested. Bacteria were inoculated by adding 100 µL of a suspension of 10^5 cfu/mL, as estimated by optical density and prepared from a culture in exponential growth phase. After 6 days of incubation at 37 °C, 30 µL of resazurin (0.01% w/v) was added to each well, incubated 48 h at 37 °C, and assessed for colour change. A change from blue to pink indicates bacterial growth. The MIC is defined as the lowest drug concentration that prevents this color change.

4.12. *In vitro* antimicrobial activity assessment of daptomycin-loaded nanocapsules

The *in vitro* activity test of daptomycin-loaded nanocapsules was carried out using too different bacterial strains: *Staphylococcus aureus* CECT 794 (methicillin sensitive) and CECT 5190 (methicillin resistant).

In a 96-well plate, different concentrations of daptomycin-loaded nanocapsules and free bedaquiline were mixed in a total volume of 100 µL MHII medium. Then, 100 µL of a 10^5 c.f.u./mL bacterial culture were added to each well.

Several control wells are established: a positive control in which 100 µL of a 10^5 c.f.u./mL bacterial culture is added to 100 µl of MHII medium; a negative control in which we only had 200 µl MHII medium; and a strain viability test in which 100 µL of a 10^5 c.f.u./mL bacterial culture is added to 100 µL of MHII medium with different concentrations of free vancomycin.

Bacteria are incubated for 18 hours at 37 ºC and MIC is recorded adding 30 µL of a resazurin solution 0.01% w/v and checking color change from blue to pink after 1 hour.

5. References

(1) Leung, E.; Weil, D. E.; Raviglione, M.; Nakatani, H. *Bull. World Health Organ.* **2011**, *89* (5), 390–392.

(2) Pacios, O.; Blasco, L.; Bleriot, I.; Fernandez-Garcia, L.; Bardanca, Mónica González Ambroa, A.; López, M.; Bou, G.; Tomas, M. *Antibiotics* **2020**, *9* (65), 1–20.

(3) Willyard, C. *Nature* **2017**, *543* (7643), 15.

(4) Kalhapure, R. S.; Suleman, N.; Mocktar, C.; Seedat, N.; Govender, T. *J. Pharm. Sci.* **2015**, *104* (3), 872–905.

(5) Nathan, C. *Nature* **2004**, *43* (October), 899–902.

(6) World Health Organization. *Global action plan on antimicrobial resistance*; 2015.

(7) WHO. *PRIORITIZATION OF PATHOGENS TO GUIDE DISCOVERY, RESEARCH AND DEVELOPMENT OF NEW ANTIBIOTICS FOR DRUG-RESISTANT BACTERIAL INFECTIONS, INCLUDING TUBERCULOSIS*; 2017.

(8) Gould, I. M.; David, M. Z.; Esposito, S.; Garau, J.; Lina, G.; Mazzei, T.; Peters, G. *Int. J. Antimicrob. Agents* **2012**, *39* (2), 96–104.

(9) Stefani, S.; Chung, D. R.; Lindsay, J. A.; Friedrich, A. W.; Kearns, A. M.; Westh, H.; MacKenzie, F. M. *Int. J. Antimicrob. Agents* **2012**, *39* (4), 273–282.

(10) Eleraky, N. E.; Allam, A.; Hassan, S. B.; Omar, M. M. *Pharmaceutics* **2020**, *12* (2), 1–51.

(11) Villanueva-Flores, F.; Castro-Lugo, A.; Ramírez, O. T.; Palomares, L. A. *Nanotechnology* **2020**, *31* (13).

(12) Lang, X.; Wang, T.; Sun, M.; Chen, X.; Liu, Y. *Int. J. Biol. Macromol.* **2020**, *154*, 433–445.

(13) Pelgrift, R. Y.; Friedman, A. J. *Adv. Drug Deliv. Rev.* **2013**, *65*, 1803–1815.

(14) Shao, K.; Zhang, Y.; Ding, N.; Huang, S.; Wu, J.; Li, J.; Yang, C.; Leng, Q.; Ye, L.; Lou, J.; Zhu, L.; Jiang, C. *Adv. Healthc. Mater.* **2014**, *4* (2), 291–300.

(15) Boisseau, P.; Loubaton, B. *Comptes Rendus Phys.* **2011**, *12* (7), 620–636.

(16) Steenbergen, J. N.; Alder, J.; Thorne, G. M.; Tally, F. P. *J. Antimicrob. Chemother.* **2005**, *55* (3), 283–288.

(17) Straus, S. K.; Hancock, R. E. W. *Biochim. Biophys. Acta - Biomembr.* **2006**, *1758* (9), 1215–1223.

(18) Gray, D. A.; Wenzel, M. *Antibiotics* **2020**, *9* (1).

(19) Lange, C.; Abubakar, I.; Alffenaar, J. W. C.; Bothamley, G.; Caminero, J. A.; Carvalho, A. C. C.; Chang, K. C.; Codecasa, L.; Correia, A.; Crudu, V.; Davies, P.; Dedicoat, M.; Drobniewski, F.; Duarte, R.; Ehlers, C.; Erkens, C.; Goletti, D.; Günther, G.; Ibraim, E.; Kampmann, B.; Kuksa, L.; De Lange, W.; Van Leth, F.; Van Lunzen, J.; Matteelli, A.; Menzies, D.; Monedero, I.; Richter, E.; Rüsch-Gerdes, S.; Sandgren, A.; Scardigli, A.; Skrahina, A.; Tortoli, E.; Volchenkov, G.; Wagner, D.; Van Der Werf, M. J.; Williams, B.; Yew, W. W.; Zellweger, J. P.; Cirillo, D. M. *Eur. Respir. J.* **2014**, *44* (1), 23–63.

(20) Diacon, A. H.; Pym, A.; Grobusch, M. P.; de los Rios, J. M.; Gotuzzo, E.; Vasilyeva, I.; Leimane, V.; Andries, K.; Bakare, N.; De Marez, T.; Haxaire-Theeuwes, M.; Lounis, N.; Meyvisch, P.; De Paepe, E.; van Heeswijk, R. P. G.; Dannemann, B. *N. Engl. J. Med.* **2014**, *371* (8), 723–732.

(21) Mahajan, R. *Int. J. Appl. Basic Med. Res.* **2013**, *3* (1), 1.

(22) De Matteis, L.; Alleva, M.; Serrano-Sevilla, I.; García-Embid, S.; Stepien, G.; Moros, M.; De La Fuente, J. M. *Mar. Drugs* **2016**, *14* (10), 175.

(23) Rajaonarivony, M.; Vauthier, C.; Couarraze, G.; Puisieux, F.; Couvreur, P. *J. Pharm. Sci.* **1993**, *82* (9), 912–917.

(24) McClements, D. J.; Rao, J. *Crit. Rev. Food Sci. Nutr.* **2011**, *51* (4), 285–330.

(25) Bouchemal, K.; Briançon, S.; Perrier, E.; Fessi, H. *Int. J. Pharm.* **2004**, *280*, 241–251.

(26) Tavares, I. S.; Caroni, A. L. P. F.; Neto, A. A. D.; Pereira, M. R.; Fonseca, J. L. C. *Colloids Surfaces B Biointerfaces* **2012**, *90* (1), 254–258.

(27) Berthold, A.; Cremer, K.; Kreuter, J. *J. Control. Release* **1996**, *39* (1), 17–25.

(28) Soria-Carrera, H.; Lucía, A.; De Matteis, L.; Aínsa, J. A.; de la Fuente, J. M.; Martín-Rapún, R. *Macromol. Biosci.* **2019**, *19* (4), 1–11.

(29) De Matteis, L.; Jary, D.; Lucía, A.; García-Embid, S.; Serrano-Sevilla, I.; Pérez, D.; Ainsa, J. A.; Navarro, F. P.; M. de la Fuente, J. *Chem. Eng. J.* **2018**, *340*, 181–191.

(30) Poh, W.; Ab Rahman, N.; Ostrovski, Y.; Sznitman, J.; Pethe, K.; Loo, S. C. J. *Drug Deliv.* **2019**, *26* (1), 1039–1048.

(31) Ritsema, J. A. S.; Herschberg, E. M. A.; Borgos, S. E.; Løvmo, C.; Schmid, R.; te Welscher, Y. M.; Storm, G.; van Nostrum, C. F. *Int. J. Pharm.* **2018**, *548* (2), 730–739.

(32) Bannunah, A. M.; Vllasaliu, D.; Lord, J.; Stolnik, S. **2014**.

(33) Alexis, F.; Pridgen, E.; Molnar, L. K.; Farokhzad, O. C. *Mol. Pharm.* **2008**, *5* (4), 505–515.

(34) Clift, M. J. D.; Rothen-Rutishauser, B.; Brown, D. M.; Duffin, R.; Donaldson, K.; Proudfoot, L.; Guy, K.; Stone, V. *Toxicol. Appl. Pharmacol.* **2008**, *232* (3), 418–427.

(35) Couvreur, P.; Puisieux, F. *Adv. Drug Deliv. Rev.* **1993**, *10* (2), 141–162.

(36) Yu, S. S.; Lau, C. M.; Thomas, S. N.; Gray Jerome, W.; Maron, D. J.; Dickerson, J. H.; Hubbell, J. A.; Giorgio, T. D. *Int. J. Nanomedicine* **2012**, *7*, 799–813.

(37) Li, F.; Zhu, A.; Song, X.; Ji, L.; Wang, J. *Int. J. Pharm.* **2013**, *453* (2), 506–513.

(38) He, C.; Hu, Y.; Yin, L.; Tang, C.; Yin, C. *Biomaterials* **2010**, *31* (13), 3657–3666.

(39) Tsai, M. L.; Chen, R. H.; Bai, S. W.; Chen, W. Y. *Carbohydr. Polym.* **2011**, *84* (2), 756–761.

(40) Kumar, A.; Dixit, C. K. *Adv. Nanomedicine Deliv. Ther. Nucleic Acids* **2017**, 44–58.

(41) Cyriac, J. M.; James, E. *J. Pharmacol. Pharmacother.* **2014**, *5* (2), 83–87.

(42) Marques, M. R. C.; Loebenberg, R.; Almukainzi, M. *Dissolution Technol.* **2011**, *18* (3), 15–28.

(43) Starýchová, L.; Žabka, M.; Špaglová, M.; Čuchorová, M.; Vitková, M.; Čierna, M.; Bartoníková, K.; Gardavská, K. *J. Pharm. Sci.* **2014**, *103* (12), 3977–3984.

(44) Nicolas, J.; Mura, S.; Brambilla, D.; Mackiewicz, N.; Couvreur, P. *Chem. Soc. Rev.* **2013**, *42* (3), 1147–1235.

(45) Han, G.; Ghosh, P.; Rotello, V. M. *Mater. Today Proc.* **2018**, *5* (8), 16763–16773.

(46) Guo, X.; Wei, X.; Chen, Z.; Zhang, X.; Yang, G.; Zhou, S. *Prog. Mater. Sci.* **2020**, *107* (April 2017), 100599.

(47) des Rieux, A.; Pourcelle, V.; Cani, P. D.; Marchand-Brynaert, J.; Préat, V. *Adv. Drug Deliv. Rev.* **2013**, *65* (6), 833–844.

(48) Rabanel, J. M.; Hildgen, P.; Banquy, X. *J. Control. Release* **2014**, *185* (1), 71–87.

(49) Dash, B. C.; Réthoré, G.; Monaghan, M.; Fitzgerald, K.; Gallagher, W.; Pandit, A. *Biomaterials* **2010**, *31* (32), 8188–8197.

(50) Zhao, Z.; Li, Y.; Xie, M. Bin. *Int. J. Mol. Sci.* **2015**, *16* (3), 4880–4903.

(51) Pietrelli, L. *Adsorption* **2013**, *19* (5), 897–902.

(52) Palomino, J.-C.; Martin, A.; Camacho, M.; Guerra, H.; Swings, J.; Portaels, F. *Antimicrobail Agents Chemother.* **2002**, *46* (8), 2720–2722.

(53) Hong, G.; Antaris, A. L.; Dai, H. *Nat. Biomed. Eng.* **2017**, *1* (1).

(54) Coya, J. M.; De Matteis, L.; Giraud-Gatineau, A.; Biton, A.; Serrano-Sevilla, I.; Danckaert, A.; Dillies, M. A.; Gicquel, B.; De La Fuente, J. M.; Tailleux, L. *J. Nanobiotechnology* **2019**, *17* (1), 1–15.

(55) Ferreira, I. S.; Bettencourt, A.; Bétrisey, B.; Gonçalves, L. M. D.; Trampuz, A.; Almeida, A. J. *Int. J. Pharm.* **2015**, *485* (1–2), 171–182.

(56) Ferreira, I. S.; Bettencourt, A. F.; Gonçalves, L. M. D.; Kasper, S.; Bétrisey, B.; Kikhney, J.; Moter, A.; Trampuz, A.; Almeida, A. J. *Int. J. Nanomedicine* **2015**, *10*, 4351–4366.

(57) Santos Ferreira, I.; Kikhney, J.; Kursawe, L.; Kasper, S.; Gonçalves, L. M. D.; Trampuz, A.; Moter, A.; Bettencourt, A. F.; Almeida, A. J. *AAPS PharmSciTech* **2018**, *19* (4), 1625–1636.

(58) Gross, M.; Cramton, S. E.; Götz, F.; Peschel, A. *Infect. Immun.* **2001**, *69* (5), 3423–3426.

(59) Taylor, S. D.; Palmer, M. *Bioorganic Med. Chem.* **2016**, *24* (24), 6253–6268.

Chapter 3

Encapsulation of disulfiram for its repurposing as an anticancer and antimicrobial agent

1. Introduction

Developing of new drugs is and expensive and time-consuming process with high failure rates which makes the industry shift to new commercial routes of treatment. Repurposing and repositioning of existing drugs have gained more popularity over the last decades.[1] One of the most prominent advantages is the skipping of the Phase I safety studies in clinical trials. Repurposed drugs enter directly into Phase IIa, which reduces not only time and cost, but also rate of failure.[2] In addition, the synthesis procedures for the drug synthesis can be utilized and there is a potential increase in the patent life of the drug.[3]

Several drugs have been repurposed over the years, one of the most famous examples been Sildenafil. This molecule was originally intended for the treatment of hypertension, but during the clinical trials it was repurposed for the treatment of erectile dysfunction. Other famous drug that could enter the market again thanks to repurposing is thalidomide. This drug was intended for morning sickness, but it is well known because of the severe skeletal birth defects in children born to mothers who took thalidomide during the first trimester of the pregnancy in the late 50's.

However, it was later demonstrated to help with the treatment of leprosy and more recently is being investigated as an anticancer drug.[4] Another drug that is currently been investigated is disulfiram.

Disulfiram, (DSF) commercially available as Antabus, is a member of the dithiocarbamate family. Traditionally, it has been used for the treatment of alcoholism.[5] DSF first used in the 1800's was as a catalyst for rubber production. In 1937, E.E. Williams observed that those workers in contact with DSF experienced unpleasant symptoms such as headache, sweating, abdominal pain etc. after alcohol intake. It was later discovered that this effect was due to the inhibition of the enzyme aldehyde dehydrogenase.[6] It was approved by the FDA to treat alcoholism in 1948. Recently, several other properties of this molecule have been discovered, as it has been demonstrated to have also anticancer activity[7,8], inhibit cataracts formation[9,10] and act as an antimicrobial agent[11–15], amongst others. Within the antimicrobial effects, DSF has demonstrated to have antimicrobial activity against MRSA.[13–15]

In this work, we are going to explore the repurposing of disulfiram as an exploratory work to evaluate its potential activity as an antimicrobial and antitumoral drug. These applications were selected due to their importance and the number of affected people all over the world.

Several trials have tested the anticancer activity of DSF against different types of tumors. These trials have tested the use of DSF for advanced solid malignancies with liver metastasis (ClinicalTrials.gov Identifier: NCT00742911), metastatic melanoma (ClinicalTrials.gov Identifier: NCT00571116, NCT00256230),

glioblastoma (ClinicalTrials.gov Identifier: NCT01777919, NCT01907165), non-small cell lung cancer (ClinicalTrials.gov Identifier: NCT00312819), and prostate cancer (ClinicalTrials.gov Identifier: NCT01118741). Although its mechanism of action is still under study, it is known that DSF inhibits cancer stem cells and proteasome activity and has a potential as an enhancer of the cytotoxicity of other anticancer drugs.[6]

Amongst the difference cancer affecting people worldwide, pancreatic ductal adenocarcinoma is the fourth leading cause of cancer death. It has a 5-year relative survival rate of 8%, due to difficult early diagnosis and high resistance to treatments. Development of new curative approaches to enhance the therapeutic effect will be of great significance in the clinical management of pancreatic cancer.[16]

Several authors have also probed that DSF possesses antibacterial activity against Meticillin-resistant *Staphylococcus aureus*.[11,14] Although the mechanism of action is still unclear, it is known that DSF form disulfides with thiol-bearing substances. Bacteria have several cofactors, metabolites and enzymes with thiol groups that can be modified by DSF. This bond is rapid, which causes an abrupt halt in bacterial metabolism, inhibiting bacterial growth.[11,14] As we have previous experience with the treatment of MRSA, as mentioned in the previous Chapter, repurpose of DSF for the treatment of MRSA infections will be tested.

DSF has been efficiently administered orally for the treatment of alcoholism for many years. However, the instability of this molecule in acidic gastric media makes it impossible to reach the concentration needed for its antimicrobial or anticancer

activity.[17]Another option would be the intravenous administration but it is also hampered by the rapid degradation of this drug in the blood stream.

The use of an efficient drug delivery system would allow to protect DSF under physiological conditions independently of the administration route, allowing us to achieve a more efficient application in the treatment of MRSA infections or cancer treatment.[18] Several works in literature proposed disulfiram encapsulation in PLGA nanoparticles, mostly for cancer treatment, and demonstrated that this strategy leads to better stability of the compound. An improved effect of the encapsulated drug with respect to the free molecule has been observed.[19,20]

Based on these results, in this work, the encapsulation of disulfiram is proposed in nanoemulsion particles stabilized with two natural polysaccharides for the treatment of MRSA infections. These nanocarriers have been previously described by the same authors for the successful of other molecules for the treatment of several diseases[21–24] and had been extensively discussed in Chapter 2. In this chapter, we demonstrated the suitability of the encapsulation system for the stabilization of DSF and its delivery for the treatment of MRSA infections and pancreatic cancer.

Thanks to the hydrophobic core of the nanoformulation and the hydrophobic nature of the drug, encapsulation efficiency and drug loading reached good values. Here, both chitosan and xanthan have been used for the stabilization of the emulsion, to compare how the charge of the nanocapsule surface affects stability and effectiveness of both types of nanocapsules. In comparison with chitosan, already explained and used in Chapter 2, xanthan is negatively charged and has small ramifications in the main polymer chain. Xanthan has proved to be great in stabilizing

nanoemulsions in other works, so it was interesting to evaluate how the change in the polymer would affect nanocapsule stabilization and interaction with cells due to its different charge and structure.[25,26]

The developed nanocarriers were compared and their physicochemical properties as well as encapsulation efficiency and disulfiram loading were analysed. Their potential against pancreatic cancer cells have been analyzed. Finally, their antibacterial efficacy against methicillin-resistant *Staphylococcus aureus* and *in vitro* safety in animal cell culture have been tested. The nanocapsules showed promising results in the preliminary studies carried out in terms of efficacy in comparison with the free drug in both studies, which opens new opportunities for the repurposing of DSF for the treatment of MRSA infections and its application in the treatment of pancreatic cancer.

2. Results and discussion

2.1. Synthesis and optimization of disulfiram-loaded nanocapsules

The method selected for the synthesis of disulfiram-loaded nanocapsules is similar to the one used in Chapter 2 for the encapsulation of bedaquiline and daptomycin. The nanocapsule core is highly suitable for the encapsulation of disulfiram, as both have a hydrophobic nature.

The synthesis method of the nanocapsules is based on spontaneous emulsification in presence of disulfiram, followed by coating with chitosan or xanthan. 25 mg of disulfiram were added to the organic phase, which contained Span 85 and oleic acid dissolved in ethanol. This mixture was added to the aqueous phase containing

Tween 20 to form the nanoemulsion. Thanks to the hydrophobic nature of disulfiram, it was expected that the drug was encapsulated into the nanoemulsion core with high encapsulation efficiency and drug loading. After the addition of the organic phase into the aqueous one, disulfiram-loaded nanoemulsion is spontaneously and rapidly formed. As explained before, the rapid diffusion of the organic solvent into the water phase which causes an increase in oil-water interfacial area, interfacial turbulence and spontaneous formation of droplets. In this case, the polymer is added immediately after the nanoemulsion formation, as it was observed that the emulsion tended to aggregate if it was left under stirring without the stabilization with the polysaccharide.

In this case, two different polysaccharides were used for the stabilization of the nanoemulsion. First, chitosan was used again, as it proved in the previous study to be able to stabilize the emulsion in bedaquiline and daptomycin-loaded nanocapsules. After addition of chitosan into the nanoemulsion solution, the mixture was stirred for 15 minutes to obtain a homogeneous distribution of the polymer chains around the nanoemulsion surface. Then the ionotropic gelation was carried out. In this study, besides the use of chitosan, it was also explored the stabilization of the emulsion with the polysaccharide xanthan. Xanthan is a polysaccharide that has been widely used for the stabilization of nanoemulsions, especially in the food industry, usually as a texture modifier (McClements_2011; Mirhosseini_2008). This polymer was used to explore how a change in the nanocapsule surface affects its effectiveness, stability or interaction with cells. In this case, instead of using Na_2SO_4 as in the case of chitosan, a first attempt of gelation was made using $CaCl_2$, as the

negative charges of xanthan would be crosslinked with the positively charged Ca^{+2}. However, it was observed that even low concentrations of calcium chloride produced huge aggregation in the nanocapsule solution. For this reason, the crosslinking of the xanthan with calcium was skipped, as the polymer is able to produce a gel only in the presence of water. This meant that xanthan gum is able to stabilize the emulsion without the need of addition of any other molecule. Scheme of the nanocapsule structure as well as the chemical structures of the components is shown in Scheme 1.

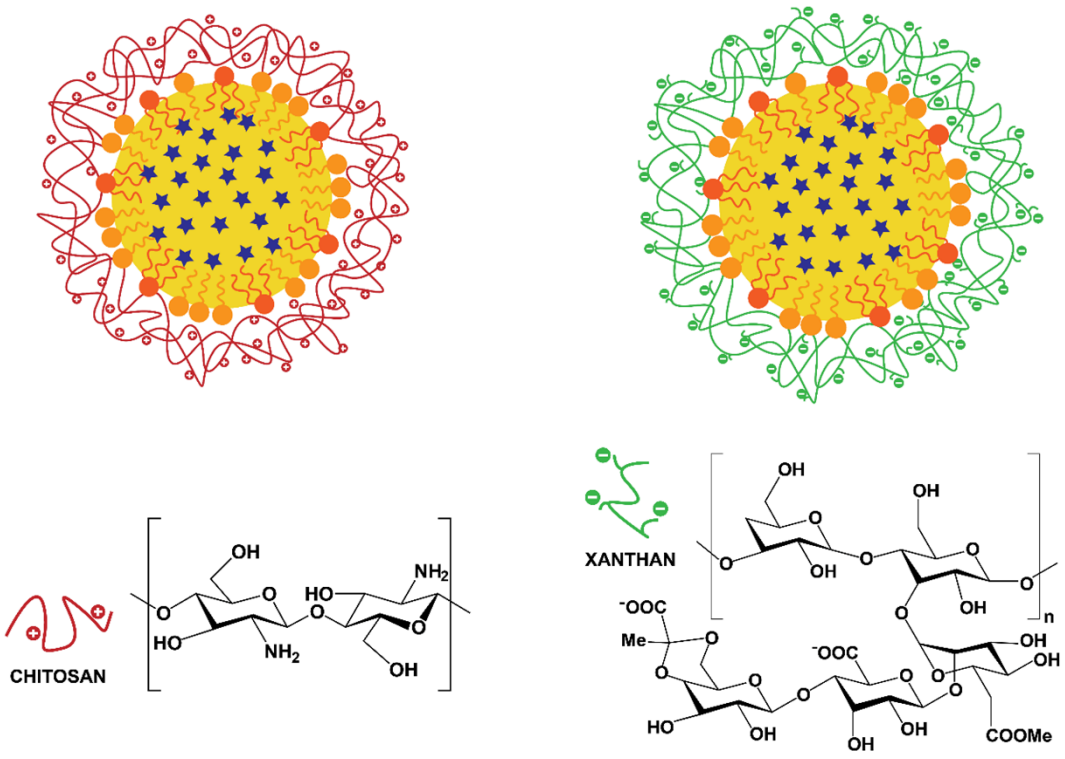

Scheme 1. Schematic representation of nanocapsule structure and chemical structures of their components

After the stabilization of the emulsion with the polymer, the nanocapsules formed were washed to remove non-encapsulated drug. In the case of chitosan-coated

nanocapsules, they were washed by applying two ultracentrifugation steps. However, in the xanthan-loaded ones, nanocapsules did not precipitate after ultracentifugation, even after 2 hours, probably due to the high viscosity of xanthan gum. For this reason, nanocapsules were washed using Amicon® centrifugal filter units, which thanks to the diameter of the pore, retains and concentrates particles but allows water and other molecules to pass through its filter. Nanocapsules were centrifuged three times and fresh water was added after each one, to remove all the non-encapsulated drug.

Once the nanocapsules were formed and purified, it was important to evaluate the effectiveness in the encapsulation of disulfiram. For this purpose, we determined encapsulation efficiency and drug loading as important factors in the pharmaceutical industry for the profitability of the developed system, as previously described in Chapter 2. Encapsulation efficiency (EE%) is defined as the percentage ratio between the amount of drug encapsulated and the drug initially added; while the drug loading (DL%) is described as the percentage ration between the amount of drug encapsulated and the amount of nanocapsule obtained.

For the determination of EE% and DL%, it was necessary to quantify nanocapsule concentration and disulfiram content in the nanocapsules. Firstly, nanocapsules concentration was calculated following the method reported in Chapter 2, by freeze-drying of an aliquot of the nanocapsules suspension and measurement of the dry weight, which allows the calculation of the concentration.

The next step was the quantification of the encapsulated disulfiram. The method is shown in Figure 1.

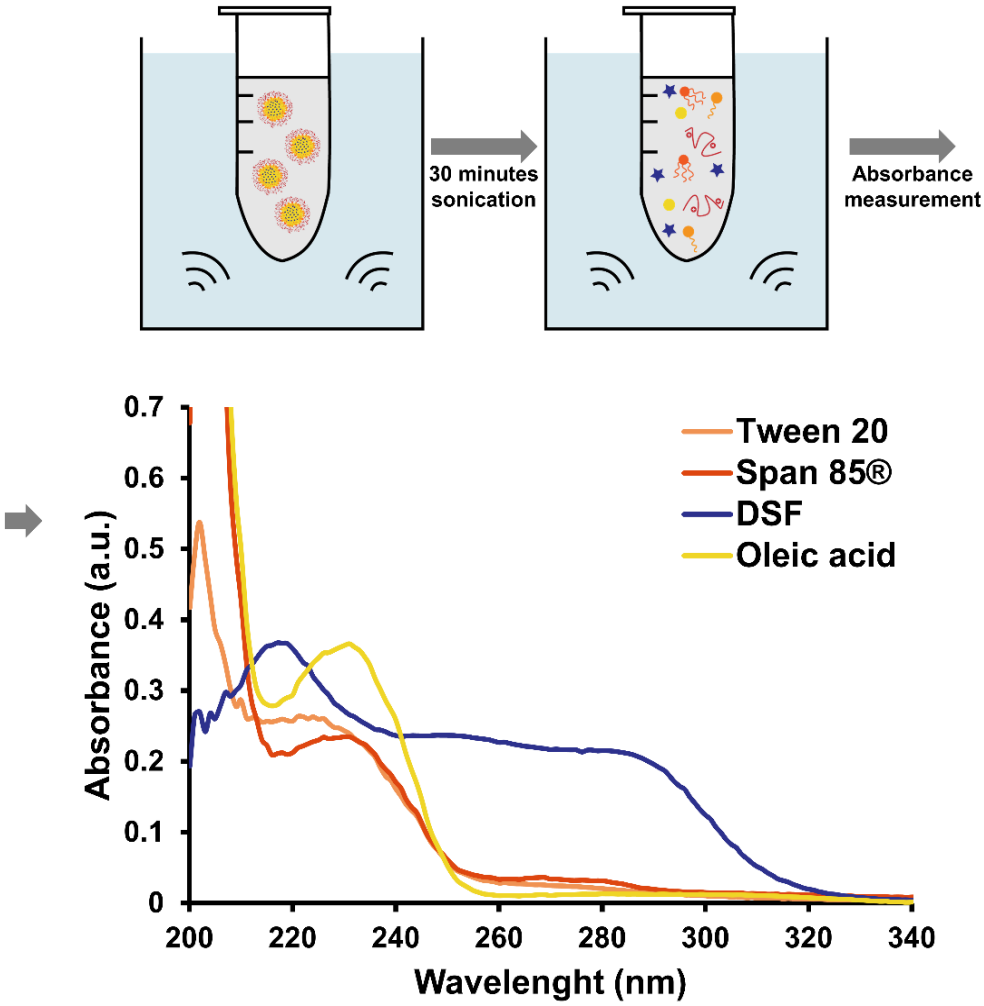

Figure 1. Schematic representation of disulfiram extraction and quantification

As shown in Figure 1, the method used for the quantification of DSF is similar to the one developed in Chapter 2 for the quantification of both bedaquiline and daptomycin. Nanocapsules were mixed with methanol and sonicated for 30 minutes to get the complete extraction of disulfiram. Then, UV-Vis spectrophotometry was carried out to quantify the amount of DSF. DSF presents a peak in the UV-vis spectra

at 280 nm, which does not interfere with the presence of surfactants in the mixture, as they have absorbance in the region of 200-240 nm.

As expected, due to the hydrophobic nature of disulfiram, both developed systems (chitosan and xanthan nanocapsules) probed to be highly efficient in the encapsulation of disulfiram in their lipidic core. Values of encapsulation efficiency (EE%) are 65 ± 5 % for the chitosan-coated nanoparticles and 60 ± 5 for the xanthan-coated ones, while drug loading values (DL%) are 44 ± 3 % and 22 ± 2 %, respectively for the two carriers. These values are comparable to the ones obtained for other molecules such as bedaquiline and daptomycin encapsulated in chitosan-coated carriers. In the case of coating with xanthan, DL% is half than in chitosan-coated nanocapsules. This can be explained by an increase in the total amount of material obtained, as the amount of polymer used in this case to stabilize the emulsion was higher. In the case of xanthan coating, double amount of polymer was added for the stabilization of the nanocapsules.

These values are comparable to the ones presented in similar studies. Wang *et al.*[27] developed long circulating disulfiram-loaded lactic-co-glucolic acid nanoparticles for the treatment of liver cancer, achieving EE% of 78.92 ± 2.16 % and DL% of 27.67 ± 3.47%. Najlah *et al*.[19] investigated the encapsulation of disulfiram into different types of liposomes for the treatment of colorectal cancer, achieving EE% values from 45 to 95% (they did not report DL% values), depending on the liposome composition. Comparing our results with this presented in literature, EE% of both chitosan and xanthan loaded nanocapsules is not the highest reported, but it is in the middle range. In the case of DL%, for chitosan-loaded nanocapsules, the value is higher

than the one reported in other type of nanocapsules in literature, meaning that our capsules are able to encapsulate disulfiram with a great capacity. Higher DL% means lower doses of nanocapsules, which will decrease the secondary effects that may produce nanocapsules themselves and also reduce costs.

2.2. Characterization of disulfiram-loaded nanocapsules

Both types of nanocapsules were characterized by Photon Correlation Spectroscopy (PCS) in order to determine their hydrodynamic diameter, size distribution and Zeta Potential which will allow us to correlate these properties with the antibacterial and anticancer efficacy. In Table 1 the hydrodynamic diameters, polydispersity index and ζ potential of both types of nanocapsules developed are reported.

Table 1. Summary of the charaterization of DSF-loaded nanocapsules

	Hydrodynamic diameter, nm	**Polydispersity index**	**Z Potential, mV**
CS-25	218.7	0.189	+25
XAN-25	91.2	0.222	-24

We can observe that the hydrodynamic diameter of nanocapsules is different depending on the coating of the emulsion, being 218.7 nm for chitosan-coated nanoemulsions and 90 nm for the xanthan ones. However, it is necessary to observe the particle size distribution to be able to understand these differences. Figure 2 presents the size distribution of nanoparticles in water.

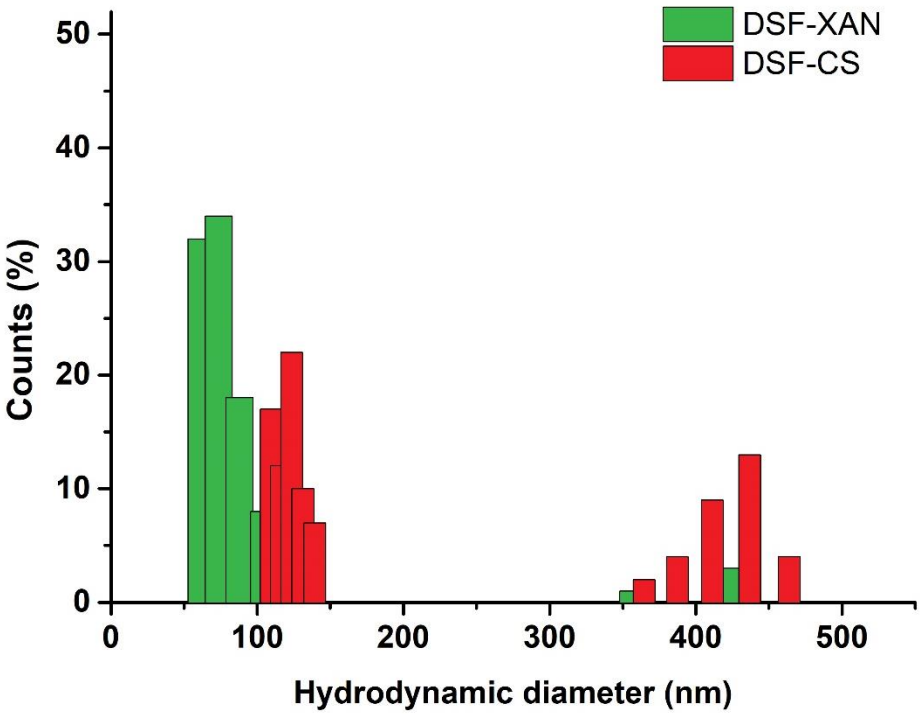

Figure 2. Size distribution of DSF-loaded nanocapsules coated with Chitosan (red) or Xanthan (red).

Observation of the size distribution of the nanocapsules in water (Figure 2, red) reveals that chitosan-coated nanocapsules present two populations: the main one with a mean diameter of around 100 nm, and a second one corresponding to 30% of the population with a diameter higher than 300 nm. We hypothesize that this population may correspond to aggregates, outlining low stability of the sample or it may also be due to the coating of several nanoemulsion cores into one chitosan layer. It can be observed that in the case of xanthan-coated nanocapsules (green) the sample presents a main population with a smaller diameter and a small population with higher diameter. As the bigger population in xanthan has a smaller percentage than in chitosan, this may outline a higher stability of the system, which

is an important parameter to take into account, as interactions with cells will differ with change in nanoparticle size and surface. Besides, this difference in size between the two types of nanocapsules may also affect the efficacy of the nanocapsules in cancer treatment and antibacterial activity, as it will influence internalization.[28] Gratton *et al.*[29] claim that optimum nanoparticle size for cell internalization is around 150 nm, although nanoparticles with bigger sizes can be also internalized into non-phagocitic cells. This would mean that internalization of nanoparticles with tendency to form aggregates of bigger size would be drastically decreased.

Characterization of the surface was carried out by measurement of the ζ Potential in KCl 1mM. Chitosan-coated nanocapsules show a ζ potential of +25 mV while the value for xanthan-coated ones is -24 ± 0.5. For both nanovehicles, absolute values are higher than 20 mV. As explained for the BQ and DP-loaded nanoparticles, this ζ potential value generates enough electrostatic repulsion between nanocapsules to prevent aggregation and guarantee colloidal stability (Bhattacharjee_2016). The coating of the nanocapsules is evidenced by the value of the ζ potential. In the case of chitosan-coated nanoparticles, the positive ζ potential values can indicate the presence of exposed amino groups. This means that nanocapsules are correctly coated by chitosan polymer. In xanthan coated ones, the negative ζ potential could be explained by the presence of carboxylic acids in the lateral chains of the polymeric coating. The difference on charge can influence cell internalization both in cancer and bacterial cells, so evaluation of the surface charge of the nanocapsules will help us understand the results obtained in future efficacy experiments.

2.3. Freeze-drying of disulfiram-loaded nanocapsules

Both developed nanocapsules were freeze-dried in order to preserve their properties during long-term storage. It is important to develop systems with that preserve their properties during long periods while maintaining the high encapsulation efficiency values. It was observed that disulfiram-loaded nanocapsules tended to macroscopically aggregate during short periods of storage time (usually about a week), both at room temperature and at 5 ^{o}C. Besides, as nanocapsules were going to be used in collaborations with other groups, the suspensions could be affected by changes in temperature during shipping. For this reason, it was decided to freeze-dry nanoparticles, which will preserve their properties for longer periods of time and shipping conditions will not be so crucial.

For the freeze-drying process, the first step was the selection of a compatible cryoprotectant. Cryoprotectants help to avoid the formation of crystals in the nanocapsule suspension, which would affect the integrity of the nanoparticles. Multiple cryoprotectants have been used in the literature, such as mannitol, lactose or sucrose.[30] In this project, we have selected mannitol. The reason is that a collaboration within the NAREB project already stablished that it was the best working for this type of nanocapsules.

After cryoprotectant selection, another important parameter to take into account is the concentration of nanocapsule and cryopreservant. Nanoparticle concentration was stablished at 10 mg/mL. Due to the concentration of the nanocapsule suspension before freeze-drying, and taking into account that cryoprotectant needed to be added to that suspension, 10 mg/mL was the higher achievable concentration.

Nanocapsule concentration needs to be as high as possible, as this would allow to achieve high concentration of nanocapsules in further experiments if needed.

For the selection of the concentration of mannitol used, three different concentrations were tested: 5%, 10% and 20 %. The concentration of cryoprotectant needs to be enough to protect nanocapsules during the freeze-drying process but not too much that it is hard to dissolve it during the reconstitution process.

For the freeze-drying process, mannitol and nanocapsules were mixed with these final concentrations, frozen with liquid nitrogen and freeze dried. The first step for the evaluation of the quality of the nanocapsules after freeze drying is observation of the cakes aspect. Then, to evaluate the nanocapsules characteristics after the process and compare them to the initial ones, they were resuspended in the same volume of water and characterization was carried out.

For the three mannitol concentrations tested, upon observation of the cakes after freeze drying and before resuspension, mannitol 5% was rejected. This was due to the fact that the cake did not maintain its integrity, collapsing and destroying the nanocapsules. This was check also by addition of water and reconstitution of the nanocapsules. Nanocapsules were completely aggregated and it was impossible to resuspend them.

Both 10 and 20% mannitol cakes presented good stability during freeze-drying, but they behaved differently after addition of water. In the case of 10% mannitol, the suspension looked homogenous, so DLS was performed to further evaluate the size distribution of nanocapsules after the cryopreservation process. In the case of 20%

mannitol, due to the low solubility of the sugar in water, the solution was not homogenous. There were some crystals presented in the suspension that were impossible to resuspend, so finally 10% mannitol was selected as the most promising cryoprotectant. Results from the size distribution of nanocapsules before and after freeze-drying is shown in Figure 3.

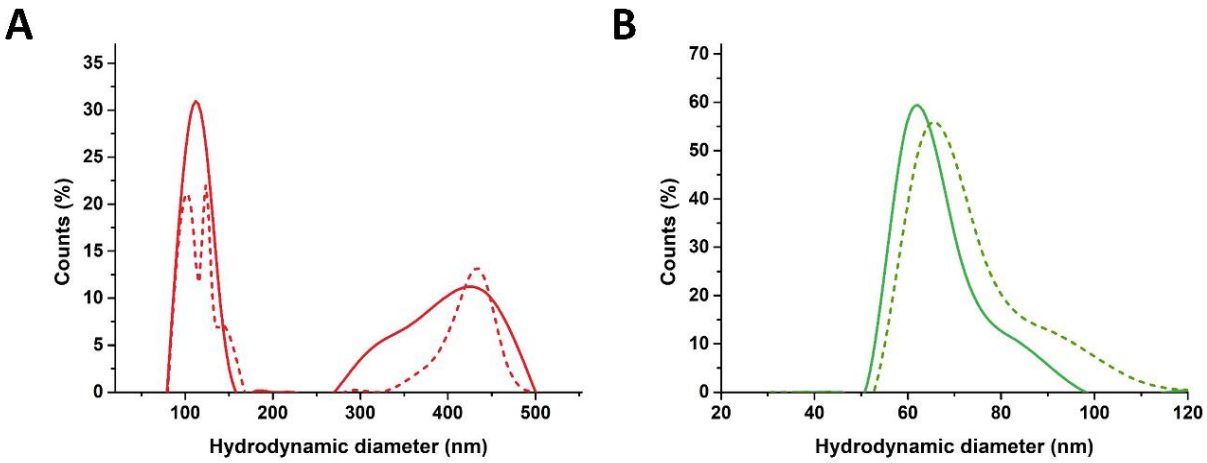

Figure 3. Size distribution of chitosan-coated (A) and xanthan-coated disulfiram-loaded nanocapsules in suspension (solid) and reconstituted after freeze-drying (dash)

As it can be seen from Figure 2, size distribution after formulation is comparable to the one before freeze-drying. This means that both nanocapsules maintain their characteristics after the preservation and mannitol 10% is a good cryopreservant.

Hereon, all the nanocapsules used were freeze-dried prior to use, as this is considered our final material, and not the non-freeze-dried suspension.

2.4. Disulfiram release study

Once the size distribution was studied and the best administration and preservation conditions determined, the next step was to determine the stability of the loaded

cargo. This means to study the release of the drug in different media of relevance. This would allow the correlation of the results observed in the *in vitro* experiments with the release from the nanocapsules.

The first step for the study of the release is the selection of the release media. For disulfiram release study, water, Dulbecco's Modified Eagle Medium (DMEM) and Muller-Hinton II (MHII) were selected.

Water is the control media, as it is the resuspension media after freeze-drying. DMEM is the cell culture media for pancreatic cancer cells. The amount of disulfiram released from the nanocapsules in this media is an important parameter to study, as it may correlate with the anticancer activity of the nanocapsules. The drug can be released before in the cell culture media before internalization which could mean that it can enter into the cells free or encapsulated in the nanocapsules. Understanding how the drug behaves in the cell culture media would help us understand further results of efficacy of the nanocapsules. This is the same for MRSA culture media, MHII, which is the third medium selected.

After selection of the media, the release protocol developed for bedaquiline-loaded nanocapsules was applied in this study, with slight modifications to mimic *in vitro* experiments using disulfiram-loaded nanocapsules.

Nanoparticles were incubated for 48 hours, as efficacy *in vitro* anticancer experiments length this amount of time and antibacterial ones 24 hours. Check points were performed at 1, 2, 3, 6, 24 and 48 hours to follow the progress. For the same reason, 37 ^{o}C were selected as incubation temperature, as it is both the

temperature of in vitro and in vivo experiments and the human corporal temperature. Nanocapsules were incubated with each release media and the concentration of disulfiram was analyzed at each time point.

Nanocapsules were separated from the release media by passing the solution through a syringe filter. Nanocapsules were retained in the filter, while the released free disulfiram and the rest of the components of the media went through (sugars, salts...). Both released drug (the one that was not retained in the filter) and the retained one were measured. To extract disulfiram from the nanocapsules, methanol was passed through the filter to break nanocapsules and take the drug out of the filter. Solutions were measured at 280 nm, as DSF calibration curve was performed at that wavelength. After measurement of the different solutions, both released and retained DSF, several problems were observed.

Firstly, DSF solubility in water is low, and if the release in the media was high, DSFf formed crystals that were retained inside the filter which made results not reproducible. Another problem was the wavelength of DSF measurement. Release media contain proteins that have absorption at 280 nm, the same wavelength used for DSF quantification, causing interference with the measurement. For this reason, we had to develop a different separation and quantification method.

It was decided to try to separate the nanocapsules using dialysis. For this purpose, disulfiram loaded nanocapsules were mixed with the release media, and place inside a 8K pore size dialysis bag. Then, this container was place into a beaker containing 50 mL of the same release media. At each time point, 1 mL of the solution was taken

from the beaker. Using this method allows disulfiram to be in a concentration under the solubility limit, avoiding the formation of crystals.

One the problem of solubility was solved, we needed to solve the quantification problem. For this purpose, a new method of quantification without the interference of proteins was developed. It was decided to complex DSF with copper ions. It has been well stablished in literature that DSF forms a complex in the presence of copper which has a green/blue color. Skowran *et. al.*[31] developed a method for the determination of the presence of DSF using thin-layer chromatography (TLC). DSF-containing solution was deposited into TLC plates and submerged into a copper sulfate solution. The spot immediately turned green. This method was explored for the measurement of the released DSF in the different media. However, quantification in TLC is difficult as the intensity of the spots need to be measured from a picture. For this reason, the complexation method was applied in solution. DSF was mixed with a solution of copper sulfate in 96-well plates, and a green coloration was observed. Upon measurement of this solution using UV-vis spectrophotometry, a clear peak appeared with a maximum absorption point at 420 nm.

To apply this quantification method to the release study, different controls were stablished. Firstly, empty nanocapsules absorbance at 420 nm was measured after addition of copper to check if that there was not interference with any of the nanocapsules components at that wavelength. No absorbance was observed in this solution. Then, the different release media themselves were measured too, and a calibration curve was performed to check the sensibility of the method. The lower detectable concentration of DSF was determined and compared with the DSF

concentrations in the release study. With this comparison it was determined that this method was not useful, as the sensitivity was too low to be able to measure disulfiram release, as it is really diluted in the beaker, so another more sensitive method should be found.

A new method based on an enzymatic assay was developed. Disulfiram is an irreversible inhibitor of hepatic aldehyde dehydrogenase (ALDH)[32], an enzyme that catalyzes the oxidation of aldehydes to carboxylic acids. So the developed method is based on the inhibition of the enzymatic conversion of acetaldehyde into acetic acid. The reaction is followed spectrophotometrically at 340nm by the accumulation of NADH, as the conversion of acetaldehyde into acetic acid also involves the transformation of NAD+ into NADH. The protocol, based on the work of Maninang and coworkers[32] with some modifications, is performed in a 96 wells microplate containing 130 µL of a reaction mixture. The concentrations of enzyme and substrate were optimized for the best performance in our reaction media. Then, 20 µL of DSF in release media of interest or the released fractions are added and incubated at 25 ^{o}C for 15 minutes. Finally, the reaction started by addition of 30 µL of NAD^{+} and the absorbance at 340 nm was measured for 1 minute.

The slope of the linear increase during the reaction time is inversely proportional to the amount of DSF in solution and is not affected by the presence of other components of the release media or nanocapsules. This was checked by adding controls with just release media, nanocapsules or nanocapsules in release media and comparing the results with the results without addition. Therefore, the method allows the quantification of the amount of DSF present in the release media thanks

to the calibration curve that is performed in each experiment. Results for water, MHII and DMEM are shown in Figure 4, only for 24 and 48 hours, as no release was detected at lower time points.

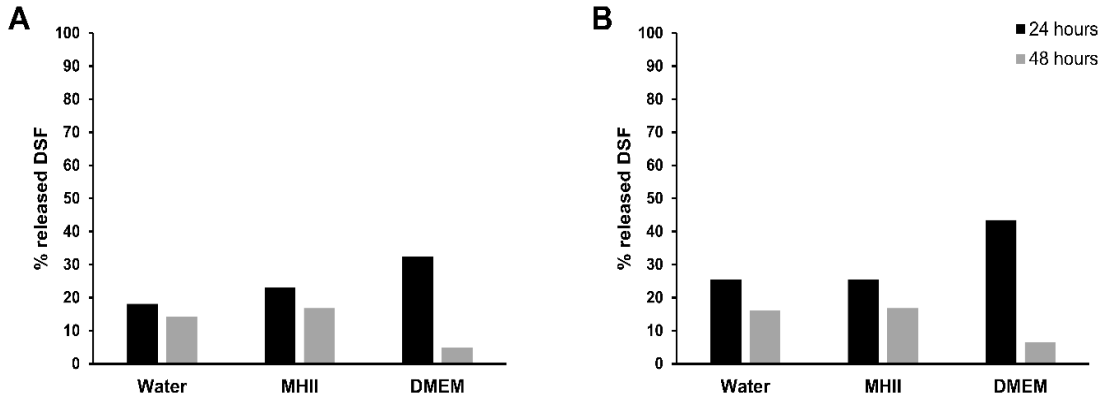

Figure 4. % released DSF from chitosan-coated (A) and xanthan-coated (B) nanocapsules in different media of interest after 24 and 48 hours

As it can be observed in Figure 4, the amount of DSF detected at 48 hours was lower than for 24 hours, which suggested that the drug was degraded in some media, especially in DMEM. To check this issue, a degradation assay was carried out. Free DSF at the same concentration used in the release experiment was added to the release media and incubated in the same conditions for 24 hours. Inhibition of ALDH was measured as explained before at different time points to check the concentration of DSF. Results of the remaining active DSF are shown in Figure 5.

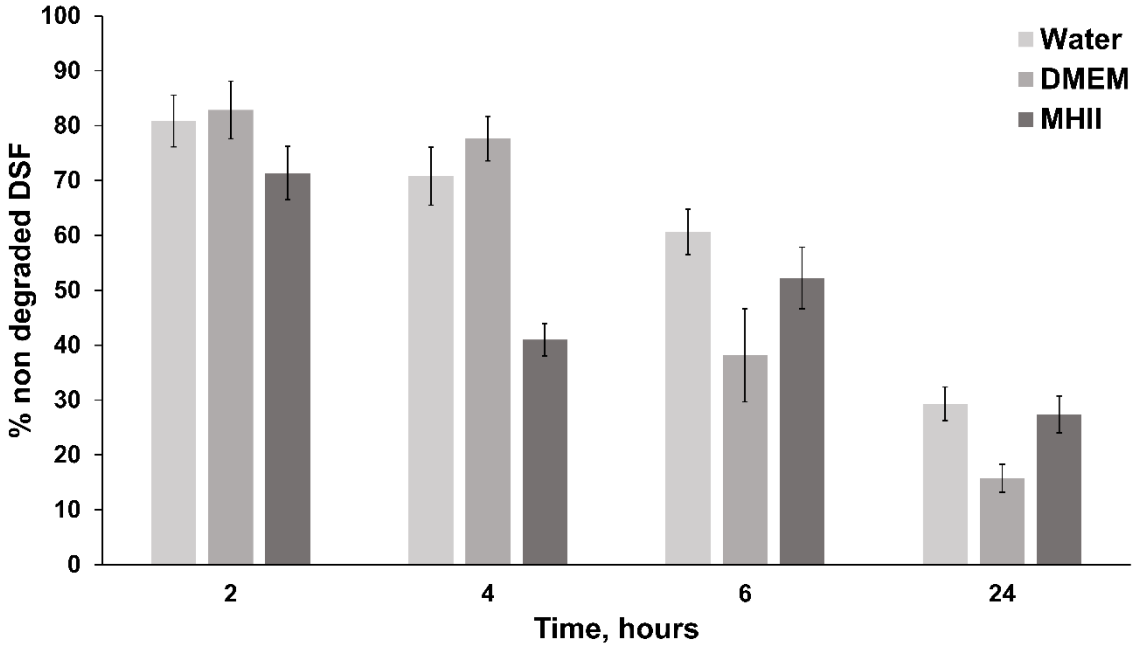

Figure 5. Degradation of disulfiram in different media

As it can be observed in Figure 5, after 2 hours, 80% of the disulfiram added to the media was still intact. After 24 hours, between 70 to 80% of the total disulfiram added has been degraded both in water and the culture media so release profile cannot be measured as the molecule disappears as it is released. This is in agreement with the fact that disulfiram is really unstable in blood, gastric media and other biological fluids.[17]

However, this result can also mean that our nanocapsules have some protective effect while the drug is in the nanocapsule core. After 24 hours, more than 50% of the total amount of DSF added in xanthan-coated nanocapsules (Figure 4) is still present in the release media, as it is able to inhibit the ALDH. This would mean that this DSF must have been protected by the nanocapsules at least during the first hours of incubation, as only 20% would be in solution and not degradated if it was released in the first minutes of reaction, as evidenced from the degradation studies.

So, although we did not get a release profile from the nanocapsules, we can conclude that our nanocapsules protect disulfiram from degradation in some extent.

2.5. Application of disulfiram-loaded nanocapsules for the treatment of pancreatic cancer

The experiments carried in this section have been performed in collaboration with Dra. Pilar Acedo and coworkers from University College London (UK).

Once nanoparticles have been developed and characterized, they are ready to be used for different applications. As already mentioned in the introduction, DSF has been repurposed for the treatment of cancer specifically, disulfiram has proved to be an effective drug for the treatment of pancreatic cancer.[16]

To check the anticancer efficiency of disulfiram loaded nanocapsules, cell proliferation of pancreatic cancer cells in the presence of nanocapsules was evaluated by reduction of 3-(4, 5-dimethylthiazol-2-yl)-2, 5-diphenyl tetrazolium bromide (MTT reagent) (MTT). Cell used in this study were PANC-1, a pancreatic ductal adenocarcinoma cell line. Cells were incubated in the presence of increasing concentrations of empty and DSF-loaded nanocapsules coated with chitosan or xanthan for 24 hours. After this time, cells were washed and the nanocapsule-containing incubation media was substituted with fresh media. PANC-1 cells were incubated for another 48 or 96 hours and MTT assay was performed. This incubation time was used to evaluate if cells are able to recover after treatment or if the drug needs some time to affect cell metabolic pathways before death can be observed. After this time, MTT was added to the cell culture media to evaluate cell proliferation. MTT is a reagent that can be reduced to formazan only by living cells, forming

crystals with a blue color. These crystals are then dissolved with dimethyl sulfoxide and the UV-vis absorbance is measured at 520 nm.

In this experiment, both the toxicity of empty and DSF-loaded nanocapsules is measured. This would allow to determine if the cell death observed is due to the nanocapsule itself or the encapsulated DSF. Results are shown in Figure 6.

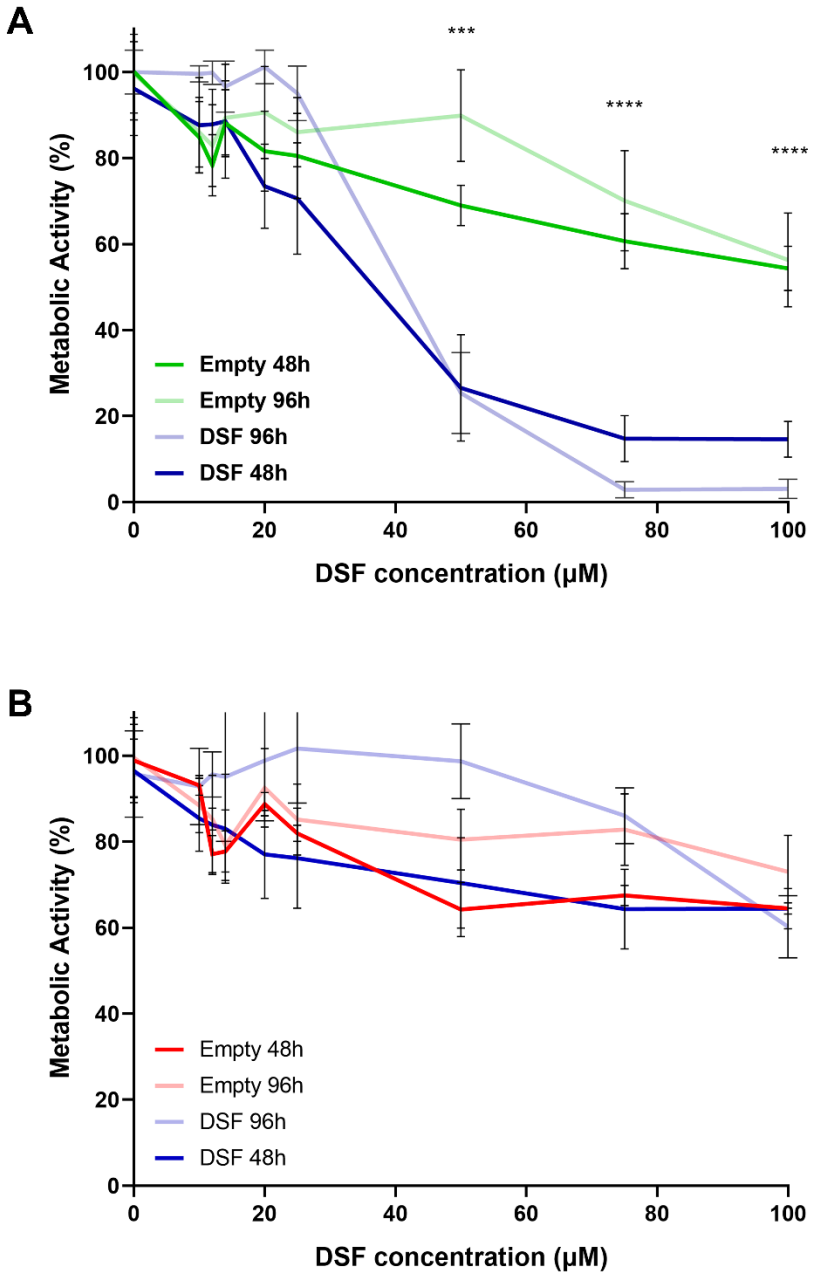

*Figure 6. . Treatment efficacy in PANC-1 of DSF-loaded nanocapsules. Metabolic activity of PANC-1 cells 48 and 96h after incubation with increasing concentrations of DSF encapsulated in xanthan (A) or chitosan (B)-coated nanocapsules compared to empty nanocapsules with the same coating. Data corresponds to mean values ± SD from at least three different experiments and statistically significant differences between empty and DSF-containing NPs at 48h are labelled as *** p<0.001, **** p<0.0001.*

Figure 6 shows the toxicity of both DSF-loaded and empty nanocapsules. The same nanocapsule concentration was used for the empty and DSF-loaded nanocapsules. However, it is expressed as a function of DSF concentration in the well to be able to compare chitosan and xanthan coated ones, as drug loading in both nanovehicles is different.

Empty xanthan-coated nanocapsules seem to be more toxic at the same concentration. However, this is due to the fact that to obtain the same concentration of DSF in the well, more xanthan-coated nanocapsules need to be added, as if we recall from Section 2.2, DL% for xanthan-coated nanocapsules is 22% while for chitosan is 44%. Therefore, nanocapsule toxicity is similar in both cases.

In terms of effectiveness of DSF-loaded nanocapsules, chitosan-coated nanocapsules have no anticancer activity. Although viability at high DSF concentrations is a bit lowed when nanocapsules are loaded with DSF, the differences with the empty ones are not enough to be considered statistically significant. However, in the case of xanthan-coated nanocapsules, statistically significant differences can be observed for DSF concentrations higher than 50 μM.

Between 48 and 96 hours of incubation after removal of nanocapsules, there is not much difference. This means that cells are not able to recover after the treatment with DSF-loaded nanocapsules. Besides, the ones that are not effective are not able to kill cancer cell even a longer incubation times.

With these results, we can determine that xanthan-coated DSF-loaded nanocapsules are the most effective in the reduction of cancer cell viability. This may

be due to the higher stability of these nanocapsules and lower diameters. As it was explained before, smaller nanoparticles internalization rates are higher that bigger ones. It is described in literature that nanoparticles with a diameter higher than 300 nm do not internalize as much as smaller nanoparticles (Gratton_2018) and it has been observed that chitosan nanocapsules have aggregates with a diameter higher than 300 nm. This may explain why xanthan-coated nanocapsules are more effective with the same concentration of DSF than chitosan-coated ones.

To try to improve DSF activity and decrease nanocapsule concentration, a combined therapy with copper was evaluated. It has been described in literature by different authors that combination of DSF with copper enhances the anticancer activity (Viola-Rhenals_2018). Again, the anticancer activity of DSF-loaded nanocapsules in combination with copper was evaluated by MTT assay. Increasing concentrations of DSF were added with 1 μM Cu(II) to PANC-1 cells and incubated for 24 hours. Cell death by MTT was evaluated immediately after removal of the nanocapsules and after 24 hours incubation with fresh media. Results are shown in Figure 7.

.

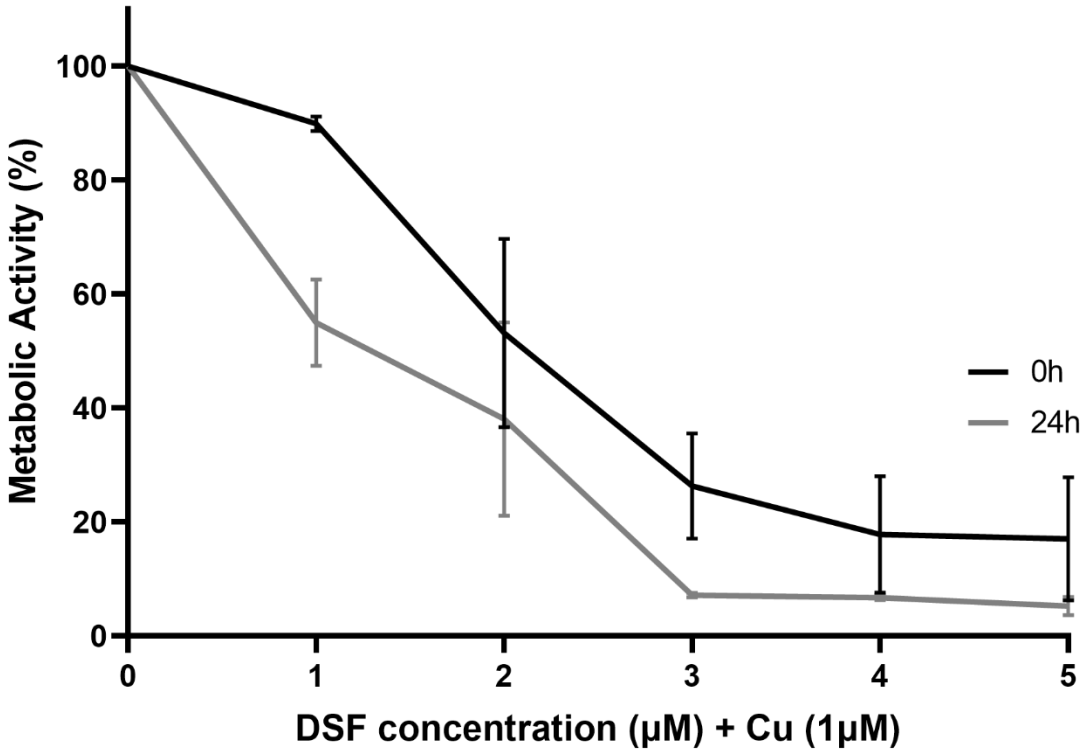

Figure 7. Metabolic activity of PANC-1 and PDX354 cells after incubation with increasing concentrations of disulfiram encapsulated in xanthan-coated nanocapsules. Values were measured at 0 and 24h after treatment.

Figure 7 show the effectivity of DSF-loaded nanocapsules in combination with copper. Although a slight increase in toxicity can be observed between 0 and 24 hours after removal, both times show good anticancer activities. Encapsulated DSF IC-50, meaning the drug concentration needed to reduce cell viability to 50%, is reduced from 40 µM to around 2 µM, which is a 20-fold reduction. Combined therapy of DSF-loaded xanthan coated nanocapsules is a promising alternative to be explored.

For this reason, the next step would be the coencapsulation of Cu/DSF into xanthan-coated nanocapsules. This was explored in several ways. First, coencapsulation was

tried by encapsulation of a previously formed DSF-Cu complex. Cu was added to an organic phase containing disulfiram. DSF-Cu complex is immediately formed, but upon addition into the aqueous phase, there was huge aggregation and the encapsulation failed. In a second trial, copper was added to the aqueous phase to try to delay the formation of the complex and avoid aggregation, but this method did not work either, producing also big aggregates.

To avoid the formation of the complex so fast, we decided to add the copper in form of copper nanoparticles. For this purpose, copper nanoparticles where synthesized following the method by Xiong *et al.* (Xiong_2011). In this method, copper nanoparticles are formed by reduction of copper with L-ascorbic acid, leading to nanoparticles of around 2 nm. Then, these nanoparticles were washed by dialysis and encapsulated into the nanocapsules. DSF was added together with the organic phase as in the standard developed method, and copper nanoparticles were either added mixed with the aqueous or xanthan solutions. Nanocapsules synthesis was continued as in the DSF-loaded ones without copper.

This method produced stable nanocapsules with a green/brown coloration due to the presence of copper and the Cu/DSF complex. At the moment, experiments are being conducted to evaluate their stability, DSF and copper concentration and later anticancer properties.

2.6. Application of disulfiram-loaded nanocapsules for the treatment of MRSA infections

These experiments carried out in this Section have been carried out in the frame of the NAREB project, in collaboration with Dr. Jose Antonio Aínsa's group (from

University of Zaragoza) and Dra. Joanna Empel's group (National Medicines Institute, Warsaw, Poland).

As already stated, it has been demonstrated that DSF has antibacterial activity against Meticillin-resistant *Staphylococcus aureus (MRSA)*. For this reason, disulfiram-loaded nanocapsules were tested as antibacterial agents against MRSA cell cultures.

The antibacterial activity was studied against different strains of *Staphylococcus aureus*. It is important to test the nanocapsules against both types of strains, methicillin-sensitive and methicillin-resistant strains, as the treatment of Staphylococcus aureus meticillin-resistant (MRSA) bacteria is very challenging and daptomycin is one of the antibiotics that are being used to fight these infections. However, its effectiveness against a sensitive (MSSA) strain as a control was also checked. Strains used are shown in Table 2 and they were selected either for being reference strains or for their importance in clinical infections.

Table 2. Staphylococcus aureus strains used in the study

Type of strain	***S*train ID**	**MSSA/MRSA[a]**
Reference strain	CECT-794	MSSA MRSAMRSA
	CECT-5190	
	MRSA252	
Clinical strain	1600/10	MRSA
	401/05	MRSA
	4281/08	MRSA
	600/07	MRSA

The antibacterial activity was studied in terms of Minimal Inhibitory Concentration (MIC), which is the minimum concentration of the antibiotic that inhibits the growth of the bacteria in a cell culture. This MIC value for encapsulated disulfiram was compared with the activity of the free antibiotic as a control. Besides, empty nanocapsules were also used as a control.

Bacteria were cultured following a standard protocol. Briefly, different amounts of disulfiram, either free or encapsulated, were coincubated with bacteria for 20 hours. After this time, the viability of the culture was evaluated by addition of resazurin to the culture. Resazurin is a blue-colored compound that is reduced to resorufin by living cells. This produces a color change in the well with living cells from blue to pink. The MIC is the lowest concentration at which no bacterial growth is observed.

During the antimicrobial experiments carried out by chitosan-loaded nanocapsules, several problems were observed. First of all, results were not reproducible between different nanocapsule batches. Besides, there were differences between different experiments of the same batch of nanocapsules. It was stated by our collaborators that chitosan-coated nanocapsules aggregated in the bacterial culture media, making it impossible to get reproducible results and it was also observed during the release studies.

As it was believed that the issue with the chitosan-coated nanocapsules was a problem of high DL%, we decided to develop a new type of chitosan-coated nanocapsules to compare their antibacterial activity with xanthan-coated ones.

For this purpose, we modified the initial amount of DSF added to the synthesis, to decrease the DL%. In this case, instead of adding 25 mg, only 10 mg were added. Besides, this reduction in DL% would produce chitosan-coated nanocapsules with a similar DL% to the xanthan-coated ones, allowing easier comparison between them.

The synthesis method was kept exactly the same and only the initial amount of DSF was decreased from 25 mg to 10 mg. The EE% and DL% of nanocapsules was determined following the same protocols already developed. Drug loading obtained was 19 ± 2% and the encapsulation efficiency 57 ± 5%. DL% obtained in this case is similar to the one in xanthan-coated nanocapsules.

Size distribution was evaluated by DLS before and after the freeze-drying process, which was performed with the same concentrations as before. If the developed nanocapsules maintained their characteristics after freeze-driying with these concentrations, they will be used for the rest of the experiments. If not, further optimization of the freeze-drying process would need to be performed. Results are shown in Figure 8.

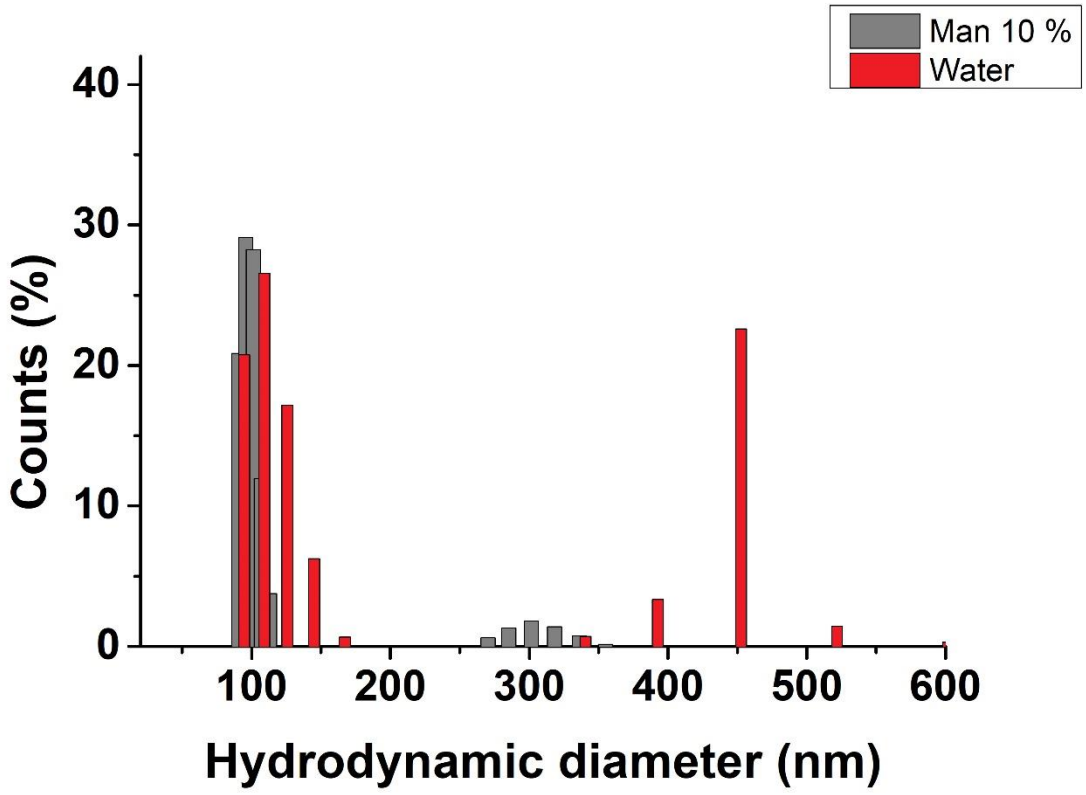

Figure 8. Size distribution of low-loading chitosan-coated nanocapsules before (solid) and after (dash) freeze-drying

These new chitosan-coated nanocapsules have a mean diameter of 208.8 nm (Figure 8). Nanocapsules present two populations before freeze-drying. The main one has a mean diameter around 100 nm, while there is a second corresponding to about 30% of the population with a diameter of around 450 nm. However, this population is highly reduced after freeze-drying, which may mean that they were aggregates that have been stabilized thanks to the presence of mannitol.

Nanocapsule surface was also characterized by ζ potential as in the previous cases, to check if capsules are correctly coated. Nanocapsules showed a ζ potential of +22 mV, which is in agreement with a coating with chitosan, due to the presence of positively charged amino groups in this polymer. Hereon, we will refer to chitosan-

coated nanocapsules used for the antibacterial experiments as the ones with a nominal loading of 10 mg.

Antibacterial experiments were performed to compare the antibacterial activity of free drug and the encapsulated into xanthan and chitosan coated nanocapsules. Results for all the strains tested are shown in Table 3.

Table 3. Comparison of MIC values of xanthan-coated and chitosan-coated disulfiram-loaded nanocapsules determined for S. aureus strains.

	***S. aureus* MSSA CECT 794**		***S. aureus* MRSA CECT 5190**		***S. aureus* MRSA MRSA252**	
	MIC (µg/mL)	**Fold increase**	**MIC (µg/mL)**	**Fold increase**	**MIC (µg/mL)**	**Fold increase**
Chitosan-coated	14	0,25x	28	0,5x	14	0,5x
Xanthan-coated	14	0,25x	28	0,5x	7	0,25x
	***S. aureus* MSSA 1600/10**		***S. aureus* MRSA 401/05**		***S. aureus* MSSA 4281/08**	
	MIC (µg/mL)	**Fold increase**	**MIC (µg/mL)**	**Fold increase**	**MIC (µg/mL)**	**Fold increase**
Chitosan-coated	28	1x	14	0,25x	28	1x
Xanthan-coated	56	2x	14	0,25x	7	0,25x
	***S. aureus* MRSA Xen30**		***S. aureus* MRSA 600/07**			
	MIC (µg/mL)	**Fold increase**	**MIC (µg/mL)**	**Fold increase**		
Chitosan-coated	56	0,5x	14	0,25x		
Xanthan-coated	28	0,25x	14	0,25x		

As it can be observed in Table 3, in almost all of the cases an improve in DSF efficacy is observed with both types of nanocapsules as nanocarriers. Only in the case of MSSA 1600/10 strain, no improvement in efficacy was observed. However, in the rest of the cases, disulfiram MIC decreases 2 or 4 times. This means that if disulfiram is encapsulated, only half disulfiram concentration is needed to kill bacteria in comparison with free drug.

In the release studies, although we could not measure disulfiram release profile from the nanocapsules, a slight protective effect was observed. The efficacy results may indicate that both type of nanocapsules can protect DSF from degradation in the biological environment and deliver it to the bacteria in an efficient way. As DSF stays in the core of the nanocapsules, it is not degraded in the culture media so DSF has a prolonged antibacterial effect. Besides, the fact that no much difference is observed between xanthan or chitosan coated nanocapsules may also be an indication that the effectiveness of the treatment is due to the protection of the drug from the media and it was independent on the polymer used. The fact that MSSA 1600/10 stain was not as susceptible as the others to encapsulated DSF can be an indication that nanocapsules are interacting with cell surface and internalizing, so different bacterial phenotypes may affect the efficacy. Further experiments need to be performed in order to determine if the difference in the polymer coating is affecting bacterial effectivity. For example, fluorescent nanocapsules could be developed in order to evaluate if there is a difference in internalization depending on the polymer coating and cell strain.

3. Conclusions

In this chapter, we presented the optimization of the synthesis of disulfiram-loaded nanocapsules for the treatment of MRSA infections and pancreatic cancer. Disulfiram has been successfully encapsulated into the developed nanocapsules with two different polymer coatings. This should allow the protection of the drug to be able to be used for repurposing objectives.

The synthesis process was already optimized for the development of empty nanocapsules in a previous work, and it also probed it suitability as a drug delivery system in other studies. Here, we tested the suitability for the encapsulation of the hydrophobic drug disulfiram and the study of the modification of the nanocapsule surface with two different polymers. The good results obtained for EE% and DL% values were expected due to the hydrophobic nature of the drug. However, stability issues were observed in chitosan-coated nanocapsules due to high-loading values.

After characterization of the nanoparticle size distribution, we could observe that all the developed nanocapsules presented a mean diameter in the submicrometric. range, which, as already mentioned, is in an appropriate range to promote interaction with living cells. However, better results were obtained for the xanthan-coated nanocapsules, as they had smaller sized and the suspension presented lower tendency to aggregation, which indicated that there may be higher internalization in cancer cells. Besides, ζ Potential was in agreement in all of the cases with the polymer coating used, which therefore served as an indicator that the nanocapsules were correctly coated.

In all the developed nanocapsules, a freeze-drying process was carried out in order to improve nanocapsule stability over time. The optimization of the cryoprotectant concentration lead to the conclusion that 10% mannitol was the optimum one. Besides, in the low-loading chitosan nanocapsules seem to have a stabilizing effect and lower aggregates were observed in solution after freeze-drying.

Efficacy experiments carried out in pancreatic cancer cells PANC-1 show diverse results for the different coating. Chitosan-coated nanocapsules presented low anticancer activity. However, good results were observed for xanthan-coated nanocapsules. Cotherapy with copper showed a 20-fold decrease in IC50 in comparison with monotherapy with DSF, which opens the way to the development of coencapsulated Cu/DSF nanocapsules.

Finally, a new type of chitosan coated nanocapsule needed to be developed for the antimicrobial assays of the nanocapsules against *Staphylococcus aureus* due to stability issues. Improved efficacy for encapsulated DSF was observed against almost all the strains tested in the experiments, for both types of nanocapsules. This indicated the protection of the drug from the environment, as free-DSF is degraded in MHII.

With the results presented here conclude that the developed DSF-loaded nanocapsules show promising characteristics for the encapsulation of DSF and the repurpose of the drug in the treatment of MRSA infections and pancreatic cancer.

4. Materials and methods

4.1. Materials

Tween® 20 and absolute ethanol were purchased from Panreac. Span® 85 (sorbitane trioleate), oleic acid (90%), chitosan (medium molecular weight), xanthan from *Xanthomonas campestris*, Aldehyde dehydrogenese (ALDH), NAD^+, acetaldehyde, copper chloride, MTT and resazurin were obtained from Sigma-Aldrich. BBLTM Mueller Hinton II (MHII) Broth Cation Adjusted is from BD Diagnostics. 100K Amicon centrifugal filter units were purchased from Merck Millipore.

The pancreatic ductal adenocarcinoma cell line PANC-1 (ATCC® CRL-1469™) was purchased from ATCC. Cells were grown in a BINDER incubator (Tuttlingen, Germany) at 37 °C in 95% humidity and 5% CO2. PANC-1 cells were cultured in DMEM (Dulbecco's Modified Eagle's Medium, Sigma Aldrich, UK) supplemented with 10% Foetal Bovine Serum (FBS, Gibco) and 1% Penicillin-Streptomycin (Gibco).

4.2. Synthesis of disulfiram-loaded nanocapsules

The general method for the synthesis of daptomycin-loaded nanocapsules was slightly modified from the already reported protocol for the obtaining of empty nanocapsules (De Matteis et al., 2016). Firstly, 10 or 25 mg of disulfiram were mixed with 40 mg of oleic acid and 100 µL of absolute ethanol. This solution was then mixed with 8.6 mL of Span® 85 in 4 mL absolute ethanol and sonicated until all the components were dissolved. Then, this organic phase was added dropwise to an aqueous phase containing 13.6 mg Tween® 20 in 8 mL water. Immediately after,

0.5 mL of a 5 mg/mL chitosan solution in acetic acid 1% (v/v) was added for the chitosan-coated nanocapsules or 1 mL of a 5 mg/mL xanthan solution in water for the xanthan-coated ones. After 15 minutes of magnetic stirring, chitosan and xanthan-coated nanocapsules followed different paths:

Chitosan-coated nanocapsules solution was added to 15 mL of 50 mM Na2SO4 solution to obtain the chitosan hydrogel and then they were washed by ultracentrifugation (24000 rpm, 30 min, 10 °C), resuspended in 10 mL of water, centrifuged again and resuspended in water. Xanthan-coated nanocapsules were washed by centrifugation in 100K amicon centrifugal filter units. Three steps of centrifugation and resuspension in water were performed. Finally, for all the nanocapsules, we measured the dry weight of the sample after freeze-drying to obtain the concentration of the nanocapsules suspension.

To improve stability during long-term storage of the disulfiram-loaded nanocapsules, 10 mg/mL nanocapsules suspension was freeze dried in the presence of 10% mannitol as a cryoprotectant. The freeze-dried formulation was resuspended in the initial volume of milliQ water before each use.

4.3. Determination of drug encapsulation efficiency and drug loading

For all the types of nanocapsules, 1.5 mg of particles were mixed with 900 µl methanol and sonicated for 30 minutes, in order to extract the encapsulated drug. The absorbance of the sample was measured at the adequate for each drug using a Varian Cary 50 UV/Vis spectrophotometer. Previously, a calibration curve of the drug in methanol was obtained. The absorbance at 282 nm was used for disulfiram.

Two values are calculated for the evaluation of the efficiency of the process, encapsulation efficiency and drug loading:

- **Encapsulation efficiency:** is the parameter that expresses the total amount of the drug that was successfully encapsulated in comparison to the amount initially added to the synthesis.

$$\mathrm{EE\%} = \frac{\text{mg encapsulated drug}}{\text{mg added drug}} \cdot 100$$

- **Drug loading:** this value expresses the amount of drug inside the capsules with respect to the total amount of capsules mass.

$$\mathrm{DL\%} = \frac{\text{mg encapsulated drug}}{\text{mg total nanocapsules}} \cdot 100$$

4.4. Characterization of the nanocapsules

Dynamic Light Scattering (DLS) analysis has been carried out using a Brookhaven 90Plus DLS instrument. Nanoparticle hydrodynamic diameter and polydispersity index (PDI) has been measured in milliQ water at the concentration of 0.05 mg/mL.

Electrophoretic mobility (ζ Potential) of nanoparticles has been determined by measuring the potential of a 0.1 mg/mL nanoparticle suspension in 1 mM KCl with a Plus Particle Size Analyzer (Brookhaven Instruments Corporation).

4.5. Release study of disulfiram-loaded nanocapsules

Release profile of the disulfiram-loaded nanocapsules was studied in water, MHII bacterial culture media and DMEM cell culture media.

In a first attempt, 10 µl of a 20 mg/ml capsules solution was mixed with 0.99 ml of each studied medium and incubated at 37 °C during 1, 2, 3 and 7 days. At each time point, the solution was passed through a syringe membrane filter (Millex syringe-driven filter unit, PVDF filter with 0.22 µm pores, from Merck Millipore) to separate the nanocapsules from the medium. Then, 900 µl methanol were passed through the filter to break the capsules and extract the antibiotic. The concentration was measured spectrophotometrically at 282 nm.

In the second protocol, 80 µg of encapsulated DSF were mixed with the release media to a total volume of 2 mL inside an 8K pore size dialysis bag. This container was placed into a beaker containing 50 mL of the same release media and incubated for 48 h at 37 ºC. At 24 and 48 hours, 1 mL of solution was taken for the analysis. In order to quantify the amount of disulfiram released from the nanocapsules suspension, we developed a new method based on an enzymatic assay of ALDH inhibition.

The protocol, based on the paper by Maninang and coworkers[1] with some modifications, is performed in a 96 wells microplate containing 130 µL of a reaction mixture with: Tris–HCl buffer 103 mM; 0.04 units/mL yALDH solution (diluted in 100 mM Tris–HCl buffer with 0.02%(w/v) BSA); KCl 100 mM; 10 mM acetaldehyde. Then, 20 µL of DSF in release media of interest or the released fractions are added and incubated at 25 ºC for 15 minutes. Finally, the reaction started by addition of 30 µL of NAD+ 2.7 mM and the absorbance at 340 nm was measured for 1 minute.

The slope of the increase in absorbance during the reaction time is inversely proportional to the amount of DSF in solution. A calibration curve with increasing amounts of DSF was performed in every experiment.

4.6. In vitro anticancer activity assessment of disulfiram-loaded nanocapsules

To determine the effectiveness of empty and disulfiram loaded xanthan and chitosan coated nanoparticles to inactivate PANC-1 cells, increasing concentrations of NPs were used. For DSF loaded NPs the concentrations are normalized to DSF encapsulated for each nanocarrier type. For each experiment, 5000 cells/well seeded in transparent flat bottom 96 well-plates, were incubated for 24 hours with the NPs at different concentrations (0 or Control, 10, 12, 14, 20, 25, 50, 75, 100μM) diluted in supplemented DMEM. After the 24h-treatment period, cells were washed with PBS and then fresh DMEM was added. MTT assays were performed 48h and 96h after treatment.

For the combined therapy, we tested different concentrations of xanthan-coated nanocapsules with our without copper until a gradual effect in cell viability was observed. Therefore, for each assay 5000 cells/well seeded in a 96 well-plate were treated for 24 hours with various concentrations of nanocapsules (0.1-100 μM) free DSF (0.01-20 μM) in combination with 1μM Cu(II). After the 24h incubation period, the plates were rinsed with PBS and replaced with fresh DMEM. MTT assays were performed at 0h, 24h, 48h and 96h after treatment.

The effect of DSF, copper(II) chloride and empty and loaded NPs in the cell proliferation rate of PANC-1 cells was evaluated by the reduction of 3-(4, 5-dimethylthiazol-2-yl)-2, 5-diphenyl tetrazolium bromide (MTT reagent) to formazan

crystals (van Meerloo, Kaspers and Cloos, 2011). A 0.5mg/ml solution of MTT was prepared immediately before use in warmed supplemented DMEM, filtered using a 0.22µm sterile Millex® syringe filter and stored at room temperature until usage. 100µl of the mixture was added to each 96 well-plate well. Promptly, the plate was covered in aluminium foil and placed in the incubator for 60 minutes. Following this time, formazan crystals were dissolved adding 100ul of DMSO per well. Subsequently, the solubilized formazan concentration was measured as optical density (OD) using an Infinite M200 PRO microplate reader (Tecan Group Ltd) at a 520nm wavelength.

The result is expressed as percentage and the closer it is to 0%, the higher is the effectiveness of the treatment in inhibiting PANC-1 proliferation.

4.7. In vitro antimicrobial activity assessment of disulfiram-loaded nanocapsules

The following experiments were performed by Dr. Ainhoa Lucía Quintanar and Dr. Joanna Empel, as part of the NAREB project.

The in vitro activity test of daptomycin-loaded nanocapsules was carried out using different bacterial strains (See Table 3). In a 96-well plate, different concentrations of disulfiram-loaded nanocapsules and free disulfiram were mixed in a total volume of 100 µl MHII medium. Then, 100 µl of a 105 c.f.u./mL bacterial culture were added to each well. Several control wells are established: a positive control in which 100 µl of a 105 c.f.u./mL bacterial culture is added to 100 µl of MHII medium; a negative control in which we only had 200 µl MHII medium. Bacteria are incubated for 18

hours at 37 ºC and MIC is recorded adding 30 µL of a resazurin solution 0.01% w/v and checking color change from blue to pink after 1 hour.

5. References

(1) Jia, Y.; Huang, T. *Cancer Manag. Res.* **2021**, *13*, 4095–4101.

(2) Kepplinger, E. E. *Biotechnol. Law Rep.* **2015**, *34* (1), 15–37.

(3) Kaul, G.; Shukla, M.; Dasgupta, A.; Chopra, S. *Future Microbiol.* **2019**, *14* (10), 829–831.

(4) Ashburn, T. T.; Thor, K. B. *Nat. Rev. Drug Discov.* **2004**, *3*, 673–683.

(5) Suh, J. J.; Pettinati, H. M.; Kampman, K. M.; O'Brien, C. P. *J. Clin. Psychopharmacol.* **2006**, *26* (3), 290–302.

(6) Jiao, Y.; N. Hannafon, B.; Ding, W.-Q. *Anticancer. Agents Med. Chem.* **2016**, *16* (11), 1378–1384.

(7) Hothi, P.; Martins, T. J.; Chen, L.; Deleyrolle, L.; Yoon, J.-G.; Reynolds, B.; Foltz, G. *Oncotarget* **2012**, *3* (10), 1124–1136.

(8) Iljin, K.; Ketola, K.; Vainio, P.; Halonen, P.; Kohonen, P.; Fey, V.; Grafström, R. C.; Perälä, M.; Kallioniemi, O. *Clin. Cancer Res.* **2009**, *15* (19), 6070–6078.

(9) Ito, Y.; Cai, H.; Koizumi, Y.; Hori, R.; Terao, M.; Kimura, T.; Takagi, S.; Tomohiro, M. *Biol. Pharm. Bull.* **2000**, *23* (3), 327–333.

(10) Wang, S.; Jiang, T.; Wang, Z. *2008 Int. Conf. Biomed. Eng. Informatics* **2008**, 596–600.

(11) Sheppard, J. G.; Frazier, K. R.; Saralkar, P.; Hossain, M. F.; Geldenhuys, W. J.; Long, T. E. *Bioorganic Med. Chem. Lett.* **2018**, *28* (8), 1298–1302.

(12) Dalecki, A. G.; Haeili, M.; Shah, S.; Speer, A.; Niederweis, M.; Kutsch, O.; Wolschendorf, F. *Antimicrob. Agents Chemother.* **2015**, *59* (8), 4835–4844.

(13) Haeili, M.; Moore, C.; Davis, C. J. C.; Cochran, J. B.; Shah, S.; Shrestha, T. B.; Zhang, Y.; Bossmann, S. H.; Benjamin, W. H.; Kutsch, O.; Wolschendorf, F. *Antimicrob. Agents Chemother.* **2014**, *58* (7), 3727–3736.

(14) Long, T. E. *Antimicrob. Agents Chemother.* **2017**, *61* (9), 1–8.

(15) Phillips, M.; Malloy, G.; Nedunchezian, D.; Lukrec, A.; Howard, R. G. *Antimicrob. Agents Chemother.* **1991**, *35* (4), 785–787.

(16) Cong, J.; Wang, Y.; Zhang, X.; Zhang, N.; Liu, L.; Soukup, K.; Michelakos, T.; Hong, T.; DeLeo, A.; Cai, L.; Sabbatino, F.; Ferrone, S.; Lee, H.; Levina, V.; Fuchs, B.; Tanabe, K.; Lillemoe, K.; Ferrone, C.; Wang, X. *Cancer Lett.* **2017**, *409*, 9–19.

(17) Shergill, M.; Patel, M.; Khan, S.; Bashir, A.; McConville, C. *Int. J. Pharm.* **2016**, *497* (1–2), 3–11.

(18) Johansson, B. *Acta Psychiatr. Scand.* **1992**, *86* (S369), 15–26.

(19) Najlah, M.; Ahmed, Z.; Iqbal, M.; Wang, Z.; Tawari, P.; Wang, W.; McConville, C. *Eur. J. Pharm. Biopharm.* **2017**, *112*, 224–233.

(20) Song, W.; Tang, Z.; Lei, T.; Wen, X.; Wang, G.; Zhang, D.; Deng, M.; Tang, X.; Chen, X. *Nanomedicine Nanotechnology, Biol. Med.* **2016**, *12* (2), 377–386.

(21) De Matteis, L.; Jary, D.; Lucía, A.; García-Embid, S.; Serrano-Sevilla, I.; Pérez, D.; Ainsa, J. A.; Navarro, F. P.; M. de la Fuente, J. *Chem. Eng. J.* **2018**, *340*, 181–191.

(22) Casadomé-Perales, Á.; Matteis, L. De; Alleva, M.; Infantes-Rodríguez, C.; Palomares-Pérez, I.; Saito, T.; Saido, T. C.; Esteban, J. A.; Nebreda, A. R.; M. de la Fuente, J.; Dotti, C. G. *Nanomedicine* **2019**.

(23) Ambrosone, A.; Matteis, L. De; Serrano-Sevilla, I.; Tortiglione, C.; Fuente, M. D. La. *ACS Biomater. Sci. Eng.* **2020**, *6*, 2893–2903.

(24) Hibbitts, A.; Lucía, A.; Serrano-Sevilla, I.; De Matteis, L.; McArthur, M.; M. de la Fuente, J.; Aínsa, J. A.; Navarro, F. *PLoS One* **2019**, *14* (9), 1–24.

(25) Xu, X.; Luo, L.; Liu, C.; McClements, D. J. *Food Hydrocoll.* **2017**, *64*, 112–122.

(26) Mirhosseini, H.; Tan, C. P.; Hamid, N. S. A.; Yusof, S. *Colloids Surfaces A Physicochem. Eng. Asp.* **2008**, *315* (1–3), 47–56.

(27) Wang, Z.; Tan, J.; McConville, C.; Kannappan, V.; Tawari, P. E.; Brown, J.; Ding, J.; Armesilla, A. L.; Irache, J. M.; Mei, Q. B.; Tan, Y.; Liu, Y.; Jiang, W.; Bian, X. W.; Wang, W. *Nanomedicine Nanotechnology, Biol. Med.* **2017**, *13* (2), 641–657.

(28) Graf, C.; Gao, Q.; Schu, I.; Noufele, C. N.; Ruan, W.; Posselt, U.; Korotianskiy, E.; Nordmeyer, D.; Rancan, F.; Hadam, S.; Vogt, A.; Lademann, J.; Haucke, V.; Ru, E. *Langmuir* **2012**, *28*, 7598–7613.

(29) Gratton, S. E. A.; Ropp, P. A.; Pohlhaus, P. D.; Luft, J. C.; Madden, V. J.; Napier, M. E.; DeSimone, J. M. *Proc. Natl. Acad. Sci.* **2008**, *105* (33), 11613 LP – 11618.

(30) Abdelwahed, W.; Degobert, G.; Fessi, H. *Int. J. Pharm.* **2006**, *324* (1), 74–82.

(31) Skowron, M.; Zakrzewski, R.; Ciesielski, W.; Rembisz, Ż. *J. Planar Chromatogr. – Mod. TLC* **2014**, *27* (2), 107–112.

(32) Maninang, J. S.; Lizada, M. C. C.; Gemma, H. *Food Chem.* **2009**, *117* (2), 352–355.

Chapter 4

Encapsulation of cloroperoxidase and magnetic nanoparticles for their use as catalytic microsupports

1. Introduction

The use of enzymes dates back thousands of years, especially in food processing, but it was not until the development of recombinant DNA technology in the 1070's that they were widely spread thanks to a more efficient production with cheaper and higher purity enzymes.[1] Enzymes are biological catalyst that are mostly preferred over traditional catalysts due to their high biocatalytic performance, chemoselectivity, stereoselectivity and regioselectivity. These characteristics make them highly desirable for their application in the industry, especially in biocatalysis, development of biosensors, environmental remediation and food, agrochemical and biomedicine industry.[2] They acquired great importance in the mid-80's for the synthesis of chiral compounds in the pharmaceutical industry, as most traditional catalysts were not enantiospecific and therefore additional purification steps were required to obtain the final product. Besides, they are considered as sustainable, efficient and environmentally responsive biocatalysts because of the reduction in the

consumption of hazardous chemicals and in the generation of toxic byproducts. This is due to the fact that enzymes are derived from renewable sources and are biocompatible and biodegradable, unlike traditional catalyst, which usually make use of toxic metals.[3] Moreover, biocatalysis is usually performed under mild conditions, without organic solvents and skipping protection and deprotection steps, which leads to a decrease of the number of steps and to more energy efficient processes.

However, in many cases, their use on large scale is hampered by low stability in the reaction conditions and high cost in production.[4] Usually, chemical reactions in the industry involve the use of organic solvents, extreme pH or high temperature, which greatly affect enzyme structure and activity. All these limitations can be overcome by enzyme immobilization. This will allow recovery and reuse of the catalytic system as well as an easy separation from the final product, which will greatly reduce costs. Moreover, immobilization improves enzyme stability to environmental conditions such as presence of organic solvents, pH or temperature, which allows the use the of the enzyme for longer periods of time in comparison with the soluble enzyme. As previously said, immobilization of enzymes on insoluble support materials is beneficial also due to increased purity of the final product, which is of great importance in food and pharmaceutical industrial applications.[3]

Over the last decades, research has been focused on the development of new support materials together with new immobilization techniques for the improvement of enzymes applicability in the catalysis industry. Early immobilization techniques provided low enzyme loadings so over the last decades, more immobilization techniques have been developed.[5]

The objective of enzyme immobilization is to retain enzyme stability and activity, for which is of greatly importance to select a suitable support and immobilization technique.[6] There are different traditional methods for enzyme immobilization: non-covalent adsorption, physical entrapment and covalent attachment, each with their own advantages and disadvantages. Non-covalent adsorption involves the passive adsorption onto hydrophobic surfaces or electrostatic interactions with charged ones. The main advantage of this method is that it does not involve coupling reagents or modification of the enzyme. However, due to the weak interactions, enzymes leak from the support, resulting in loss of activity and catalyst. Covalent immobilization techniques involve the stable attachment by covalent bonding to the support. The covalent bond can be either formed with some of the groups naturally present in the enzyme structure, or by previous modification of the enzyme. The first approach is easier as it does not require previous modification of the enzyme, however, it is not possible in some enzymes as they do not have reactive groups, or it can modify the active site reducing enzyme catalytic activity. Modification of the enzyme previous to immobilization requires additional steps that can also affect enzyme activity and increases costs. The best approach to overcome the negative influence of covalent bonding to enzyme activity and prevent enzyme leaking from the support is physical entrapment.[5]

After selection of the entrapment method, the support is another important aspect. In recent years, nanostructured materials emerged as promising support materials that can overcome traditional immobilization matrices thanks to their high surface to volume ratio and high capacity to load the enzymes. Enzymes can be entrapped

within the nanomaterial pores or coating or bound to the surface. When the catalyst is entrapped, nanomaterials provide a biocompatible microenvironment surrounding the enzyme that usually protects them from denaturation in the recycling process. Entrapment in nanomaterials can also improve their stability towards the presence of organic solvents, pH or temperature or can even improve catalytic performance. Besides, immobilization in nanomaterials also improves reusability in several reaction cycles and separation from the reaction mixture.

Several types of nanoparticles can be used for enzyme immobilization. For example, silica is a well-known material that has been extensively used for enzyme immobilization. Silica surface can be functionalized with different groups that can covalently bind enzymes. Polymer nanofibers can also be used as enzyme immobilizer and thanks to its high porosity they usually have large enzyme loading per unit mass. Other nano immobilizers include gold nanoparticles, or zinc oxide.[7]

Among the different kinds of nanoparticles available nowadays, magnetic nanoparticles offer great advantages thanks to their ease in separation upon application of a magnetic field.[8] This allows the avoidance of centrifugation or filtration steps, which usually results in stability of the enzyme for longer periods of time, thanks to milder recovery conditions.[9]

This type of nanoparticles has been extensively used for enzyme immobilization but in most of the cases coating of the surface has been performed. This surface modification protects the core from degradation and prevents the nanoparticles from aggregation due to magnetic interaction between the magnetic cores or interactions

with the environment, which translates into better colloidal stability and therefore a higher activity of the enzyme.

Several methods have been used for magnetic nanoparticle coating, such as coating with silica or different kinds of polymers. Amongst the polymers used, many works present systems with good stability and efficiency using polyvinyl alcohol (PVA), polyethylene glycol (PEG) or polysaccharides.[10,11] Polysaccharides offer great advantages over other synthetic polymers, as they are abundant, biodegradable and cheap.[12]

We decided to develop a magnetic support for CPO immobilization through the encapsulation of magnetic iron oxide nanoparticles in a multi-shell support of chitosan and sodium alginate. As in Chapter 2 and 3, we have used a nanoemulsion-based core for the encapsulation of the magnetic nanoparticles, which assures easy recovery of the support upon the application of a magnetic field. This core is then coated with the polysaccharides of choice: alginate and chitosan, to provide a good microenvironment of the enzyme and protect the whole support improving its stability and reusability.

Among the polysaccharides currently used for the immobilization of enzymes, we have selected chitosan and sodium alginate as they are both biodegradable, non-toxic and biocompatible and present opposite charges.[13–15] The negative charge of sodium alginate is due to the presence of carboxyl groups, while chitosan is positive at pH values below 6.0 due to the presence of amino groups that come from the deacetylation of chitin. Both polymers have been used for the coating of magnetic

nanoparticles[16,17] to obtain biocompatible and sustainable supports. Besides, the presence of charge groups enables an easy interaction with the biomolecules of interests as well as between them, allowing multicoating of the supports. It has also been demonstrated before that chitosan is also able to create a good microenvironment for our enzyme of choice.[18]

In this particular work, we have selected the enzyme chloroperoxidase as a model enzyme. This project has been carried out as a collaboration with Prof. Nicoletta Spreti from Universitá dell'Aquila and the work has been developed in the frame of two PhD thesis, Dra. Francesca Di Renzo and this one. CPO has been previously studied by that group and presents good stability and activity in polysaccharide coated supports.[18,19] Chloroperoxidase from *Caldaromyces fumago* (CPO) is a highly glycosylated heme enzyme which possesses a great industrial interest due to its ability to catalyze many reactions of large-scale interest, i.e. sulfooxidation, epoxidation and oxidative halogenation. The main disadvantage of this enzyme is its sensitivity to high concentration of oxidants, essential for its activity, which limits its industrial applications.[20]

As previously mentioned, enzyme low stability in reaction mixture can be overcome by entrapment of the enzyme to protect it from the surrounding environment. This strategy has been widely used in the literature, but different groups have used different supports. Muñoz-Guerrero *et al.*[21] immobilized CPO onto different mesoporous materials and one of the supported enzymes showed 3-times higher catalytic activity for styrene epoxidation in comparison with the free enzyme. Jiao *et al.*[22] also immobilized CPO onto mesoporous silica and evaluated its stability by

measurement of the decolorization of Crocein Orange G. In this case, immobilized enzyme showed improved thermal stability and higher stability in the presence of organic solvents. Wang and coworkers [23] and Cui and coworkers[24] both developed magnetic supports for the immobilization the CPO. Both works show improved stability and reusability in comparison with the free enzyme. A Au@Fe3O4 support was developed by Gao *et al.*[25] for the simultaneous immobilization of glucose oxidase and CPO in a layer by layer assembly and demonstrated that both enzymes exhibited good reusability and thermostability in the nanoreactor. Titanium oxide was used by Lu *et al*. [26] and Muñoz-Guerrero *et al.*[27] and the supports showed higher catalytic activity in the decolorization of crocein orange G and epoxidation of styrene respectively. Other supports have also been used by some authors such as ZnO nanowire/silica composites[28], alumina nanorods[29], graphene oxide nanosheets[30] or Eupergit ® C[31].

In our case, our research group has previously developed a hybrid polymer-silica matrix synthesized by sol-gel. As mentioned before, the chitosan coated composite was the most effective in creating the best microenvironment for enzyme catalytic activity[18], so that is why it was selected.

As it has been previously demonstrated that chitosan favors CPO activity, entrapment of the enzyme was always performed on this polymer. Alginate was able to interact with chitosan thanks to its opposite charge generating different magnetic supports depending on the combination of shells. The addition of another coat to the microsupport allows to improve stability towards the presence of other component in the reaction media All of the supports were characterized and catalytic performance

and reusability were evaluated to select the best performing one in view of large-scale applications

2. Results and discussion

2.1. Magnetic micro-supports: structure and synthesis

The encapsulation system developed in this thesis offers great advantages for enzyme immobilization for catalysis applications. Thanks to the hydrophobic core and polymeric coating, we have different compartments in which we can encapsulate different molecules, enzymes, particles or whatever is needed.

For the development of magnetic microsupport for CPO reutilization, we decided to encapsulate magnetic nanoparticles in the core, as they are a very interesting building block because their offer easy separation of the immobilization support when exposed to a magnet. Among all the synthesis method, we have selected a previously optimized co-precipitation method[32] to obtain iron oxide nanoparticles with a diameter between 5 and 10 nm. This synthesis method offers the possibility to produce nanoparticles in high amounts and produces naked nanoparticles that can be coated with any material of choice in further steps.

In our case we chose polydopamine for the coating, as it has been demonstrated in the group that favors the following encapsulation of magnetic nanoparticles in a nanoemulsion based system by improving their affinity for the nanoemulsion components. In fact, previous studies performed in the group on the encapsulation of naked nanoparticles using the same nanoemulsion strategy led to very unsatisfactory results in terms of encapsulation efficiency and homogeneity of the whole system obtained. A thin shell of polydopamine was formed around the

magnetic nuclei through spontaneous oxidative polymerization of dopamine under slightly basic pH. Dopamine was added to the nanoparticle suspension to allow firstly the coordination on iron oxide surface through catechol group and subsequently its polymerization to form an organic thin layer of polydopamine surrounding the inorganic nuclei[33] as shown in Figure 1. Polydopamine allows to passivate the surface of iron oxide nanoparticles, preventing any deterioration of their crystalline nature and therefore any possible loss of magnetic properties.

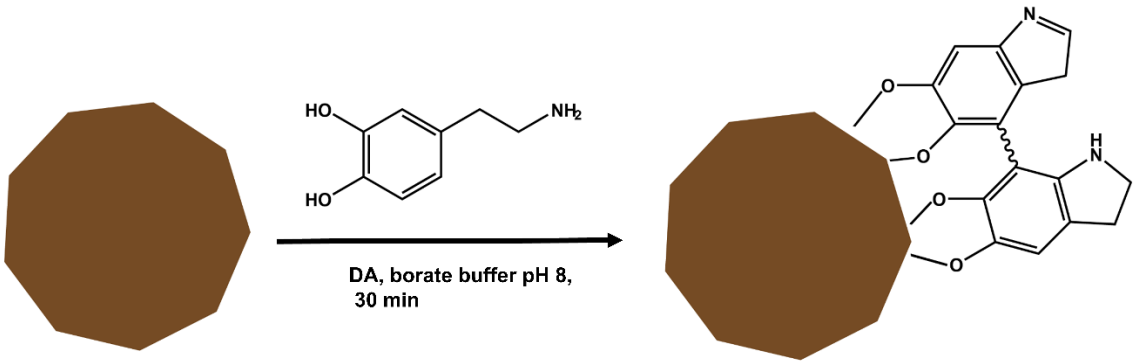

Figure 1. Schematic representation of dopamine (DA) polymerization on MNPs surface

After the polydopamine coating, nanoparticles added during the formation of the nanoemulsion core, previously described in the preceding chapters. The stabilization of these cores was obtained using natural polysaccharides, sodium alginate and chitosan, that formed a nanohydrogel shell around the magnetic nanoemulsion nuclei. These polymers were chosen mostly for their biocompatibility and availability but also for their versatility to form nanoparticles and coatings. Different kinds of interactions and both synthetic and natural polymers can be used. Although synthetic polymers can be tailored to meet specific properties, natural polymers as the polysaccharides used in this work have the advantage of being abundant in nature,

they are biodegradable, cheaper and present greener extraction/production processes.[12] Besides, thanks to the opposite charge of chitosan and alginate, we can develop multilayered nanocapsules to improve stability and tailor surface characteristics of the support.

After a first interaction of the polymer with the cores to favor their adsorption on micelle aggregates, the mixture was put in contact with a Na_2SO_4 and $CaCl_2$ solution, respectively in the case of chitosan and sodium alginate, to produce the interaction between polymer chains necessary to obtain the gelation of the polymeric coating.

CPO will be entrapped in the polymer structure, as it will allow easier diffusion of the substrate to the enzyme, facilitating the catalysis. Besides, in previous studies carried out by De Matteis *et al* [18], it was observed that CPO entrapped in both alginate and chitosan had good catalytic activity.

Apart from the iron oxide magnetic nuclei, the organic nature of the support makes it sensitive to reaction conditions. The search for the most robust coating was necessary to avoid any loss of support properties during the recycling process of the catalytic nanosystem. So, in order to select the most efficient system for enzyme immobilization, different strategies were developed, involving different combinations of the two polysaccharides on the surface of the magnetic nanoemulsion based supports.

The first approach consisted in the covalent crosslinking of chitosan network containing the immobilized CPO. For this purpose, BS^3 was used as a covalent crosslinker as it was previously used in other studies for the functionalization of chitosan-coated nanocapsules. In this case, the crosslinker was added to the chitosan-coated microsupports in borate buffer pH 8.2. This pH assures that the

amino group in chitosan is not protonated and it is able to react with BS^3. This strategy has some drawbacks, as BS^3 crosslinks the amino groups in the chitosan layer but is able to react also with the amino groups in CPO. This can rigidify the enzyme structure limiting its catalytic activity, so measurement of the catalytic activity will be important to check if the microsupport is efficient after BS^3 crosslinking or the rigidification reduced the catalytic performance of the enzyme.

In a different strategy for microsupport improvement, mixed polymer layer was used to reinforce the support and protect it from the reaction media conditions. In particular, chitosan and sodium alginate were used in two different combinations (inner chitosan shell, outer alginate shell or the opposite combination) as reported in Figure 1. For this purpose, the previously synthesized microsupports, ALG or CS monolayer, were exposed to a second coating with the opposite polymer. In both cases, the microsupport was resuspended in acetate buffer pH 5 to assure that both polymers are charged and are able to interact with each other thanks to their opposite charge.

Independently on the coating strategy, chitosan was chosen to create an optimal microenvironment for enzyme entrapment thanks to its superior stabilizing effect on CPO, as observed in our previous work.[19] So, in all tested combinations of coatings, enzyme was always entrapped in chitosan shell. This means that although 5 microsupports were characterized, ALG was only tested as the previous step to the ALG-CS synthesis, as CPO was not entrapped in ALG microsupport.

In the end, five different magnetic supports were obtained: CS, ALG, CS-ALG, ALG-CS and CS-BS^3, and a scheme is shown in Figure 2. All of them undergo to full

characterization and stability assays to assess their performances in terms of material properties and enzyme reusability.

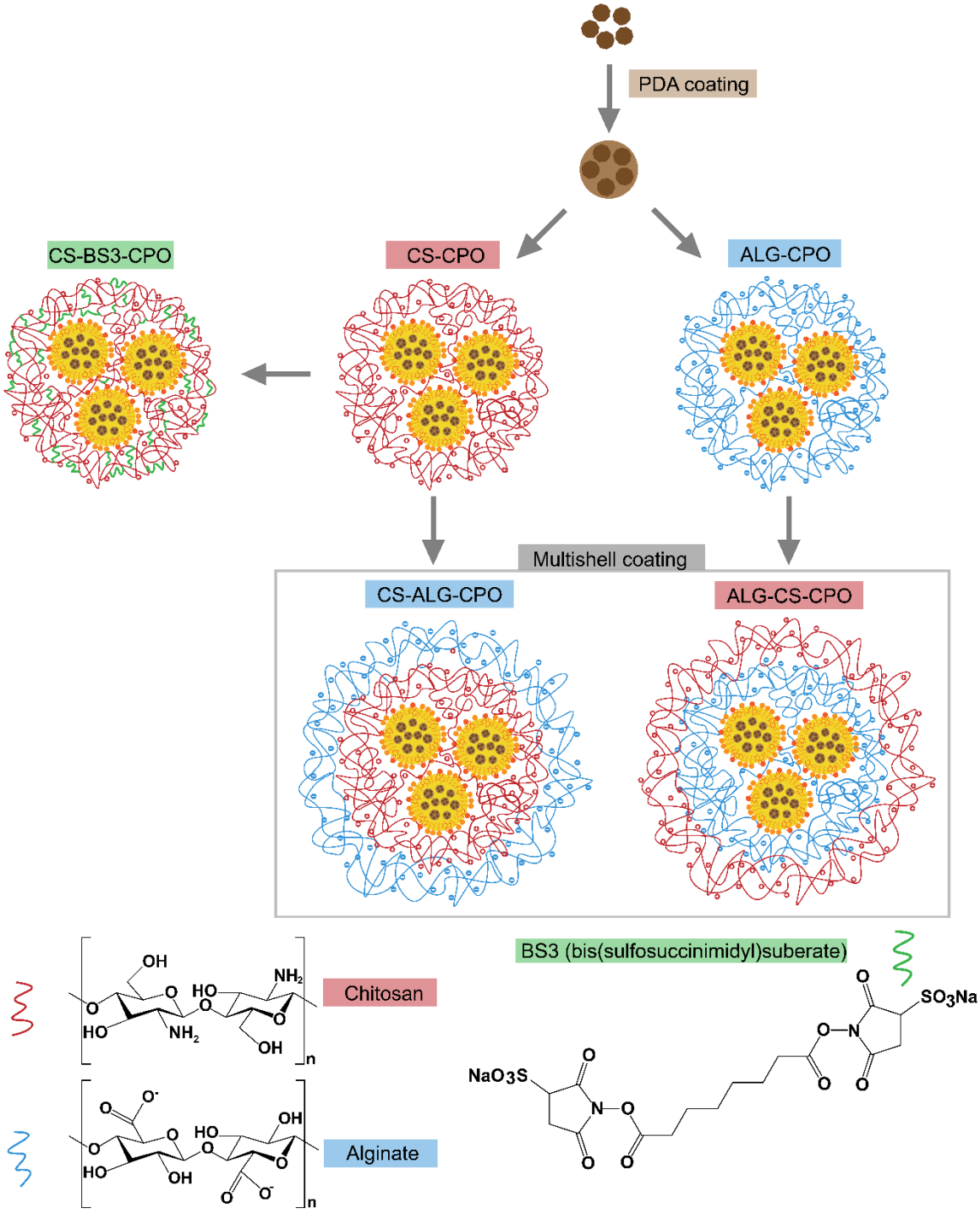

Figure 2. Schematic representation of the developed microsupports

2.2. Magnetic micro-supports characterization

Characterization of the magnetic microsupports started by studying and confirming the modifications on the shell. For this purpose, we used different techniques to confirm the presence of the different polymers coating the magnetic cores: FTIR and Z-potential analysis.

Firstly, FTIR spectra of the magnetic nanoparticles coated with polydopamine and the optimized supports coated with the different polymers shells are reported in Figure 3.

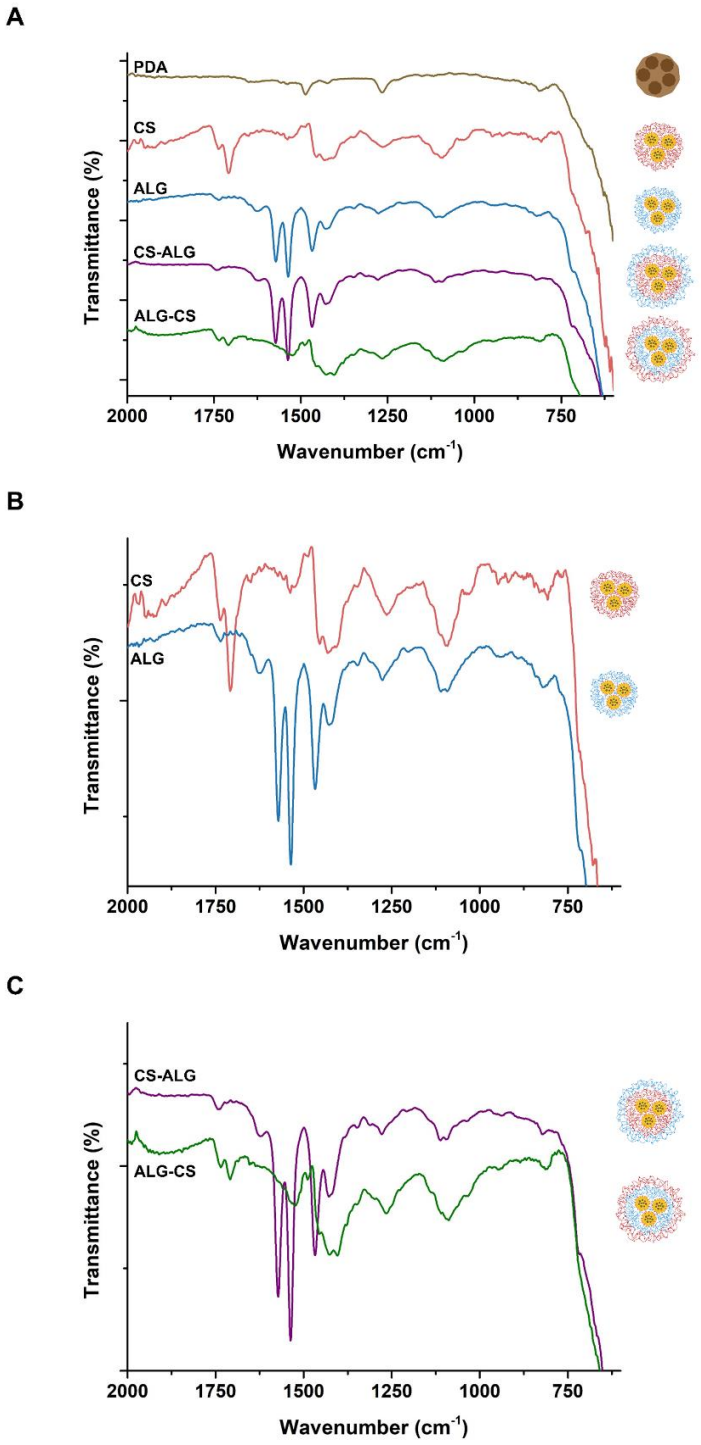

Figure 3. FTIR analysis of magnetic micro-supports: A) comparison of FTIR spectra of all micro-supports; B) comparison between single shell micro-supports (ALG and CS); C) comparison between double shell micro-supports (CS-ALG and ALG-CS).

FTIR spectra of all the coating steps were registered to be able to follow all the surface modifications. We report all the spectra together in Figure 3A to be able to compare between them, while in Figure 3B and 3C the comparison between single shell systems and the double-shell ones are reported for a more accurate description. Naked emulsion spectrum is not reported, as it was not possible to record FTIR spectra of the emulsion without coating due to low stability of the system. For this reason, we are not able to determine if the components of the emulsion are present on the spectra or not, as after polymer addition peaks corresponding to the surfactants are not present in the spectra recorded. However, due to increase in turbidity of the solution during the emulsion synthesis step, it can be determined that the nanoemulsion has been formed.

From Figure 3B it can be observed that the method used to obtain the coating of the nanoemulsion cores by covering them with one coat of the polysaccharides is very effective since the peaks corresponding to most representing vibrations of the polymers structure can be recognized in both cases.

In particular, in CS single coated microsupports (red line), bands at 1648 and 1540 cm^{-1} could be attributed to the stretching of C-O (amide I) and N-H bending (amide II) of chitosan, respectively. Moreover, absorption bands, characteristic of the polysaccharide structure, appear at 1100 cm−1 (stretching of C-O-C glyosidic bridge) and 1030 cm^{-1} (skeletal vibrations involving the C-O stretch).

In the case of ALG single shell micro-supports (blue line), the characteristic absorption bands related to the asymmetric and symmetric stretching of –COO- groups are shifted to 1536 and 1465 cm^{-1} with respect to the pure polymer (1595

and 1405 cm^{-1}). These shifts could be due to the interactions between the polymer and the components of the nanoemulsion or with the Ca^{2+} ions used for crosslinking. In the case of double-shell supports, Figure 3A and 3C show that the spectra correspond only to the external layer and the internal one is not observed in any case. This may be explained by a masking effect of the outer shell probably due to interactions established between both layers. However, to make sure that both layers are present and the addition of the second one does not remove the previous layer, another characterization technique was applied.

ζ potential analysis was carried out to describe the changes on micro-support surface, especially in the case of single and double layer coatings. Results are reported in Figure 4.

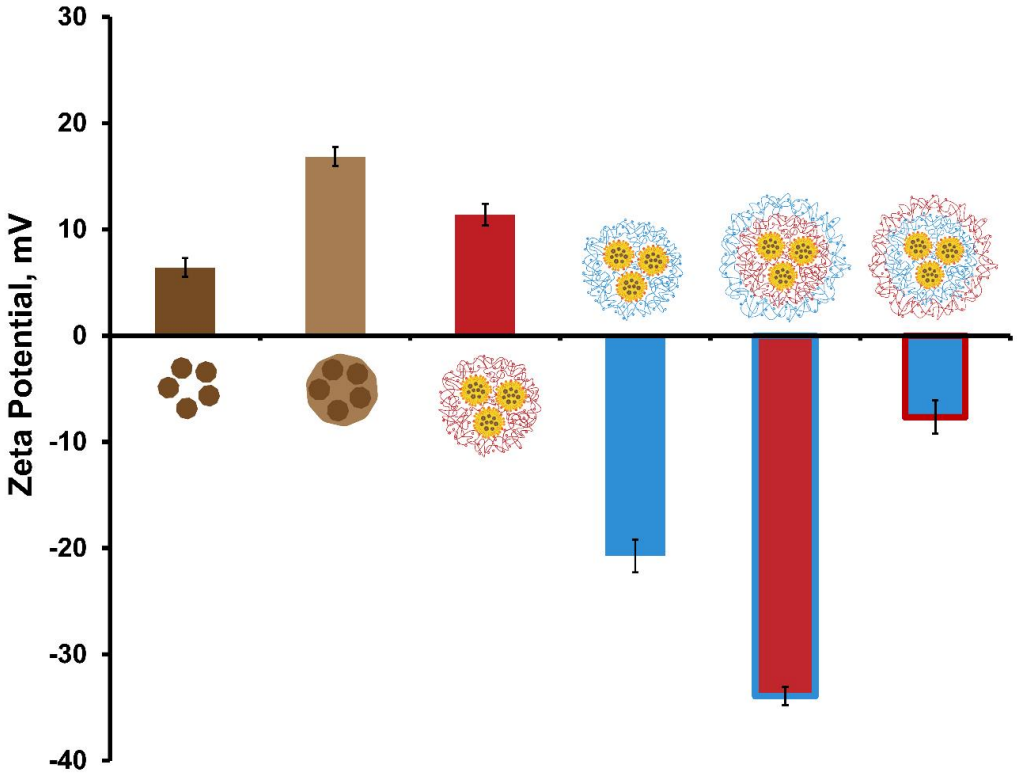

Figure 4. Z-potential analysis of magnetic micro-supports with and without polymeric shells.

It resulted from the analysis that the potential of the surface of the obtained magnetic supports clearly reflected the nature or combination of the polysaccharides used. As expected, CS single coated microsupports (red bar) present a positive potential (+11 ± 1 mV) due to the presence of amine groups in the surface, while ALG single coated microsupports (blue bar) show negative potential (-21 ± 2 mV) because of the carboxylic groups.

In the case of double coated nanoparticles, the outer alginate layer over chitosan (red bar with blue outline) presents a high negative potential (-34 ± 1 mV). As observed in the single layer alginate coating (blue bar), alginate coating presents higher ζ potential absolute value in comparison with chitosan one, so in the CS-ALG, high negative ζ potential observed will be due to a masking effect of alginate over chitosan. In the opposite combination (ALG-CS), the chitosan outer layer, having a lower ζ potential absolute value, is not able to mask completely the negative charge of the alginate which would explain the slightly negative potential (-8 ± 2 mV) observed. However, the presence of chitosan is confirmed by the increase in the potential in comparison with the single coated alginate microsupports.

This confirms the hypothesis that double layer microsupports have been obtained, although the inner layers were not easily recognized in the FTIR spectra.

The morphological characterization of the materials produced in this work has been carried out using the Transmission Electron Microscopy (TEM) for the magnetic nanoparticles and Environmental Scanning Electron Microscopy (ESEM) for the magnetic micro-supports that required softer conditions during the analysis. When we tried to use TEM for the morphological study of the microsupports, they showed to be very sensitive to conventional operative conditions and no images were

obtained. This is due to the fact that upon interaction with the electron beam, due to the sensitiveness of the material, sample appears to be melting, and no image can be taken, as the sample disappears before. In Fig. 5, images referring to TEM analysis of iron oxide nanoparticles naked (A) and coated with polydopamine (B) are reported, together with ESEM images referring to CS-ALG and ALG-CS magnetic micro-supports (Fig. 5C and D respectively).

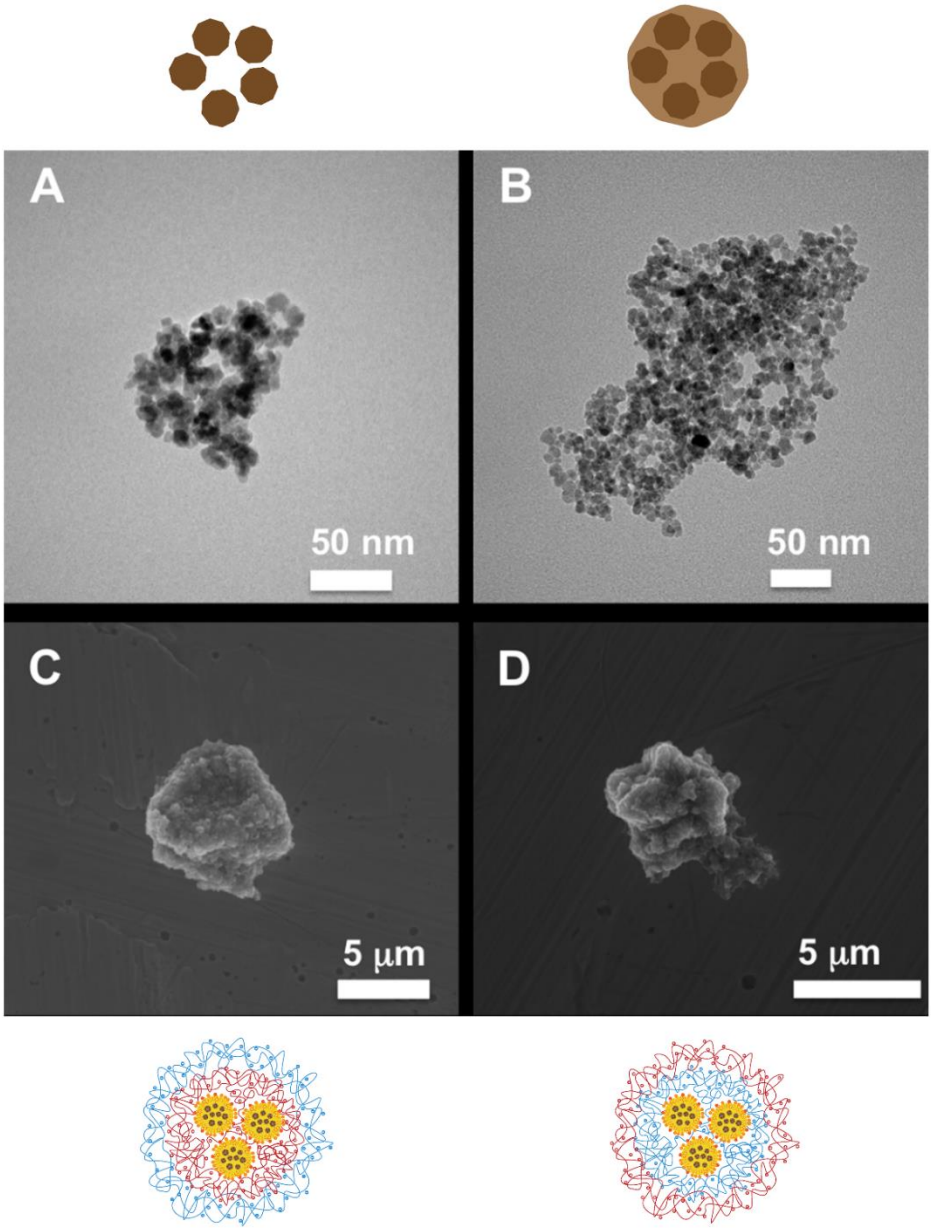

Figure 5. A) TEM image of iron oxide nanoparticles; B) TEM image of polydopammine-coated iron oxide nanoparticles; C) ESEM image of CS-ALG magnetic micro-support and D) ESEM image of ALG-CS magnetic micro-support.

It is possible to appreciate from the images that naked magnetic nanoparticles, as well as the polydopamine coated ones, have a size around 5–10 nm. If we observe these images, it looks like these small nanoparticles are aggregated in larger

clusters, but this effect can be addressed to the sample preparation method and especially to the drying effect of samples in water suspension.[34] In the case of PDA coating, it can be also due to the formation of aggregates during the polymerization reaction. This effect can be corroborated by the fact that both kind of nanoparticles are very stable in water suspension over long periods of time at room temperature and no precipitation or change of appearance was observed.

In ESEM images, we can observe that after the encapsulation, these small nanoparticles are incorporated into the emulsion core and then probably several cores are surrounded by the polymeric layer, leading to the formation of micro-supports with a size of a few microns. This effect seemed to be independent from the combination of polymeric coatings, as shown in Figure 5C and D.

2.3. Functional stability of magnetic micro-supports

Before testing the catalytic activity of the microsupports, it was very important to test the stability of the support in the reaction media. This would allow us to check if the microsupports are suitable for the final application or we needed to develop other options. The reaction mixture consists of phosphate buffer at pH 2.9, containing the substrate (monochlorodimedone), KCl and H_2O_2. These components, especially phosphate buffer with acidic conditions, can affect the stability of the supports. Acidic pH can destabilize the polymeric coating of the support due to change in polymer changer. Besides, it is reported that polydopamine coating is not stable under acidic conditions[35] and as polydopamine-coated nanoparticles are contained in the core of the structure, any release of dopamine would mean that there has been a disruption in the integrity of the microsupport.

The chemical stability of the developed micro-supports in the reaction medium was measured in terms of dopamine release during time. The supports were put in contact with phosphate buffer pH 2.9 used in the enzymatic reaction and any release of polydopamine and/or dopamine was measured spectrophotometrically.

The results reported here have been performed in phosphate buffer and not in the complete reaction medium. It was previously checked that identical results were obtained using the complete reaction medium, with the substrate, KCl and H_2O_2, but only phosphate buffer was used to avoid the waste of reactants. As the same results were obtained with or without complete reaction media, it can be confirmed that the degrading effect has to be completely addressed to the buffer composition and pH. Stability results obtained using the developed magnetic micro-supports without enzyme are reported in Figure 6. The point at time 0 refers to incubation in the aqueous storage medium in which no release of dopamine/polydopamine was observed. In this case, the choice of using micro-supports without the enzyme and an incomplete reaction medium was a matter of economy of the process, as the results are the same, and waste of expensive reactants was unnecessary.

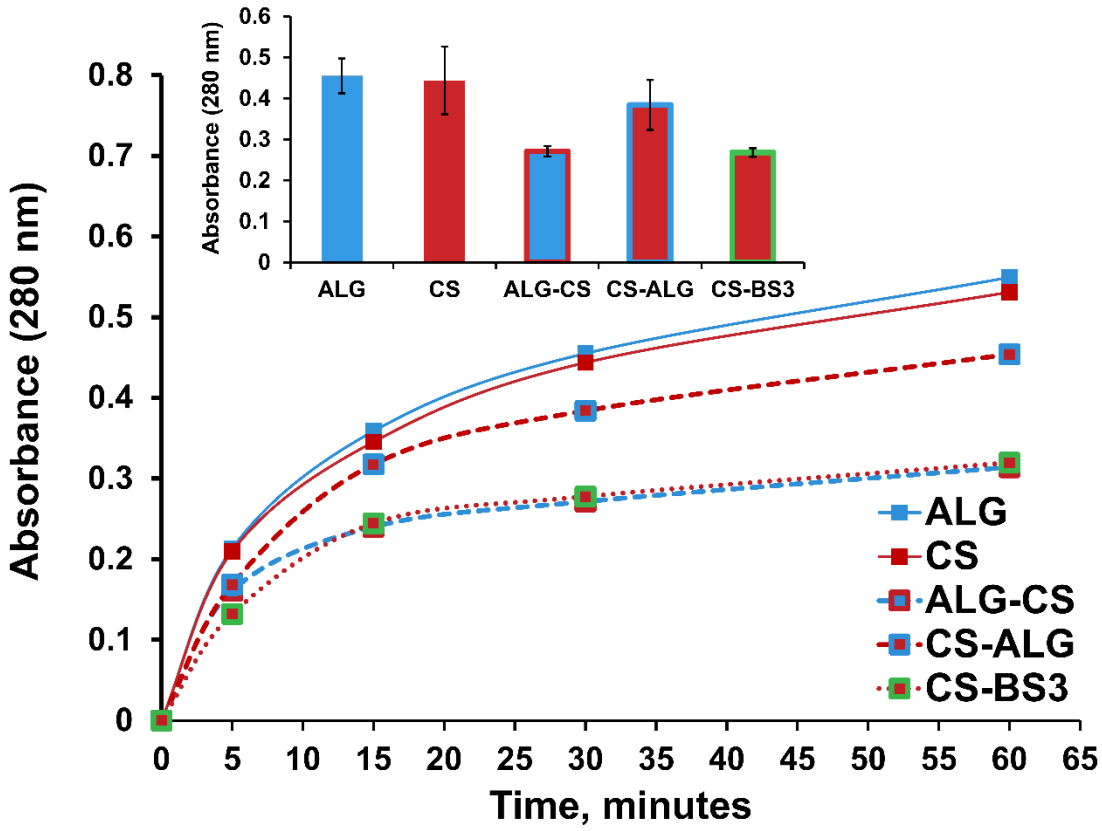

Figure 6. Stability assay of magnetic micro-supports. Dopamine/polydopammine release in phosphate buffer 10 mM pH 2.75. Inset: data referring to 30 minutes incubation.

As observed in Figure 6, it was found that both ALG and CS single polymer shell did not protect the support from the release of components. In fact, we observed a great amount of dopamine release from the iron oxide magnetic nanoparticles surface. This would mean that upon addition of the microsupports to the reaction medium, the protective shell would be swelled due to the acidic pH and the presence of phosphate ions. In the case of ALG, this can be explained by the fact that sodium phosphate salt leads to the wash out of the Ca^{2+} ions that are holding the alginate structure around the emulsion core, leading again to the aperture of the hydrogel network.[36,37] For the CS support, the acidic condition of the phosphate buffer triggers

swelling of the polymer, also destroying the coating. According to the literature, the residual amino groups of chitosan can be ionized in acidic buffers, which contributes to the electrostatic repulsion between adjacent ionized residual $–NH_2$ groups of chitosan leading to chain expansion and eventually increases the water uptake of the gels.[38] This swelling of the polymer will eventually lead to degradation of polydopamine from the core of the supports due to the acidic pH that, as already mentioned, is not stable at low pH. The rigidified structure CS-BS3, in which the polymer is covalently crosslinked with BS^3, should reduce the polymer swelling, increasing microsupport stability.

As observed in Figure 6, this strategy improved the stability of the microsupport, explained by the decrease in the absorbance at 280 nm, meaning that there was decrease in the release of dopamine (the absorbance after 60 minutes of single layer supports is 0.5 while for CS-BS^3 is 0.3). This same effect was observed using the support with a sodium alginate internal shell and an outer chitosan layer (ALG-CS has an absorbance of 0.3) but only a very small improvement was observed using the inverted shell combination (CS-ALG has an absorbance of 0.45). This would mean that chitosan internal shell and sodium alginate outer layer behaved like the support with a single chitosan shell. This could mean that the chitosan swelling is reduced in the ALG-CS by stabilization by alginate and phosphate ions are not able to penetrate enough in the structure to destabilize alginate inner coating. In the CS-ALG coating, the alginate structure would not be stabilized by the inner CS, leading to reduced stability. These results will help understand the catalytic activity of the microsupports.

2.4. Chloroperoxidase immobilization and catalytic performances

After enzyme immobilization, it was important to determine the encapsulation efficiency. For this purpose, we investigated the presence of free CPO in both supernatants of the encapsulation process by SDS-PAGE analysis (Figure 7).

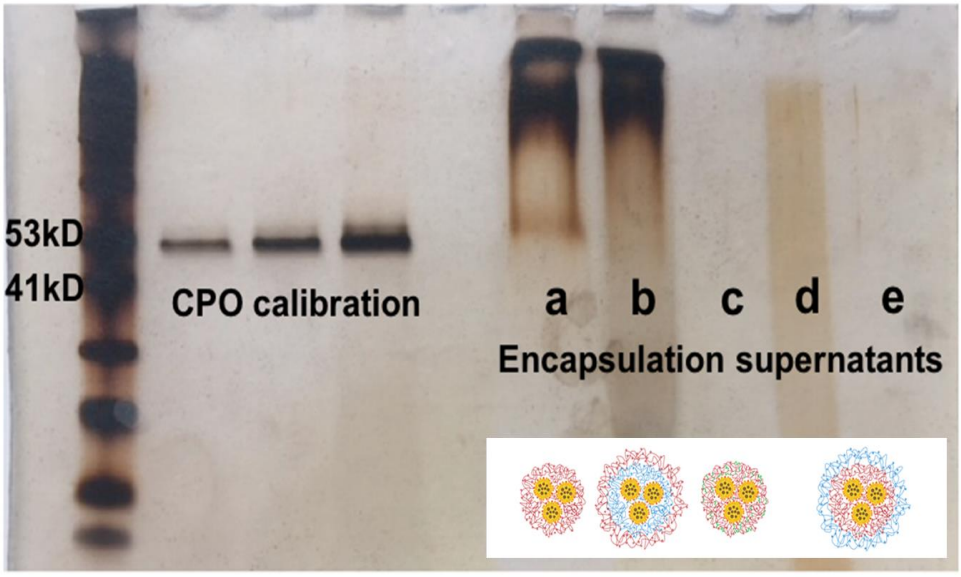

Figure 7. SDS-PAGE analysis of encapsulation supernatants: a) CS supernatant, b) ALG-CS MMS supernatant, c) CS-BS3 supernatant MMS, d) CS-ALG washing solution before gelation and e) CS-ALG supernatant of gelation.

In Figure 7, we can observe the results from the SDS-PAGE electrophoresis. Supernatants of encapsulation when dialyzed to eliminate excess reactants of the synthesis and then freeze dried and concentrated up to a maximum theorical concentration of 6 µL of CPO/mL. After running the SDS-PAGE electrophoresis, the gel was stained using silver staining to reveal the band intensities, which intensity was estimated using Image J software. To determine the amount of CPO present in these bands, a calibration curve was also performed in the same experiment with

increasing quantities of CPO. Comparison of supernatant band intensity with the calibration curve gave CPO concentration in the supernatant. After calculations, it was determined that only 8% of total CPO added during entrapment CS was detected in the supernatant. During BS^3 crosslinking reaction of CS supports, enzyme leaching is less than 5% and the same result is observed during ALG coating of CS coated supports (CS-ALG). This result of less than 5% of enzyme leaching is the limit of detection of the technique, and it is due to the fact that no band is detectable.

In the case of entrapment of CPO in ALG-CS, at least 95% of the total CPO added is encapsulated. These results confirm that the entrapment efficiency of CPO in the reaction conditions is optimum and that these supports are suitable for the catalytic assay and CPO is entrapped in the microsupport.

The developed magnetic microsupports with encapsulated enzyme were used to test the activity and reusability of the catalytic systems for monochlorodimedone (MCD) conversion to dichlorodimedone (DCD). This reaction is used as a model as it is easy to follow due to decrease in the absorbance at 280 nm when MDC is converted into DCD. Reaction conditions, in terms of enzyme/substrate ratio and concentrations, were the same that the authors used in previous studies.[19] A description of the whole process (catalytic assay and recycling) is reported in Scheme 1.

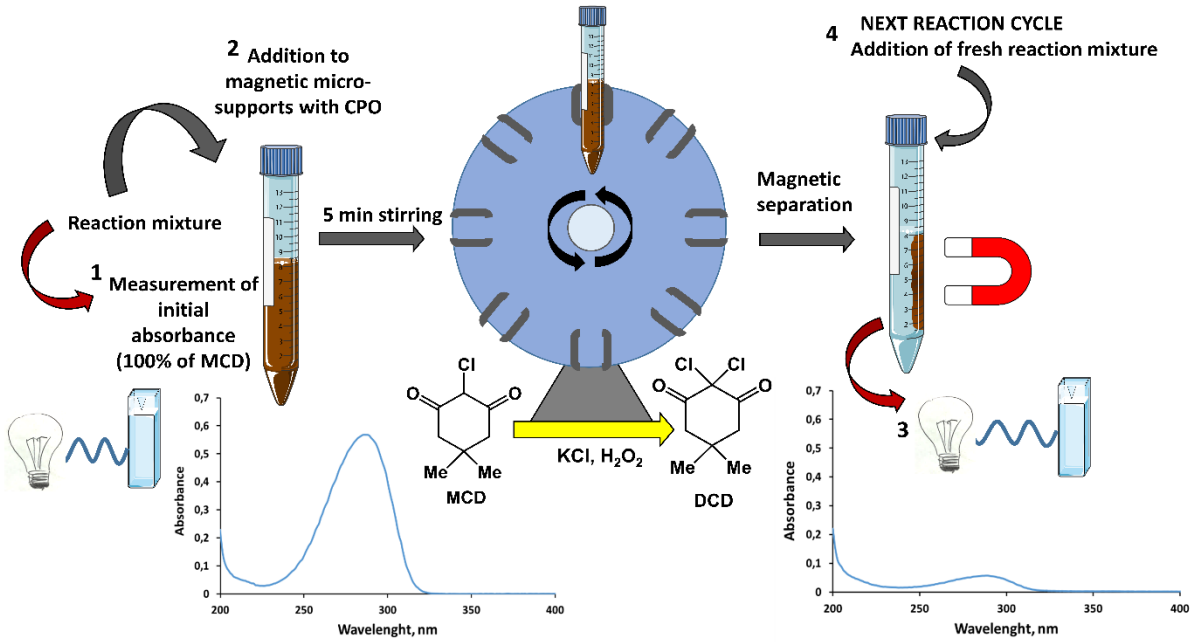

Scheme 1. General description of catalytic assay and recycling procedure.

Scheme 1 presents the catalytic assay and recycling process that was followed in this experiment. Firstly, a reaction mixture containing all the reactants but the microsupports was prepared. Absorbance at 280 nm of this solution was measured and the absorbance result was considered as a 100% of MCD (Step 1 in Scheme 1). Then, this reaction mixture was added to the magnetic microsupports with CPO entrapped, and this solution was agitated for 5 minutes for the reaction to take place (Step 2 of Scheme 1). To calculate the reaction yield, the reaction mixture was separated from the microsupport using a magnet and the absorbance of the solution was measured again (Step3 of Scheme 1). If a conversion of 100% was obtained (no absorbance at 280 nm) micro-supports were recovered and put in contact with a fresh reaction mixture to be reused in a second reaction cycle (Step 4 of Scheme 1). The process was repeated until the conversion yield was not 100%. If the

absorbance was not 0 after 5 minutes, there was some MCD (substrate) in the reaction mixture, meaning that the reaction was not complete. The reaction mixture was mixed again with the microsupport and they were let in contact for longer periods of time for the reaction to be complete.

First attempts were performed using a washing step with phosphate buffer solution between cycles in order to remove excess reactants from the previous cycles. However, this step was skipped in these final results as the reaction was always complete and there was no substrate in the reused support. Besides, it was observed that this washing step caused high stress in the microsupport probably due to compactation and drying during the separation process, which lead to slightly lower reusability efficiency in terms of number of consecutive cycles of reaction.

Results of the substrate conversion in the first reaction cycle for the different supports are shown in Figure 8.

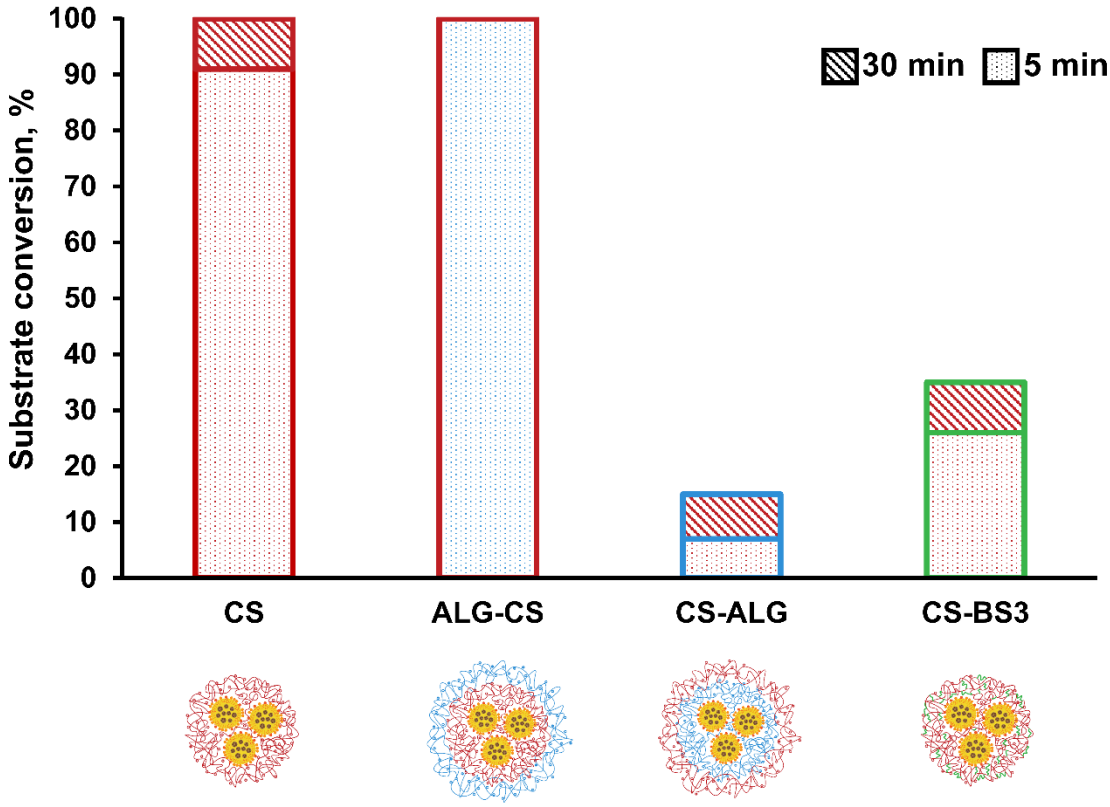

Figure 8. Reaction yields after the first reaction cycle.

The conversion yields were evaluated in a first reaction cycle and shown in Figure 8. It can be observed that dotted part of the bar shows the substrate conversion after 5 minutes of reaction. If this conversion was not completed, the reaction was carried out for 25 more minutes and the results are reported in the striped part. Results show that CPO encapsulated in the CS-ALG, as well as in the CS and CS-BS^3, showed almost no activity at the first reaction cycle, even when the support was left for 30 minutes in contact with the substrate. The lack of activity of entrapped CPO in the case of alginate outer shell could be addressed to poor substrate diffusion through the polymeric shell and not that much in enzyme loss of activity. However, in the

case of CS-BS[3], as mentioned before, crosslinking of the enzyme amino groups can lead to rigidification of the protein structure. Covalent linking to the polymer network and the consequent decrease in the flexibility or the distortion of the active site would probably result in the inactivation of the catalyst. For the microsupports in which the enzyme is exposed in the outer layer (CS and ALG-CS), we can observe more than 95% conversion after 5 minutes so both supports were tested in terms of reusability (Figure 9).

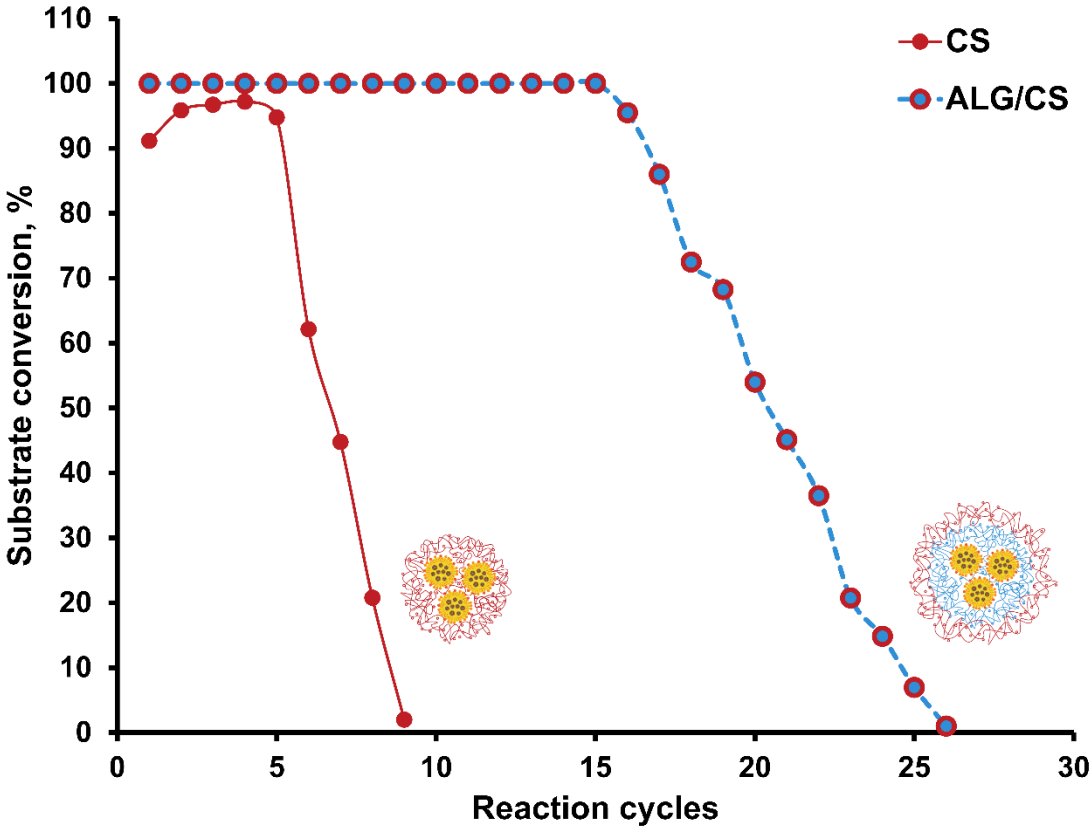

Figure 9. A) B) Reusability of chitosan-coated (CS) and double shell coated micro-supports with alginate inner shell (ALG-CS).

Results of reusability of the supports showing higher substrate conversion are shown in Figure 9. Substrate conversion is represented in relation with the cycle number.

These results were obtained measuring the substrate conversion in several cycles as explain in Scheme 1. It can be observed, that in the case of CS, the substrate conversion is higher than 90% for the first 5 reaction cycles but it is dramatically decreased in sixth circle. The substrate conversion was almost 0 after 9 reaction cycles. In the case of ALG-CS, we could observe a much higher reusability of the system which is in agreement with the higher chemical stability observed during the CPO leaching assay. The catalytic system was able to convert the substrate with a 100% of efficiency during 16 consecutive reaction cycles. The following cycles, as substrate conversion was not 100% after 5 minutes, longer reaction times were required. The system still presented a 23% of conversion at cycle 23. The difference in the two systems reusability can be explained by the stability observed in the previous experiment of dopamine release. In the case of CS, the reduced stability would mean that the enzyme is progressively leached from the support which would ultimately mean that the amount of enzyme in the microsupport after few cycles would be greatly reduced.

To confirm this hypothesis, the presence of free enzyme in the washing steps of encapsulation and in the reaction mixture was checked. For this purpose, the supernatants (without the microsupport) were mixed with reaction mixture and substate conversion was evaluated. If enzyme leaked from the support, substrate conversion would be more than 0%, as there will be enzyme in the mixture. If substrate conversion was 0%, no enzyme would be leaking as no microsupport with entrapped enzyme was added. In the case of CS, leaching of the catalyst was detected and a 77% and 97% of conversion were measured respectively in the encapsulation medium and conditioning medium after 15 min of incubation with the

reaction mixture. In the case of ALG-CS, no conversion was observed. This confirms that the difference in reusability is due to the different stability of the microsupports and a prolonged entrapment of the enzyme in the system.

The reusability obtained with CPO entrapped in ALG-CS supports was comparable or even better than that reported in literature for other magnetic support with immobilized CPO. The same number of cycles and a 62% activity was obtained by Cui and coworkers[24] using magnetic nanoparticles as the support. Results clearly confirmed that chitosan-based materials represent a very suitable microenvironment for chloroperoxidase immobilization and reuse, as observed in previous studies.[19] The best results found in literature for CPO reusability were carried out by Jiao and coworkers[22] by entrapment of CPO in mesoporous silica matrix, which is a totally different carrier than the one presented in this thesis. In their research, CPO was entrapped by electrostatic interactions and they get 61% of enzyme initial activity after 20 cycles of reuse. In their case, they immobilized CPO by LBL assembly through avidin-biotin affinity binding. Other studies were found, but none of them obtained such high reusability as the one observed for our carrier. The most interesting comparison would be to evaluate the number of substrates converted to product per mg or unit of enzyme, however, this study could not be carried out as this information was not possible to be calculated from the published studies.

3. Conclusions

Enzyme immobilization in magnetic supports offers many advantages for the reusability of the catalytic system. The use of these supports allows to easily

separate the catalyst from the reaction medium and to reuse it during several reaction cycles, highly improving the cost-effectiveness of synthetic processes. In this chapter, we demonstrate the capability of the developed synthesis method for future application in the catalytic industry. The versatility of the system allows an easy encapsulation of the magnetic nanoparticles in the core of the microsupport which allows the simple recovery of the catalyst and its reusability. On the other hand, the flexibility in the selection of the polysaccharide coating allowed the development of different microsupports to evaluate the best microenvironment for the enzyme of interest.

The possibility of combining different polymers to obtain multi polysaccharide shells has been successfully explored together with the covalent crosslinking of chitosan for the improvement of polymer shell rigidity and therefore its stability. Interesting differences in micro-supports chemical stability under reaction conditions have been observed. Among the most stable magnetic supports obtained, the one that combine an alginate inner shell and a chitosan outer shell, containing the entrapped enzyme, showed the best reusability of the catalytic system, allowing 25 consecutive cycles of model substrate conversion. This result indicates that the catalytic properties of the enzyme are preserved by protecting it from the effect of denaturing agents and probably through a physical stabilization of the protein in the microenvironment of the support as expected. The combination allows good stabilization of the inner core thanks to the alginate layer and optimal enzyme microenvironment and substrate diffusion thanks to the chitosan outer layer. On the basis of the interesting results obtained, future works will be devoted to test the developed system for the catalysis

of more interesting reactions catalyzed by chloroperoxidase for synthesis of fine chemicals.

The optimization of the support properties carried out in this study to obtain a magnetic support with a stabilizing polymer shell demonstrated that supported catalysts with superior properties could be obtained developing smart materials that gather properties of their different components. Therefore, besides the exploration of the applicability of entrapped CPO in other interesting reactions, the developed system allows easy modification of the support surface to be applied in the entrapment of other enzymes of interest. Thanks to its versatility, it would also allow the entrapment of different enzymes to develop a multienzymatic system in which the different steps of a reaction could be done in just one step.

4. Materials and methods

4.1. Materials

Chloroperoxidase (CPO, EC 1.11.1.10) from *Caldariomyces fumago*, as a crude suspension (26,776 U/mL), Monochlorodimedone (MCD, 2-chloro-5,5-dimethyl-1,3-cyclohexanedione), alginic acid sodium salt, Span® 85 (sorbitanetrioleate) (Croda International PLC, Cowick Hall Snaith, UK), oleic acid, chitosan (medium molecular weight), iron(II) chloride tetrahydrate ($FeCl_2 \cdot 4H_2O$), iron(III) chloride hexahydrate ($FeCl_3 \cdot 6H_2O$) and dopamine hydrochloride were acquired from Sigma-Aldrich. Tween® 20 (Croda International PLC, Cowick Hall Snaith, UK) was obtained from Panreac. Iron standard solution was purchased from Across Organics. Bis(sulfosuccinimidyl) suberate (BS3) was obtained from Pierce Biotechnology.

Water (double processed tissue culture) used in all micro-supports synthesis and 14 kDa dialysis tubing cellulose membrane were purchased from Sigma. Mini-PROTEAN® TGX Stain-Free Gels 8–16% and Pro-Sieve® Color Protein Markers were acquired from Bio-Rad and Lonza respectively.

4.2. Synthesis of magnetic nuclei

Magnetite nanoparticles were prepared following a previously optimized co-precipitation method.[32] $FeCl_3 \cdot 6H_2O$ and $FeCl_2 \cdot 4H_2O$ in a 3:1 ratio were dissolved in 18 mL of water and 6 mL of 30% $NH_3 \cdot H_2O$ were added drop wise under gentle stirring to form magnetic nuclei. After 20 min, magnetite nanoparticles were precipitated magnetically to remove the reactants and they were washed three times with water to remove the excess reactants. Finally, they were suspended in 10 mL of water.

To obtain polydopamine coating, 240 mg of dopamine were dissolved in 80 mL of 0.1M borate buffer pH 8. Then, 76 mg of MNP, measured in terms of iron content, were added to the solution that was stirred for 30 min for the dopamine polymerization. Then, the coated magnetic nanoparticles were separated from the non-magnetic PDA particles by using a magnetic rack. PDA-coated magnetic nanoparticles (PDA-MNP) were washed three times with water and suspended in 10 mL of fresh water.

4.3. Synthesis of polysaccharide-stabilized micro-supports

Micro-supports cores were obtained using a nanoemulsion method similar to the one described in Chapter 2 but slightly modified for the encapsulation of MNP. 30 mg of PDA-MNP were added to 4 mL of water solution containing 6.8 mg Tween® 20.

Then, the organic phase containing 4.3 mg Span® 85 and 20 mg oleic acid in 2 mL absolute ethanol was added to the aqueous phase under stirring. Nanoemulsion spontaneously and almost immediately formed. Then, 0.25 mL of a 5 mg/mL chitosan solution in acetic acid 1% (v/v) or 1.25 mL of a 10 mg/mL alginate solution in water were added to stabilize the obtained nanoemulsion. In the last step of the synthesis, chitosan-coated nanoemulsion supports (CS) were added to 20 mL of 50mM Na_2SO_4 under manual stirring. In the case of alginate-coated supports (ALG), supports were washed twice with water before they were added to 20 mL of a 10% $CaCl_2$ solution. Both kind of micro-supports were washed three times with water and resuspended in 2 mL of fresh water.

4.4. Synthesis of external extra shell

25 mg of ALG or 10 mg in the case of CS were resuspended in 6 mL 50mM acetate buffer pH 5 under stirring. Then 0.65 mL of a 10 mg/mL sodium alginate solution or 0.25 mL of 5 mg/mL chitosan solution were added drop-wise respectively to the CS or ALG suspensions and kept under stirring for 30 min. Finally, alginate-externally coated micro-supports (CS-ALG) were washed twice with water and they were added to 20 mL of a 10% $CaCl_2$ solution, while chitosan-externally coated micro-supports (ALG-CS) were added to 20 mL of 50mM Na_2SO_4 under manual stirring. Both kind of double-coated micro-supports were washed three times with water and they were resuspended in 2 mL of fresh water.

4.5. Stabilization of chitosan magnetic micro-supports with BS^3

For the crosslinking of CS, 200 nmol of bis(sulfosuccinimidyl) suberate (BS3) were added drop-wise to a solution of 10 mg of microsupports in 40 mL of 10mM borate

buffer pH 8.2 and they were kept under stirring for 30 min. Micro-supports were washed twice with water and resuspended in 2 mL.

4.6. Characterization of polysaccharide-coated magnetic micro-supports

Iron content of micro-supports in water was obtained spectrophotometrically using a Varian Cary 50 UV/Vis spectrophotometer. Magnetic micro-supports were dissolved in a solution of nitric acid/hydrochloric acid. Then, a solution of KSCN 0.75M was used to form a complex with Fe(III) that absorbs visible light at 484 nm. Iron concentration was obtained using a calibration with iron standard solution.

The encapsulation efficiency of MNP in polysaccharidic micro-supports was obtained calculating the ratio between the amount of iron encapsulated (recovered amount), measured dissolving the final material, and the amount of iron added during nanoemulsion formation (initial amount). The iron loading has been calculated from the ratio between the amount of iron recovered after encapsulation and the total weight of the final material obtained after freeze-drying.

Z Potential of supports has been determined by measuring the potential of a 0.05 mg/mL nanoparticle suspension in 1mM KCl solution with a Plus Particle Size Analyzer (Brookhaven Instruments Corporation).

Fourier Transform Infrared Spectroscopy analysis was carried out in a JASCO FTIR-4100 Fourier transform infrared spectrometer in a frequency range of 600–4000 cm^{-1} with 2 cm^{-1} resolution and a scanning number of 32.

MNP and MNP-PDA wered observe in brightfield imaging in FEI Tecnai T20 operated at 200 kV. Samples were resuspended in ethanol under sonication, putting a drop of the suspension on a TEM carbon grid and letting it to dry at room temperature in air atmosphere before observation in the microscope.

Samples were analyzed by means of Environmental Scanning Electron Microscopy (ESEM) in a QUANTA-FEG 250 microscope. The sample was analyzed without any previous treatment. The observation was carried out using a cooling stage (at approximately 1 °C) at humidity conditions of approximately 100%.

4.7. Stability assay

The stability of the support under reaction conditions was evaluated by incubating 5 mg of each magnetic microsupport with phosphate buffer 10mM pH 2.75 and measuring the release of dopamine during time by spectrophotometry at 280 nm.

4.8. Chloroperoxidase encapsulation

26,78 U of CPO (1 µL) were added to 0.25 mL of chitosan 5 mg/mL, before chitosan shell synthesis, depending on the material to be prepared, after nanoemulsion formation or after alginate first shell synthesis and the rest of the synthesis process was kept the same.

The encapsulation efficiency of the enzyme was evaluated by sodium dodecyl sulfate polyacrylamide gel electrophoresis analysis (SDS-PAGE). Supernatants of encapsulation, as well as of the conditioning solution (phosphate buffer), were analyzed to quantify CPO content. Supernatants from encapsulation process were dialyzed overnight using 14 kDa dialysis tubing celullose membrane. All samples

were freeze-dried in a Telstar Cryodos freeze-dryer and concentrated at a maximum theoretical concentration of up to 6 μL of enzyme per milliliter of solution. Samples were denatured by boiling them in presence of a SDS/β-mercaptoethanol mixture before being loaded into the gel. Silver staining method was used to reveal the electrophoretic gels and band intensities were estimated by using ImageJ software. Calibration curve was performed by loading CPO samples at known concentrations (1–3 μL of enzyme per milliliter of solution) so the amount of enzyme in the supernatants was determined by comparison.

4.9. Catalytic assay

The chlorination of monochlorodimedone to dichlorodimedone was used as model reaction for chloroperoxidase catalytic assay. 10 mg of the corresponding micro-support were washed with 1 mL of 10mM phosphate buffer pH 2.75. Micro-supports were separated from the buffered washing solution using a magnetic rack and the solution was recovered to evaluate the leaching of enzyme from the micro-supports. Then, the previously recovered micro-supports were mixed with 4 mL of buffered reaction mixture containing 3.6 mL of 3.19·10−4M MCD solution prepared using 3.19·10−2MKCl in phosphate buffer pH 2.9 and 0.4 mL of 4.6mM H2O2 and kept under stirring for 5 min. After each reaction cycle, micro-supports were separated from the mixture using a magnetic rack. The supernatants were analyzed spectrophotometrically and the reaction yield was determined in terms of monochlorodimedone absorbance decrease and calculated as ratio percentages between the reaction mixture absorbance before and after a reaction cycle of 5 min (Absfinal/Absinitial×100). If conversion was complete, the catalytic system was

recycled directly (without any washing treatment) by adding a freshly prepared reaction mixture. In the case of an incomplete conversion after 5 min, the reaction mixture and the micro-supports were left to react again during a longer time. Magnetic micro-supports without immobilized enzyme were also tested as negative controls in terms of catalytic activity using the same reaction conditions and also to discard any absorption of the substrate on micro-supports. Freshly prepared micro-supports were used in all experiments. They were washed with water, resuspended and kept at 4.0 °C when experiment length did not allow their continuous use. All sets of experiments were reproduced several times under identical operating conditions in order to increase the accuracy of the findings.

4.10. Leaching assay

To quantify the possible leaching of the enzyme, the activity of the washing supernatants was assessed mixing 1 mL of the supernatant of the coating and entrapment process with 9 mL of the reaction mix which contained 0.4 mL of H_2O_2 4.6 mM and 8.6 mL of a $1.15 \cdot 10^{-4}$ M MCD/$1.15 \cdot 10^{-2}$ M KCl solution in phosphate buffer pH 2.9. The activity of released CPO was determined as ratio percentages between the reaction mixture absorbance at 278 nm before and after a reaction cycle of 5 min.

5. References

(1) Sheldon, R. A.; Woodley, J. M. *Chem. Rev.* **2018**, *118* (2), 801–838.

(2) Bilal, M.; Ashraf, S. S.; Ferreira, L. F. R.; Cui, J.; Lou, W. Y.; Franco, M.; Iqbal, H. M. N. *Int. J. Biol. Macromol.* **2020**, *162*, 1906–1923.

(3) Sheldon, R. A.; Pereira, P. C. *Chem. Soc. Rev.* **2017**, *46* (10), 2678–2691.

(4) Madhavan, A.; Sindhu, R.; Binod, P.; Sukumaran, R. K.; Pandey, A. *Bioresour.*

Technol. **2017**, *245*, 1304–1313.

(5) Homaei, A. A.; Sariri, R.; Vianello, F.; Stevanato, R. *J. Chem. Biol.* **2013**, *6* (4), 185–205.

(6) Ahmad, R.; Sardar, M. *Biochem. Anal. Biochem.* **2015**, *4* (2), 178.

(7) Cipolatti, E. P.; Valério, A.; Henriques, R. O.; Moritz, D. E.; Ninow, J. L.; Freire, D. M. G.; Manoel, E. A.; Fernandez-Lafuente, R.; De Oliveira, D. *RSC Adv.* **2016**, *6* (106), 104675–104692.

(8) Polshettiwar, V.; Luque, R.; Fihri, A.; Zhu, H.; Bouhrara, M.; Basset, J. M. *Chem. Rev.* **2011**, *111* (5), 3036–3075.

(9) Chamoli, S.; Yadav, E.; Hemansi, H.; Saini, J. K.; Verma, A. K.; Navani, N. K.; Kumar, P. *Int. J. Biol. Macromol.* **2020**, *164*, 1729–1736.

(10) Shakya, A. K.; Nandakumar, K. S. *Nanobiocatalysts for Industrial Applications*; Elsevier Inc., 2018.

(11) Netto, C. G. C. M.; Toma, H. E.; Andrade, L. H. *J. Mol. Catal. B. Enzym.* **2013**, *85–86*, 71–92.

(12) Palma, S. I. C. J.; Roque, A. C. A. *J. Nanosci. Nanotechnol.* **2017**, *17* (7), 4410–4431.

(13) Mallakpour, S.; Behranvand, V. *Express Polym. Lett.* **2016**, *10* (11), 895–913.

(14) Sundar, S.; Kundu, J.; Kundu, S. C. *Sci. Technol. Adv. Mater.* **2010**, *11* (1), 014104.

(15) Jayakumar, R.; Menon, D.; Manzoor, K.; Nair, S. V.; Tamura, H. *Carbohydr. Polym.* **2010**, *82* (2), 227–232.

(16) Sojitra, U. V.; Nadar, S. S.; Rathod, V. K. *Carbohydr. Polym.* **2017**, *157*, 677–685.

(17) Sahin, S.; Ozmen, I. *J. Mol. Catal. B Enzym.* **2016**, *133*, S25–S33.

(18) De Matteis, L.; Germani, R.; Mancini, M. V.; Savelli, G.; Spreti, N.; Brinchi, L.; Pastori, G. *J. Mol. Catal. B Enzym.* **2013**, *97*, 23–30.

(19) De Matteis, L.; Germani, R.; Mancini, M. V.; Di Renzo, F.; Spreti, N. *Appl. Catal. A Gen.* **2015**, *492*, 23–30.

(20) Van Rantwijk, F.; Sheldon, R. A. *Curr. Opin. Biotechnol.* **2000**, *11* (6), 554–564.

(21) Muñoz-Guerrero, F. A.; Águila, S.; Vazquez-Duhalt, R.; Alderete, J. B. *J. Mol. Catal. B Enzym.* **2015**, *116*, 1–8.

(22) Jiao, R.; Tan, Y.; Jiang, Y.; Hu, M.; Li, S.; Zhai, Q. *Ind. &Eengineering Chem. Res.* **2014**, *53*, 12201–12208.

(23) Wang, W.; Xu, Y.; Wang, D. I. C.; Li, Z. *J. AM. CHEM. SOC.* **2009**, *131*, 12892–

12893.

(24) Cui, R.; Bai, C.; Jiang, Y.; Hu, M.; Li, S.; Zhai, Q. *Chem. Engeneering J.* **2015**, *259*, 640–646.

(25) Gao, F.; Jiang, Y.; Hu, M.; Li, S.; Zhai, Q. *Mater. Des.* **2016**, *111*, 414–420.

(26) Lu, J.; Cheng, L.; Wang, Y.; Ding, Y.; Hu, M.; Li, S.; Zhai, Q.; Jiang, Y. *Mater. Des.* **2017**, *129* (620), 219–226.

(27) Muñoz-Guerrero, F. A.; Águila, S.; Vazquez-duhalt, R.; Torres, C. C.; Campos, C. H.; Alderete, J. B. *Top Catal* **2016**, *59*, 387–393.

(28) Jin, X.; Li, S.; Long, N.; Zhang, R. *Appl. Biochem. Biotechnol.* **2017**, 1–15.

(29) Juarez-Moreno, K.; León, J. N. D. De; Zepeda, T. A.; Vazquez-Duhalt, R.; Fuentes, S. *J. Mol. Catal. B. Enzym.* **2015**, *115*, 90–95.

(30) Salcedo, K.; Torres-ramírez, E.; Haces, I.; Ayala, M. *Biocatalysis* **2015**, *1*, 33–43.

(31) Ding, Y.; Cui, R.; Hu, M.; Li, S.; Zhai, Q.; Jiang, Y. *J. Mater. Sci.* **2017**, *52* (17), 10001–10012.

(32) De Matteis, L.; Custardoy, L.; Fernández-Pacheco, R.; Magén, C.; De La Fuente, J. M.; Marquina, C.; Ibarra, M. R. *Chem. Mater.* **2012**, *24* (3), 451–456.

(33) Gu, X.; Zhang, Y.; Sun, H.; Song, X.; Fu, C.; Dong, P. *J. Nanomater.* **2015**, *2015*.

(34) Franken, L. E.; Boekema, E. J.; Stuart, M. C. A. *Adv. Sci.* **2017**, *4* (5), 1–9.

(35) Wei, H.; Ren, J.; Han, B.; Xu, L.; Han, L.; Jia, L. *Colloids Surfaces B Biointerfaces* **2013**, *110*, 22–28.

(36) Pajic-Lijakovic, I.; Levic, S.; Hadnadev, M.; Stevanovic-Dajic, Z.; Radosevic, R.; Nedovic, V.; Bugarski, B. *Biochem. Eng. J.* **2015**, *103*, 32–38.

(37) Lević, S.; Pajić Lijaković, I.; Dorević, V.; Rac, V.; Rakić, V.; Šolević Knudsen, T.; Pavlović, V.; Bugarski, B.; Nedović, V. *Food Hydrocoll.* **2015**, *45*, 111–123.

(38) Qu, X.; Wirsén, A.; Albertsson, A. C. *Polymer (Guildf).* **2000**, *41* (12), 4589–4598.

Chapter 5

Encapsulation of holmium vanadate nanoparticles for their use as contrast agents

1. Introduction

MRI is one of the most powerful diagnosis imaging tool in the medical field. It has the advantages of being noninvasive and having high penetration power.[1] It is commonly used for the visualization of organs and tissues as it provides soft tissue contrast and high spatial resolution.[2] MRI contrast is based on difference on density of protons and relaxation times between tissues when they are exposed to a strong magnetic field. The different density of protons is mainly based to the difference in water content between organs. When the nuclei of the atoms are exposed to the magnetic field, their spins align together and precess under a specified frequency. Then, a resonance frequency in the radio-frequency range is introduced to the nuclei and the protons get to the excited state. When this pulse disappears, the nuclei relax to their initial state through two different pathways: T1 relaxation or longitudinal or T2 or transversal. In T1, the decreased net magnetization recovers to the initial state. In T2, the induced magnetization on the perpendicular plane disappears by dephasing of the spins. The main drawback of this technique is the sensitivity due to

low difference between normal and anormal tissues. Increase in this contrast is traditionally achieved by external probes called contrast agents. Traditionally, contrast agents are classified into positive and negative contrast agents. Positive or T1 contrast agents enhance the signal in T1-weighted images while negative or T2 agents darken T2-weighted images.[1]

Nowadays, MRI is conducted at low magnetic fields (0.5 – 1 T) using superparamagnetic iron oxide nanoparticles as negative contrast agents[3], and Gd^{+3} chelates as positives ones[4]. However, new research is being conducted for the development of new MRI equipment working at higher magnetic fields (7 to 9 T) to reduce acquisition time and increase image sensitivity as they have better signal-to-noise ratio and spatial/temporal resolution.[5,6] The main problem associated with this new research line is the lack of adecuate contrast agents. Both of the traditionally used contrast agents, superparamagnetic iron oxide nanoparticles (negative ones) and Gd^{+3} chelates (positive ones), only work for lower magnetic fields (< 1.5 T). For this purpose, new contrast agents for high magnetic fields are needed.

Among the different alternatives, lanthanides such as Dy^{3+} and Ho^{3+} compounds are considered as one of the best candidates due to their high magnetic moment. Some research has been carried out for the development of Ho^{3+} complexes as contrast agents. However, it was found that they have short circulation time and low targeting ability.[5] Another approach is the synthesis of Ho^{+3} containing nanoparticles. Nanoparticle circulation time and elimination pathways can be controlled by controlling their size and surface. Besides, modification of the surface can control also the target tissue. Recently developed Ho^{+3} containing nanoparticles are based

on fluorides. However, chemical stability of these nanoparticles is limited in physiological environment.[7]

An interesting alternative to the use of fluorides is the use of vanadates. Vanadates have already probe to be good candidates for bioimaging, as $GdVO_4$ nanoparticles showed good contrast at low fields.[8]

In a recent published paper, Gomez-González *et. al.*[9] developed a wet chemical method for the synthesis of Holmium vanadate nanoparticles with a mean diameter of 60 nm. These nanoparticles were then functionalized with poly(acrylic acid) showing great properties to be used as contrast agents at high magnetic fields (9.4 T). However, they probed to have low stability in physiological media and good ethanol stability.

For this reason, encapsulation was proposed as an alternative strategy for the development of stable, high contrast agents at high magnetic fields. Among the different alternatives for nanoparticle encapsulation, due to the good compatibility shown in organic solvents, encapsulation into an emulsion coated with chitosan seemed a great alternative, as this type of nanoparticles already showed good encapsulation efficiency for hydrophobic molecules.[10]

As in previous chapters, spontaneous emulsification was chosen for emulsion synthesis as it is an easy synthesis that does not require expensive equipment or high temperatures, thus not affecting nanoparticle integrity. Low stability of the nanoemulsion requires coating of the surface to improve nanoemulsion life.[11] For this purpose, polysaccharides have proven to be good candidates due to high biocompatibility and biodegradability. Among them, chitosan was chosen as it was previously reported that is a great option for emulsion stabilization.[12,13] Besides,

thanks to the amine groups in the surface, it is easy to functionalize, opening a possibility to develop targeted nanoparticles towards the tissue of interest. For this reason, $HoVO_4$ nanoparticles were encapsulated into chitosan coated nanoemulsions. These nanocapsules were characterized in terms of nanoparticle loading, cell toxicity, MRI imaging performance and biodistribution in murine models.

2. Results and discussion

2.2. Synthesis and characterization

The nanoparticles selected for encapsulation were synthesized in the Instituto de Ciencia de Materiales de Sevilla (ICMS) by Dr. Manuel Ocaña´s group. These nanoparticles are synthesized by a wet chemical method based on the homogeneous precipitation reactions in polyol medium. They were coated with poly(acrylic acid) (PAA) to stabilize them and present a mean diameter of around 60 nm.[9]

The method selected in this work for the encapsulation of holmium vanadate nanocapsules is similar to the ones used in previous chapters and adapted from De Matteis *et at* (2016)[12], regarding the development of empty nanocapsules. Nanocapsules consist in a nanoemulsion core with a hydrophobic nature coated with the polysaccharide chitosan. Thanks to the hydrophobicity of the core, we believe it would be highly compatible with the developed nanoparticles, as they proved to be stable in ethanol solutions in a previous work. [12]

As explained in previous chapters, the synthesis method is based on a spontaneous emulsification followed by coating with chitosan by ionotropic gelation. Quantities of the components for the nanocapsules were maintained the same as in the synthesis

of empty ones, as ratios were adequate for the production of nanoemulsions by spontaneous emulsification.

In this case, the nanoparticles were previously mixed with the organic phase, containing Span 85® and oleic acid in ethanol. Then, this solution was added dropwise to the aqueous one, containing Tween 20. Two different amounts of nanoparticles (2 and 4 mg) were added in order to determine which worked better for the rest of the assays. Hereon, NC2 will be the nanocapsules with the initial amount of 2 mg and NC4 the ones with 4 mg. The amount of nanoparticles added need to be enough to achieve good contrast in the MRI images, but not too much that we reach the maximum loading capacity of the nanocapsules. This would lead to waste of nanoparticles, as the ones above the loading capacity will not be able to be encapsulated.

After the dropwise addition of the organic phase into the aqueous phase, the nanoparticle-loaded nanoemulsion is spontaneously formed. An increase in the turbidity of the solution indicates that the emulsion is formed[14]. After 15 minutes of stirring the emulsion reaches the equilibrium[15] and the chitosan solution is added for the coating and stabilization of the emulsion. Chitosan coating stabilizes the nanoemulsion as they are not thermodynamically stable systems [16], but also improve interactions with cells and allows further modification of the nanocapsule surface.[12]

After 15 minutes of incubation, stabilization of chitosan was performed by ionotropic gelation, achieving a homogeneous coating of the nanoemulsion with the polymer chains. Nanocapsules were added to a sodium sulphate solution, which produces the crosslinking of chitosan thanks to the positively charged amino groups in chitosan and the negative charges of the sulphate ions.[17,18] Besides, as stated

before, sodium salts reduce the solubility of chitosan, compacting the coating structure.

After the ionotropic gelation, nanocapsules were washed by ultracentrifugation. Excess reactants and non-encapsulated nanoparticles were eliminated from the final suspension of nanocapsules. In the ultracentrifugation conditions, non-encapsulated nanoparticles were not able to precipitate, remaining in the supernatant.

To evaluate the suitability of the system for the encapsulation of holmium vanadate nanoparticles, we determined encapsulation efficiency and nanoparticle loading. As stated before, encapsulation efficiency (EE%) is defined as the amount of nanoparticle encapsulated per amount of drug initially added; while the nanoparticle loading (DL%) is described as the milligrams of nanoparticles encapsulated per mg of nanocapsule obtained. For the determination of these two parameters, it was necessary to quantify the nanocapsule concentration as well as nanoparticle content. Nanocapsule concentration was calculated by freeze-drying of an aliquot of the suspension and subsequent quantification of the dry weight. This allowed the quantification of the total amount of nanomaterial, meaning nanocapsule and nanoparticle.

To determine the amount of encapsulated nanoparticles, we extracted them from the core of the nanocapsules. Approximately 1 mg of nanocapsule were mixed in 900 µL of methanol and sonicated for 30 minutes. Non encapsulated nanoparticles show a unique absorbance spectrum with a prominent peak at 278 nm (Figure 1), that does not interfere with the absorption peaks of the rest of the components of the nanocapsules.

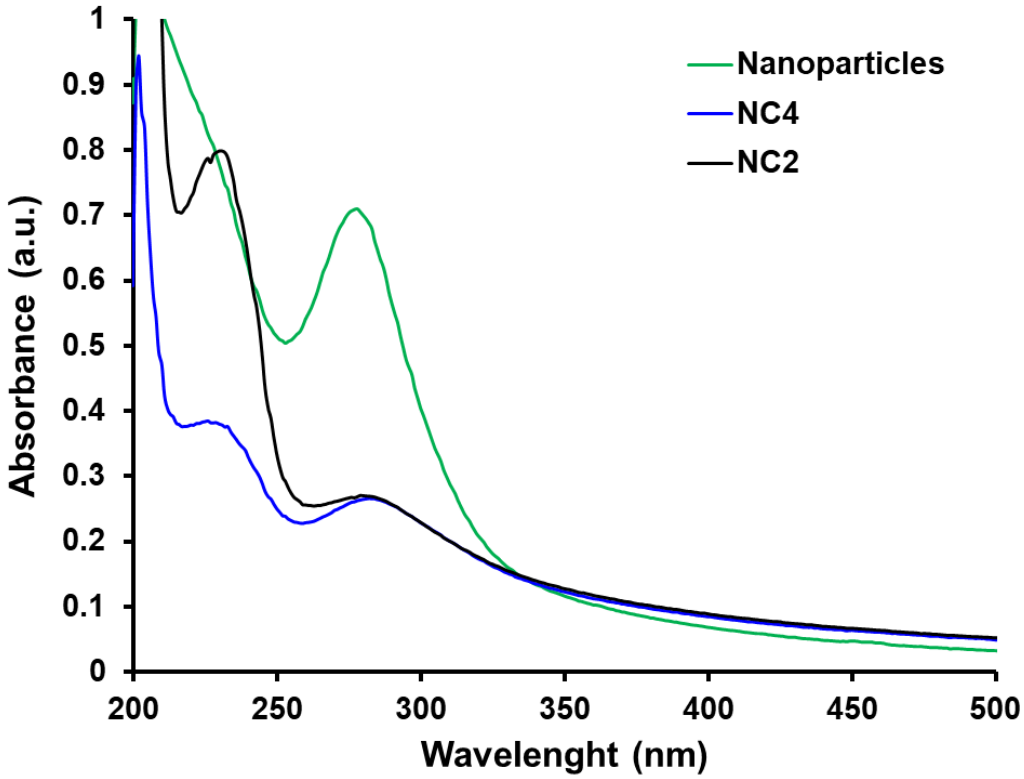

Figure 1. UV-vis spectra of non-encapsulated nanoparticles, nanocapsules loaded with 4 mg of NP (NC4) and 2 mg (NC2)

In Figure 1, it can be observed that nanoparticles and digested nanocapsules have the same peak of absorbance at 278 nm. This would mean that we can clearly observe that nanocapsules have holmium vanadate nanoparticles encapsulated. To quantify the amount of nanoparticles encapsulated, we carried out a calibration curve with increasing amounts of nanoparticles to correlate with the amount of nanoparticles in the nanocapsules. The results of EE% and DL% are shown in Table 1.

Table 1. Encapsulation efficiency (EE%) and drug loading (DL%) of nanoparticle loaded nanocapsules measured by UV-vis and ICP

	Measured by UV-vis		Measured by ICP	
	EE%	**DL%**	**EE%**	**DL%**
NC2	68	3.8	90	5
NC4	74	8.8	97	11.5

As it can be observed in Table 1, EE% values for both NC2 and NC4 are around 70%, which is a acceptable value and similar to the ones obtained for other types of molecules for this type of nanocapsules. DL% values also show that the amount of nanoparticles per mg of nanocapsule increases with the increase of added nanoparticle to the synthesis.

To corroborate the results obtained by UV-vis, we quantified the amount of Ho^{+3} present in the nanocapsule suspension by ICP. For this purpose, nanocapsule suspension was digested with aqua regia to completely dissolve the Ho^{+3} and after dilution with milli-Q water, they were measured by Inductively Coupled Plasma High Resolution Mass Spectroscopy (ICP-HRMS) by the group of Dr. Manuel Ocaña. Data regarding these results are shown in Table 1.

It can be observed that for both types of nanocapsules, both EE% and DL% values are higher in comparison with those obtained by UV-vis spectra. Values obtained by ICP-HRMS are about 1.3 % higher in comparison with the UV-vis ones. This would mean that we are underestimating the amount of nanoparticles when we measure then by UV-vis spectra. For this reason, ICP-HRMS was always used for quantification for the rest of the experiments, using only UV-vis measurements for a quick estimation of the Ho content.

Nanocapsules were characterized by DLS to determine their hydrodynamic diameter and size distribution. Size is an important parameter to evaluate as it influences nanoparticle stability and interaction with biological membranes[19]. Nanocapsules diameter was studied in water and size distribution is Shown in Figure 1.

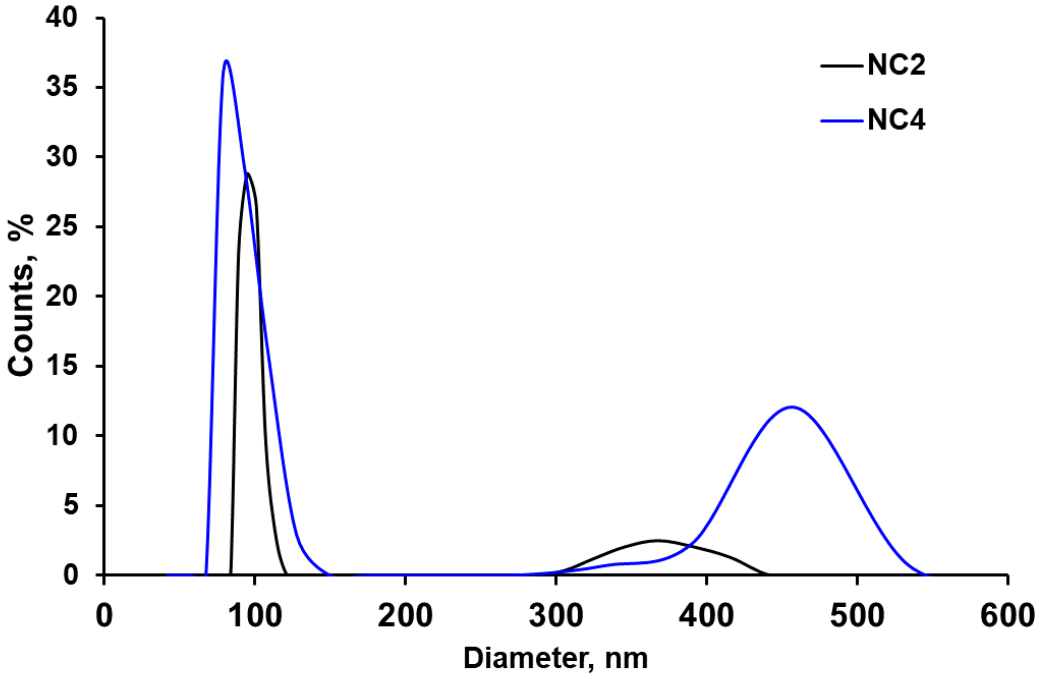

Figure 2. Size distribution of holmium vanadate encapsulated nanoparticles at the two different loadings tested

Figure 1 shows the size distribution of the loaded-nanocapsules with the 2 different initial amounts of nanoparticles. In both cases, we can observe a small population of around 100 nm, which may correspond to nanocapsules loaded with lower amounts of nanoparticles (as holmium vanadate nanoparticles have a main diameter of 65 nm). In the case of NC2, a small population with a mean diameter of 350 nm is observed. In the NC4, this population is bigger and more abundant, with a main

diameter of 450 nm. This population will correspond to the nanocapsules loaded with bigger amounts of nanoparticles. Due to the size of the encapsulated nanoparticles, which is around 60 nm, nanocapsule diameter should increase a lot with higher loading of nanocapsules, explaining this bigger population. Besides, it was observed small aggregates during the sample preparation for DLS, that could not be measured and that probably correspond nanocapsules with the highest loading. This would mean that this bigger population do not correspond to aggregates of nanocapsules in this case, but to a difference in the loading of the nanocapsules.

2.3. Magnetic properties

Relaxivity measurements were performed in order to determine the magnetic properties of the loaded nanocapsules and their performance as negative contrast agents. Relaxivity of a contrast agent reflects how the relaxation rate of a solution changes with concentration and they are calculated as the slope of the graph obtained by plotting 1/T2 vs concentration of the contrast agent and are represented as r_2 ($mM^{-}s^{-}$). This value depends on the temperature of the measurement, field strength and the medium in which the contrast agent is disolved. In this project, relaxivity was measured at 1.5 T and 9.4 T. As stated in the introduction, nowadays, lower magnetic fields such as 1.5 T are commonly used, however, as these nanocapsules are intended for their use at higher fields, 9.4 T was also tested. Results of r_2 are shown in Figure 3.

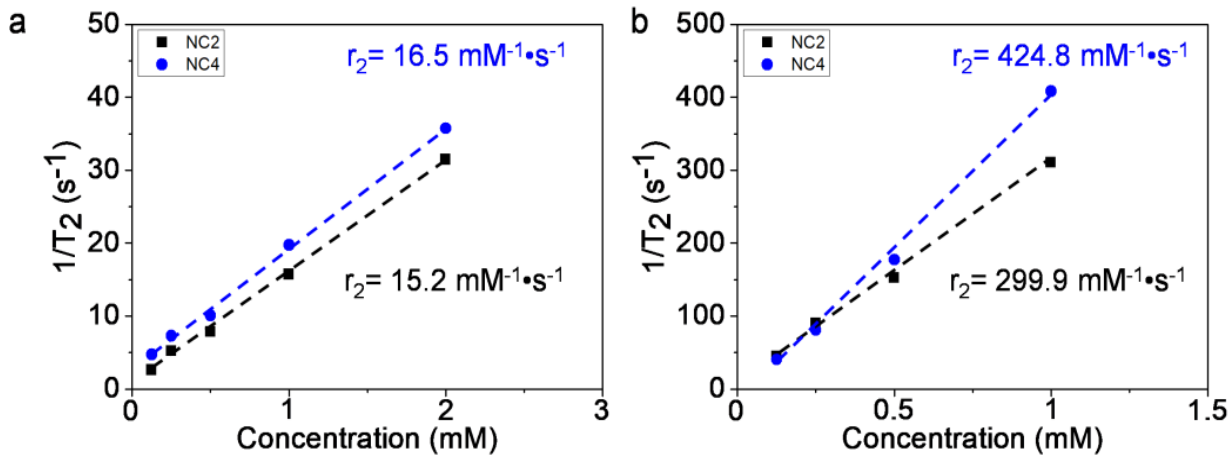

Figure 3. Plot of 1/T2 vs Ho concentration of NC2 (black) and NC4 (blue) were calculated at 1.44 T (A) and 9.4 T (B).

Figure 3 shows relaxivity values of both types of nanocapsules at 1.44 and 9.4 T. It can be observed that the measured relaxivity is similar for both nanocapsules at lower field but increases dramatically at 9.4 T. This is a surprising behavior as the amount of Ho is the same for both nanocapsules and it could mean that there is a nanometric effect affecting relaxivity such as aggregation in the core in NC4. Despite these differences, r2 values are high enough, especially in the case of NC4 nanocaspules to be applied as negative contrast agents and comparable to the ones obtained with the non-encapsulated nanoparticles.[9] T_2-weighted phantom images at 9.4 T were also obtained and are shown in Figure 4.

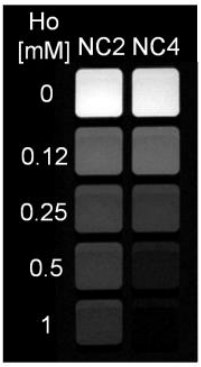

Figure 4. T_2-weighted phantom images at 9.4 T of NC2 and NC4

In Figure 4, T_2-weigthed phantom image of both types of nanocapsules can be observed. In both cases, and especially in NC4, it can be observed a darkening of the MRI signal with increasing concentration of nanocapsules. This means that they behave as effective negative contrast agents, as the more nanocapsules present in a tissue, the darker the image would look. Tissues with a lower amount of nanoparticles will not have a darkening of the image in comparison with the initial one.

It was decided to select only NC4 as they are the ones that present better performance as contrast agents. Specially in the phantom images, it can be observed that NC4 require lower concentration to darken the images and therefore are better negative contrast agents.

2.4. Cell viability

To determine if nanocapsules are suitable for their application as contrast agents for *in vivo* experiments, firstly toxicity *in vitro* needed to be checked. For this purpose, human foreskin fibroblast (HFF-1) were chosen and incubated with increasing amounts of nanocapsules. Results are shown in Figure 5.

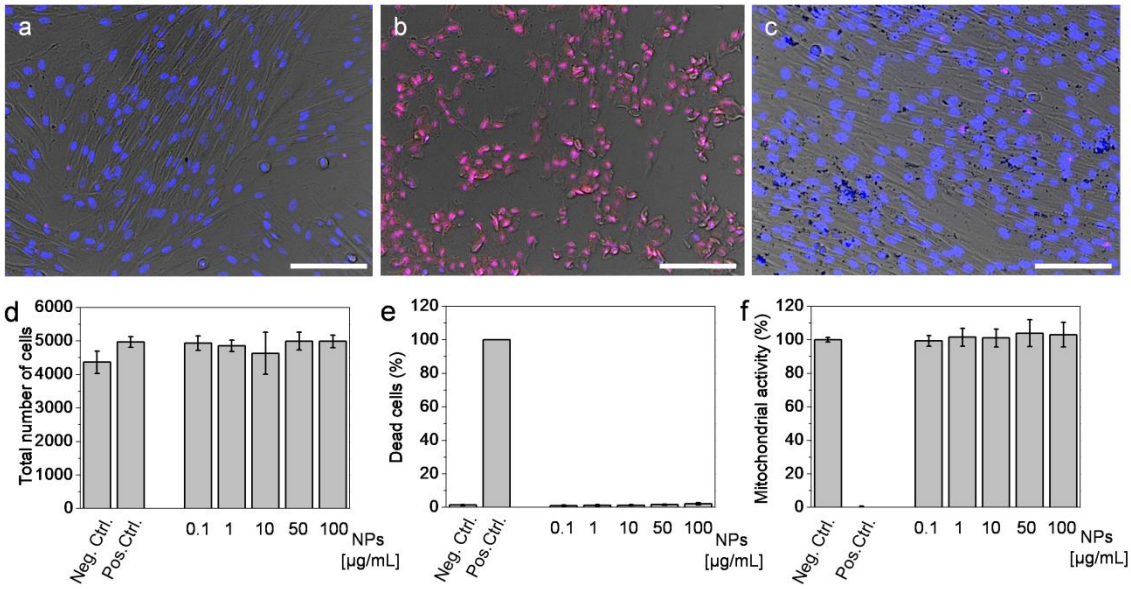

Figure 5. Optical microscopy images of HFF-1 cells: a) negative control, b) positive control, c) cells exposed to 100 µg/ml of NC4. Images show the merge of brightfield (grey), DAPI (blue) and TO-PRO-3 Iodine (red). Scale bar is 100 µm. d) Total number of cells per well exposed to increasing concentration of NPs. e) Percentage of dead cells exposed to increasing concentration of NPs. f) MTT assay of cells exposed to increasing concentration of NPs. Tested concentrations were from 0.1 µg/mL to 100 µg/ml.

Figure 5 shows the results for the toxicity test of nanocapsules with the cell line HFF-1. Figure 5a-c show the optical microscopy images of HFF-1 cells incubated with NC4 (C), a negative control (A) and a positive control (B). Images show a merge image of brightfield, DAPI (blue) and TO-PRO-3 iodine (red). Brightfield image allows the evaluation of cell morphology and determination if the exposition to NC affects cell morphology. As it can be observed, cells exposed to NC4 show similar morphology to the negative control, that are normal living cells. If NC4 were affecting cell morphology and function, they would be similar to the positive control (5B), in which 20% ethanol is added to affect cell function.

Fluorescent image shows staining with DAPI in blue and TO-PRO-3 iodine in red. DAPI is a fluorescent dye that associates with double-stranded DNA, therefore staining cell nucleus. TO-PRO-3 iodine is a fluorescent dye that is only able to penetrate into dead cell with a compromised membrane, but is impermeant to live cells. Therefore, red staining mean that cells are dead whereas living cells will only have a blue cell nucleus staining.[20] In Figure 5A and C it can be observed that both the negative control and cells incubated with NC4 show almost no red fluorescent signal, meaning that they are viable cells. However, positive control, incubated with ethanol, show a great percentage of dead red cells.

Figure 5D shows the number of total cells and figure 5E shows the number of death cells. These numbers were obtained counting the total number of DAPI stained nucleus for the total number of cells, and the number of TO-PRO-3 iodine stained cells for the death ones. It can be again observed that there is not statistically significant difference ($p < 0.05$) between control cells and NC incubated cells, even for the highest concentration of NC.

Mitochondrial activity was also checked as a control for cell toxicity. In this case, MTT assay was performed and results are shown in Figure 5F. Cells incubated with increasing concentrations of NC4 show viability similar to the control and almost 100% of viability, showing that at the tested concentrations NC4 do not affect cell viability and can be used in the *in vivo* tests.

2.5. *In vivo* biodistribution

Once the toxicity was checked, the biodistribution of NC4 was studied as potential contrast agents for MRI. NC were injected intravenously in murine models and pharmacokinetics (PK) were followed by dynamic T2 image by MRI and shown in Figure 6.

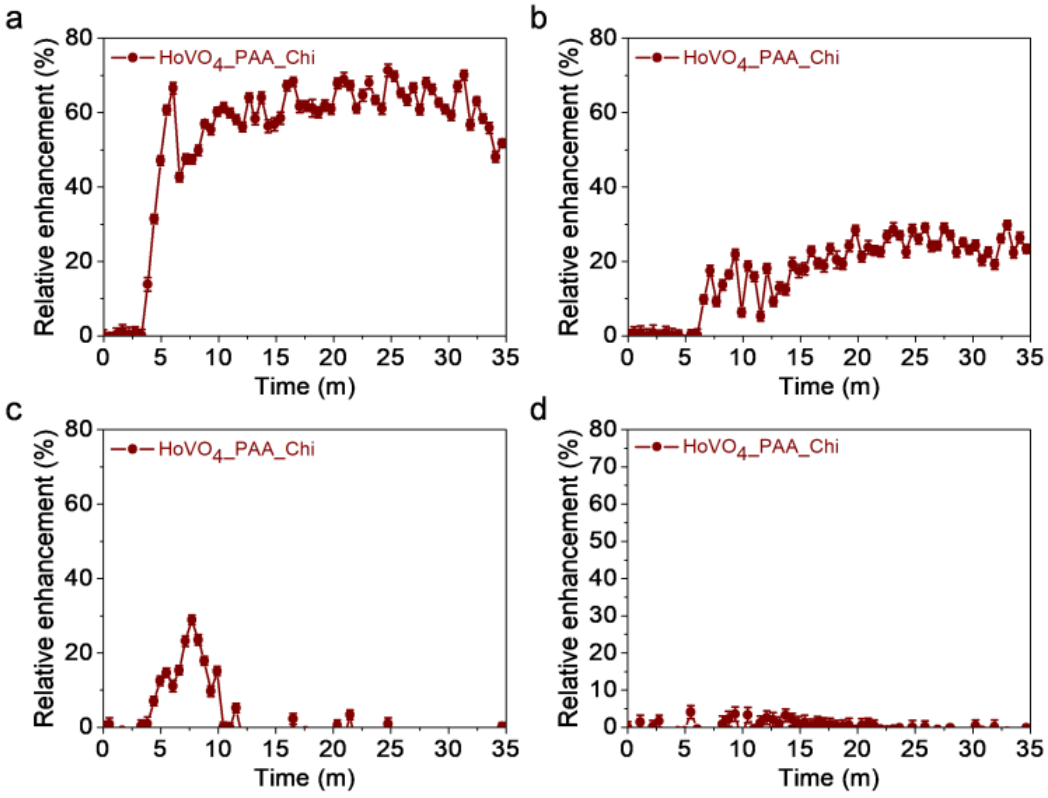

Figure 6. Representative in vivo time courses of NC4 after being intravenously injected in mice for liver (a), spleen (b), kidney (c) and muscle (d).

As shown in Figure 6, PK is different for the different organs. Liver shows a rapid increase of the relative enhancement, meaning that NC are quickly captured by this organ (Figure 6a). The accumulation in spleen is lower than in liver but it also keeps

constant after 1 h, meaning that nanocapsules are retained there (Figure 6b). In the case of kidneys, the signal increases after injection but recovers the basal state after some minutes, meaning there is no retention in this organ and that the increase in the signal is due to circulating NC. No increase is observed in muscle (Figure 6d). Overall, this profile would mean that nanocapsules are recognized by the mononuclear phagocyte system and are rapidly cleared from the bloodstream by liver Kupffer cells and spleen macrophages.[20] Besides PK, high resolution T_2-weigthed images were acquired before and 1 hour after injection of the nanocapsules and are shown in Figure 7.

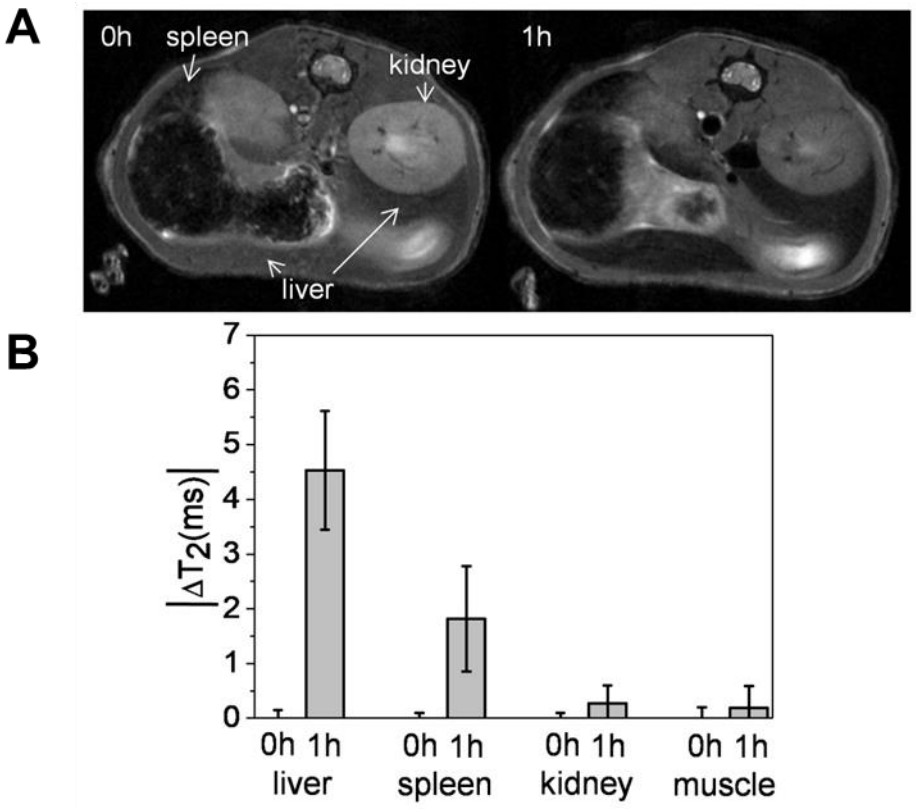

Figure 7. A. Representative T2-weighted high-resolution MR images acquired at 0h and 1h following the intravenous injection of NC4 (5 mg Ho /kg). B. Quantification of the average changes in the main tissues (n=3) in the transverse relaxation rate (R2) at 1 h after the intravenous injection of NC4

Figure 7 shows high resolution T2-weigthed images as well as quantification of the average changes in the main tissues in R2 after 1 hour. In Figure 7A, we can clearly observe darkening of the liver and spleen, which would be in agreement with the results obtained before, showing great accumulation of NC in both liver and spleen. This can be further confirmed by the decrease in T2 of 4.5 ms in liver and 1.8 ms in spleen observed in Figure 7B. These results also agree with the lower uptake of spleen in comparison with liver.

3. Conclusions

In this chapter, we presented the optimization of the synthesis of nanocapsules for the encapsulation of holmium vanadate nanoparticles.

The synthesis process was already optimized for the development of empty nanocapsules in previous works and tested for the suitability of different drugs in previous chapters. Here, the method probed to be suitable for the encapsulation of holmium vanadate nanoparticles with good encapsulation efficiency and drug loading at the two tested nanoparticle initial amount added. It was expected that they have good EE% due to their stability in ethanol, so these results were expected.

After characterization of the nanoparticle size distribution, we could observe that the developed nanocapsules presented two populations that could mean that there are nanocapsules with different loading of nanoparticles. Bigger nanocapsules would correspond to the ones with higher loading, as the nanoparticles that are being encapsulated have a mean diameter of 65 nm. This percentage of larger

nanoparticles is higher for the NC4, which is in agreement with the higher DL% observed.

Relaxivity measurements performed at both 1.44 T and 9.4 T showed good r2 values meaning that nanocapsules could be used as negative contrast agents. Besides, a higher r2 value is observed for NC4 at 9.4 T, which could mean aggregation of the nanoparticles in the nanocapsule core. Phantom images shown best behavior of the NC4 as contrast agents so these nanocapsules were chosen for the rest of the experiments.

Toxicity analysis of nanocapsules showed that they do not affect cell morphology or membrane integrity as observed microscopically at any of the tested concentrations. Besides, they show that they do not affect either mitochondrial activity so it was determined that at the tested concentrations, the developed nanocapsules are not toxic.

Finally, *in vivo* studies demonstrated that they have a great potential as high field T2 MRI contrast agents. However, biodistribution of nanocapsules, that are mostly retained in liver and spleen and their low circulation time, makes them not suitable for tumor targeting.

4. Materials and methods

4.2. Materials

Tween® 20 and absolute ethanol were purchased from Panreac. Span® 85 (sorbitane trioleate), oleic acid (90%), chitosan (medium molecular weight) and resazurin were obtained from Sigma-Aldrich. Inc. Phosphate Buffered Saline (PBS)

without PBS without Ca++, Mg++ or phenol red and RPMI (Roswell Park Memorial Institute) medium were obtained from Lonza.

4.3. Synthesis of nanoparticle-loaded nanocapsules

The general method for the synthesis of nanoparticle-loaded nanocapsules was slightly modified from the already reported protocol for the obtaining of empty nanocapsules (De Matteis et al., 2016). Firstly, different amounts of nanoparticles (2 or 4 mg) were mixed an organic solution composed of 8.6 mg Span 85 and 40 mg oleic acid in 4 mL absolute ethanol. This solution was added dropwise to an aqueous phase containing 13.6 mg Tween 20 in 8 mL MilliQ water under magnetic stirring. The solution was left under stirring for 15 minutes for the formation of the nanoemulsion and then we added 2.5 mg of a 5 mg/mL chitosan solution in acetic acid 1% (v/v). After another 15 minutes of stirring, the chitosan-coated nanoemulsion was added to 15 mL of 50 mM Na_2SO_4 under manual stirring. Capsules were separated from Na_2SO_4 through ultracentrifugation (24000 rpm, 30 minutes, 10˚C), washed with 10 mL of milliQ water, centrifuged again and resuspended in water. The concentration of the nanocapsules in water suspension was obtained by measuring the weight of 200 µL of sample after freeze-drying.

1 mg of nanocapsules were mixed with 900 µL methanol and sonicated for 30 minutes, in order to extract the encapsulated nanoparticles. The absorbance of the sample was measured at 278 nm for each drug using a Varian Cary 50 UV/Vis spectrophotometer. Previously, a calibration curve of non encapsulates nanoparticles in methanol was obtained.

Two values are calculated for the evaluation of the efficiency of the process, encapsulation efficiency and drug loading:

• Encapsulation efficiency: is the parameter that expresses the total amount of nanoparticle that was successfully encapsulated in comparison to the amount initially added to the synthesis.

$$EE\% = \frac{mg\ NP\ encapsulated}{mg\ NP\ added} \cdot 100$$

• NP loading: this value expresses the amount of nanoparticle inside the capsules with respect to the total amount of capsules mass.

$$Nanoparticles\ loading = \frac{mg\ NP\ encapsulated}{mg\ NC} \cdot 100$$

For the quantification by ICP-HRMS, nanoparticles were digested with aqua regia (a mixture of three parts of HCl and one part of HNO3). Briefly, 2.5 mL of aqua regia were added to 25 µL of a solution of nanoparticles in a volumetric flask. The mixture was left overnight. Then, milli-Q water was added to complete the total volume of 25 mL.

4.4. Characterization of the nanocapsules

Dynamic Light Scattering (DLS) analysis has been carried out using a Brookhaven 90Plus DLS instrument. Nanoparticle hydrodynamic diameter has been measured in milliQ water at the concentration of 0.05 mg/mL.

4.5. *In vitro* transverse relaxivities (r_2)

Low magnetic field measurements were performed on a Bruker Minispec system (Bruker BioSpin, Rheinstetten, Germany), using the Carl-Purcell-Meiboom-Gill

(CPMG) sequence. At high field, T_2 values were measured on a Bruker Biospec MRI system (Bruker Biospec, Bruker BioSpin, Ettlingen, Germany) using a 64-echo Carl-Purcell-Meiboom-Gill (CPMG) imaging sequence (TE values from 7.5 ms to 640 ms). The relaxivity, r_2, at both magnetic fields was calculated from the slope of the linear fit of the relaxation rate ($1/T_2$) versus the concentration of Ho.

Regions of interest (ROIs) were drawn on the first image of the image sequence and the intensity values were extracted and fit to the following equations:

$$M_Z(t) = M_0(1-e^{-TR/T_1})$$

$$M_{XY}(t) = M_0 e^{-TE/T_2}$$

where M_z and M_{xy} are the signal intensities at time TR or TE, and M_0 is the signal intensity at equilibrium.

4.6. Cytotoxicity evaluation

Cell morphology studies and "live-dead" assay. The HFF-1 cells were plated at a density of $1x10^4$ cells/well in a 96-well plate at 37ºC in 5% CO_2 atmosphere (200 µL per well, number of repetitions = 5). After 24 h of culture, the medium inside the wells was replaced with fresh medium containing the nanocapsules in varying concentrations from 0.1 µg/mL to 100 µg/ml. After 24 h, ethanol 20% was added to the positive control wells. After 15 min, all the wells were stained with DAPI (4',6-Diamidino-2-phenylindole) (dilution 1:3000) to label nuclei in all cells, although with stronger labeling in live cells, and TO-PRO-3 Iodine to only label dead cells (dilution 1:1000). The cell morphology images were acquired using a Perkin Elmer Operetta High Content Imaging System with a 20x LWD 0.45 NA air objective lens. 5 well replicas for each condition were analyzed with 10 random image fields captured per

well. For each field, fluorescence images for DAPI and TO-PRO-3, plus a brightfield image were captured. Cell mortality percentages were calculated automatically by Operetta Harmony software, whereby all nuclei (dead and alive) were identified from the DAPI staining and the percentage of dead cells was then determined by the number of nuclei also possessing high levels of TO-PRO-3 staining.

MTT assay. HFF-1 cells were plated at a density of $1x10^4$ cells/well in a 96-well plate at 37 ºC in 5 % CO_2 atmosphere (200 µl per well, number of repetitions = 5). After 24 h of culture, the medium in the wells was replaced with fresh medium containing nanocapsules in varying concentrations from 0.1 µg/mL to 100 µg/mL. After 24 h, the supernatant of each well was replaced by 200 µL of fresh medium with 3-[4,5-dimethylthiazol-2-yl]-2,5-diphenyl tetrazolium bromide (MTT) (0.5 $mg \cdot mL^{-1}$). After 2 h of incubation at 37 ºC and 5 % CO_2, the medium was removed, the formazan crystals were solubilized with 200 µl of DMSO, and the solution was vigorously mixed to dissolve the reacted dye. The absorbance of each well $[Abs]_{well}$ was read on a microplate reader (Dynatech MR7000 instruments) at 550 nm. The relative cell viability (%) and its error related to control wells containing cell culture medium without nanoparticles were calculated by the equations:

$$RCV(\%) = \left(\frac{[Abs]_{test} - [Abs]_{Pos.Ctrl.}}{[Abs]_{Neg.Ctrl.} - [Abs]_{Pos.Ctrl.}}\right) \times 100$$

$$Error(\%) = RCV_{test} \times \sqrt{\left(\frac{\sigma_{test}}{[Abs]_{test}}\right)^2 + \left(\frac{\sigma_{\mathrm{Ctrl}}}{[Abs]_{Ctrl.}}\right)^2}$$

where σ is the standard deviation. Triton X-100 was added to the positive control wells.

4.7. MRI studies

Animal experiments. Male Balb/c mice (*n* = 3 per group) with ca. 20 g in weight, provided by Charles River, were used for *in vivo* experiments. These experiments were performed in accordance with the ethical guidelines of our local ethical committee and consistent with national regulations for the care and use of laboratory animals (R.D. 53/2013).

Experiments in mice. MRI experiments were conducted on the 9.4 T Bruker Biospec system. The system was equipped with a 400 mT/m gradients and a 40 mm quadrature bird-cage resonator. All the in vivo experiments were performed using the following experimental scheme: i) acquisition of high resolution T_2-weighted images, ii) acquisition of T_2 parametric images (quantitative), iii) intravenous injection of the nanoparticles, iv) acquisition of a dynamic sequence of T_2-weighted images (pharmacokinetics time-courses), v) acquisition of high resolution T_2-weighted images and vi) acquisition of T_2 parametric images (quantitative). High resolution T_2-weighted images were acquired using a turbo-RARE sequence with respiratory gating (TE = 27 ms, TR = 1000 ms, 4 averages, 156 μm in-plane resolution and 1 mm slice thickness). Quantitative T_2 measurements were also performed using a multi-echo spin echo CPMG sequence (TEs ranging from 7 ms to 448 ms, TR = 3500 ms, FOV = 4 cm, matrix size = 128x128, slice thickness = 1 mm). The T_2 time-courses were followed by using a turbo-RARE sequence with the same parameters indicated above, but only 1 average to improve temporal resolution (1 image every 30 seconds).

5. References

(1) Na, H. Bin; Song, I. C.; Hyeon, T. *Adv. Mater.* **2009**, *21* (21), 2133–2148.

(2) Cheng, W.; Ping, Y.; Zhang, Y.; Chuang, K. H.; Liu, Y. *J. Healthc. Eng.* **2013**, *4* (1), 23–46.

(3) Wang, Y.-X. J. *Quant. Imaging Med. Surg.* **2011**, *1* (1), 35–40.

(4) Aime, S.; Botta, M.; Terreno, E. *Adv. Inorg. Chem.* **2005**, *57*, 173–237.

(5) Norek, M.; Kampert, E.; Zeitler, U.; Peters, J. A. *J. Am. Chem. Soc.* **2008**, *130* (15), 5335–5340.

(6) Rohrer, M.; Bauer, H.; Mintorovitch, J.; Requardt, M.; Weinmann, H.-J. *Invest. Radiol.* **2005**, *40* (11), 715–724.

(7) Lisjak, D.; Plohl, O.; Vidmar, J.; Majaron, B.; Ponikvar-Svet, M. *Langmuir* **2016**, *32* (32), 8222–8229.

(8) Nuñez, N. O.; Rivera, S.; Alcantara, D.; De la Fuente, J. M.; García-Sevillano, J.; Ocaña, M. *J. Chem. Soc. Dalt. Trans.* **2013**, *42* (30), 10725–10734.

(9) Gómez-Gónzalez, E.; Núñez, N. O.; Caro, C.; García-Martín, M. L.; Fernández-Afonso, Y.; De La Fuente, J. M.; Balcerzyk, M.; Ocaña, M. *Inorg. Chem.* **2021**, *60* (1), 152–160.

(10) De Matteis, L.; Jary, D.; Lucía, A.; García-Embid, S.; Serrano-Sevilla, I.; Pérez, D.; Ainsa, J. A.; Navarro, F. P.; M. de la Fuente, J. *Chem. Eng. J.* **2018**, *340*, 181–191.

(11) Xu, X.; Luo, L.; Liu, C.; McClements, D. J. *Food Hydrocoll.* **2017**, *64*, 112–122.

(12) De Matteis, L.; Alleva, M.; Serrano-Sevilla, I.; García-Embid, S.; Stepien, G.; Moros, M.; De La Fuente, J. M. *Mar. Drugs* **2016**, *14* (10), 175.

(13) García-Embid, S.; Di Renzo, F.; De Matteis, L.; Spreti, N.; M. de la Fuente, J. *Appl. Catal. A Gen.* **2018**, *560*, 94–102.

(14) McClements, D. J.; Rao, J. *Crit. Rev. Food Sci. Nutr.* **2011**, *51* (4), 285–330.

(15) Bouchemal, K.; Briançon, S.; Perrier, E.; Fessi, H. *Int. J. Pharm.* **2004**, *280*, 241–251.

(16) McClements, D. J. *Adv. Colloid Interface Sci.* **2018**, *253*, 1–22.

(17) Tavares, I. S.; Caroni, A. L. P. F.; Neto, A. A. D.; Pereira, M. R.; Fonseca, J. L. C. *Colloids Surfaces B Biointerfaces* **2012**, *90* (1), 254–258.

(18) Berthold, A.; Cremer, K.; Kreuter, J. *J. Control. Release* **1996**, *39* (1), 17–25.

(19) Bannunah, A. M.; Vllasaliu, D.; Lord, J.; Stolnik, S. **2014**.

(20) Gómez-González, E.; Caro, C.; Martínez-Gutiérrez, D.; García-Martín, M. L.;

Ocaña, M.; Becerro, A. I. *J. Colloid Interface Sci.* **2021**, *587*, 131–140.

Chapter 6

Future perspectives

Oil-in-water emulsions can be found in a variety of food and beverage products and delivery systems. As already stated in Chapter 1 (Introduction), emulsions can be formed using either high-energy or low-energy methods. For the synthesis of emulsion using high-energy approaches, specialized equipment such as a homogenizers or microfluidizers are required for the formation of the small droplets. The use of this machines highly increases the cost and complexity of the procedure.[1,2] On the other hand, low-energy approaches do not need specialized equipment and rely on the physicochemical properties of the molecules involved in the emulsion formation. Droplets are generated by mixing or change on the environmental conditions such as temperature or pH.

The main advantage of high-energy methods is scalability of the process and the high ranges of components that can be used. This is why they are well-stablished in the industry and are the most commonly used methods. However, low-energy methods require only simple mixers, which is a great advantage to be applied in the industry.[1,3]

As stated before, two different methodologies can be used for the synthesis of emulsions using low-energy methods: thermal methods and isothermal methods.

Thermal methods need a rapid change in temperature, which is difficult to implement in the industry for large volumes of fluids. For this reason, isothermal methods, which rely in a change in system composition are more promising.[4–6]

Among the isothermal methods, spontaneous emulsification is the easiest to implement. In this case, an organic phase is added to an aqueous phase, as opposed to phase inversion method, in which the aqueous phase is added to the organic one. As the volume of the organic phase is usually less, spontaneous emulsification is usually preferred.[1,2]

Traditionally, spontaneous emulsification uses high amounts of synthetic surfactants. This leads to high cost and toxicity concerns, so there has been a recent movement toward the use of natural emulsifiers. Several natural emulsifiers have been used including proteins, polysaccharides and phospholipids.

Phospholipids are of great interest as they contain both hydrophilic and hydrophobic groups. This makes them easily able to orient at the oil-water interface. There are a variety of sources that phospholipids can come from including soybeans, rapeseeds, or sunflowers. The main drawback of the use of natural surfactants is the difficult optimization process, especially for the spontaneous emulsification method.[7,8] Some researchers have reported the synthesis of emulsions by spontaneous emulsification and high-energy methods using sunflower phospholipids.[8,9]

For this reason, the next step for the modification of the developed nanocapsules would be the modification of the surfactants used for the nanoemulsion formation. In addition to this, the oil could be modified to in order to understand if the system is versatile enough to be able to encapsulate different types of oils.

A few experiments have been carried out for this purpose, as a first glance in this research line. At a first approach, several pure phospholipids were chosen to be used as surfactants and their structures are shown in Figure 1.

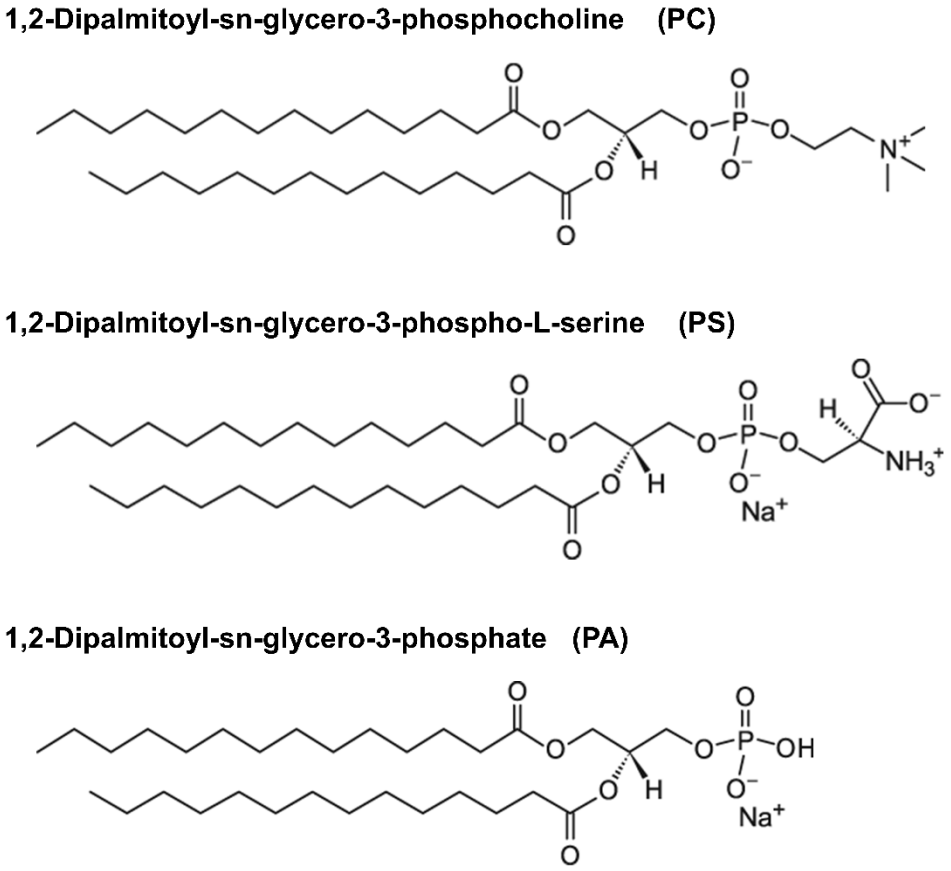

Figure 1. Chemical structures of the phospholipids used for the nanoemulsion synthesis

As shown in Figure 1, all the chosen surfactants have the same lipid (palmitic acid) and they are modified with different moieties in the phosphate group. Changing the properties of the polar head allows the evaluation of how this group affect nanoemulsion synthesis. In the future, it can be also studied how the change in the lipids of the phospholipid affect nanoemulsion structure. The different phospholipid heads that were chosen had different charges and structures. PC is positively

charged, PS is amphiphilic while PA is not modified and has the bare negatively charged phosphate acid. With this, we would have and overall negatively charged one (PA), a positively charged one (PS) and a neutral one (PC). In addition to that, three different oils were chosen and their structures are shown in Figure 2.

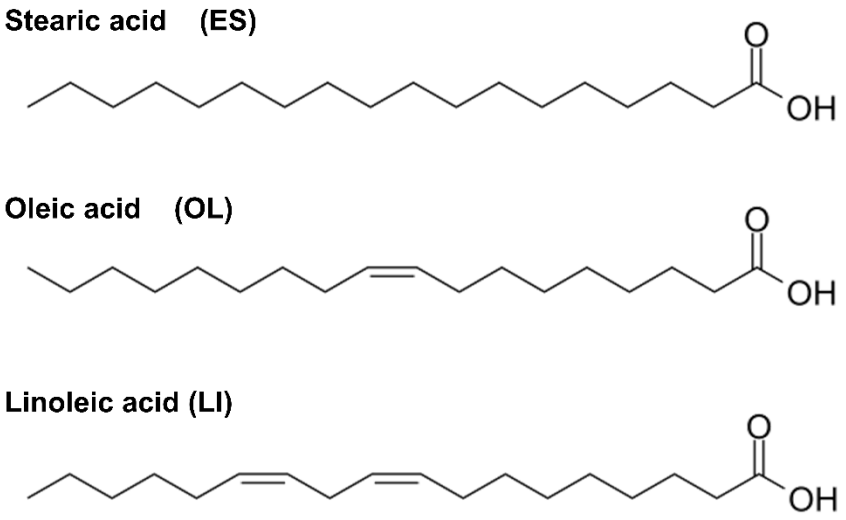

Figure 2. Chemical structures of the oils used for the nanoemulsion synthesis

As observed in Figure 2, all the oils selected contain the same number of carbons, and differ in the number of double bonds in their structure: ES has no double bonds, OL has one and LI two. With this selection, as with the phospholipid case, we wanted to eliminate as many variants as possible, and changing just one parameter of the oils (in this case, the number of double bonds). In future experiments, the number of carbon could be changed too, and even oil mixtures of oils with different characteristics.

With these components, it was decided to create a matrix for the synthesis of all the possible combinations (Table 1). In addition to natural phospholipids, Tween 20 (TW) was used as a control surfactant.

Table 1. Matrix of the different combination of components for the synthesis of the nanoemulsions. In red, the ones that did not work, in green the ones that did

Oil/Surfactant	TW	PC	PS	PA
ES				
OL				
LI				

As shown in Table 1, 15 different nanoemulsions were synthesized combining the different components. In all the cases, the synthesis process was carried out similarly to the one performed in the previous chapters. First, the oil and the phospholipids were mixed with ethanol. In the case of the ones with TW, the oil was mixed with ethanol and TW with water. In all the case, the aqueous phase was added into the organic one under stirring. After 15 minutes of stirring at room temperature, xanthan was added. This polymer was chosen instead of alginate or chitosan because it does not need further steps for stabilization of the coating, such as addition of sodium sulfate or calcium chloride. This allows the reduction of the number of parameters affecting the final synthesis of the nanoemulsions. For all the cases, after 15 minutes of stirring after xanthan addition, nanocapsules were washed 3 times using Amicon® centrifugal filter units.

In Table 1, colors of the matrix represent if the synthesis process worked or not. The cases that worked (in green) were the combinations of OL with TW, PC and PA and

LI with the same surfactants. It is believed that these combinations worked because a change in the turbidity of the suspension occurred, indicating the formation of a nanoemulsion.[7,10] In the case of the ones that did not work (in red), either no change was observed, or precipitation of any component occurred.

In the cases that did not work, all the combinations with PS or ES, some changes in the nanoemulsion synthesis conditions could be performed in the future, such as changes of the solvent, temperature or components ratios, but for these first tests these oil/surfactant combinations were just discarded and the ones that worked were selected.

To characterize the nanocapsule, hydrodynamic diameter and size distribution were measured to check if the different oil/surfactant mixtures affected nanocapsule size. All the nanocapsules were measured at the same concentration in water in order to be able to compare the results. Results for size distribution for all the types are shown in Figure 3.

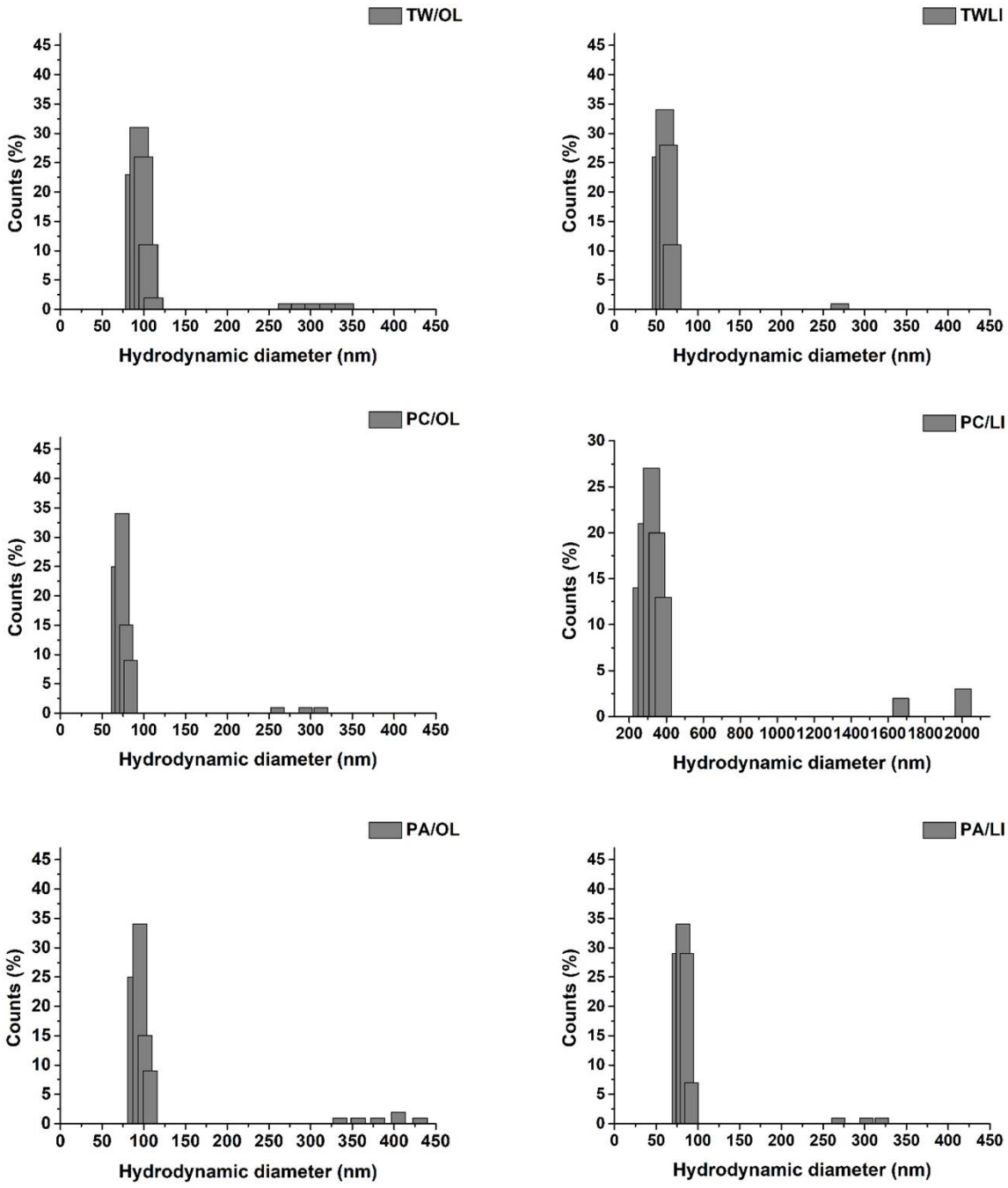

Figure 3. Size distribution measured by DLS of the different oil/surfactant combinations measured by DLS

Results shown in Figure 3 show the size distribution of the 6 nanocapsules obtained with the 6 oil/surfactant combinations that worked. TW containing nanocapsules

have a mean diameter of 95 nm and 65 nm for the combination with OL and LI, respectively. This result is in agreement with the possible formation of stable nanoemulsions coated by xanthan, meaning that both combinations worked and that we could use them in future experiments. In the case of PC, for its combination with OL, nanocapsules show also a mean diameter of 70 nm. However, for the combination with LI nanocapsules show a mean diameter of 330 nm, which is much higher than expected. Besides, there is also a small population of capsules in the micrometric range, and it could be observed macroscopic aggregation of the nanocapsules. This would mean that possibly this combination is not forming stable nanocapsules, as they are aggregating in short periods of time. In the future, some experiments could be performed to adjust oil/surfactant ratio or the solvent used during the synthesis to be able to develop a more stable system. For both PA combinations, we can observe that they have a mean diameter of 95 nm and 80 nm for OL and LI, respectively. As in the TW case, these diameters are in agreement with good nanoemulsion formation, as diameter in within the expected range, and no aggregation was observed.

With this results, we have a first approximation of which combination of oil/surfactant worked better and for which ones some parameter would need adjustment. For example, it was already determined, that working with stearic acid in these conditions was not easy as its melting point is 69.3 ^{o}C, so it is solid at room temperature conditions, unlike oleic and linoleic acid, which both are in a liquid state. This could be affecting nanoemulsion formation, as with all the tested surfactants nanoemulsion was not formed.

In the case of the phospholipids that we tried, only PS did not work. One of the reasons that this could have happened is because it is the one presenting lower ethanol solubility. This would limit its dissolution in ethanol, which is the solvent for the nanoemulsion formation. It shows better solubility in solvents like chloroform which cannot be used for spontaneous emulsification as the organic solvent need to be miscible with water, so probably this phospholipid would not work for the synthesis of nanoemulsions using this method.

With these results, we have a first approximation as what to expect next. Firstly, nanocapsules should be further characterized, especially in terms of toxicity, to check if the substitution of the surfactant lowers nanocapsule toxicity. After that, other phospholipids and oils could be selected in order to understand better which parameters are critical for nanoemulsion formation. For example, oils with a different number of carbon could be selected or phospholipids with different lipids such as oleic o estearic. This work opens a new door to understanding how the nanoemulsion core can be synthesized in a more natural way and in the future also how this changes affect the encapsulation of different molecules.

General conclusions

Nanoparticles have attracted the interest of many researchers from different research fields over the past decades due to their unique properties. One of the most explored applications is their use as nanocarriers. Nanocarriers are nanomaterials able to transport substances, such as drugs, proteins or other nanoparticles. Their interest has grown because they allow the vehiculization of molecules with low solubility in water, targeting the site of action, the protection from degradation or even immobilization of molecules to separate them from the rest of the medium.

Among the different nanocarriers, in this thesis we have selected a synthesis method to obtain nanocapsules with tunable properties. In a previous work, we developed a synthesis method for the synthesis of empty nanocapsules that combine a nanoemulsion core, formed by spontaneous emulsification and a polymeric shell. The core was coated with chitosan to stabilize the emulsion and modify the surface properties. In this thesis, we used this nanocapsules for the encapsulation of different molecules with different properties. We believed that, thanks to the hydrophobic core, we would be able to encapsulate hydrophobic molecules and that the polymeric coating could help to entrap hydrophilic ones. Due to the nature of this type of nanocapsules, surface properties could be tuned by changing the polymer coating to meet the needs of the application, allowing better suitability of the

nanocapsule surface to the final application and also by grafting the surface with functional molecules. Even several polymers could be used for the coating of the surface to improve the stability or efficacy needed.

For example, chitosan was used in Chapter 2 and 5 due to its effectiveness for cell internalization of nanocapsules. Besides, its easy modification was also really useful in Chapter 2 for the addition of targeting molecules such as trimannoside.

But not only chitosan was suitable for the coating of these nanocapsules. Xanthan has proven to be also very effective in the stabilization of the nanocarriers. For example, in Chapter 3, disulfiram-loaded nanocapsules were coated with chitosan or xanthan for the application of the nanocapsules in the treatment of pancreatic cancer and MRSA infections. Both nanocapsules proved to be very effective in the antimicrobial assays against MRSA infections. However, xanthan-coated ones were more effective in killing pancreatic cancer cells, probably thanks to an improvement of the nanocapsule stability with xanthan coating.

In Chapter 4, we developed carriers with a third polysaccharide: alginate. In this case, the negative charge of this polymer allowed easy interaction with the positively charge chitosan. Chitosan was needed for the entrapment of the enzyme immobilized in this study, as it proved in previous works that it created the best microenvironment for the activity of the enzyme. Thanks to combination of chitosan and alginate in the capsule surface, we obtained the best possible carrier to be used in catalysis.

These examples proved that selection of the suitable polysaccharide for the nanocapsule coating is really important, as the efficiency of the nanocarrier will greatly depend on it. Besides, it demonstrates that we are able to coat the nanoemulsion with different natural polysaccharides after the correct optimization of the coating method, which was developed specifically for each project.

To evaluate the properties of the nanocapsules as carriers, several molecules and nanoparticles were selected to be encapsulated with different final applications. In this manner, we would be able to evaluate the suitability of this type of nanocarriers to encapsulate multiple molecules and nanoparticles and would help us predict which ones could work in future experiments.

Thanks to the experiments performed and explained during the different chapters of this thesis, we concluded that our system is suitable for the encapsulation of hydrophobic molecules that can be solubilized in the nanoemulsion mixture. For example, in Chapter 2, the antibiotic bedaquiline was encapsulated for the treatment of *Mycobacterium tuberculosis* infections with great results for encapsulation efficiency and drug loading values. The hydrophobic drug disulfiram was also encapsulated and the results are shown in Chapter 3. On the other hand, we could also prove the possibility to encapsulate hydrophilic molecules with a hydrophobic moiety, such as daptomycin.

But these nanocarriers also proved that they are able to encapsulate proteins or even inorganic nanoparticles. In Chapter 5, holmium vanadate with a mean diameter of 65 nm were successfully encapsulated. In Chapter 4, magnetic iron oxides particles together with the enzyme chloroperoxidase were entrapped in different

compartments of a capsule: CPO in the chitosan layer and magnetic nanoparticles in the emulsion core the polymer coating of the carriers.

All the developed nanocapsules showed great efficiency results thanks to their optimization process and the correct selection of their characteristics. In all the cases, new methods had to be developed for the evaluation of these characteristics depending on the molecule encapsulated. Iin Chapter 2, we developed new methods for the quantification of the amount of encapsulated antibiotic, release in different media of interest or the surface modification. These developed methods could be slightly modified to be applied in different projects, such as in Chapter 3. In Chapter 4, determination of the nanocarrier stability in the reaction media and development of a new method for catalysis evaluation were also developed.

We could conclude that we have effectively developed a new versatile nanocarrier that was successful on the encapsulation of multiple and different cargos such as drugs, nanoparticles and proteins. New methods for the coating of these nanocapsules with different polysaccharides have been established too, and have demonstrated that the selection of the surface coating has great impact in the final efficiency of the nanocarrier.

These developed nanocapsule could be modified in the future by substituting the synthetic surfactants for natural ones such as phospholipids. This modification would allow the obtaining of totally natural nanocapsules, which could improve toxicity issues to cells. Besides, using of different phospholipids with different polar heads together with the modification of the oil inside the nanoemulsion could help us modify

the nanocapsule structure and their encapsulation efficiencies for different molecules to finally make them the best possible nanocarrier for each application.

Conclusiones generales

Las nanopartículas han atraído el interés de muchos investigadores de diferentes campos de investigación durante las últimas décadas debido a sus propiedades únicas. Una de las aplicaciones más exploradas es su uso como nanoportadores. Los nanoportadores son nanomateriales capaces de transportar sustancias, como fármacos, proteínas u otras nanopartículas. Su interés ha crecido porque permiten la vehiculización de moléculas con baja solubilidad en agua, dirigiéndose específicamente al sitio de acción, la protección contra la degradación o incluso la inmovilización de moléculas para separarlas del resto del medio.

Entre los diferentes nanoportadores, en esta tesis hemos seleccionado un método de síntesis para obtener nanocápsulas con propiedades ajustables. En un trabajo anterior, desarrollamos un método de síntesis para la síntesis de nanocápsulas vacías que combinan un núcleo de nanoemulsión, formado por emulsificación espontánea y una capa polimérica. El núcleo se revistió con quitosano para estabilizar la emulsión y modificar las propiedades de la superficie. En esta tesis, utilizamos estas nanocápsulas para la encapsulación de diferentes moléculas con diferentes propiedades. Se creía que, gracias al núcleo hidrófobo, se podría encapsular moléculas hidrófobas y que el recubrimiento polimérico podría ayudar a atrapar las hidrófilas. Debido a la naturaleza de este tipo de nanocápsulas, las

propiedades de la superficie podrían afinarse cambiando el recubrimiento de polímero para satisfacer las necesidades de la aplicación, permitiendo una mejor adecuación de la superficie de la nanocápsula a la aplicación final y también modificando la superficie con moléculas funcionales. Incluso se podrían usar varios polímeros para el revestimiento de la superficie para mejorar la estabilidad o eficacia necesarias.

Por ejemplo, el quitosano se utilizó en los capítulos 2 y 5 debido a su eficacia para mejorar la internalización celular de las nanocápsulas. Además, su fácil modificación también fue útil en el Capítulo 2 para la modificación de su superficie con moléculas diana como el trimanósido.

Pero no solo el quitosano es adecuado para el recubrimiento de estas nanocápsulas. El xantano también ha demostrado ser muy eficaz en la estabilización de los nanoportadores. Por ejemplo, en el Capítulo 3, se recubrieron nanocápsulas cargadas de disulfiram con quitosano o xantano para la aplicación de las nanocápsulas en el tratamiento del cáncer de páncreas y las infecciones por SARM. Ambas nanocápsulas demostraron ser muy efectivas en los ensayos antimicrobianos contra infecciones por SARM. Sin embargo, las recubiertas de xantano fueron más efectivas para matar las células de cáncer de páncreas, probablemente gracias a una mejora de la estabilidad de la nanocápsula con el recubrimiento de xantano.

En el capítulo 4, se desarrollaron vehículos con un tercer polisacárido: el alginato. En este caso, la carga negativa de este polímero permitió una fácil interacción con el quitosano de carga positiva. El quitosano era necesario para el atrapamiento de

la enzima inmovilizada en este estudio, ya que se demostró en trabajos anteriores que creaba el mejor microambiente para la actividad de la enzima. Gracias a la combinación de quitosano y alginato en la superficie de la cápsula, obtuvimos el mejor portador posible para ser utilizado en catálisis.

Estos ejemplos demostraron que la selección del polisacárido adecuado para el recubrimiento de la nanocápsula es realmente importante, ya que la eficiencia del nanoportador dependerá en gran medida de ello. Además, demuestra que somos capaces de recubrir la nanoemulsión con diferentes polisacáridos naturales tras la correcta optimización del método de recubrimiento, que fue desarrollado específicamente para cada proyecto.

Para evaluar las propiedades de las nanocápsulas como portadoras, se seleccionaron varias moléculas y nanopartículas para encapsularlas con diferentes aplicaciones finales. De esta forma, podríamos evaluar la idoneidad de este tipo de nanotransportadores para encapsular múltiples moléculas y nanopartículas y nos ayudaría a predecir cuáles podrían funcionar en futuros experimentos.

Gracias a los experimentos realizados y explicados durante los diferentes capítulos de esta tesis, llegamos a la conclusión de que nuestro sistema es apto para la encapsulación de moléculas hidrófobas que pueden solubilizarse en la mezcla de nanoemulsión. Por ejemplo, en el Capítulo 2, se encapsuló el antibiótico bedaquilina para el tratamiento de infecciones por *Mycobacterium tuberculosis* con excelentes resultados en cuanto a eficacia de encapsulación y valores de carga de fármaco. El fármaco hidrófobo disulfiram también se encapsuló y los resultados se muestran en

el Capítulo 3. Por otro lado, también pudimos probar la posibilidad de encapsular moléculas hidrófilas con un resto hidrófobo, como la daptomicina.

Pero estos nanoportadores también demostraron que son capaces de encapsular proteínas o incluso nanopartículas inorgánicas. En el Capítulo 5, se encapsuló con éxito nanopartículas vanadato de holmio con un diámetro medio de 65 nm. En el Capítulo 4, las partículas magnéticas de óxido de hierro junto con la enzima cloroperoxidasa fueron atrapadas en diferentes compartimentos de una cápsula: CPO en la capa de quitosano y nanopartículas magnéticas en el núcleo de la emulsión el recubrimiento polimérico de los portadores.

Todas las nanocápsulas desarrolladas mostraron gran eficiencia gracias a su proceso de optimización y la correcta selección de sus características. En todos los casos, se tuvieron que desarrollar nuevos métodos para la evaluación de estas características en función de la molécula encapsulada. En el Capítulo 2, se desarrollaron nuevos métodos para la cuantificación de la cantidad de antibiótico encapsulado, la liberación en diferentes medios de interés o la modificación de la superficie. Estos métodos desarrollados pudieron modificarse ligeramente para ser aplicados en diferentes proyectos, como en el Capítulo 3. En el Capítulo 4, también se desarrollaron métodos para la determinación de la estabilidad del nanotransportador en los medios de reacción y el desarrollo de un nuevo método para la evaluación de la catálisis.

Podríamos concluir que hemos desarrollado efectivamente un nuevo nanotransportador versátil que tuvo éxito en la encapsulación de cargas múltiples y diferentes, como medicamentos, nanopartículas y proteínas. También se han

establecido nuevos métodos para el recubrimiento de estas nanocápsulas con diferentes polisacáridos y han demostrado que la selección del recubrimiento superficial tiene un gran impacto en la eficiencia final del nanotransportador.

Estas nanocápsulas desarrolladas podrían modificarse en el futuro sustituyendo los tensioactivos sintéticos por otros naturales como los fosfolípidos. Esta modificación permitiría obtener nanocápsulas totalmente naturales, lo que podría mejorar los problemas de toxicidad celular. Además, el uso de diferentes fosfolípidos con diferentes cabezas polares junto con la modificación del aceite dentro de la nanoemulsión podría ayudarnos a modificar la estructura de la nanocápsula y sus eficiencias de encapsulación para diferentes moléculas para finalmente convertirlas en el mejor nanoportador posible para cada aplicación.

List of publications

1. Bento, R., Pagán, E., Berdejo, D., de Carvalho, R.J., **García-Embid, S.**, Maggi, F., Magnani, M., de Souza, E.L., García-Gonzalo, D., Pagán, R. Chitosan nanoemulsions of cold-pressed orange essential oil to preserve fruit juices (2020) International Journal of Food Microbiology, 331, art. no. 108786

2. González-Mancebo, D., Becerro, A.I., Corral, A., **García-Embid, S.**, Balcerzyk, M., Garcia-Martin, M.L., de la Fuente, J.M., Ocaña, M. Design of a nanoprobe for high field magnetic resonance imaging, dual energy X-ray computed tomography and luminescent imaging (2020) Journal of Colloid and Interface Science, 573, pp. 278-286.

3. **García-Embid, S.**, Di Renzo, F., De Matteis, L., Spreti, N., M. de la Fuente, J. Magnetic separation and high reusability of chloroperoxidase entrapped in multi polysaccharide micro-supports (2018) Applied Catalysis A: General, 560, pp. 94-102.

4. De Matteis, L., Jary, D., Lucía, A., **García-Embid, S.**, Serrano-Sevilla, I., Pérez, D., Ainsa, J.A., Navarro, F.P., M. de la Fuente, J. New active formulations against M. tuberculosis: Bedaquiline encapsulation in lipid nanoparticles and chitosan nanocapsules (2018) Chemical Engineering Journal, 340, pp. 181-191.

5. Artiga, Á., **García-Embid, S.**, De Matteis, L., Mitchell, S.G., de la Fuente, J.M. Effective in Vitro Photokilling by cell-adhesive gold nanorods (2018) Frontiers in Chemistry, 6 (JUN), art. no. 234.

6. Martín-Rapún, R., de Matteis, L., Ambrosone, A., **García-Embid, S.**, Gutiérrez, L., de la Fuente, J.M.Targeted nanoparticles for the treatment of Alzheimer's disease (2017) Current Pharmaceutical Design, 23 (13), pp. 1927-1952.

7. De Matteis, L., Alleva, M., Serrano-Sevilla, I., **García-Embid, S.**, Stepien, G., Moros, M., De La Fuente, J.M. Controlling properties and cytotoxicity of chitosan nanocapsules by chemical grafting (2016) Marine Drugs, 14 (10), art. no. 175.

Abreviations

ºC	Celsius degree
ALDH	Aldehydehydrogenase
ALG	Alginate
BQ	Bedaquiline
BS^3	Bis(sulfosuccinimidil)suberate
Cryo-TEM	Cryogenic Transmission Electro Microscopy
CS	Chitosan
CPO	Cloroperoxidase
DSD	Dichlorodimedone
DL%	Drug loading
DLS	Dynamic Light Scattering
DP	Daptomycin
DSF	Disulfiram
EE%	Encapsulation Eficiency
FTIR	Fourier-transform infrared spectroscopy
IS	Intestinal Simulated Media
Li	Linoleic acid
MCD	Monoclorodimedone

MHII	Mueller Hinton II
MIC	Minimal Inhibitory Concentration
MRI	Magnetic Resonance Imaging
MRSA	Meticillin-Resistant *Staphylococcus aureus*
MTT	3-(4,5-dimethylthiazol-2-yl)-2,5-diphenyltetrazolium bromide
NC	Nanocapsule
NIR	Near-infrarred region
NP	Nanopartice
PA	Phosphatidic acid
OL	Oleic acid
PBS	Phosphate Buffered Solution
PC	Phosphatidil choline
PCS	Photocorrelation Spectroscopy
PDI	Polydispersity Index
PEG	Polyethylenglycol
PLGA	Poly(lactic-co-glycolic) acid
ROS	Reactive Oxygen Species
rpm	Revolution per minute
SDS-PAGE	Sodium dodecyl sulfate polyacrylamide gel electrophoresis
SEM	Scanning Electron Microscopy
TEM	Transmission Electron Microscopy
TRI	Trimannose
TW	Tween 20

UV-vis	Ultraviolet-visible
WHO	World Health Organization
XAN	Xanthan